UNIVERSITY OF CALIFORNIA SAN DIEGO

Chemical tools to modulate stem cell differentiation through glycocalyx engineering

A dissertation submitted in partial satisfaction of the
requirements for the degree Doctor of Philosophy

in

Chemistry

by

Matthew Russell Naticchia

Committee in charge:

Professor Kamil Godula, Chair
Professor Michael Burkart
Professor Mark Fuster
Professor Thomas Hermann
Professor Patricia Jennings

2022

The Dissertation of Matthew Russell Naticchia is approved, and it is acceptable in quality and form for publication on microfilm and electronically.

University of California San Diego

2022

TABLE OF CONTENTS

LIST OF FIGURES

LIST OF TABLES

LIST OF SCHEMES

LIST OF ABBREVIATIONS

AIBN	azobisisobutyronitrile
AF488	AlexaFluor 488
BMP	bone morphogenic protein
Boc	bitertbutyldicarbonate
BSA	bovine serum albumin
CPD	critical point dryer
CTA	chain transfer agent
DCM	dichloromethane
DiI	1,1'-dioctadecyl-3,3,3'3'-tetramethylindocarbocyanine perchlorate
DMF	N, N-dimethylformamide
DPBS	Dulbecco's phosphate buffer saline
DPPE	1,2-dipalmitoyl-sn-glycero-3- phosphoethanolamine
EB	embryoid body
ECM	extracellular matrix
Ext1	exostosin 1
FBS	fetal bovine serum
FGF	fibroblast growth factor
Flk1	fetal liver kinase 1
GAG	glycosaminoglycan
GP	glycopolymer
GPC	gel permeation chromatography
GlcNAc	N-acetylglucosamine
HS	heparan sulfate
IMDM	Iscove's modified Dulbecco's media
KO-DMEM	knockout Dulbecco's modified eagle medium
LIF	Leukemia inhibitory factor
mESC	murine embryonic stem cell
SEM	scanning electron microscope
PCR	polymerase chain reaction
PhOH	phenol
RAFT	reversible addition fragmentation chain transfer
THF	tetrahydrofuran
TMSCl	trimethylsilyl chloride
WT	wild type
3D	three dimensional

ACKNOWLEDGEMENTS

I would like to thank Dr. Kamil Godula for for his support and mentorship throughout my graduate degree. I would like to thank Dr. Mia Huang and Dr. Steve Verespy, who helped me grow as a scientist and provided valuable insight. I'd like to thank Dr. Dan Honigfort and Dr. Greg Trieger for aiding me in my job search. I'd like to thank (future Dr.) Logan Laubach for all the hard work he put in as an undergraduate and Masters student, working with me on several projects. I'd also like to thank the rest of the Godula lab. You all became a second family to me and made my PhD experience worthwhile.

I would like to thank my family for all their love and support. Without my mom, dad, brother and sister (and the dogs), I would never have made it this far. Even from across the country, your love and support has meant the world to me. Finally I'd like to thank Yanice Benitez (and of course Peanut) for being with me every step of my PhD. The road wasn't always easy, but having you as a partner on this journey has made it a little easier.

Notes About the Chapters

Chapter 2, in full, is a reprint of the material as it appears: M. R. Naticchia, L.K. Laubach, D.J. Honigfort, S. C. Purcell, K. Godula. *Biomaterials Science* – Spatially controlled glycocalyx engineering for growth factor patterning in embryoid bodies. The dissertation author is the primary co-author of this manuscript.

Chapter 3, in full, is a reprint of the material as it appears: M. R. Naticchia, L.K. Laubach, E.M. Tota, T. M. Lucas, M.L. Huang, K. Godula. *ACS Chemical Biology* – Embryonic stem cell engineering with a glycomimetic FGF2/BMP4 co-receptor drives

mesodermal differentiation in a three-dimensional culture . The dissertation author is the primary author of this manuscript.

Chapter four, in full, is currently being prepared for submission for publication. M. R. Naticchia, S. Verespy, D. Kozirovskiy, C. Seitz, Z. Gaieb, B. Timm, M. L. Huang, R. Amaro, K. Godula. Small molecule inhibitor of heparan sulfate biosynthesis enable transient reprogramming of stem cell glycocalyx to control differentiation. The dissertation author was the primary researcher and author of this material.

VITA

Education

2014 Bachelor of Arts, Biochemistry and Molecular Biology, The College of Wooster

2016 Master of Science, Chemistry, UC San Diego

2022 Doctor of Philosophy, Chemistry, UC San Diego

Publications

M. R. Naticchia, L. K. Laubach, E. M. Tota, T. M. Lucas, M. L. Huang, K. Godula, Embryonic Stem Cell Engineering with a Glycomimetic FGF2/BMP4 Co-Receptor Drives Mesodermal Differentiation in a Three-Dimensional Culture. *ACS Chem. Biol.* **13**, 2880–2887 (2018).

M. R. Naticchia, L. K. Laubach, D. J. Honigfort, S. C. Purcell, K. Godula, Spatially controlled glycocalyx engineering for growth factor patterning in embryoid bodies. *Biomater. Sci.* **9**, 1652–1659 (2021).

T. M. Lucas, C. Gupta, M. O. Altman, E. Sanchez, **M. R. Naticchia**, P. Gagneux, A. Singharoy, K. Godula, Mucin-mimetic glycan arrays integrating machine learning for analyzing receptor pattern recognition by influenza A viruses. *Chem*. **7**, 3393–3411 (2021).

S.C. Purcell, **M.R. Naticchia**, N. Marroquin, J. L. Follmar, H. J. C. Ng, K. Godula. HS-aptamer chimeras enable embryonic stage-specific glycocalyx engineering. *In preparation*

M. R. Naticchia, S. Verespy, D. Kozirovskiy, C. Seitz, Z. Gaieb, B. Timm, R. Amaro, K. Godula. Small molecule inhibitor of heparan sulfate biosynthesis enable transient reprogramming of stem cell glycocalyx to control differentiation. *In preparation*

ABSTRACT OF THE DISSERTATION

by

Matthew Russell Naticchia

Doctor of Philosophy in Chemistry

University of California San Diego, 2022

Professor Kamil Godula, Chair

The ability to self-replicate and differentiate into all three germ layers gives stem cells great therapeutic potential. However, regulation of differentiation is complex, requiringspatial, temporal and molecular cues to reach a desired lineage. Growth factor (GF) signaling is key in regulating stem cell differentiation, however these signals alone are not

sufficient for efficient and homogeneous differentiation. Additional tools are needed to understand these differentiation pathways, and further control them for therapeutic gain.

Heparan sulfate (HS) glycosaminoglycans serve as co-receptors for many GFs and could be a valuable tool for driving differentiation. However, approaches that utilize HS to manipulate cellular signaling has been minimal due to the size and

heterogenious nature of these biomolecules. Sulfation is dynamic along the chain, with modifying enzymes present around the cell surface, and biosynthesis of HS is non-templated. This makes understanding the key interactions in a pathway difficult and synthesis of mimetics difficult.

To achieve chemical control over differentiation, chemically-defined synthetic tools are necessary to mimic the ability to bind GFs without the structural heterogeneity and complexity. Further, methods are needed for overwriting the native HS so that these tools can be used transiently. In this dissertation, I present methods for the preparation of synthetic HS mimetics and a novel inhibitor of HS biosynthesis and demonstrate their efficacy in the context of stem cell differentiation. In chapter 2, I introduce a method for forming GF gradients using chemically defined HS mimetics. In chapter 3, I use these HS-mimetics to achieve mesodermal differentiation in spheroid culture. In chapter 4, I developed novel inhibitor of HS biosynthesis to arrest mESCs in a pluripotent state and one that is compatible with glycocalyx remodeling techniques.

1 Heparan Sulfate and its role in stem cell biology

1.1 Structure and biosynthesis of heparan sulfate

Glycans are ubiquitously found in nature, serving as the first point of contact for cells with the outside environment. These glycans serve as both a physical barrier, protecting cells from pathogens[1], and play a key role in signaling events, ranging from self-recognition[2] to protein and growth factor binding[3]. The range of function is largely driven by the diverse structures that can be made from a large pool of monosaccharide building blocks[4], varying glycosidic bond linkages and potential for branched structures[5]. Further, the non-templated synthesis of these structures allows for a dynamic response to the outside environment.[6] These cell surface glycans within the glycocalyx form a diverse microenvironment that is vital for proper cellular function.

Within the glycocalyx is a class of glycans called glycosaminoglycans (GAGs). These biomolecules are found in all human tissue, and different GAG classes are responsible for a variety of cellular functions. All GAGs share a common core tetrasaccharide, consisting of xylose, two galactose residues and a glucuronic acid. The identity of the monosaccharides that extend the GAG chain give rise to four distinct classes: heparan sulfate (HS), chondroitin sulfate (CS)/dermatan sulfate (DS), keratan sulfate (KS) and hyaluronic acid.[7] GAGs form extended linear structures, comprised of repeating disaccharide subunits that can stretch hundreds of disaccharides in length. The full extent of their function is still being elucidated; however, their function is often tied to their disaccharide composition and additional modifications (i.e. sulfation, isomerization), tissue localization and the cellular microenvironment that they belong.[8,9]

Of these classes of glycans, glycosaminoglycans, and in particular heparan sulfate (HS), play a vital role in growth factor signaling.[10] HS is an O-linked glycan that is

comprised of alternating glucuronic acid (GlcA) and N-acetylglucosamine (GlcNAc) residues, extending off a core tetrasaccharide. Xylose is first attached to the proteoglycan backbone through serine/threonine residues. Two distinct galactosyltransferases add the next two galactose residues to the core. The final piece of the core tetrasaccharide in HS is a glucuronic acid residue. The core is then extended with the Ext1/2 proteins and functionality of these chains can be modulated through isomerization of GlcA to iduronic acid (IdoA) and from sulfation of the monosaccharides (Fig. 1.1A).[11] These sulfation events can occur at the de-acetylated nitrogen of GlcNAc and on the C3/C6 and C2 hydroxyl groups of the GlcNAc or uronic acid residues, respectively (Fig. 1.1B).[12,13] Sulfation is often found in clusters along the HS chain, and encode binding motifs for growth factors and proteins, such as thrombin.[14,15] To properly induce a cell signaling event, GFs often form complexes with membrane associated HS and their receptor kinases.[16] Secreted or shed HS can act as reservoirs for GFs, maintaining a local concentration nearby the cellular membrane.[17] Removal of the sulfate groups via secreted sulfatase or enzymatic depolymerization of the chain, releasing the bound GFs from the ECM.[18,19]

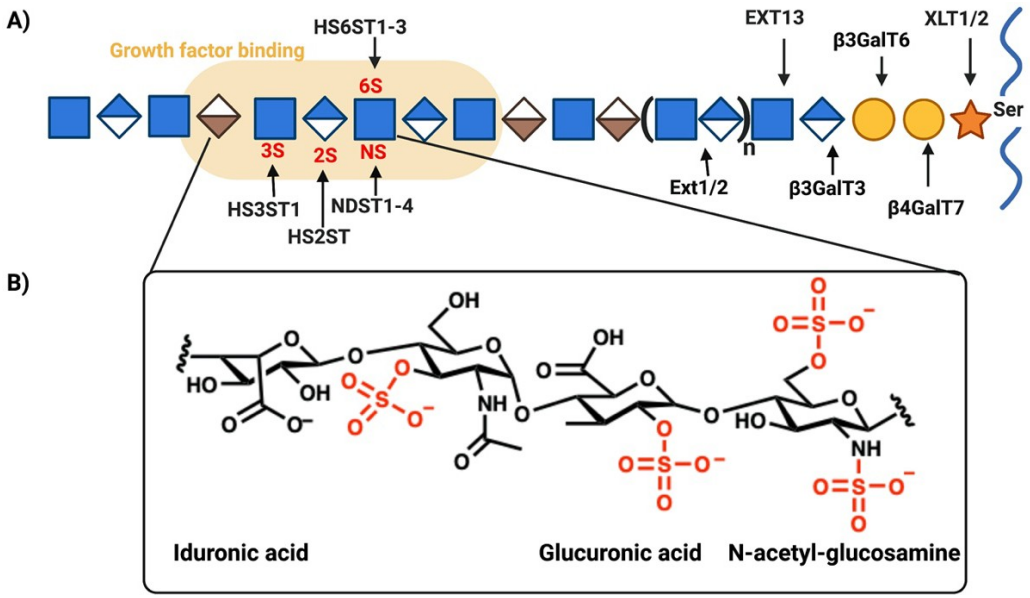

Figure 1.1. Heparan sulfate structure and biosynthesic enzymes. A) The core tetrasaccharide consists of Xylose (orange star), two galactose residues (yellow circle) and a glucuronic acid (blue/white diamond). The core is extended by the Ext1/2 proteins in repeating glucuronic acid and n-acetyl-glucosamine (blue square). The monosaccharides can be modified through sulfation, or glucuronic acid can be isomerized into iduronic acid (brown/white diamond). Patches of high sulfation along the chain serve as binding sites for growth factors. B) Chemical structure and potential sulfation sites of N-acetyl-glucosamine and glucuronic acid.

1.2 Role of heparan sulfate in stem cell differentiation

Stem cell differentiation requires physical/spatial,[20] temporal[21] and molecular cues[22] to proper proliferate and differentiate into their proper cellular specification. During embryogenesis, growth factor gradients are established as differentiating cells produce and release growth factors. They begin to migrate and self-organize within the physical space of the developing embryo. The timing of the activation of these pathways are vitally important for both cellular localization and lineage specification. HS is expressed throughout this process, although distinct proteoglycans[22] and sulfation[23] epitopes along the HS chain are expressed along the HS chain differentially depending on the location and cell type.

In early differentiation of mouse embryonic stem cells (mESC), FGF2 and BMP4 are the determining growth factor signals in determining which germ layer is formed. Both growth factors utilize HS as a co-receptor (Figure 1.2A).[24,25] FGF2 is required for mESCs to exit the pluripotent state, and sustained FGF2 signal leads to neuroectodermal differentiation, characterized first by the expression of the biomarker Sox1[26], followed by Nestin and βIII-tubulin (Fig. 1.2B, left).[27] This process occurs through MAPK activation ultimately ERK phosphorylation, as FGF2 forms a ternary complex with two receptor tyrosine kinases (FGFRs) and HS, that binds both the growth factor and receptor.[28]

To reach the other two primary germ layers, FGF2 is still required initially to prime stem cells for exit of the pluripotent state, however BMP4 signaling quickly becomes the dominant signaling pathway. While the full extent of the role of HS in BMP4 signaling is still unclear[29], HS is required for binding of BMP4 and subsequent signaling. Binding of BMP4 to HS and a receptor complex comprised of a dimer of dimers (BMPRs) results in phosphorylation of Smad-1, -5 or -8, upon which it forms a trimer and translocates to the nucleus (Fig. 1.2B, right). There it serves as a transcription factor that activates the *id* family of genes.[30]

Removal of HS from the cell surface arrests mESCs in a pluripotent state and prevents binding and signaling of FGF2 and BMP4 (Fig. 1.2B, middle).[31] Knocking out the *ext1* gene, responsible for elongation of the HS chain, results in early developmental defects. Differentiation of *Ext1*$^{-/-}$ mESCs results in maintenance of pluripotency markers, such as *oct4* and *nanog*.[32] Normal differentiation via FGF2 or BMP4 can be rescued if these cells are given exogenous HS structures.

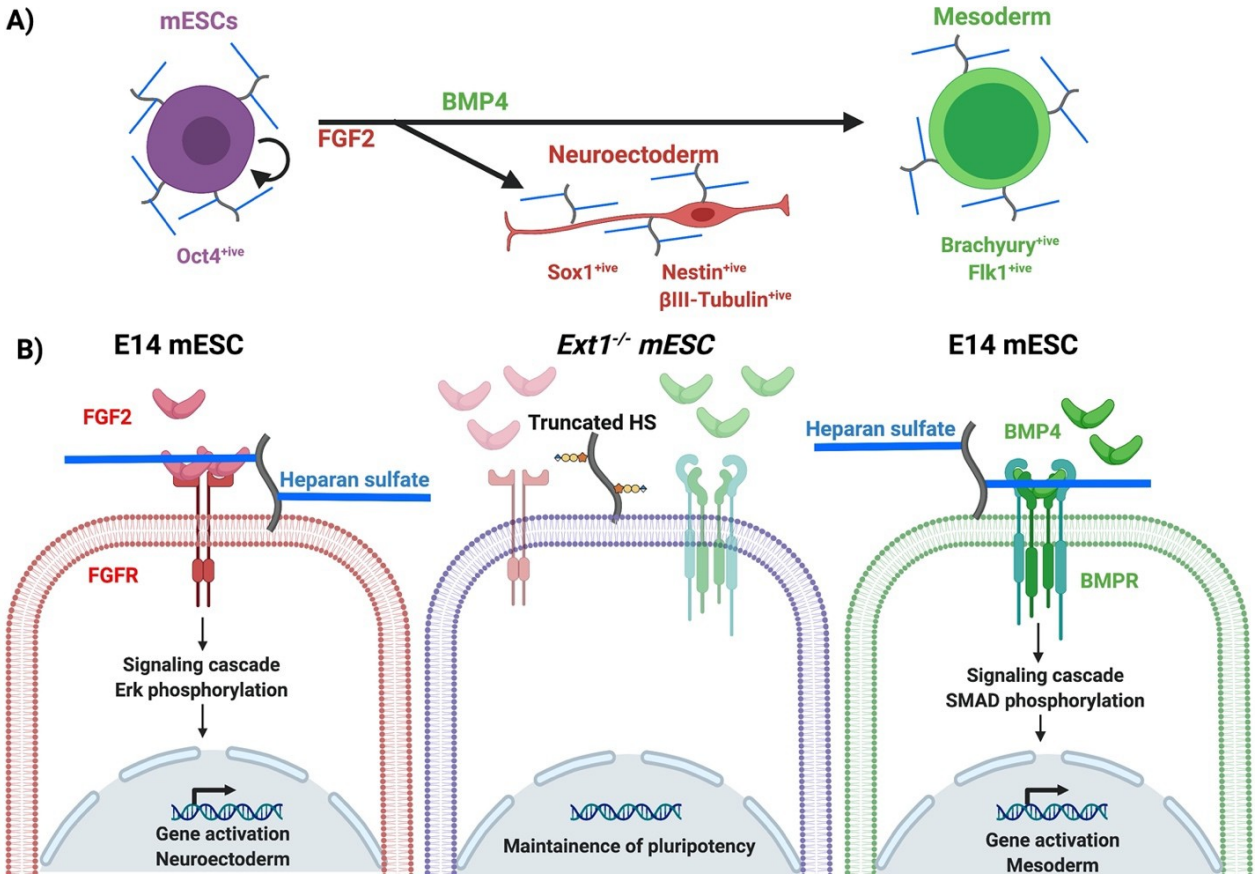

Figure 1.2. Mouse embryonic stem cell differentiation pathways and their growth factor signals. A) Pluripotent stem cells propagate until receiving an FGF2 signal, where it begins to leave the pluripotent state. Continued FGF signalling leads to neural precursor cells, and further neuroectodermal lineages. Introduction of BMP4 soon after exit of the pluripotent state directs differentiation towards mesodermal lineages. B) Mouse embryonic stem cells use heparan sulfate as a co-receptor for both FGF2 (left, red) and BMP4 (right, green). *Ext1*$^{-/-}$ mESCs do not produce functional heparan sulfate chains, and these signaling pathways cannot occur, arresting the cells in a pluripotent state.

1.3 Challenges in controlling stem cell differentiation

Despite their potential as a therapeutic, hematopoietic stem cells are the only class of FDA approved stem cell treatment. To achieve the full potential of stem cells as therapeutics, tight control over the differentiation products must be achieved. While addition of exogenous GFs can drive differentiation towards a particular lineage, typical differentiation protocols still yield heterogeneous mixtures of cells and poor overall yield. Stem cell therapies require a large number of cells, so scalable protocols with high yields

are necessary. Further, loss of control over differentiation can lead to a host of complications such as formation of teratomas.[33]

HS structures have potential to further improve lineage specification, but the compositional heterogeneity and the lack of simple and powerful methods for controlling their synthesis has limited advancement in structure-activity relationship studies, and therefore we lack a full understanding of the HS structures required for specific GF binding and signaling activation.[34] Heparin is widely used clinically as a drug, but heparin suffers from being a heterogeneous polysaccharide with units of differential sulfation and a broad binding profile. It is therefore necessary to develop HS structures with more defined structures. Further, any exogenous HS structure would need to out-compete native HS structures, or native structures would need to be transiently removed. While genetic knockouts hold value as a tool for understanding HS and HS-GF interactions, genetic knockout stem cell lines do not hold value as a functional therapeutic.

1.4 HS mimetics as tools for controlling stem cell differentiation

Chemoenzymatic synthesis has pushed the limits of HS mimetic technology, however the preparation of HS polysaccharides is laborious, and controlling sulfation pattern difficult to achieve. The scale of chemoenzymatic HS polysaccharides is dwarfed by the size of the native structures. Advances in mass spectroscopy techniques have allowed for identification and isolation of specific glycan structures.[35] And binding techniques, such as SPR, has helped identify the minimum binding scaffold for sets of GFs.[36] But these methods lack spatial information and these oligosaccharides tend to lack biological activity.

To introduce sufficiently large glycan structures, many have turned to introducing smaller sub-units in a multivalent arrangement.[37,38] This confers the advantages of high

avidity, without necessitating laborious synthetic techniques that may limit diversity of sulfation patterns. One of the first such structures utilized a glycodendrimer to bind FGF2. The multivalent display of the oligosaccharides significantly increased both GF binding and cellular response.[37] Since then, other researchers have adopted similar approaches, advancing the technology towards further elongated glycan structures[38] or scaffolds that resemble the underlying proteoglycan.[39]

While full length, chemically characterized HS material are still out of reach, creative solutions have been demonstrated and continue to be developed by a variety of research teams. The next three chapters describe my efforts to develop HS-mimetic materials and tools to manipulate HS in the context of stem cell biology. Chapter 2 describes the development of HS GAG mimetics and characterization of these for patterning of FGF2 within 3-D spheroids. Chapter 3 takes advantage of the GF binding ability of this material to stimulate differentiation towards mesodermal lineages in spheroid culture. Finally, chapter 4 introduces a novel inhibition strategy for maintaining pluripotency in mESCs. Collectively, these chapters demonstrate the versatility of the HS-mimetic materials and their broad utility in different biological applications, providing the foundation for their future development toward biomedical applications.

1.5 References

1. S. K. Linden, P. Sutton, N. G. Karlsson, V. Korolik, M. A. McGuckin, Mucins in the mucosal barrier to infection. *Mucosal Immunol*. **2008.** 1, 183–197.

2. R. Amon, E. M. Reuven, S. Leviatan Ben-Arye, V. Padler-Karavani, Glycans in immune recognition and response. *Carbohydrate Research*. **2014.** 389, 115–122.

3. M. Schuldiner, O. Yanuka, J. Itskovitz-Eldor, D. A. Melton, N. Benvenisty, Effects of eight growth factors on the differentiation of cells derived from human embryonic stem cells. *PNAS*. **2000.** 97, 11307–11312

4. R. D. Cummings, J. M. Pierce, The Challenge and Promise of Glycomics. *Chemistry & Biology*. **2014.** 21, 1–15.

5. B. Mulloy, G. W. Hart, P. Stanley, in *Essentials of Glycobiology*, A. Varki, R. D. Cummings, J. D. Esko, H. H. Freeze, P. Stanley, C. R. Bertozzi, G. W. Hart, M. E. Etzler, Eds. (Cold Spring Harbor Laboratory Press, Cold Spring Harbor (NY), ed. 2nd, **2009**; http://www.ncbi.nlm.nih.gov/books/NBK1898/).

6. H. Xiao, R. Wu, Quantitative investigation of human cell surface N -glycoprotein dynamics. *Chemical Science*. **2017.** 8, 268–277.

7. A. Varki, R. D. Cummings, J. D. Esko, P. Stanley, G. W. Hart, M. Aebi, A. G. Darvill, T. Kinoshita, N. H. Packer, J. H. Prestegard, R. L. Schnaar, P. H. Seeberger, *Essentials of Glycobiology* (Cold Spring Harbor Laboratory Press, 2017; https://www.ncbi.nlm.nih.gov/books/NBK310274/) .

8. D. Xu, J. D. Esko, Demystifying Heparan Sulfate–Protein Interactions. *Annual Review of Biochemistry*. **2014.** 83, 129–157.

9. J. L. Dreyfuss, C. V. Regatieri, T. R. Jarrouge, R. P. Cavalheiro, L. O. Sampaio, H. B. Nader, Heparan sulfate proteoglycans: structure, protein interactions and cell signaling. *Anais da Academia Brasileira de Ciências*. **81**, 409–429 (2009).

10. X. Lin, Functions of heparan sulfate proteoglycans in cell signaling during development. *Development*. **2004.** 131, 6009–6021.

11. K. Sugahara, H. Kitagawa, Heparin and Heparan Sulfate Biosynthesis. *IUBMB Life*. **2002**. 54, 163–175.

12. P. Jemth, J. Kreuger, M. Kusche-Gullberg, L. Sturiale, G. Giménez-Gallego, U. Lindahl, Biosynthetic oligosaccharide libraries for identification of protein-binding heparan sulfate motifs. Exploring the structural diversity by screening for fibroblast growth factor (FGF)1 and FGF2 binding. *J. Biol. Chem.* **2002.** 277, 30567–30573.

13. N. Dani, M. Nahm, S. Lee, K. Broadie, A Targeted Glycan-Related Gene Screen Reveals Heparan Sulfate Proteoglycan Sulfation Regulates WNT and BMP Trans-Synaptic Signaling. *PLoS Genet*. **2012.** 8, e1003031.

14. A. N. Teien, U. Abildgaard, M. Höök, The anticoagulant effect of heparan sulfate and dermatan sulfate. *Thrombosis Research*. **1976.** 8, 859–867.

15. K. D. Rodgers, J. D. San Antonio, O. Jacenko, Heparan sulfate proteoglycans: A GAGgle of skeletal-hematopoietic regulators. *Dev. Dyn.* **2008.** 237, 2622–2642.

16. S. K. Nigam, K. T. Bush, Growth factor–heparan sulfate "switches" regulating stages of branching morphogenesis. *Pediatr Nephrol*. **2014.** 29, 727–735.

17. K. C. Kirkbride, B. N. Ray, G. C. Blobe, Cell-surface co-receptors: emerging roles in signaling and human disease. *Trends in Biochemical Sciences*. **2005.** 30, 611–621.

18. J. Kopf, P. Paarmann, C. Hiepen, D. Horbelt, P. Knaus, BMP growth factor signaling in a biomechanical context. *BioFactors*. **2014.** 40, 171–187.

19. C. K. M. Tripathi, J. Banga, V. Mishra, Microbial heparin/heparan sulphate lyases: potential and applications. *Appl Microbiol Biotechnol*. **2012.** 94, 307–321.

20. S. Tada, T. Era, C. Furusawa, H. Sakurai, S. Nishikawa, M. Kinoshita, K. Nakao, T. Chiba, S.-I. Nishikawa, Characterization of mesendoderm: a diverging point of the definitive endoderm and mesoderm in embryonic stem cell differentiation culture. *Development*. **2005.** 132, 4363–4374.

21. R.-H. Fu, Y.-C. Wang, S.-P. Liu, C.-M. Huang, Y.-H. Kang, C.-H. Tsai, W.-C. Shyu, S.-Z. Lin, Differentiation of Stem Cells: Strategies for Modifying Surface Biomaterials. *Cell Transplantation*. **20**, 37–47 (2011).

22. A. G. Smith, Embryo-Derived Stem Cells: Of Mice and Men. *Annual Review of Cell and Developmental Biology*. **17**, 435–462 (2001).

23. R. J. Baldwin, G. B. ten Dam, T. H. van Kuppevelt, G. Lacaud, J. T. Gallagher, V. Kouskoff, C. L. R. Merry, A Developmentally Regulated Heparan Sulfate Epitope Defines a Subpopulation with Increased Blood Potential During Mesodermal Differentiation. *STEM CELLS*. **26**, 3108–3118 (2008).

24. C. E. Johnson, B. E. Crawford, M. Stavridis, G. Ten Dam, A. L. Wat, G. Rushton, C. M. Ward, V. Wilson, T. H. van Kuppevelt, J. D. Esko, A. Smith, J. T. Gallagher, C. L. R. Merry, Essential alterations of heparan sulfate during the differentiation of embryonic stem cells to Sox1-enhanced green fluorescent protein-expressing neural progenitor cells. *Stem Cells*. **25**, 1913–1923 (2007).

25. R. Padera, G. Venkataraman, D. Berry, R. Godavarti, R. Sasisekharan, FGF-2/fibroblast growth factor receptor/heparin-like glycosaminoglycan interactions: a compensation model for FGF-2 signaling. *FASEB J.* **13**, 1677–1687 (1999).

26. S. A. Khan, M. S. Nelson, C. Pan, P. M. Gaffney, P. Gupta, Endogenous heparan sulfate and heparin modulate bone morphogenetic protein-4 signaling and activity. *Am. J. Physiol., Cell Physiol.* **294**, C1387-1397 (2008).

27. M. L. Huang, R. A. A. Smith, G. W. Trieger, K. Godula, Glycocalyx Remodeling with Proteoglycan Mimetics Promotes Neural Specification in Embryonic Stem Cells. *Journal of the American Chemical Society*. **136**, 10565–10568 (2014).

28. J. Schlessinger, A. N. Plotnikov, O. A. Ibrahimi, A. V. Eliseenkova, B. K. Yeh, A. Yayon, R. J. Linhardt, M. Mohammadi, Crystal Structure of a Ternary FGF-FGFR-Heparin Complex Reveals a Dual Role for Heparin in FGFR Binding and Dimerization. *Molecular Cell*. **6**, 743–750 (2000).

29. B. Bragdon, O. Moseychuk, S. Saldanha, D. King, J. Julian, A. Nohe, Bone Morphogenetic Proteins: A critical review. *Cellular Signalling*. **23**, 609–620 (2011).

30. M. Kretzschmar, J. Doody, J. Massagu, Opposing BMP and EGF signalling pathways converge on the TGF-β family mediator Smad1. *Nature*. **389**, 618–622 (1997).

31. R. J. Holley, C. E. Pickford, G. Rushton, G. Lacaud, J. T. Gallagher, V. Kouskoff, C. L. R. Merry, Influencing Hematopoietic Differentiation of Mouse Embryonic Stem Cells using Soluble Heparin and Heparan Sulfate Saccharides. *J. Biol. Chem.* **286**, 6241–6252 (2011).

32. M. Mossahebi-Mohammadi, M. Quan, J.-S. Zhang, X. Li, FGF Signaling Pathway: A Key Regulator of Stem Cell Pluripotency. *Frontiers in Cell and Developmental Biology*. **8** (2020) (available at https://www.frontiersin.org/article/10.3389/fcell.2020.00079).

33. W. Zakrzewski, M. Dobrzyński, M. Szymonowicz, Z. Rybak, Stem cells: past, present, and future. *Stem Cell Res Ther*. **10**, 68 (2019).

34. U. Häcker, K. Nybakken, N. Perrimon, Heparan sulphate proteoglycans: the sweet side of development. *Nat Rev Mol Cell Biol*. **6**, 530–541 (2005).

35. T. M. Puvirajesinghe, Jeremy. E. Turnbull, Glycoarray Technologies: Deciphering Interactions from Proteins to Live Cell Responses. *Microarrays (Basel)*. **5** (2016), doi:10.3390/microarrays5010003.

36. M. L. Huang, K. Godula, Nanoscale materials for probing the biological functions of the glycocalyx. *Glycobiology*. **26**, 797–803 (2016).

37. A. Pulsipher, M. E. Griffin, S. E. Stone, L. C. Hsieh-Wilson, Long-Lived Engineering of Glycans to Direct Stem Cell Fate. *Angew. Chem. Int. Ed.* **54**, 1466–1470 (2015).

38. M. L. Huang, E. M. Tota, S. Verespy, K. Godula, Glycocalyx Scaffolding to Control Cell Surface Glycan Displays. *Current Protocols in Chemical Biology*. **10**, e40 (2018) .

39. G. W. Trieger, S. Verespy, P. L. S. M. Gordts, K. Godula, Efficient Synthesis of Heparinoid Bioconjugates for Tailoring FGF2 Activity at the Stem Cell–Matrix Interface. *Bioconjugate Chem.* **30**, 833–840 (2019).

2 Spatially controlled glycocalyx engineering for growth factor patterning in embryoid bodies

2.1 Introduction

Embryonic stem cells (ESCs) and induced pluripotent stem cells (iPSCs) have the capacity to differentiate into any cell type of the adult body.[1] They provide an important tool to study the process of embryogenesis and organismal development[2] and hold promise for a range of biomedical applications.[3] A key challenge in realizing their full potential is in translating differentiation protocols established in 2D in vitro cultures to the highly complex 3D environments of tissues in vivo.[4,5] 3D spheroids formed from ESCs and iPSCs, such as embryoid bodies (EB),[6] offer a convenient laboratory system to bridge this gap. EBs have the capacity to undergo spontaneous self-patterning into ordered multicellular structures;[7] however, harnessing this potential for reliable production of functional tissue and organ replacements will require achieving better spatial and temporal control over cell differentiation in these systems.[8] Current methods for engineering the microenvironment and self-organization of stem cell spheroids focus primarily on directing the delivery, release and diffusion of differentiation cues, such as growth factors (GFs) and small molecule morphogens.[9,10] For instance, spatial control over cell differentiation in EBs has been accomplished through their exposure to GF gradients in microfluidic devices[11,12] or through encapsulation in hydrogels with controlled GF release (Fig. 2.1A).[13,14]

The inherent challenge in these approaches is a restricted transport of morphogens into the spheroids through their outer shell composed of tightly associated cells and dense deposits of extracellular matrix (ECM).[15,16] Imbedding of GF laden microparticles with stem cells during EB aggregation overcomes this challenge; however,

it provides limited control over the localization of the GF source within the spheroid (Fig. 2.1A).[17,18] Here, we present an alternative chemical method for generating gradients of GFs in EBs, which takes advantage of the restricted macromolecular transport across the spheroid boundary (Fig. 2.1B). Our approach utilizes lipid-modified glycopolymers (**GP**s) with tunable size and affinity for GFs, which insert directly into the plasma membranes of ESCs and promote GF adhesion. Pre-assembly of the amphiphilic glycomimetics into nanoscale glycopolymer vesicles (**GPV**s) with defined dimensions enables tuning of their diffusion into the EBs, upon which they undergo fusion with the plasma membranes of ESCs to produce gradients of cells with enhanced GF-affinity (Fig. 1B).

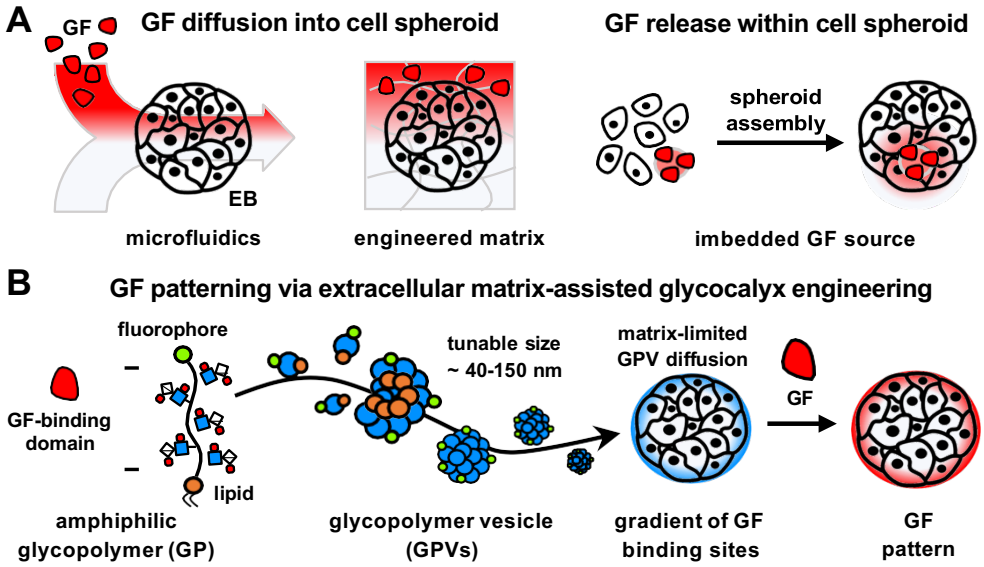

Figure 2.1. Growth factor (GF) gradient engineering in stem cell spheroids. (A) Prior methods utilize exposure of spheroids to GF gradients in microfluidic devices and engineered hydrogels or through imbedding of GF-laden microparticles in the spheroid core. (B) The present approach uses cell surface engineering with glycomimetics to tailor stem cell interactions with GFs. Amphiphilic GF-binding glycopolymers (**GP**s) assemble into glycopolymeric vesicles (**GPV**s) with tunable size and extracellular matrix penetrance. Upon entry into the spheroid, the **GPV**s fuse with cell membranes, forming gradients of stem cells with enhanced GF affinity.

2.2 Results

The glycomimetics are inspired by heparan sulfate (HS) glycosaminoglycans (GAGs), which are sulfated polysaccharide coreceptors for GFs on surfaces of cells and regulators of their activity,[19] including during stem cell differentiation.[20] Synthetic GAG mimetics have emerged as readily accessible biomaterials with capacity to bind and regulate the activity of a range of HS-binding proteins. Comprising linear polymeric scaffolds decorated with variously sulfated synthetic disaccharides representing the elementary structural motif of HS, soluble HS-mimetic glycopolymers have been shown to attenuate B cell chemotaxis induced by the chemokine RANTES[21] or inhibit breast cell metastasis in mouse models by blocking the activity of matrix heparinases.[22]

We have developed HS-mimetic polymers with affinity for various GFs comprising enzymatically derived HS disaccharides.[23,24] Endowing the polymers with phospholipid tails allowed for their targeting to the plasma membranes of ECSs. There, the materials served as functional surrogates for native GAGs, activated signaling by FGF2 and BMP4, and promoted neural and mesodermal differentiation, respectively. We envisioned that the phospholipids, which allows for insertion of the HS mimetics into the plasma membranes of cells, also give the **GP**s amphiphilic character and should promote their assembly into GPVs (Fig. 2.1B). Polymer length as well as the size and charge of their glycans should allow for tuning of **GPV** size and penetrance into the EBs (Fig. 2.1B). To test this hypothesis, we generated a panel of **GP**s ranging in size from short (**S**, degree of polymerization, DP $\sim$ 40) to medium (**M**, DP$\sim$ 125) and long (**L**, DP$\sim$ 300) and glycosylated either with the 2,6-O-disulfated HS-derived disaccharide, ΔUA2S-GlcNAc6S (D2A6), or the monosaccharides N-acetylglucosamine (GlcNAc) and its 6-O-sulfated derivative, GlcNAc-6S (Fig. 2.2A). The **GP**s were derived from a Boc-protected poly-(3-

N-methylaminooxypropyl)-acrylamide precursors (**P1**) generated by RAFT[25] polymerization of monomer 1 in the presence of a dipalmitoyl phospholipid-containing chain transfer agent CTA and the radical initiator, AIBN (Fig. 2.2A).[23] The RAFT process furnished precursors **P1** with good control over molecular weight and dispersity (Đ), as determined by size exclusion chromatography (SEC, Fig. 2.2B and Table 2.2). The polymeric precursors **P1** were elaborated in four steps to produce glycopolymers **GP** labeled with AlexaFluor488 (AF488) for visualization (Fig. 2.2A). First, the trithiocarbonate chain end groups in polymers **P1** were cleaved with n-butylamine to release a reactive thiol, which was capped immediately with AF488-maleimide. The protective Boc groups were then removed by treatment with trimethylsilyl chloride in phenol to yield polymers **P2** with exposed N-methylaminooxy side chains for subsequent ligation of reducing glycans.[26] The extent of polymer labeling (AF488) was determined by UV-VIS at this stage to be ∼0.7–0.8 fluorophores per polymer chain (Table 2.3). Finally, heating of intermediates **P2** with the mono- and disaccharides at 50 °C under acidic conditions (acetate buffer, pH = 4.5), followed by size filtration yielded the desired **GP**s (Fig. 2C). The fraction of glycosylated side chains was determined for each glycopolymer by 1H NMR spectroscopy and ranged from ∼40–50% for the charged glycans, D2A6 and GlcNAc-6S, to ∼50–60% for the neutral monosaccharide, GlcNAc (Fig. 2.2C and Table 2.4).

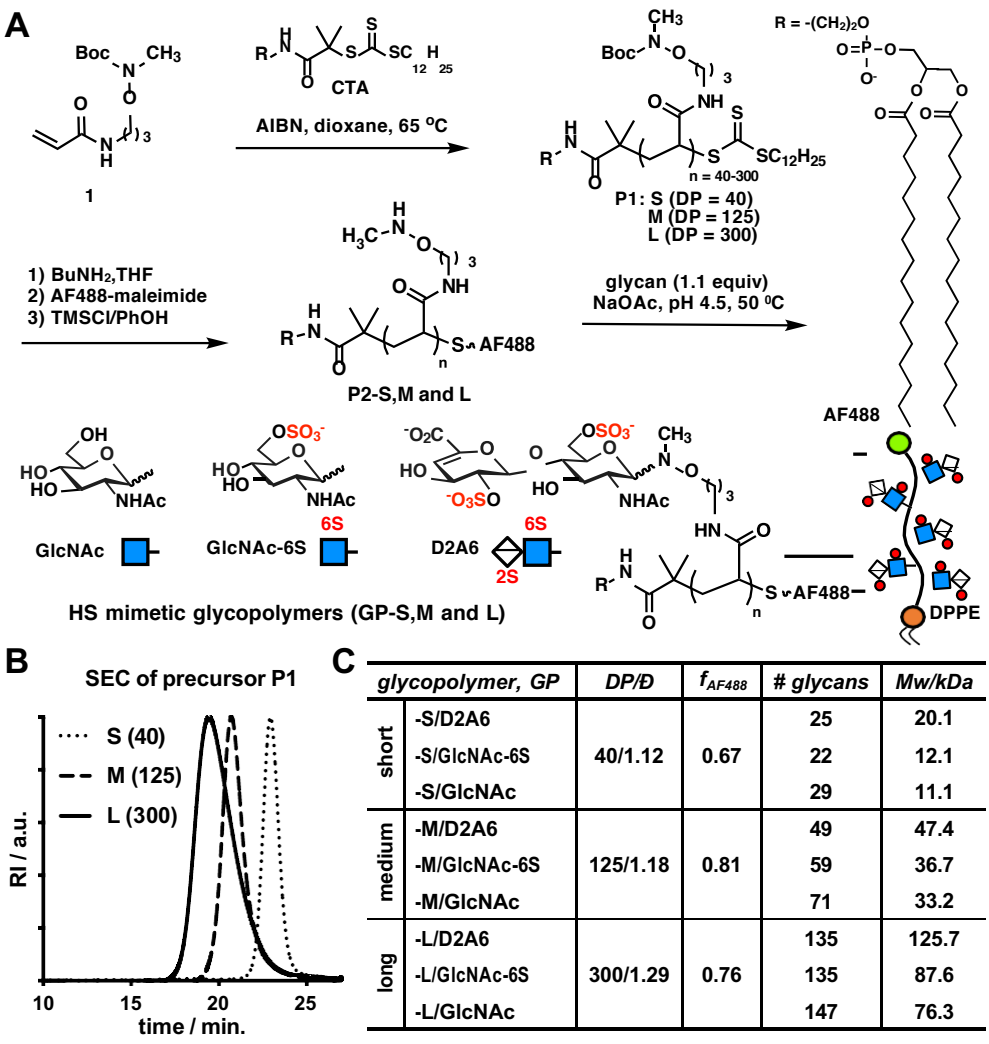

	glycopolymer, GP	DP/Đ	f_{AF488}	# glycans	Mw/kDa
short	-S/D2A6	40/1.12	0.67	25	20.1
	-S/GlcNAc-6S			22	12.1
	-S/GlcNAc			29	11.1
medium	-M/D2A6	125/1.18	0.81	49	47.4
	-M/GlcNAc-6S			59	36.7
	-M/GlcNAc			71	33.2
long	-L/D2A6	300/1.29	0.76	135	125.7
	-L/GlcNAc-6S			135	87.6
	-L/GlcNAc			147	76.3

Figure 2.2. Synthesis and characterization of HS-mimetic glycopolymers, GP. (A) Short (S), medium (M), and long (L) GPs were assembled from a RAFT-derived polymeric precursor P1. (B) Size exclusion chromatography (SEC) traces of P1-S, M and L (DP = 40, 125 and 300, respectively). (C) Structural characteristics of GPs. DP = degree of polymerization, Đ = dispersity, fAF488 = fraction of AlexaFluor 488 (AF488)-labeled chains.

We evaluated the affinity of the negatively charged HS-mimetic glycopolymers for FGF2, which induces ECSs toward neural commitment.[20] Using ELISA with surface-immobilized FGF2 (Fig. 2.6), we measured strong binding for polymers **GP-D2A6** carrying the 2,6-O-disulfated HS disaccharides (Kd,app =2–7 nM). The observed affinity was comparable to that of heparin (Kd,app = 6 nM), which is a highly sulfated form HS. The monosaccharide-modified polymers **GP-GlcNAc-6S** showed no measurable FGF2

binding activity (Fig. 2.6). Dynamic light scattering (DLS) analysis of the **GP** solutions in PBS buffer (pH = 7.4) confirmed their assembly into **GPV**s with sizes of ~40–150 nm (Fig. 2.3 and 2.7). Using the fluorescent lipophilic dye, DiI, we determined the critical vesicle-forming concentration (cvc) of the **GP**s in the range of 0.1–0.3 μM regardless of polymer length (Fig. 2.X). The molecular weight (Mw) of the polymers scaled linearly with their length (DP). The steepest rise in Mw was observed for the disaccharide containing polymers, **GP-D2A6**, followed by the monosaccharide polymers **GP-GlcNAc-6S** and **GP-GlcNAc** (Fig. 3A). Accordingly, the short (S), medium (M), and long (L) glycopolymers **GP-D2A6** afforded the largest **GPV**s (Fig. 2.3B and 2.7, Table 2.5) with diameters (d**GPV**) of 44 ± 1, 106 ± 9, and 139 ± 12 nm, respectively (Fig. 3B and C). The monosaccharide analogs **GP-GlcNAc-6S** and **GP-GlcNAc** gave **GPV**s of approximately equal sizes for each polymer length: 42 ± 8 and 36 ± 1nm(S), 64 ± 5 and 65 ± 4 nm (M), and 74 ± 13 and 84 ± 24 nm (L). Polymers without the lipids remained dissolved and did not form **GPV**s. Our DLS data indicate that the **GPV** size is determined primarily by the DP and Mw of the glycopolymers but not their charge, which was reflected in the zeta potential of the vesicles (Fig. 2.3D and Table 2.5).

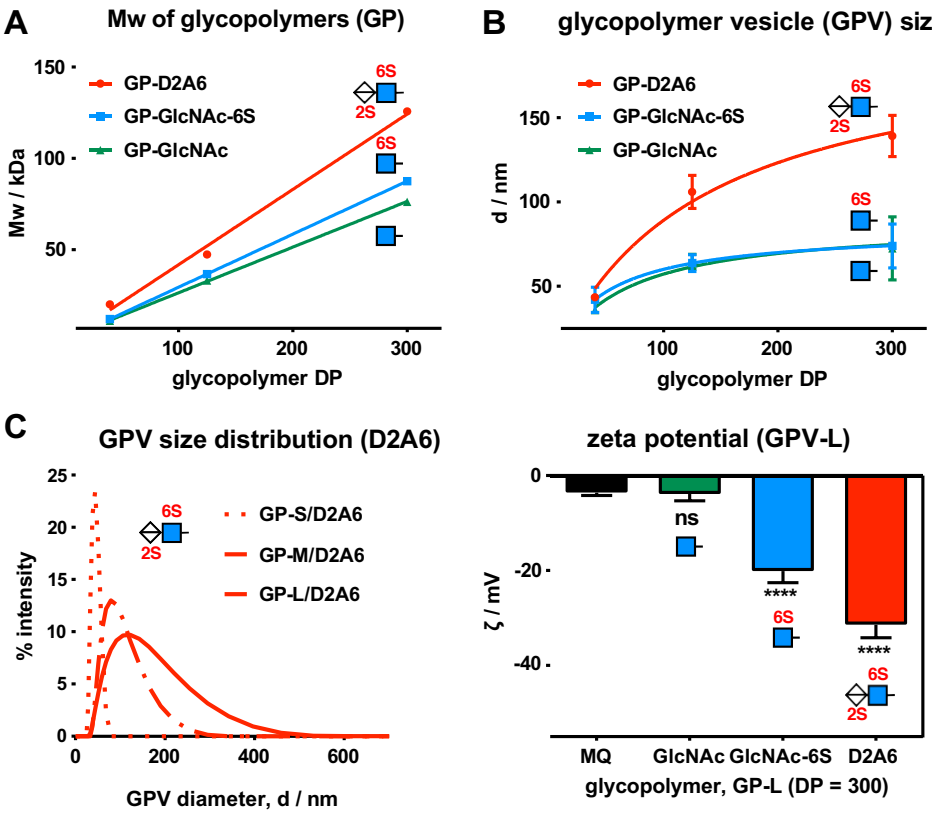

Figure 2.3. Assembly of amphiphilic HS-mimetic glycopolymers (**GP**s) into glycopolymeric vesicles (**GPV**s) with tunable diameter. (A) Mw of glycopolymers **GP** increased proportionally with polymer DP and glycosylation. (B) Short (S), medium (M), and long (L) GPs (3 μM) assembled in water into **GPV**s. Polymer Mw, but not charge, determined **GPV** diameter. (C) Size distributions for GPVs formed by polymers **GP-D2A6**. (D) Zeta potential of **GPV**s (shown for glycopolymers **GP-L**), MQ = MilliQ water, ****p < 0.001.

The single short hydrophobic dipalmitoyl lipid tail attached to the much more extended hydrophilic glycosylated segment of the **GP**s is likely to drive the formation of vesicles rather than micelles,[27] with the latter expected to produce much smaller particle sizes than those observed by DLS. The **GPV**s, which form during the glycopolymer assembly, remain stable in solution over a range of concentrations (0.3–10.0 μM) according to DLS measurements (Fig. 2.9). The **GPV**s can be disrupted by the addition a detergent, such as TritonX-100 (Fig. 2.7). Irreversible aggregation of the **GPV**s was observed after freezing, drying, or prolonged storage in solution.

We envisioned that differential size-dependent diffusion of the **GPV**s through the ECM network of EBs, followed by their fusion with ESC membranes, would establish gradients of HS mimetic-remodeled stem cells with increasing FGF2 affinity (Fig. 1B). To eliminate background FGF2 binding from endogenous HS glycans on ESCs, we used mutant cells missing the gene, exostosin-1 (*ext1*), which encodes for a glycosyltransferase involved in HS chain polymerization.[19] Unable to produce functional HS, the Ext1$^{-/-}$ ESCs lack the ability to bind many HS-dependent GFs, including FGF2.[28]

Since HS also contributes to cell adhesion and deposition of matrix proteins (e.g., fibronectin),[29] we first analyzed the effects of the *ext1* gene deletion on EB formation and ECM organization. Wild type (*wt*) E14 and Ext1$^{-/-}$ ESCs were aggregated into EBs under embryonic conditions in the presence of LIF using the hanging drop method (Fig. 2.4A).[30] After 2 days, both cell lines formed EB spheroids with normal morphology and sizes of ~100–200 μm (Fig. 2.4B and 2.10). Scanning electron microscopy (SEM) imaging confirmed the formation of ECM deposits on the surface of EBs from both cell lines (Fig. 2.4C and 2.11). Immunohistological analysis of the EBs confirmed the lack of HS expression by Ext1$^{-/-}$ ESCs, which resulted in visible accumulation of fibronectin toward the EB periphery, while collagen distribution was affected to a much lesser degree (Fig. 2.4D and Fig. 2.12). The ability of Ext1$^{-/-}$ ESCs to form EBs and deposit ECM, we reasoned, should influence **GPV** penetrance into the spheroids.

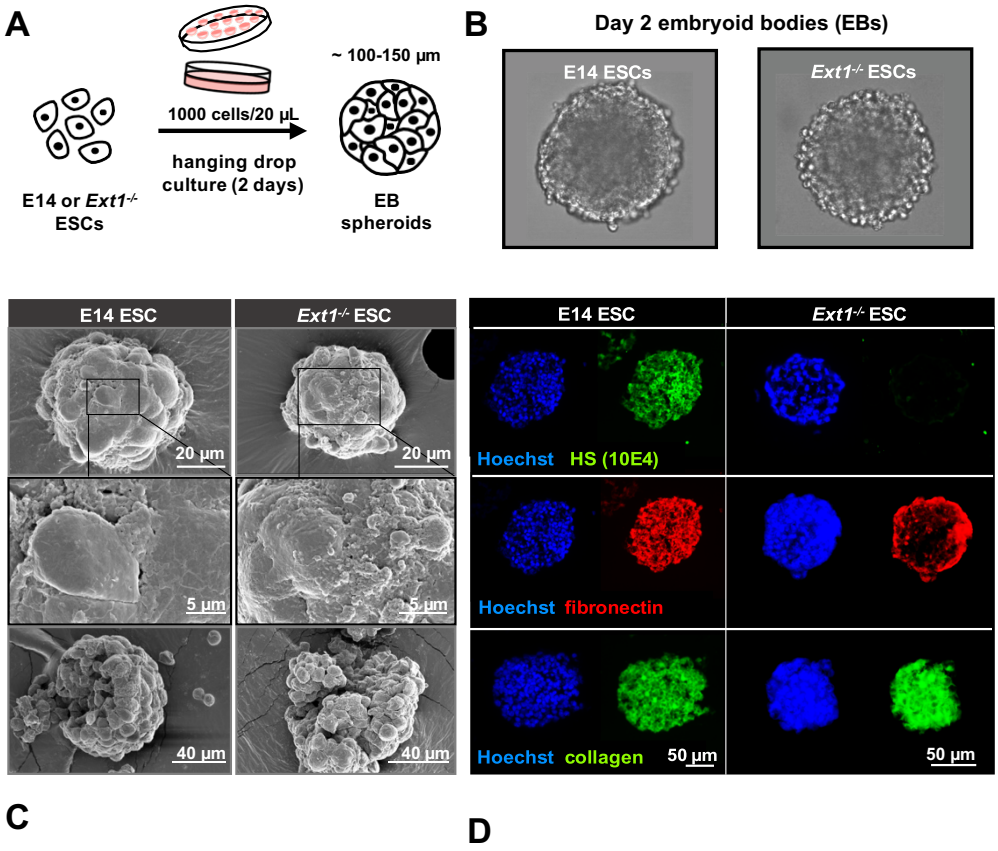

Figure 2.4. Formation and characterization of embryoid bodies (EBs). (A) E14 and Ext1$^{-/-}$ ESCs were aggregated in hanging drops in the presence of LIF for 2 days. (B) Optical microscopy confirmed normal EB formation. (C) SEM images show similar level of ECM deposition on the surfaces of EBs from both cell lines. (D) Immunostaining with anti-HS antibody, 10E4, confirmed lack of HS expression by Ext1$^{-/-}$ ESCs. Loss of HS led to accumulation of fibronectin toward the outer regions of the EBs but had no effect on collagen deposition (blue = Hoechst 33342 nuclear stain).

Next, we set to test whether the **GPV**s can remodel the glycocalyx of ESCs in a gradient pattern after diffusion into the EBs (Fig. 2.5). In addition to their size, EB penetrance of the **GPV**s is likely to be determined by their concentration in the media and the duration of treatment. We examined these parameters by first incubating day 0 Ext1$^{-/-}$ ESC EBs with 0.1, 1.0 and 3.0 µM fluorescently labeled **GP-M/GlcNAc-6S** in serum-free media. After 2 h at 37 °C, the EBs were washed to remove excess **GPV**s, fixed, and imaged by confocal microscopy to assess glycopolymer distribution.

Focusing on our aim to exploit the size-limited diffusion of **GPV**s in the EB environment to engineer GF affinity gradients, we performed remodeling experiments with

the FGF2-binding HS mimetics, **GP-D2A6**. We have previously shown that installation of glycopolymers carrying the D2A6 disaccharide at the surface of Ext1$^{-/-}$ ESCs restored FGF2 binding and signaling activity,[23] thus providing functional surrogates for cell-surface HS. While the *wt* E14 ESCs express endogenous HS structures that produce uniform FGF2 binding across the EB, the Ext1$^{-/-}$ ESCs HS mutants lack affinity for FGF2 and provide a clean slate for the pattering of the GF (Fig. 2.5C).

Treatment of day 0 Ext1$^{-/-}$ ESC EBs with **GP-D2A6** polymers of all three lengths under the optimized conditions (3.0 μM, 1 h, 37 °C) resulted in patterns of remodeled cells analogous to those observed for the model monosaccharide polymers GP-GlcNAc-6S (Fig. 5D and A, green). The shortest polymers **GP-S/D2A6** (d**GPV** = 44 nm) gave full coverage of the EB interior similar to its monosaccharide derivative GP-S/GlcNAc-6S which forms **GPV**s of comparable size (d**GPV** = 42 nm). By contrast, the medium-sized polymer **GP-M/D2A6** (d**GPV** = 106 nm) exhibited lower EB penetrance and generated a steeper fluorescence gradient compared to **GP-M/GlcNAc-6S** (with d**GPV** = 64 nm). The same trend continued for the pair of longest polymers, **GP-L/D2A6** (d**GPV** = 139 nm) and **GP-L/GlcNAc-6S** (d**GPV** = 74 nm), which showed the lowest penetrance and remained localized primarily on the EB periphery. Our observations are consistent with **GP** diffusion into the EB spheroids being determined primarily by the size of their **GPV**s independent of the structure and charge state of their glycans, which provides an element of predictability and tunability.

The patterns of cell-surface anchored HS-mimetics, **GP-D2A6**, in turn, defined the distribution of FGF2 adhesion sites in the Ext1$^{-/-}$ ESC EBs, which were visualized by incubation with recombinant FGF2 followed by immunostaining (Fig. 5D, red, and Fig.

2.20 and 2.21). No FGF2 signal was observed in EBs treated with polymers **GP-GlcNAc6S** (Fig. 2.22), confirming that the GF binding is glycan dependent and the display of the HS mimetics GP-D2A6 on the surface of mESCs is required to constrain FGF2 localization.

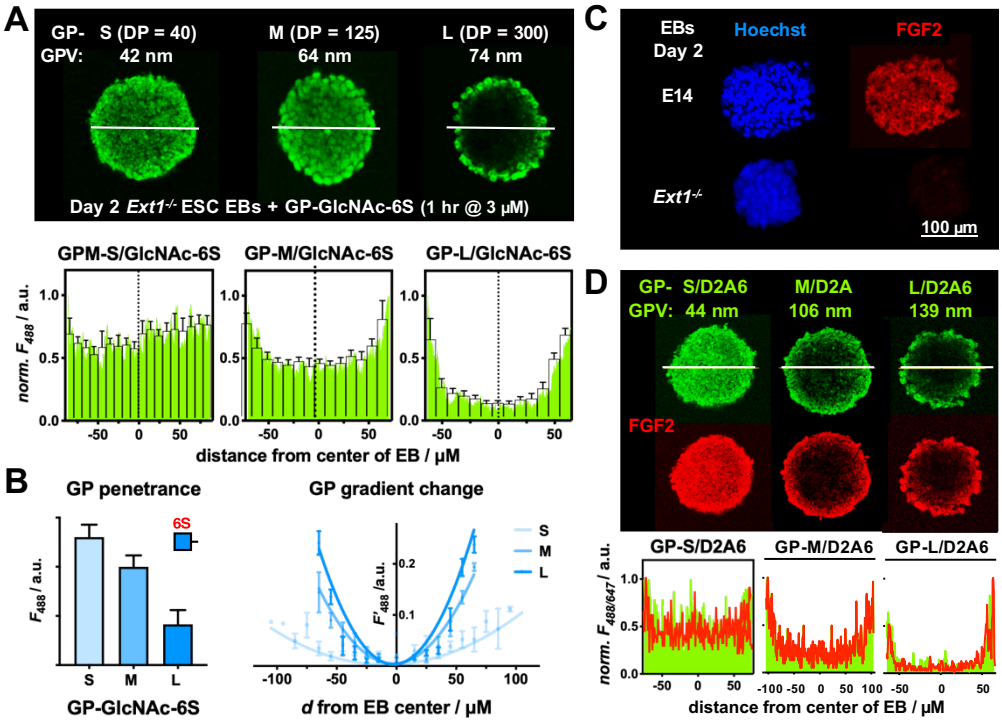

Figure 2.5. Engineering FGF2 affinity gradients in EB spheroids. (A) Top: Fluorescence confocal micrographs of EB cross-sections at midpoint after treatment with short (S), medium (M), and long (L) AF488-labeled glycopolymers GP-GlcNAc-6S. Bottom: Normalized fluorescence intensity (green) and bin histogram analysis (bars, 1 bin = 10 μm) of AF488 signal (F_{488}) along a line passing through EB center. (B) Total fluorescence intensity (F488) and rate of intensity change with distance from EB center (F'_{488}). (C) FGF2 (red) binds to *wt* E14 but not Ext1$^{-/-}$ ESCs in EBs. (D) Fluorescence micrographs and normalized line fluorescence for FGF2 (red) binding to EBs remodeled with glycopolymers GP-D2A6 (green).

2.3 Conclusions

We have developed a novel, facile method for generating GF gradients in multicellular spheroids using cell membrane engineering with synthetic GF co-receptors. By exploiting the assembly of amphiphilic glycopolymers into nanoscale vesicles with tunable diameters, we were able to control their diffusion into EB spheroids. Upon entry,

the GPVs fused with the membranes of nearby stem cells and introduced new adhesion sites for FGF2 at their surface. By using Ext1$^{-/-}$ ESCs lacking endogenous HS, we were able to limit FGF2 adhesion only to cells remodeled with appropriately glycosylated HS mimetics. The formation of vesicles and their fusion into the membranes of cells within EBs provides a unique delivery method for glycan-based receptors to the surface of cells in complex systems. In departure from existing methods for gradient patterning in 3D spheroids, which rely on the controlled diffusion and release of recombinant GFs, the current approach achieves GF patterning by tailoring their interactions at the cell surface and, thus, provides control over the activity of endogenous GFs. The cell surface engineering method can be extended to other types of cells and HS-dependent signaling molecules, and we expect its utility to increase further with the continuing improvements in HS mimetic design[21,22] and with the emergence of new tools for the genetic[31] and chemical[32] manipulation of HS expression in living cells. Further, we expect that the discovery of assembly of amphiphilic glycomaterials into tunable and stable vesicles capable of direct fusion with cell membranes will open new modalities for glycocalyx engineering in increasingly complex biological systems.

2.4 Materials and Methods

2.4.1 Reagents and Instrumentation

All chemical reagents and solvents used for the synthesis of monomer **1**,[34] lipid chain transfer agent (**CTA**),[35] and polymeric precursors **P1** and **P2** were purchased from Aldrich Chemicals and used as received unless otherwise specified. RAFT polymerization was carried out under standard Schlenk technique conditions using inert atmosphere of N_2 by adopting previously published procedure.[23] Glycans and reactive fluorophores for

the assembly of glycopolymers GP as well as all biological reagents and their sources (including catalog numbers) are listed in Table 2.1. Glycan conjugation reactions to assemble glycopolymers GP were maintained at 50°C using a Biorad MyCycler thermocycler (Hercules, CA).

Table 2.1 Biological Reagents

Material	Supplier	Catalog No.
Human recombinant FGF2	Cell Signaling Technologies	8910
Anti-mouse IgG Alexa Fluor 350 conjugate	Life Technologies	A11045
BCA Protein Assay	Thermos Sci Pierce Biotech	P123225
DPBS (w/o Ca and Mg)	Mediatech Inc (Conrning)	21-031-CM
Quick Spin Columns Sephadex G-50, fine	Roche Diagnostics	11273973001
BSA, Fraction V	Spectrum	A3611
Fetal Bovine Serum	Sigma Aldrich	12303C
GlcNAc-6S sodium salt	Sigma Aldrich	108321-79-5
ΔUA2S-GlcNAc6S Na3	Dextra	H1005
Anti-mouse IgG AF647	Cell Signaling Technologies	4410S
SecureSeal spacers (100 μM silicon)	Grace Biolabs	654008
Prolong gold anti-fade	Invitrogen	P36930
KO DMEM	Gibco-ThermoFisher Scientific	10829018
IMDM	GE Healthcare Life Sciences	SH3022802
Alexa Fluor 488 c5-maleimide	Life Technologies	A10254
Anti-Fibronectin (rabbit polyclonal)	Abcam	ab2413
Anti-heparan sulfate (10E4, mouse IgM)	Amsbio	370255
Anti-Collagen I (Rabbit polyclonal)	Abcam	Ab34710
Anti-mouse IgG AF488	ThermoFisher	A28175
PD10 prepacked columns	GE Healthcare	W13286057
1.7ml Eppendorf tubes	Genemate	490003-228
Murine *wt* E14TG2a and *Ext1*$^{-/-}$ ESCs	Gift by Prof. Cathy Merry, University of Nottingham	
TMB solution	Invitrogen	00-4201-56
Heparin	Sigma Aldrich	B9806
anti-FGF basic (rabbit polyclonal)	Sigma Aldrich	F3393

2.4.1.1 Proton nuclear magnetic resonance.

^{1}H NMR spectra of glycopolymers and their precursors were obtained on a 300 MHz (Bruker) or 500 MHz (Joel) NMR spectrometer, using deuterated solvents ($CDCl_3$) for the polymer precursors, **P**, and PBS in D_2O adjusted to pH=7.4 with DCl for glycopolymers, **GP**). The spectra were analyzed using MestReNova or TopSpin software and are reported in parts per million (ppm) on the δ scale relative to the residual solvent as an internal standard (for ^{1}H NMR: $CDCl_3$ = 7.26 ppm, PBS in D_2O = 4.79 ppm). Data are reported as follows: chemical shift, multiplicity (s = singlet, d = dou- blet, dd = doublet of doublets, t = triplet, q = quartet, br = broad, m = multiplet), and integration.

2.4.1.2 Size exclusion chromatography (SEC).

Polymer size (Mw and DP) and dispersity (Đ) analysis for polymers **P1**, **P1.5** and **P2** was performed on a Hitachi Chromaster system equipped with an RI detector and a 5 µm, mixed bed, 7.8 mm I.D. x 30 cm TSK gel column (Tosoh Bioscience). The polymers were analyzed in DMF (0.2% w/v LiBR, 70°C) using an isocratic method with a flow rate of 0.7 mL/min. PEO standards were used to construct calibration curve.

2.4.1.3 Dynamic light scattering (DLS), Zeta potential and plate reader analysis of CVC.

Sizing and surface charge analysis of **GPVs** were performed using a Malvern ZetaSizer Nano-ZS90 instrument with a 633 nm laser at a 90° scattering angle. Particle sizes were measured for polymers **GP** diluted to 3 µM in PBS (pH = 7.4) using a low volume ZEN0118 cuvette equilibrated to 37°C. Samples were run in triplicate, and the size of resultant micelles were calculated from the intensity readout. To measure zeta potentials, samples were diluted to 3 µM in MilliQ water and measured at 37 °C using a DTS1070 zeta cell. Critical vesicle concentration (CVC) analysis was done in 96-well

plates using the SpectraMax I3x plate reader (Molecular Devices). Fluorescence at 580 nm was recorded for all polymer concentrations in duplicate. The two-fold dilution series of **GPs** were diluted in PBS (pH = 7.4) at

2.4.1.4 Scanning electron microscopy (SEM).

SEM imaging of EBs was performed using FEI Apreo Scanning electron microscope. Fixed EB samples were prepared for SEM imaging by drying using a critical point dryer (Tousimis AutoSamdri 815A), followed by sputter coating with Iridium metal using an Emitech K575X Iridium Sputter Coater.

2.4.1.5 Histological analysis.

Histological analysis was performed using fluorescence microscopy (Keyence BZX-700 Fluorescent Microscope) of paraffin-embedded EB slices (5 μm) produced on microtome. Collected images were processed and analyzed using ImageJ software.

2.4.2 Statistical analysis.

Statistics were performed using PRISM software. All biological experiments were performed in at least 2 experimental replicates and microscopy images were acquired and analyzed for at least 5 EBs per experimental condition. Presented are at least 5 representative images for each condition. All data were plotted as mean values ± standard deviation. Statistical analysis was performed using ANOVA.

2.4.3 Synthesis of glycopolymer mimetics

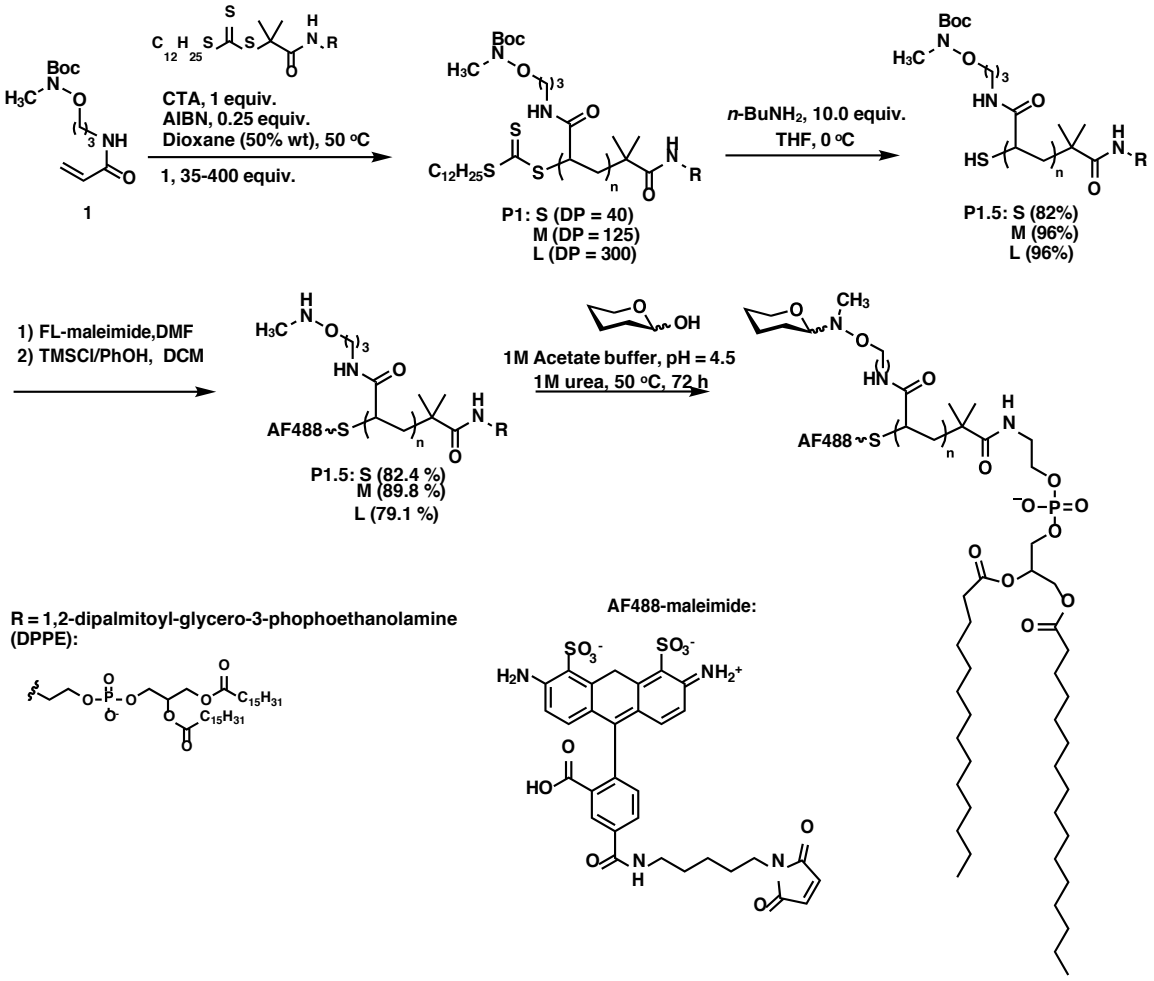

Scheme 2.1. Synthesis and structural characterization of HS-mimetic **GP**s

2.4.3.1 Synthesis of glycopolymer precursor P1

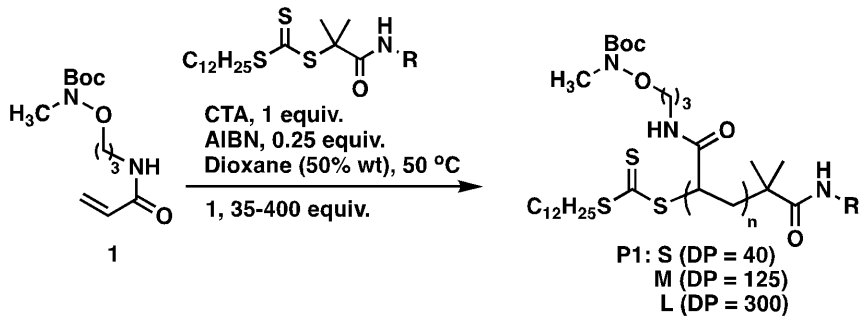

Scheme 2.2. Synthesis of polymer precursor 1, **P1**.

Anhydrous dioxane was purified by passage through alumina. A flame-dried Schlenk flask (10 mL) equipped with a magnetic stir bar was charged with DPPE-lipid trithiocarbonate chain transfer agent, **CTA**[23] and monomer **1**[23]. A stock solution of AIBN in dioxane (c = 30 μM) was added followed by additional dioxane to a final concentration of **1** at 50 wt%. The was flask was closed with a rubber septum, connected to a Schlenk line, and the content was degassed thoroughly by 3 freeze-pump-thaw cycles in liquid N_2. After the last cycle, the flask was backfilled with N_2 and submerged into an oil bath (65°C). The reaction was allowed to stir at that temperature for 5-10 hrs. After this time, the reaction was stopped by adding ether (200 μL) and the solution was precipitated into hexanes (20 mL) with stirring. The yellow precipitate was collected, re-disclosed in ether and precipitated into hexanes again. This was repeated one more time. The yellow polymer was dissolved in chloroform and dried under vacuum 3 times to remove residual hexanes. After drying under vacuum overnight, the final polymer products **P1** were obtained as pale-yellow solids. The products were analyzed by SEC (0.2% LiBr/DMF) and ^{1}H NMR ($CDCl_3$, Fig 2.23).

Table 2.2. Reagent stoichiometry, conditions, yields, and characterization for precursors **P1.**

P1-	monomer 1 mg (equiv.)	CTA mg (1 equiv.)	AIBN mg (0.25 equiv.)	time hr	conv, 1 %	yield, P1 mg (%)	Mw kDa	DP, P1	
								cal.	SEC
S	149 (35)	17	0.67	5	96.0%	136 (81.9)	11.3	34	36
M	380 (150)	10	0.40	8.5	96.0%	362 (92.8)	32.2	144	124
L	508 (400)	5	0.20	10	98.0%	481 (94.3)	64.9	392	303

2.4.3.2 Aminolysis of chain end trithiocarbonate group (P1.5).

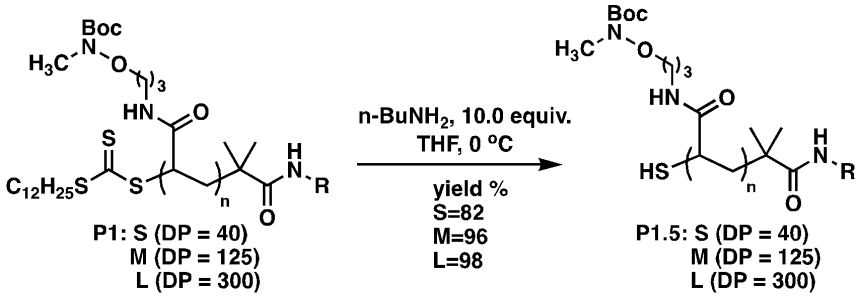

Scheme 2.3. Aminolysis of chain end trithiocarbonate group.

A flame-dried Schlenk flask (10 mL) equipped with a magnetic stir bar was charged with (20.0 mg, 1.76 μmol **P1-S**, 0.62 μmol **P1-M**, 0.30 μmol **P1-L**, 1 equiv.). Stock solution of *n*-butylamine (300 μl, 20 mM) in tetrahydrofuran was added to flask. The was flask was sealed with a rubber septum, connected to a Schlenk line, and the content was degassed thoroughly by 3 freeze-pump-thaw cycles in liquid N_2. After the last cycle, the flask was back- filled with N_2 and the reaction was allowed to proceed for 2 h at 0°C. After this time, the reaction was stopped by adding ether (200 μL) and the solution was precipitated into hexanes (20 mL) with stirring. The pale-yellow precipitate was collected, re-dissolved in

ether and precipitated into hexanes again. This was repeated one additional time. The pale-yellow polymer was dissolved in chloroform and dried under vacuum 3 times to remove residual hexanes. After drying under vacuum overnight, the final polymer products **P1.5** were obtained as pale-yellow solids and characterized by SEC (0.2% LiBr/DMF) and ^{1}H NMR ($CDCl_3$, Fig. 2.X). The polymers remain in their reduced state when stored in solid form. In solution, they undergo oxidative dimerization via disulfide bonds visible by SEC, which can be reversed by the addition of β-mercaptoethanol. The ability to dimerize increases with decreasing polymer size.

2.4.3.3 Labeling of chain end thiols with AF488 maleimide.

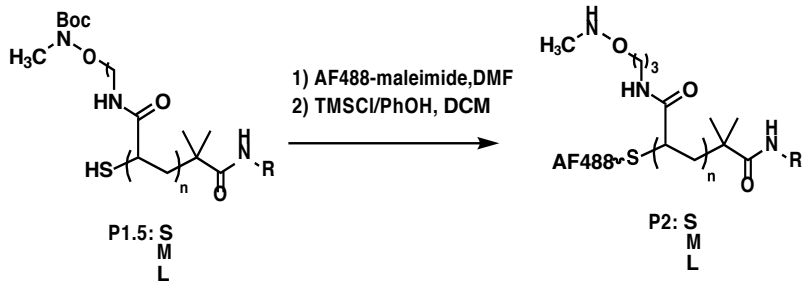

Scheme 2.4. Labeling of chain end thiols

A 4mL glass vial was charged with **P1-S**, (10.0mg, 0.880 μmol, 1 equiv.), **P1-M** (15.0 mg, 0.466 μmol, 1 equiv.) and **P1-L** (20.0 mg 0.308 μmol, 1 equiv.) with a magnetic stir bar, vacuumed and then pumped with N_2 through a rubber septum. Alexa Fluor 488 C5-maleimide (1.00 mg, 1.39 mmol, 1.5 equiv.) was dissolved in dry DMF (694 μL) to a concentration of 2 mM and added to the to the reaction vial. The polymer dissolved and the resulting solution was thoroughly degassed by three freeze pump-thaw-cycles. The reaction proceeded overnight under N_2 at ambient temperature covered in foil. After this time, the reaction was stopped by adding ether (200 μL) and the solution was precipitated

into hexanes (20 mL) with stirring. The bright red precipitate was collected, redissolved in ether and precipitated into hexanes again. This was repeated one additional time. The polymer was dissolved in chloroform and dried under vacuum 3 times to remove residual hexanes. The crude polymer containing excess fluorophore was used in the next step without further purification.

2.4.3.4 Side-chain Boc-group deprotection.

Table 2.3. Yields and AF488 labeling efficiency for products **P2**

P2	yield / %	AF488 labeling / %
-S	82	67
-M	90	81
-L	79	76

A solution of phenol (3M) and trimethylsilyl chloride (TMSCl, 1M) solution was made in dichloromethane (DCM). The resulting solution (500 µl) was added to 4ml vial containing crude product from previous reaction. Reaction was stirred and allowed to proceed for two hours at ambient temperature. After this time, the reaction was stopped by precipitation in ether (4 mL) with stirring. Ether was removed and polymer **P2** was dried under vacuum. The pink solid polymers were redissolved in Milli-Q filtered water while stirring and purified on a PD-10 pre-packed column according to manufacturer instructions to separate the fluorophore from the labeled polymers P2. These were then frozen and lyophilized overnight. Analysis by UV-Vis and ^{1}H NMR ($CDCl_3$, Fig 2.X) was performed to determine ligation efficiency and purity of the polymers.

2.4.3.5 Assembly of glycopolymers

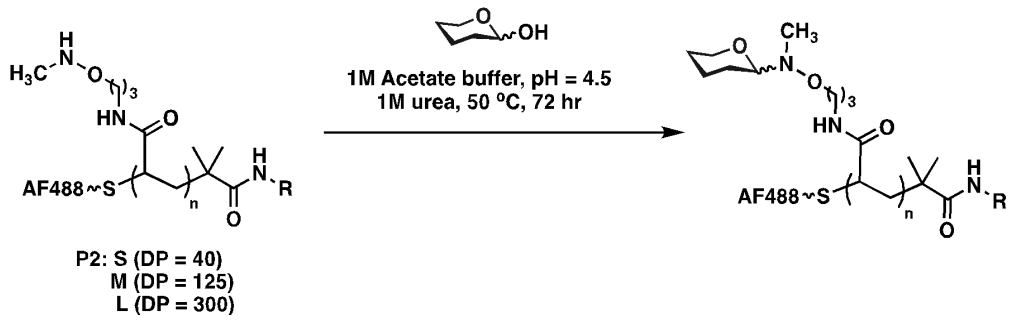

Scheme 2.5. Assembly of glycopolymers

Precursors **P2** were dissolved in sodium acetate buffer (1M, pH = 4.5) containing urea (1 M) to aminooxy side chain concentration of 200 mM. The solutions were added to the glycans in 20 µL PCR tubes, sealed and heated in a thermocycler at 50oC for 72 hours. The resulting glycopolymers **GP** were purified on Quick Spin columns to remove unreacted glycans and eluted with PBS buffer in D20 for NMR analysis. UV-Vis was used to determine **GP** concentrations based on their AF488 labels. ^{1}H NMR data (D_2O, Fig. 2.X) were collected for all polymers and used to assess polymer purity and to calculate glycan ligation efficiency as described previously.[23] The **GPs** were used immediately. If storage is required, the polymers should be kept as solutions in dark at ambient temperature or refrigerated. The samples should not be stored for more than 2 days, frozen or dried to prevent aggregate formation. DLS analysis is recommended prior to their use in biological assays to check for aggregates.

Table 2.4. Reaction conditions, yield and ligation efficiency for **GP**s

P2 stock μL	**GlcNAc** mg (1.1 equiv.)	**GlcNAc-6s** mg (1.1 equiv.)	**D2A6** mg (1.1 equiv.)	**yield, GP** %	**glycan ligation efficiency** %
P2-S					
45.6	2.22			74	61
45.8		2.86		82	53
44.2			1.90	77	40
P2-M					
40.2	2.23			70	50
40.8		2.90		81	47
41.3			1.91	83	33
P2-L					
7.50	2.15			76	46
14.3		2.94		75	54
13.5			1.78	77	42

2.4.4 FGF2 binding to sulfated HS-mimetics by ELISA

Primary antibodies against FGF2 were immobilized on the surface of 96-well tissue culture treated plates as a 10 μg/mL solution in 1% BSA/DPBS overnight at 4°C. After washing 3X with DPBS, a 10 nM solution of FGF2 in 1% BSA/DPBS was added for 2 hr at ambient temperature. Wells were washed with 0.05% Tween-20 in DPBS and blocked with 1% BSA/DPBS for 1 hr at ambient temperature. Biotinylated glycopolymers **GP** or heparin were then added to the wells at increasing concentrations (0-100 nM) for 1 hr at ambient temperature before the wells were washed three times with 0.05% Tween-20 in DPBS. Streptavidin-HRP (diluted 1:1000 in 1% BSA/DPBS) was added for 30 min at ambient temperature. The wells were then washed 3X 0.05% Tween-20 in DPBS. Next,

100 µL of 1X TMB substrate was added to the wells for 2-5 min before 100 µL of 2N sulfuric acid was added to quench the colorimetric reaction. The absorbance was read at 450 nm. Each condition was performed in triplicate wells. Data were analyzed and fitted using Prism.

2.4.5 Dynamic Light Scattering (DLS) and Zeta potential analysis.

Particle sizes and Zeta potentials were obtained using with a 633 nm laser at a 90° scattering angle. Particle sizes were measured for glycopolymers GP (3 µM) in PBS (pH = 7.4) in a low volume ZEN0118 cuvette equilibrated at 37 °C. Each sample was run in triplicate and the GPV diameters were calculated from intensity weighted signal distributions. To measure zeta potentials, glycopolymers GP were diluted to 3 µM in MilliQ water and measured at 37 °C using a DTS1070 zeta cell. Disruption of GPVs was accomplished by adding TritonX-100 (MP biomedicals 807423) **GP2-M/GlcNAc6S** (3 µM) in PBS to a final detergent concentration as indicated. The resulting solution was mixed gently via pipette, equilibrated at 37 °C, and intensity weighted size distributions were collected in triplicate. All graphs were processed in Prism. Plotted are mean values and standard deviations. We observed no measurable DLS for solutions of **GP-GlcNAc6S** polymers lacking lipid modifications (not shown).

2.4.6 Determination of critical concentration of vesicle formation.

DiI lipophilic dye (0.5 mg/mL) was incubated with a two-fold dilution series of **GP-S, GP-M** and **GP-L** (10 µM to 0.01 µM) overnight at room temperature. Each condition was done in duplicate. After incubation, fluorescence was measured at the maximum emission wavelength of DiI (580 nm). Two separate trend lines were observed for each length GP using Semi-log nonlinear regression analysis. Critical vesicle concentration

(cvc) was determined to be at the intersection of the two trend lines. All data was analyzed using the PRISM software.[36]

2.4.7 Embryonic stem cell (ESC) culture.

2.4.7.1 General culture conditions

Ext1$^{-/-}$ and E14 mouse embryonic stem cell lines were passaged at 37°C with 5% CO_2. They were expanded in 0.1% gelatin-coated T flasks with media consisting of Knockout-DMEM supplemented with 1% 200 mM L-glutamine, 1% non-essential amino acids, 0.1% 2-mercaptoethanol, 10% of fetal bovine serum and 0.01% LIF. Cell culture and EB formation were performed using standard sterile cell culture techniques without the addition of antibiotics. Flow cytometry analysis was performed on BD Accuri C6 flow cytometer and analyzed with FlowJo software.

2.4.7.2 EB formation via hanging drop.

Cells were diluted in media and deposited in 20 µl drops (~1000 cells per droplet) onto the lid of a 150 x15 mm Petri dish at day -2.[37] The bottom plate of the Petri dish was filled with sterile de-ionized water to keep a moist environment during EBs aggregation. After two days, the EBs were washed into 1.7 mL Eppendorf tubes and used for glycopolymer incorporation experiments.

2.4.8 Analysis of EBs by SEM.

Day 0 EBs were fixed for 3 hours at 0°C in 2.5% glutaraldehyde in 0.1M sodium cacodylate trihydrate solution. After fixation, the EBs were washed 3 times with 0.1M sodium cacodylate solution and soaked in 1% OsO4 solution in 0.1M sodium cacodylate for 1 hour at room temperature. The EBs were then washed 3 times with the 0.1M sodium cacodylate and dehydrated in aqueous ethanol at increasing concentrations: 10, 30, 50,

70, 85, 95, 100% ethanol. The EBs were kept at each dilution for 5 min and dried using a critical point dryer. The EBs were collected onto carbon tape, placed on SEM metal stages, sputter coated gold and imaged at a voltage of 5.0 kV, current of 0.10 nA, and wavelength of 112 nm.

2.4.9 Histological characterization of E14 and Ext1$^{-/-}$ ESC EBs.

EBs formed after two days were fixed in 10% formalin at room temperature for 30 min. After fixation, EBs were embedded in 1% agarose and left to solidify. Agarose blocks were placed in cassettes with Optimal Cutting Temperature Compound (OCT) and frozen in dry ice in 2-butanol. Microtome slices (5 μm) were placed on glass slides, dried overnight and fixed in 10% formalin and permeabilized in methanol (10 min). Blocking with 1% BSA was followed by primary antibody (Table 2.5) for 1 hr at ambient temperature. After that time, slides were washed three times with BSA solution, then incubated for 1 hr with secondary antibody or hr-FGF2 (100 nM). The slides are washed with BSA solution three more times, then incubated with Hoescht solution (1000x) for 10 min at ambient temperature. Slides are washed again and prolong antifade and cover slips are added to mount the slides. All images were acquired on Keyence fluorescent microscope at 20x magnification.

Table 2.5. Immunohistological staining reagents and conditions.

Antibody	Species	Dilution
α-collagen I	Rabbit IgG	1:1000
α-fibronectin	Rabbit IgG	1:300
α-HS (10E4)	Mouse IgM	1:300
α-mouse IgM AF488 conjugate	Goat IgG	1:2000
α-rabbit IgG AF488 conjugate	Goat IgG	1:1000
α-rabbit IgG AF647 conjugate	Goat IgG	1:1000

2.4.10 Cell surface remodeling with HS-mimetic GPVs and FGF2 staining.

The HS- mimetics are diluted to experimental concentrations in serum free media and then added to EBs. After incubation for 1 or 2 h at 37 °C, the EBs are washed three times with DPBS and fixed with 4% PFA. Human FGF2 0.5mg/ml is added overnight to fixed EBs in buffer (1% BSA in DPBS, pH 7.4) at 4°C. After FGF2 binding, EBs were washed for 6 h with BSA solution three times.

2.4.11 Cytotoxicity of glycopolymers.

To assess whether the **GPs** were cytotoxic to cells, viability was tested in Ext1$^{-/-}$ ESC EBs using ethidium bromide homodimer (EtBr) and calcein AM as a live/dead stain. EBs were incubated with the polymers (3 μM) for 1 hr, then washed with dPBS and the medium was replaced. After 8 hr, EBs were dissociated in Accutase for 15 min and stained with a solution of EtBr (50 μM) and calcien AM (50 μM) and analyzed with flow cytometry. Percentage of viable cells were determined by gating for fluorescence.

2.4.12 EB Slide Mounting for fluorescence confocal imaging.

The EBs were then mounted with Prolong Gold Antifade solution onto microslides. The EBs were mounted between three 8x9 mm Secure-Seal Imaging Spacers (50 μm

thick) to prevent damage to the EBs. The slides were dried overnight and imaged with the Leica SP5 confocal microscope

2.4.13 Confocal imaging and analysis.

Images of EBs (100-200 μM) were imaged in a multiphoton mode (792 nm). The full z-stack was collected for each EB, with laser gain gradient compensation in- creasing from 0 to 60% through the EB to maintain laser penetration. The images were processed using ImageJ software. Line graphs were generated by measuring fluorescent intensity across the widest cross sections with a line passing through the center of the EB. The line fluorescence intensity values were normalized to AF488 maximum intensity for each EB.

2.4.13.1 Image histogram analysis.

To remove noise caused by heterogeneity of cell distribution within the EBs, line graphs were binned in 10 μm increments. Bin intensities were used to determine Area under the curve, and slope of fluorescent curves and were averaged from five EBs of roughly similar size.

2.4.14 Flow cytometry analysis of cell surface labeling with GPs.

After remodeling of EBs with **GP**s, EBs were dissociated by Accutase with light vortexing at ambient temperature. After 15 min, Accutase was neutralized by a 5 min incubation at 37 °C. The cells were pelleted, washed and resuspended in DPBS, and analyzed by flow cytometry (AF488).

2.4.14.1 Statistical analysis.

Analysis of flow cytometry data was done using Flowjo software. Cell populations were identified using untreated ESCs dissociated from EBs, and cell debris and

aggregates were excluded through gating. The unlabeled population was set as 0% **GP** (AF488)-labeled population. A minimum of 10,000 cells was used for each sample to ensure statistical significance of population shifts.

2.5 Acknowledgments

The authors thank Dr. Ryan Porell (UCSD) and Dr. Mia Huang (TSRI) for valuable discussions and their insights on experimental methods and data analysis. We also thank Dr. Cathy Merry (University of Not- tingham) for providing us with ESCs. We wish to acknowledge the UCSD Microscopy Core Facility (via NINDS P30 Grant: P30NS047101) for assistance with fluorescence confocal imaging. SEM work was performed at the San Diego Nanotechnology Infrastructure (SDNI) of UCSD, a member of the National Nanotechnology Coordinated Infra-structure (NNCI) supported by NSF grant ECCS-1542148. We thank UCSD Mouse Phenotyping Core at the GRTC (supported via NHLBI grant P01HL107150) for assistance with histological analysis.This work was supported by NIH Director's New Innovator Award 1DP2HD087954-01 via NICHD. M.R.N. and S.C.P. were supported by GAANN fellowships (U.S. Dept. Of Education, P200A150251). K.G. was supported in part by the Alfred P. Sloan Foundation (FG-2017- 9094) and the Research Corporation for Science Advancement via the Cottrell Scholar Award (24119).

Chapter 2, in full, is a reprint of the material as it appears: M. R. Naticchia, L.K. Laubach, D.J. Honigfort, S. C. Purcell, K. Godula. *Biomaterials Science* – Spatially controlled glycocalyx engineering for growth factor patterning in embryoid bodies. The dissertation author is the primary co-author of this manuscript.

2.6 Supporting Information

Spatially controlled glycocalyx engineering for growth factor patterning in embryoid bodies

Matthew R. Naticchia,[‡[a]] Logan K. Laubach,[‡[a]] Daniel J. Honigfort,[[a]] Sean C. Purcell,[[a]] and Kamil Godula*[[a,b]]

[a]Department of Chemistry and Biochemistry and [b]Glycobiology Research and Training Center, University of California San Diego, 9500 Gilman Drive, La Jolla, CA 92093-0358, USA

‡ Authors contributed equally.
*** Corresponding author:** kgodula@ucsd.edu

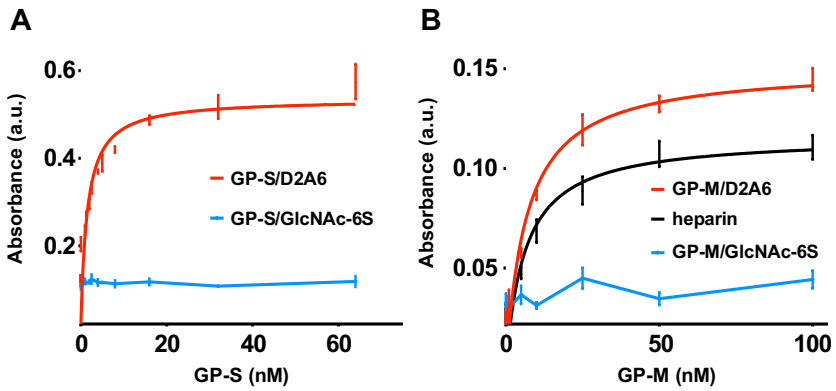

C

GP	$K_{d,app}$ [nM]
-S/D2A6	1.4 ± 0.3
-S/GlcNAc-6S	n.a.
-M/D2A6	6.7 ± 1.2
-M/GlcNAc-6S	n.a.
heparin	6.2 ± 1.8

Figure 2.6. FGF2 binding to sulfated HS-mimetic glycopolymers via ELISA. FGF2 interactions with short (A) and medium (B) glycopolymers **GP-S/D2A6** and **GP-S/GlcNAc-6S.** Heparin was used as positive control (B, black). C) Table of Kd,app for the binding of GPs and heparin to immobilized FGF2.

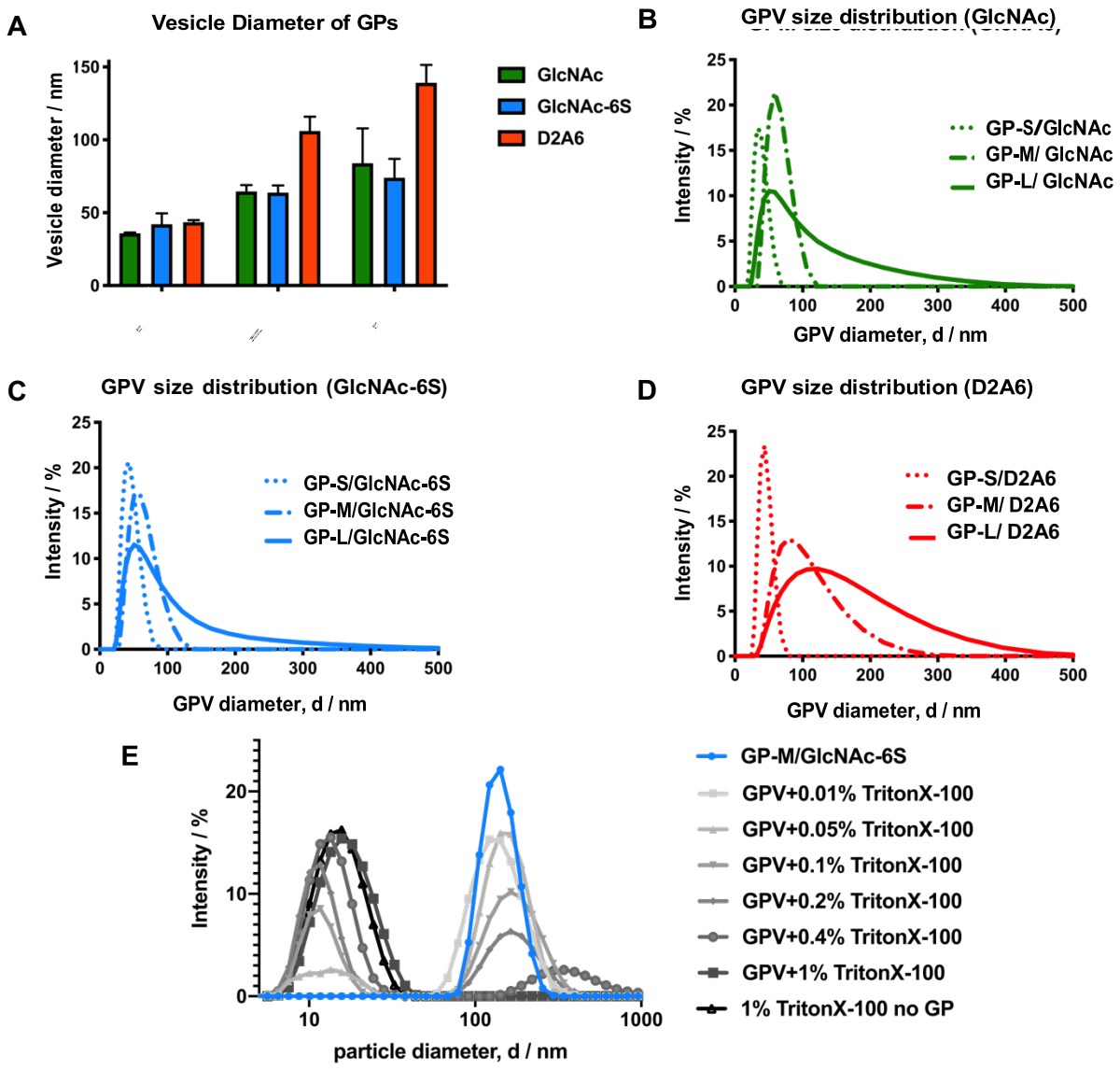

Figure 2.7. Determination of **GPV** sizes by DLS. A) Diameters for **GPV**s assembled from small (S), medium (M) and large (L) glycopolymers **GP**. B-D) Size distributions for **GPV**s according to glycan type. E) Disruption of **GPV**s with triton-X detergent (shown for **GP2-M/GlcNAc-6S**).

Table 2.5. Diameters and Zeta potentials of **GPVs**.

glycopolymer, GP		d_{GPV}, nm	**zeta potential**, mV
-S	**D2A6**	43.5 ± 1.3	-
	GlcNAc-6S	42.0 ± 7.5	-
	GlcNAc	35.8 ± 0.6	-
-M	**D2A6**	106.1 ± 9.9	-
	GlcNAc-6S	63.8 ± 5.0	-
	GlcNAc	64.5 ± 4.5	-
-L	**D2A6**	139.2 ± 12.3	-31.43 ± 2.71
	GlcNAc-6S	74.0 ± 13.0	-20.10 ± 2.44
	GlcNAc	84.0 ± 23.9	-3.89 ± 1.39
-	Milli Q water	-	-3.57 ± 0.58

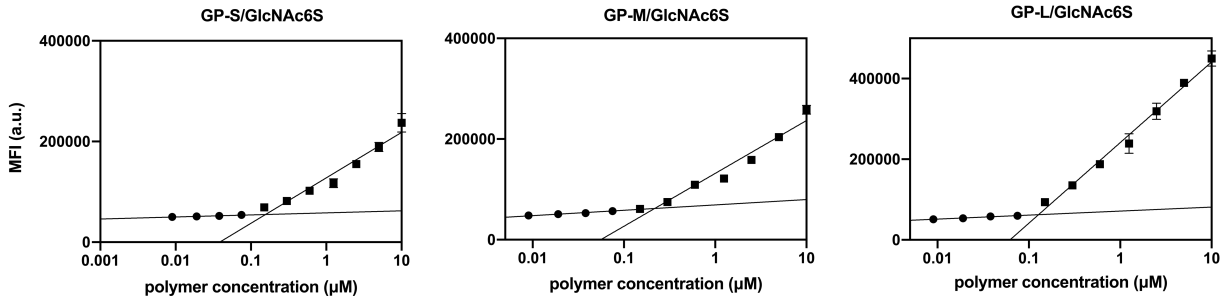

Figure 2.8. Critical vesicle-forming concentration (cvc) for **GP**s via DiI fluorescence. The formation of **GPV**s was measured in the presence of the hydrophobic fluorophore, DiI, over a range of polymer concentrations (0.01 μM - 10 μM) of the short (S), medium (M), and long (L) polymers **GP-GlcNAc-6S**. Change in the slope of the linear regions of DiI fluorescence indicates **GPV** formation. The intersection point was used to determine the CVC for the polymers, as follows: 0.17 μM (**GP-S/GlcNAc-6S**), 0.23 μM (**GP-M/GlcNAc-6S**) and 0.13 μM (**GP-L/GlcNAc-6S**).

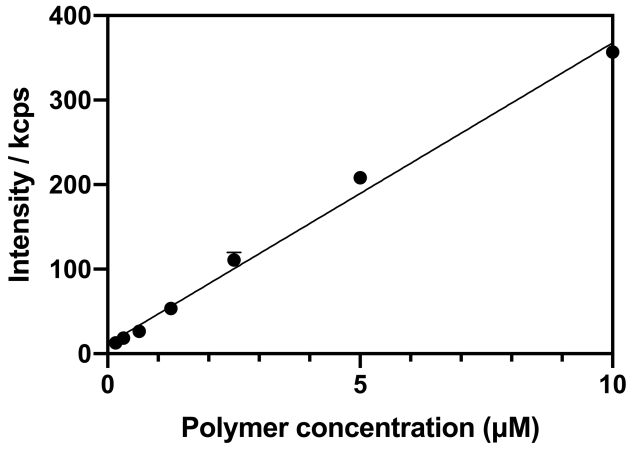

Figure 2.9. Stability of **GPV**s after dilution in PBS buffer via DLS. **GPV**s derived from **GP-M/GlcNAc6S** form at concentrations ranging from 10.0 μM to 0.31 μM, which is the lower detection limit of the DLS assay and above the cvc for **GP-M/GlcNAc-6S.**

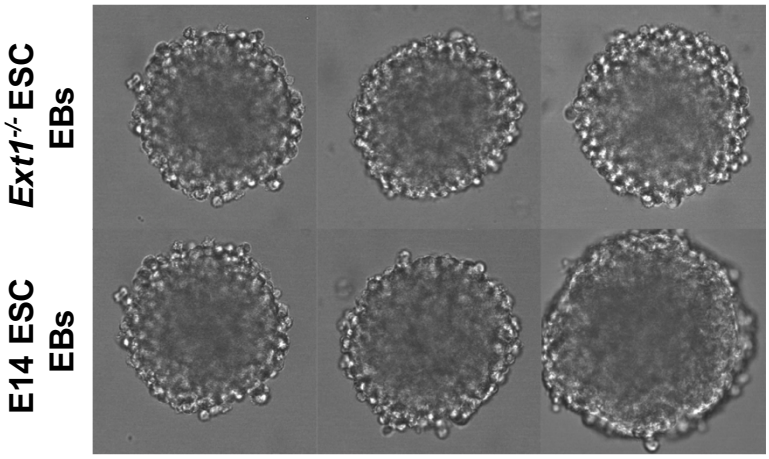

Figure 2.10. Bright field optical micrographs of Day 0 E14 and *Ext1*$^{-/-}$ ESC EBs.

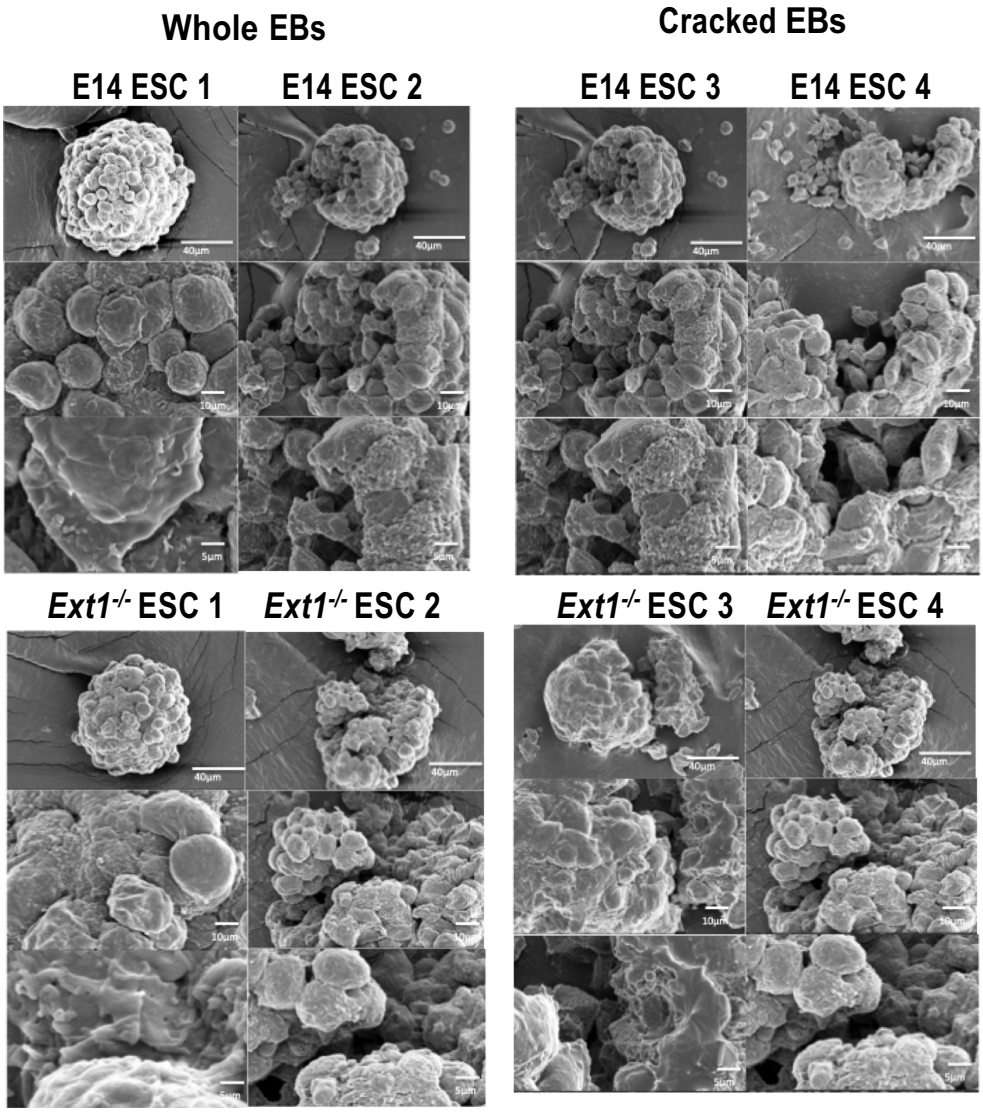

Figure 2.11. SEM images of E14 and Ext1$^{-/-}$ ESC EBs (extended data from Figure 4C). Whole E14 and Ext1$^{-/-}$ ESC EBs (left, replicates #1 and 2) show surface deposition of ECM. When E14 and Ext1$^{-/-}$ ESC EBs (right, replicates #3 and 4) are cracked open by crushing the EBs with the metal stage, increasingly closer packing of cells is observed at the periphery of the EBs.

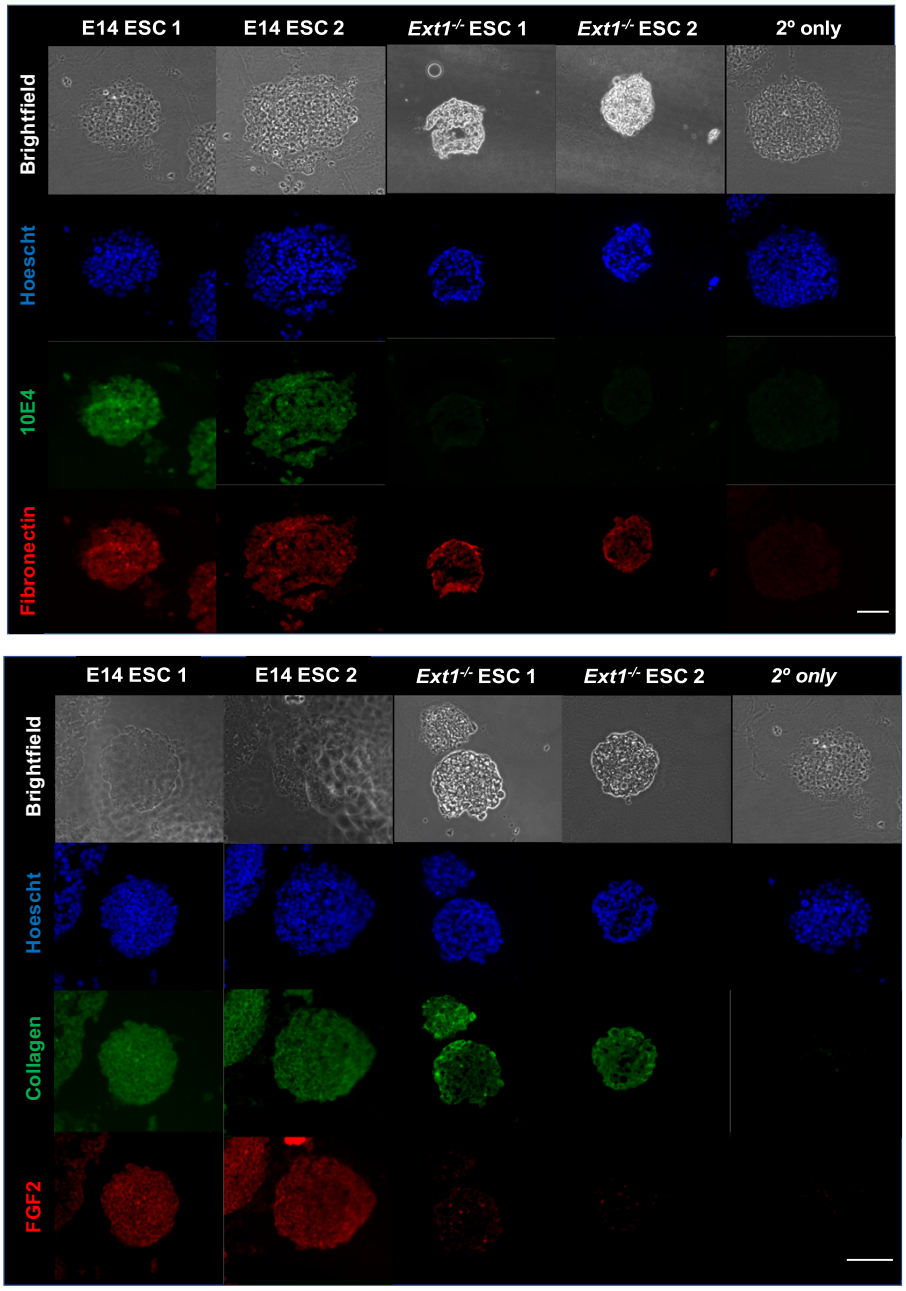

Figure 2.12. Histological slices of E14 and Ext1$^{-/-}$ EBs (extended data for Fig 4D and Fig 5C). (Top) Day 2 EBs formed from *wt* E14 ESCs stained for HS (green), while Ext1$^{-/-}$ ESCs, which lack the ability to biosynthesize HS, do not show staining above background. Both cell lines produced fibronectin, however Ext1$^{-/-}$ ESC EBs have higher fibronectin localization on the outer shell of the EB. (Bottom) EBs from both cell lines express collagen (green) throughout the EBs. As expected, only E14 ESC EBs bind FGF2 (red). Blue = Hoechst 33342 nuclear stain. Two representative EBs are shown for each condition. Scale bar represents 50 μm.

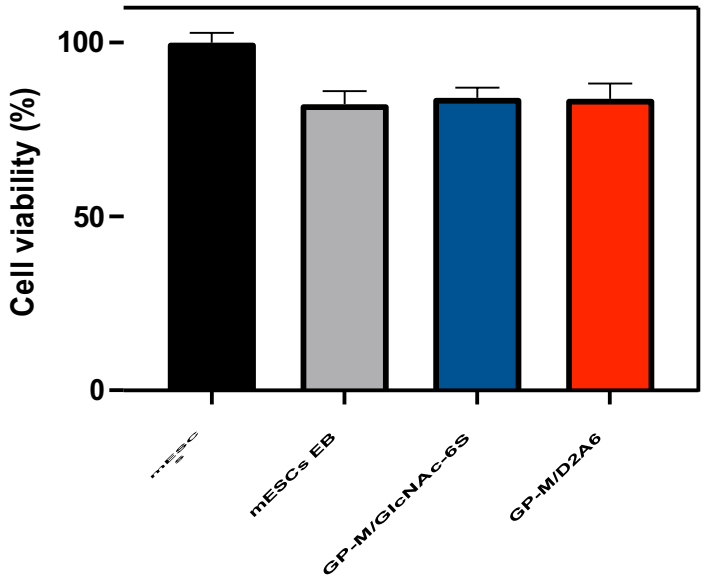

Figure 2.13. Cytotoxicity of **GP**s. Cytotoxicity of the glycopolymers **GP-M/GlcNAc-6S** and **GP- M/D2A6** was assessed in monolayer and EB Ext1$^{-/-}$ ESC culture using calcein AM and ethidium bromide homodimer live/dead stain. Some cell death was observed in EB culture compared to ESCs grown in a monolayer. Remodeling of the EBs with the polymers (3 μM) did not cause significant increase in cell death.

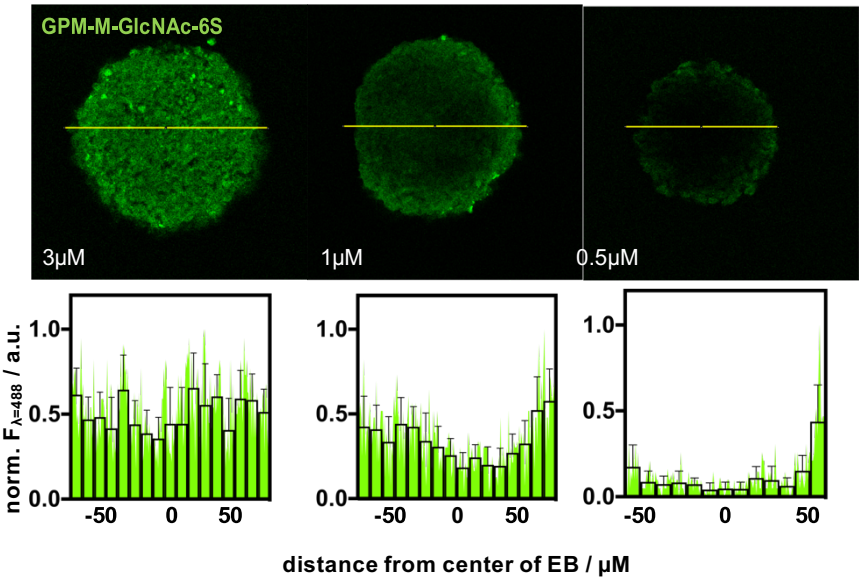

Figure 2.14. Concentration dependence of **GP-M/GlcNAc-6S** labeling of Day 0 Ext1$^{-/-}$ ESC EBs (t = 2 hr).

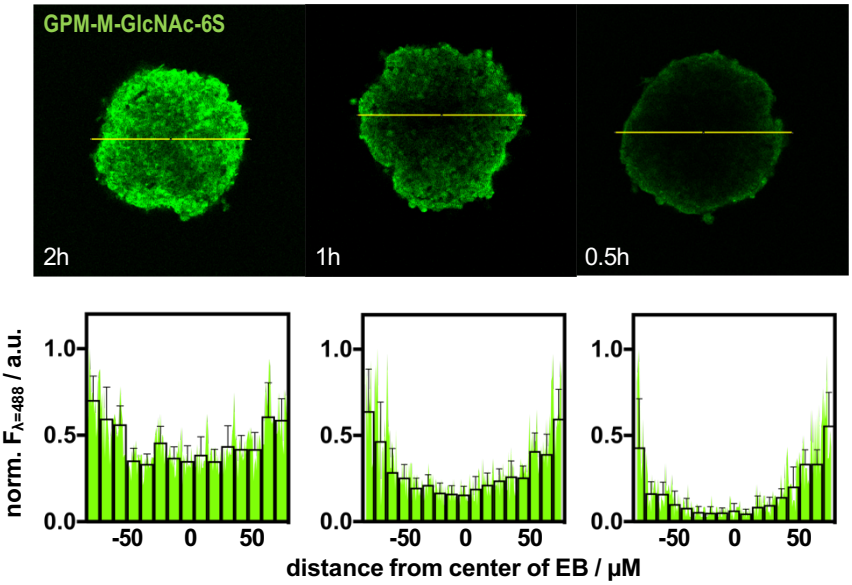

Figure 2.15. Time dependence of **GP-M/GlcNAc-6S** labeling of Day 0 Ext1$^{-/-}$ ESC EBs (c = 3 µM).

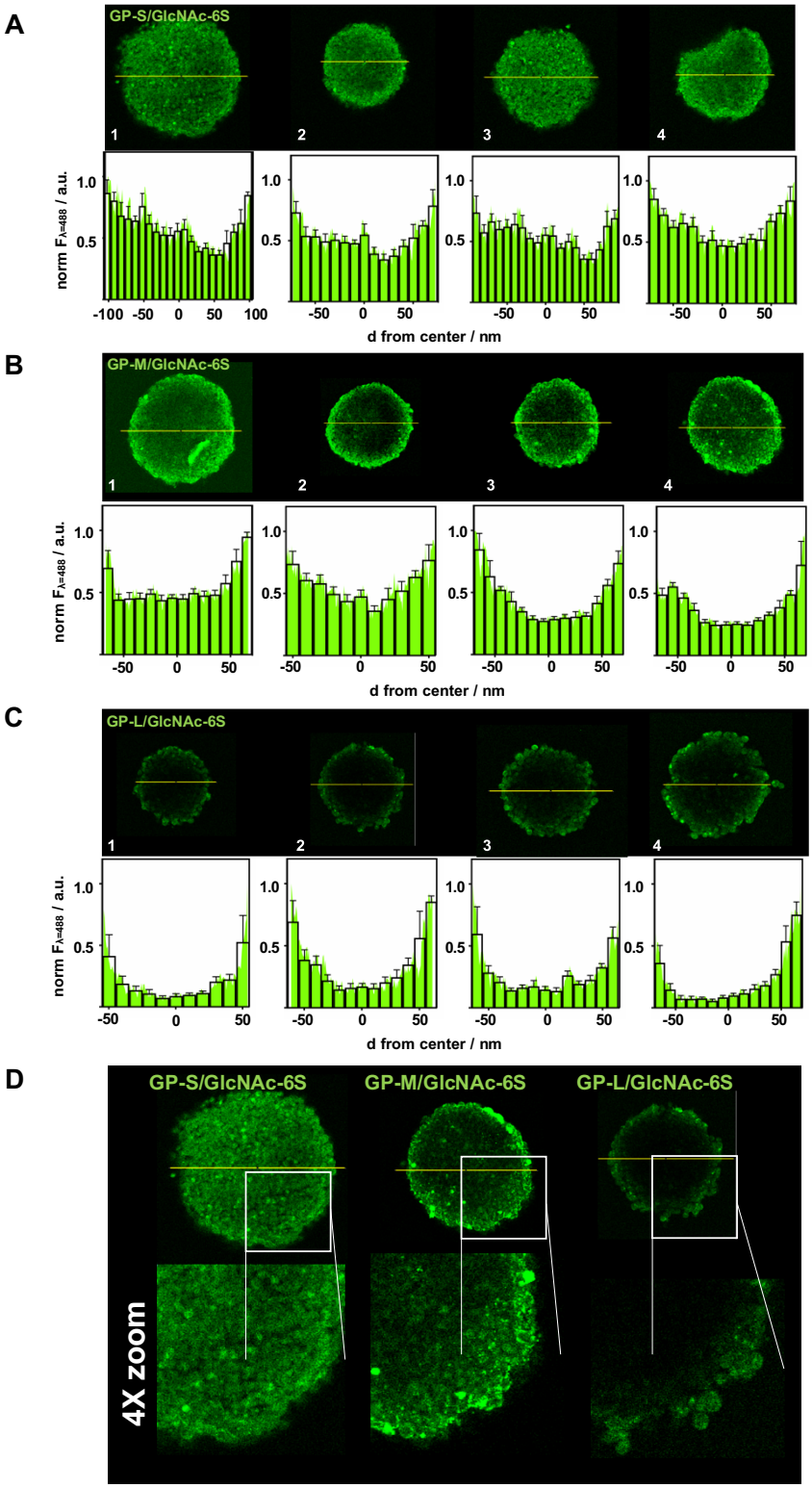

Figure 2.16. Size dependence of **GP-GlcNAc6S** diffusion in Ext1-/- ESC EBs (extended data for Fig 5A). A-C) Fluorescence micrographs and intensity histograms for EBs (4 replicates per condition) remodeled with short (S), medium (M) and long (L) **GP**s. D) Enlarged outer regions of EBs.

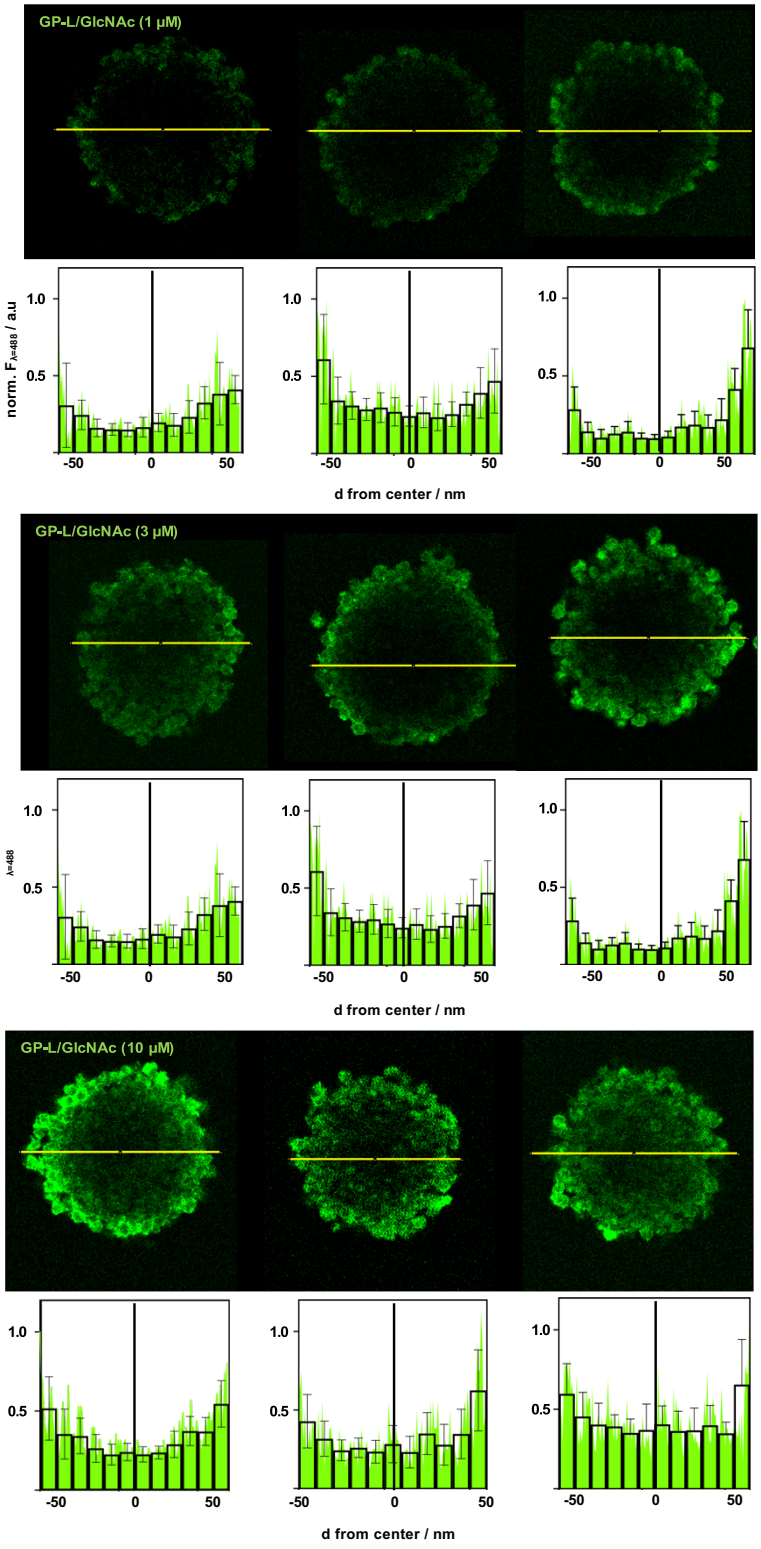

Figure 2.17. Remodeling of Ext1$^{-/-}$ ESC EBs with **GP-L/GlcNAc** polymers (1.0, 3.0 and 10 µM). The neutral **GP-L/GlcNAc GPV**s do not show increased penetrance into EBs compared to the sulfated **GP-L/GlcNAc-6S**.

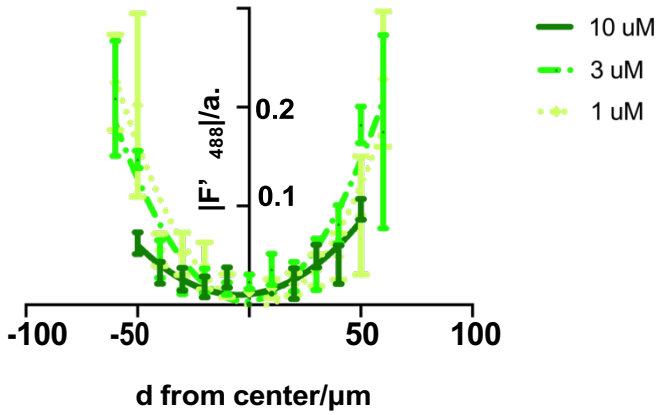

Figure 2.18. Gradient change for Ext1$^{-/-}$ ESC EB remodeling with **GP-L/GlcNAc6S** (1, 3, 10 μM, 1hr). Increasing **GP** concentration results in further **GPV** penetrance into EBs and shallower **GP** gradient.

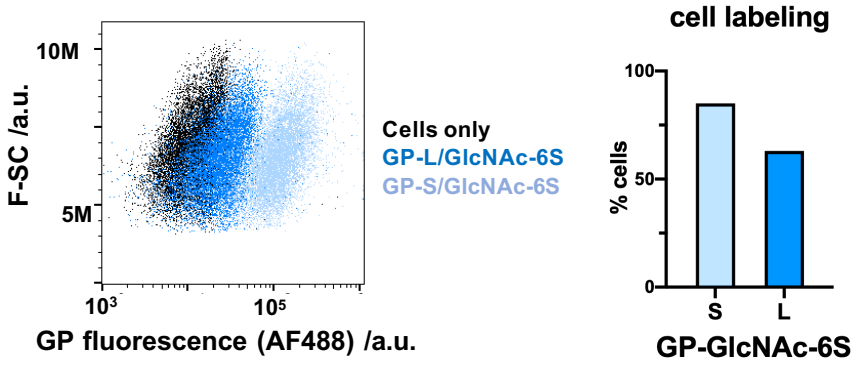

Figure 2.19. Cell surface incorporation of **GP-GlcNAc6S** after EB remodeling. Forward scattering plotted against AF488 fluorescence intensity (Left) and a bar graph representation of cell population shifts (Right) after EB treatment with the short (S) and long (L) glycopolymers **GP-GlcNAc6S** (3 μM, 1hr) and dissociation with accutase.

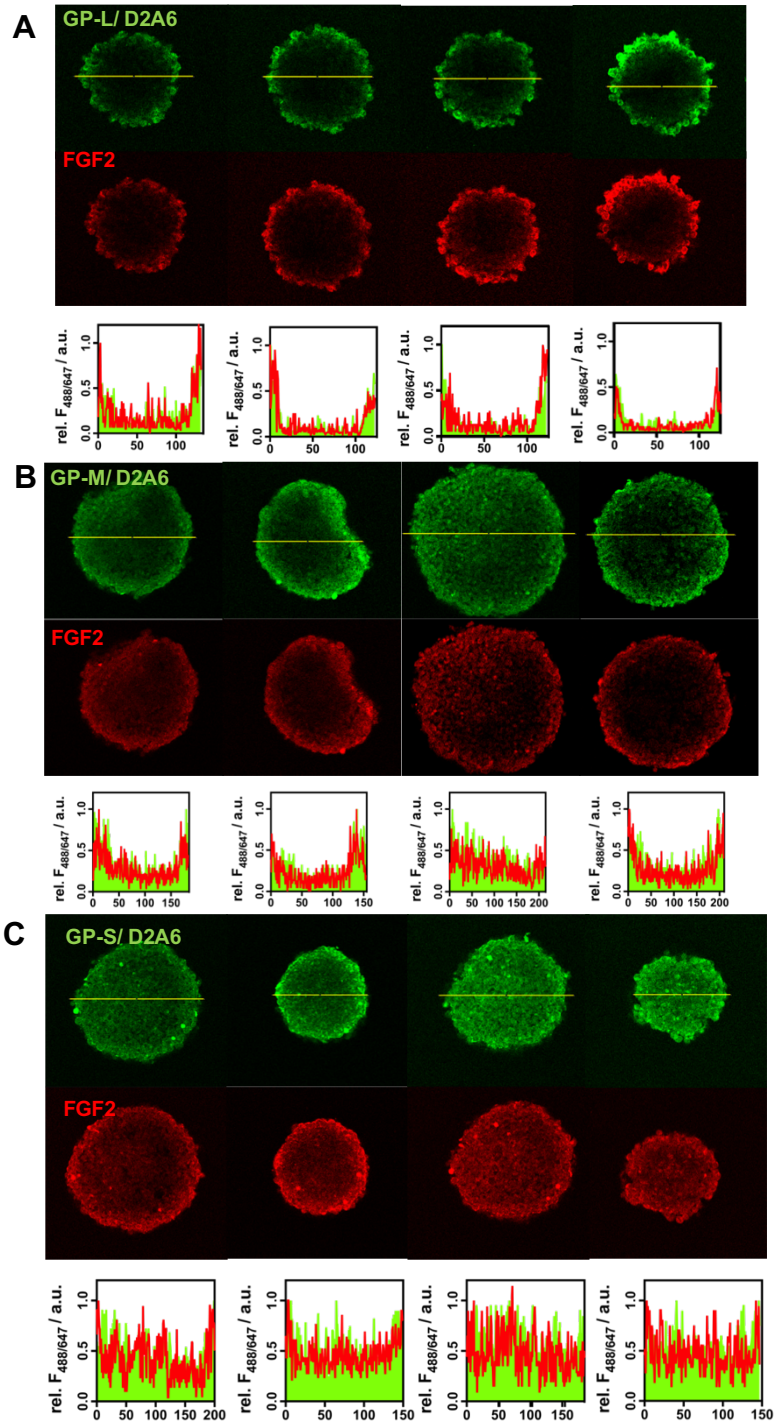

Figure 2.20. FGF2 localization in EBs remodeled by **GP-D2A6** (extended data from Figure 5D). (A-C) Fluorescence micrographs and line intensity graphs for EBs (4 replicates per condition) stained with FGF2 (red) after treatment with short (S), medium (M), and long (L) glycopolymers **GP-D2A6** (green).

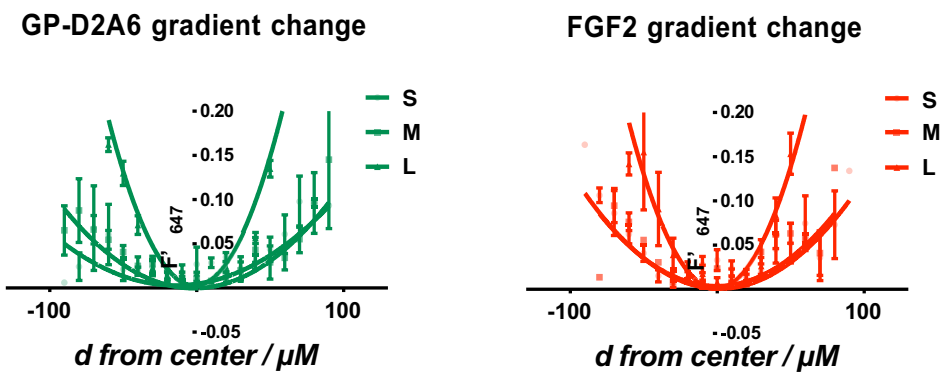

Figure 2.21. Gradient change for FGF2 binding to Ext1$^{-/-}$ ESC EBs remodeled with **GP-D2A6**. Change in line fluorescence intensity between bins with distance from EB center for glycopolymers **GP-D2A6** (green) and FGF2 (red).

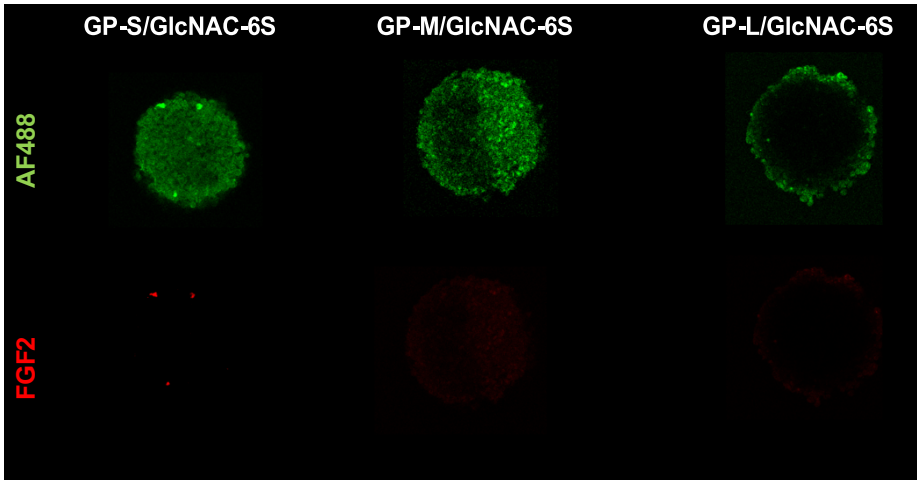

Figure 2.22. FGF2 staining of EBs remodeled with **GP-GlcNAc6S** (3 μM, 1 h). No FGF2 signal (red) above background was observed in EBs after incorporation of the short (S), medium (M) and long (L) glycopolymers **GP-GlcNAc6S** glycopolymers (green).

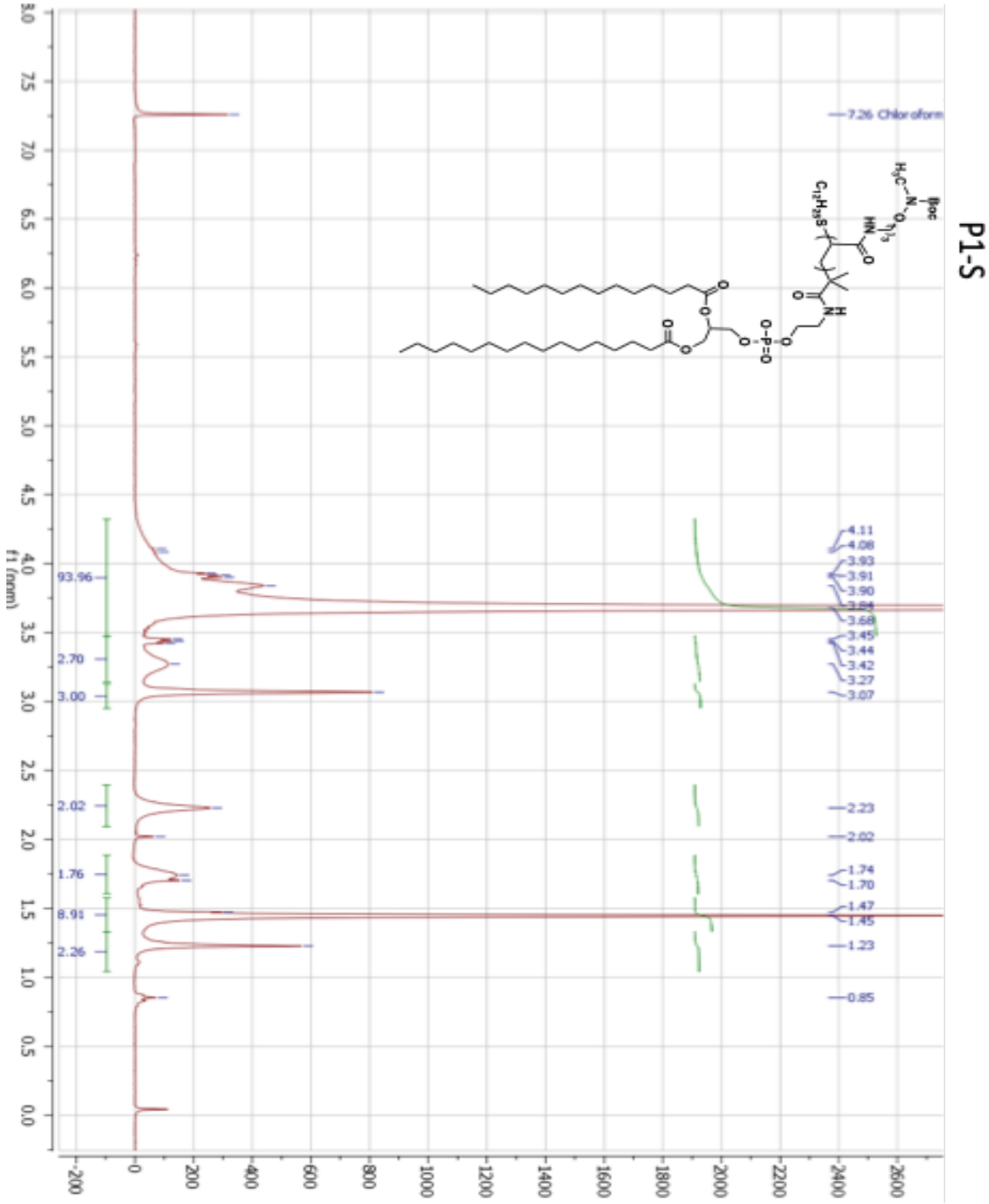

Figure 2.23. H NMR spectrum of **P1-S** (300MHz, $CDCl_3$)

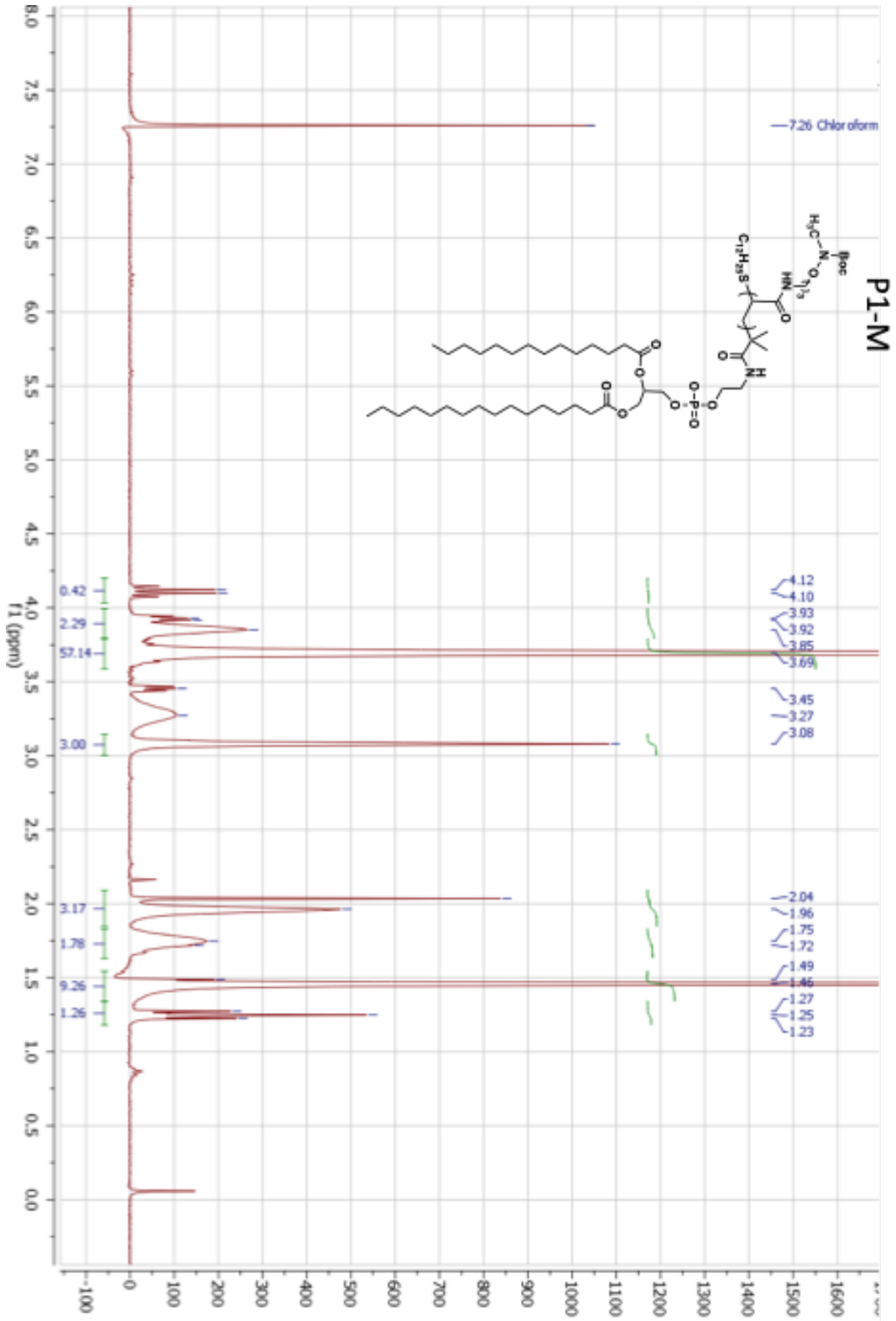

Figure 2.24. H NMR spectrum of **P1-M** (300MHz, $CDCl_3$)

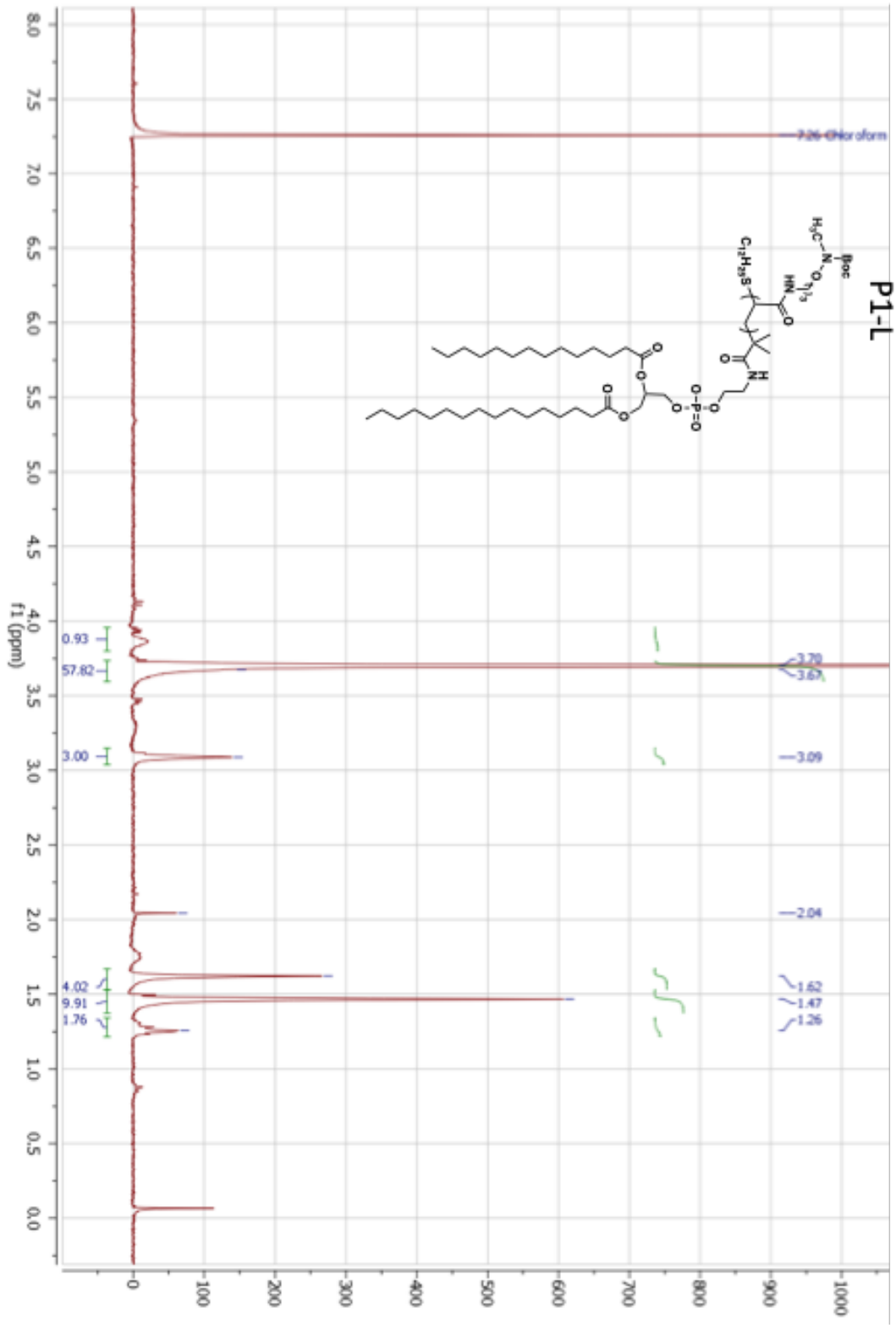

Figure 2.25. H NMR spectrum of **P1-L** (300MHz, $CDCl_3$)

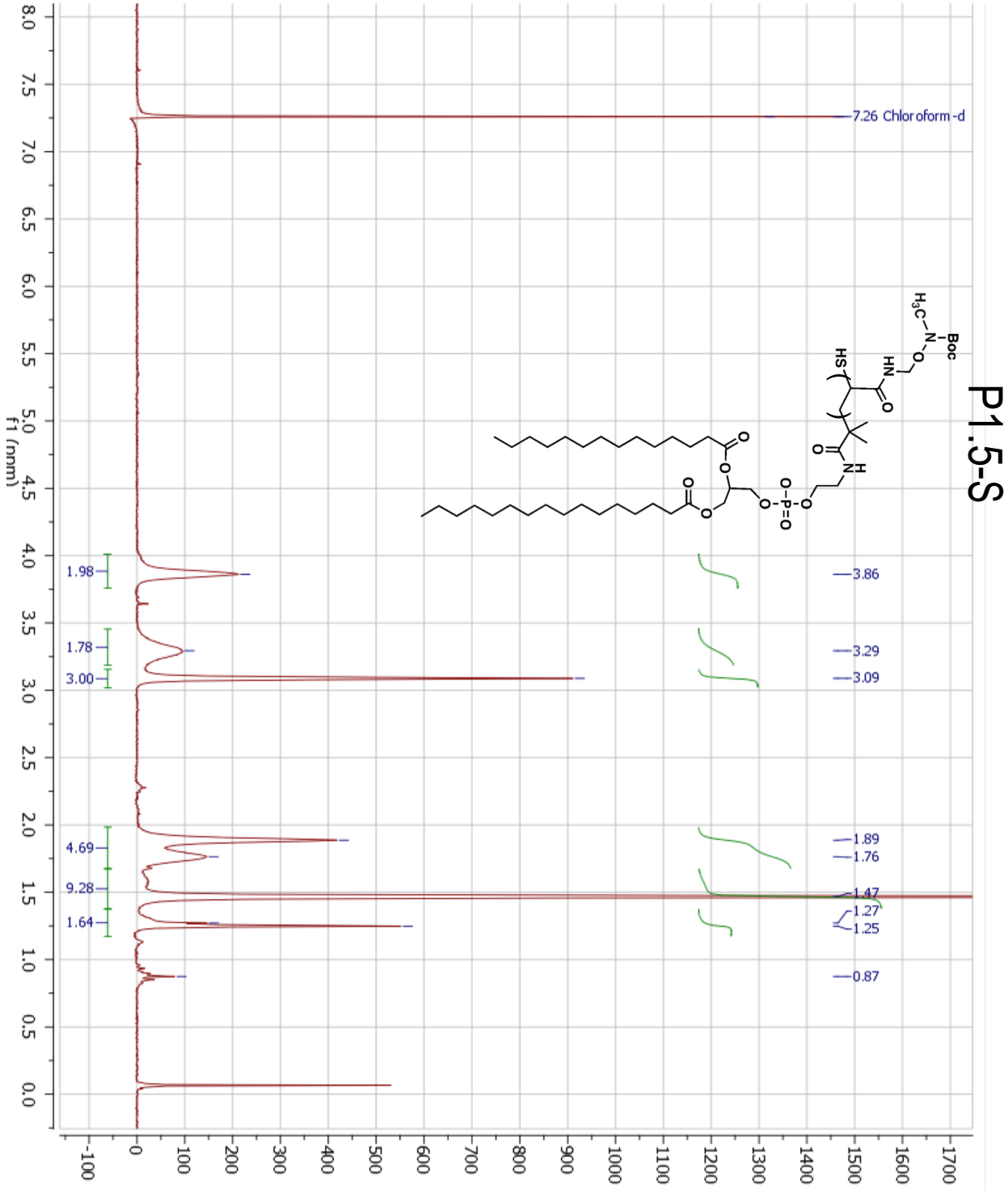

Figure 2.26. H NMR spectrum of **P1.5-S** (300MHz, $CDCl_3$)

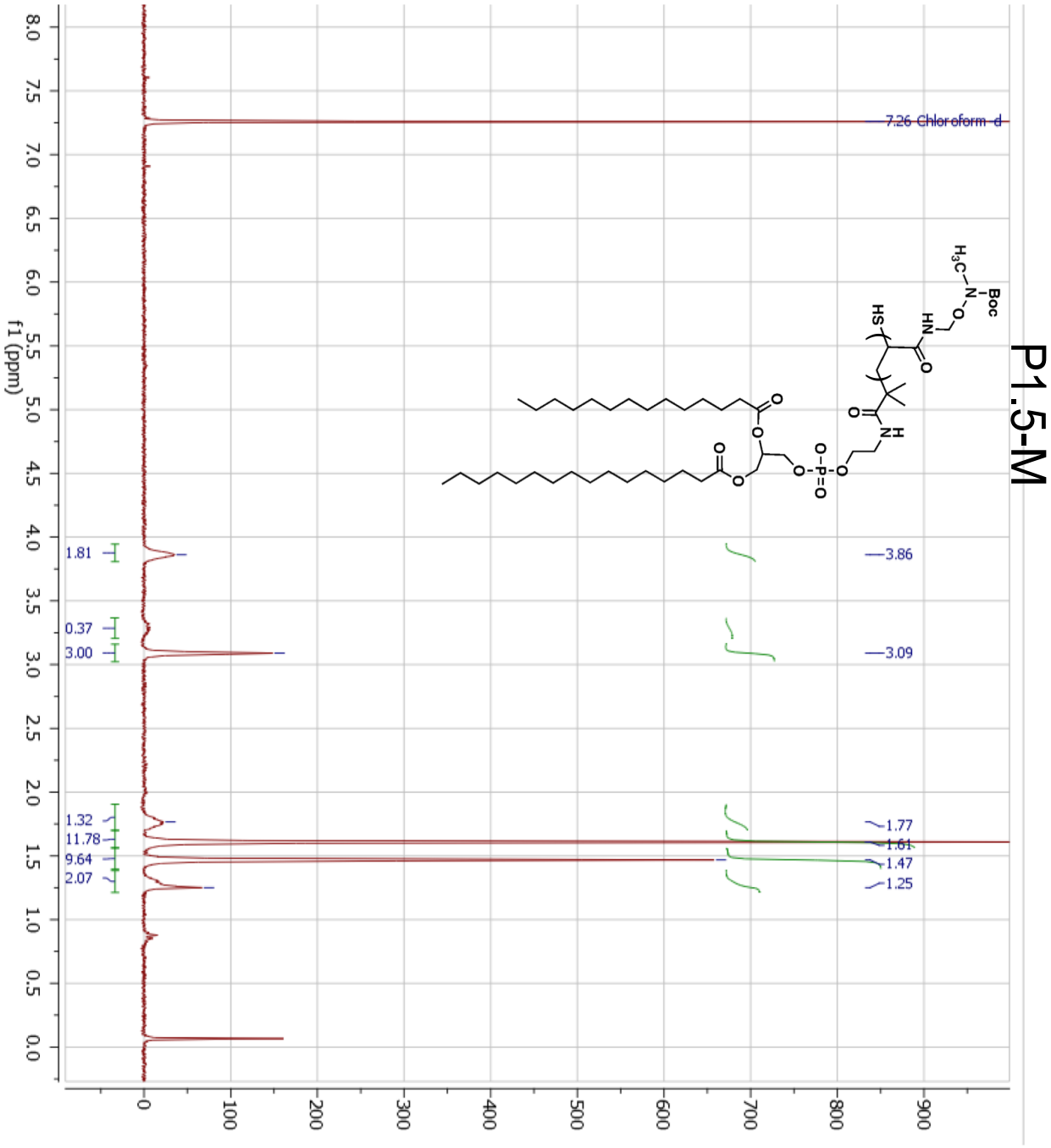

Figure 2.27. H NMR spectrum of **P1.5-M** (300MHz, $CDCl_3$)

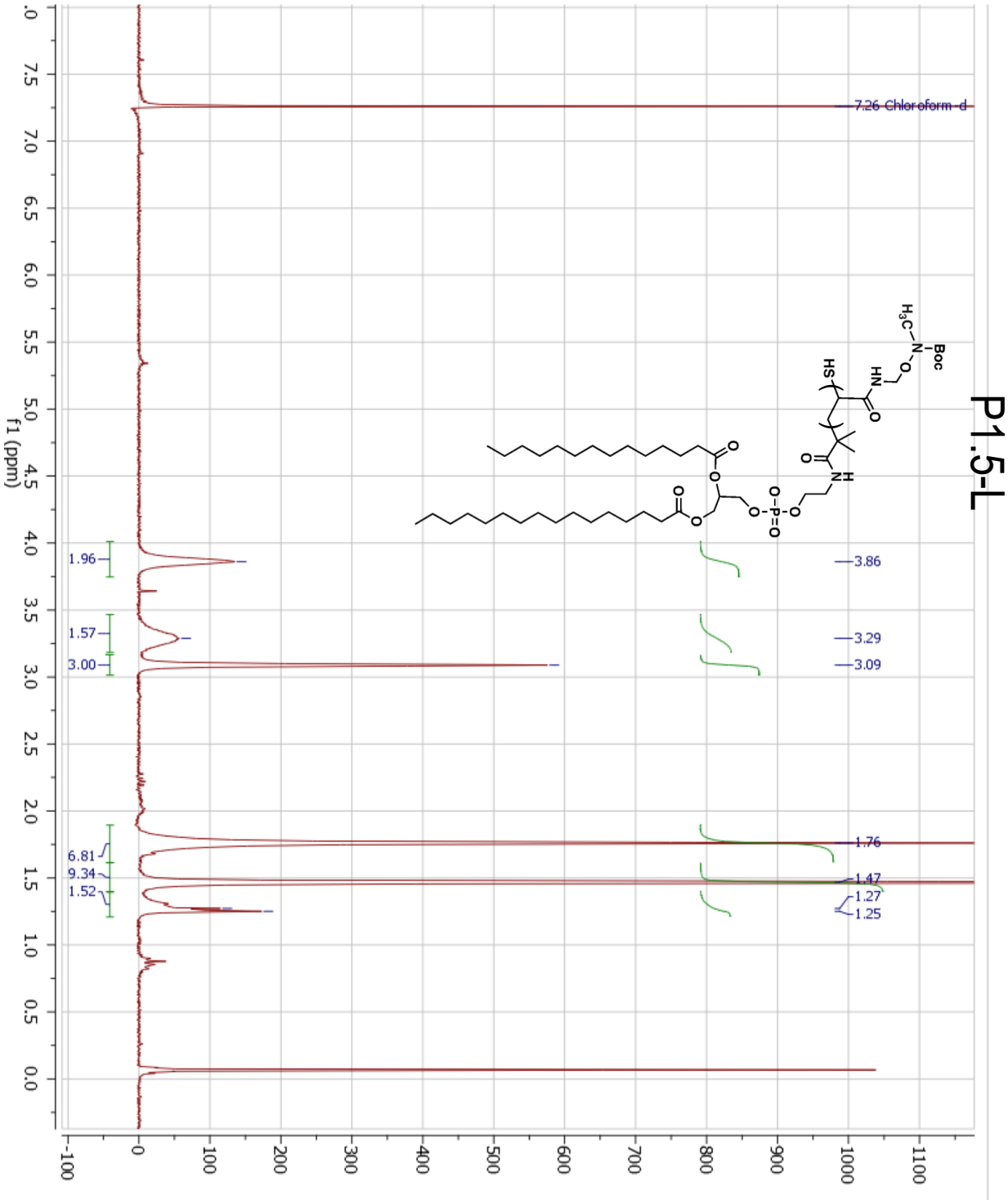

Figure 2.28. H NMR spectrum of **P1.5-L** (300MHz, $CDCl_3$)

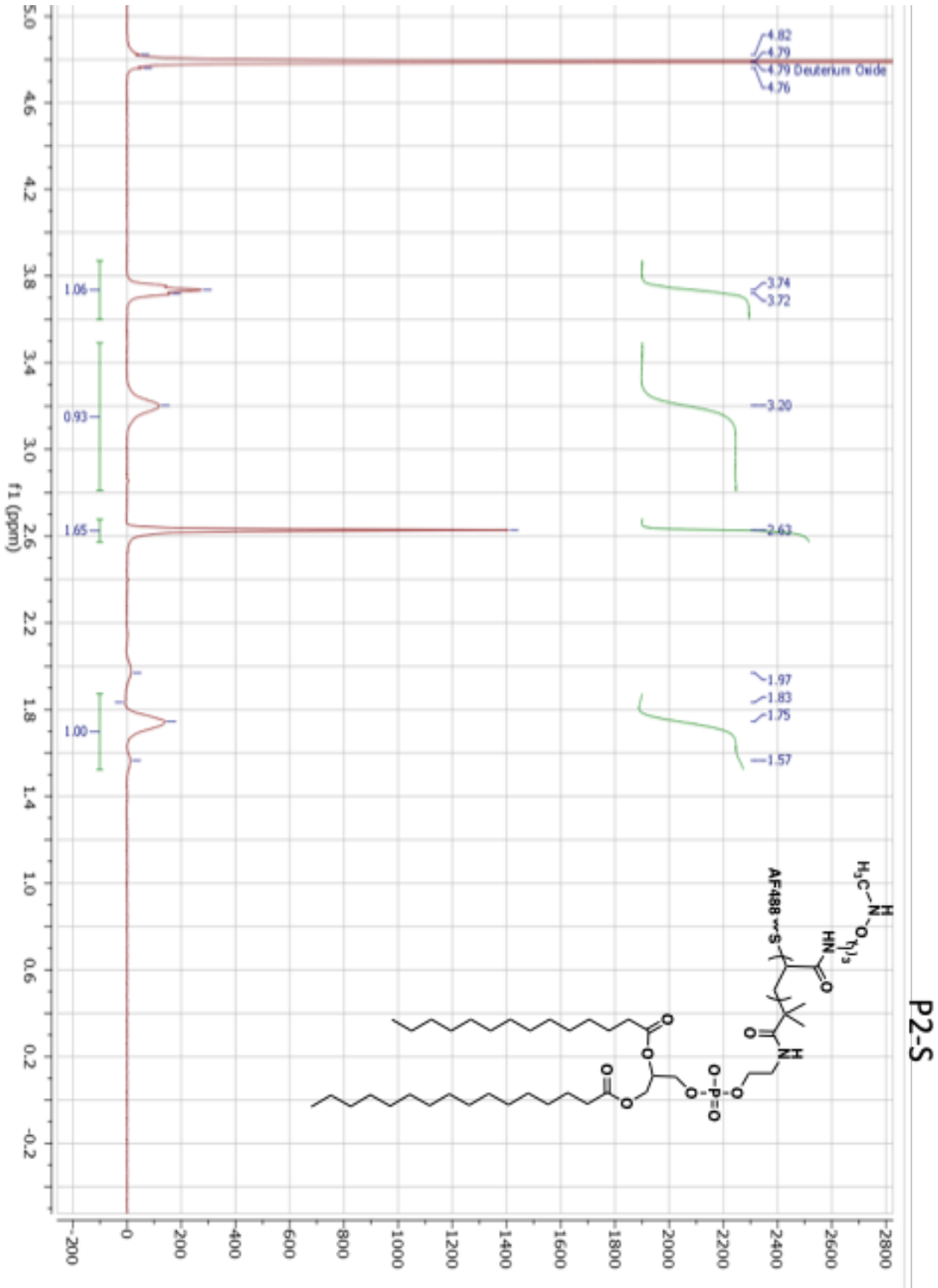

Figure 2.29. H NMR spectrum of **P2-S** (300MHz, D_2O)

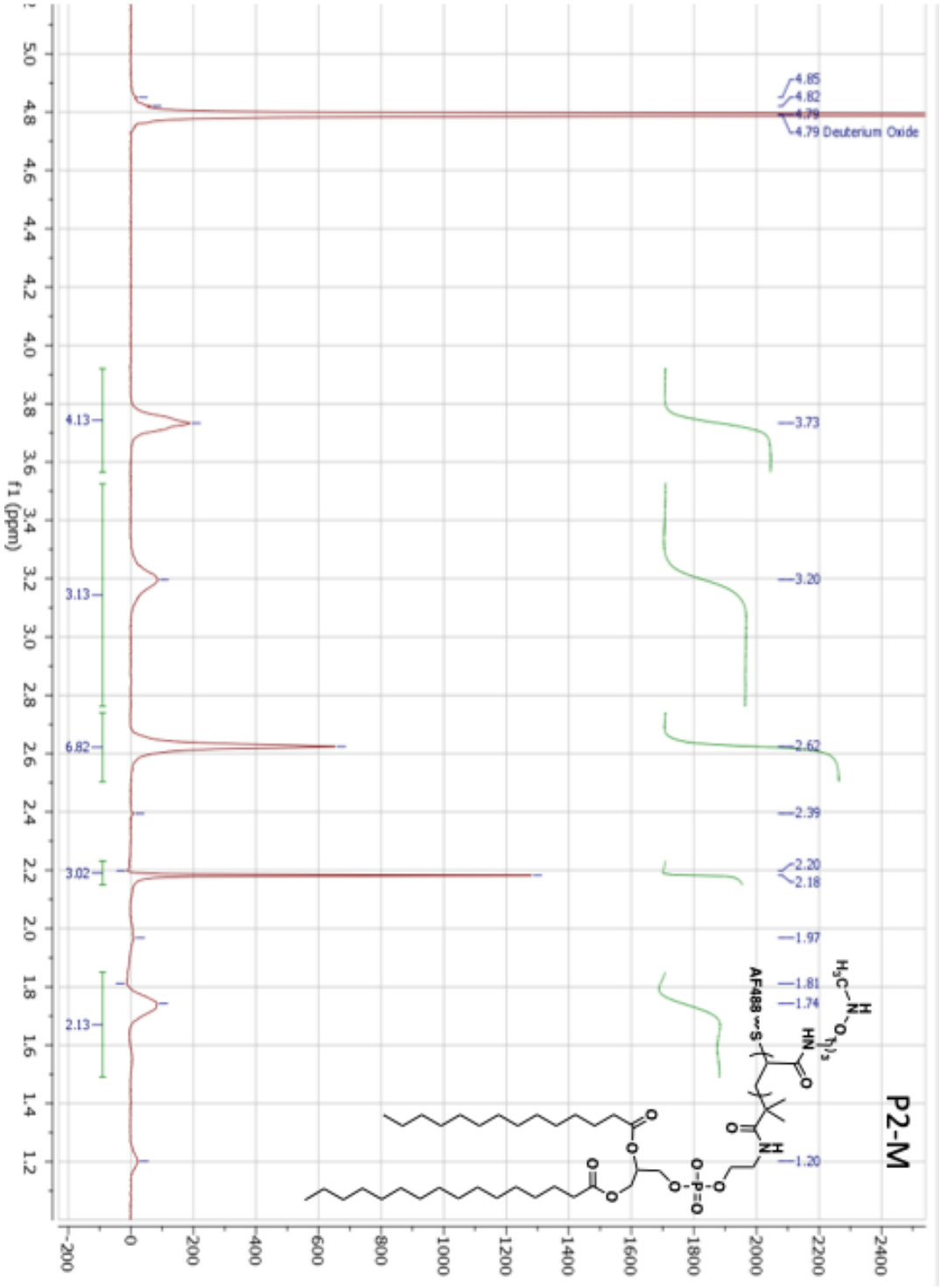

Figure 2.30. H NMR spectrum of **P2-M** (300MHz, D_2O)

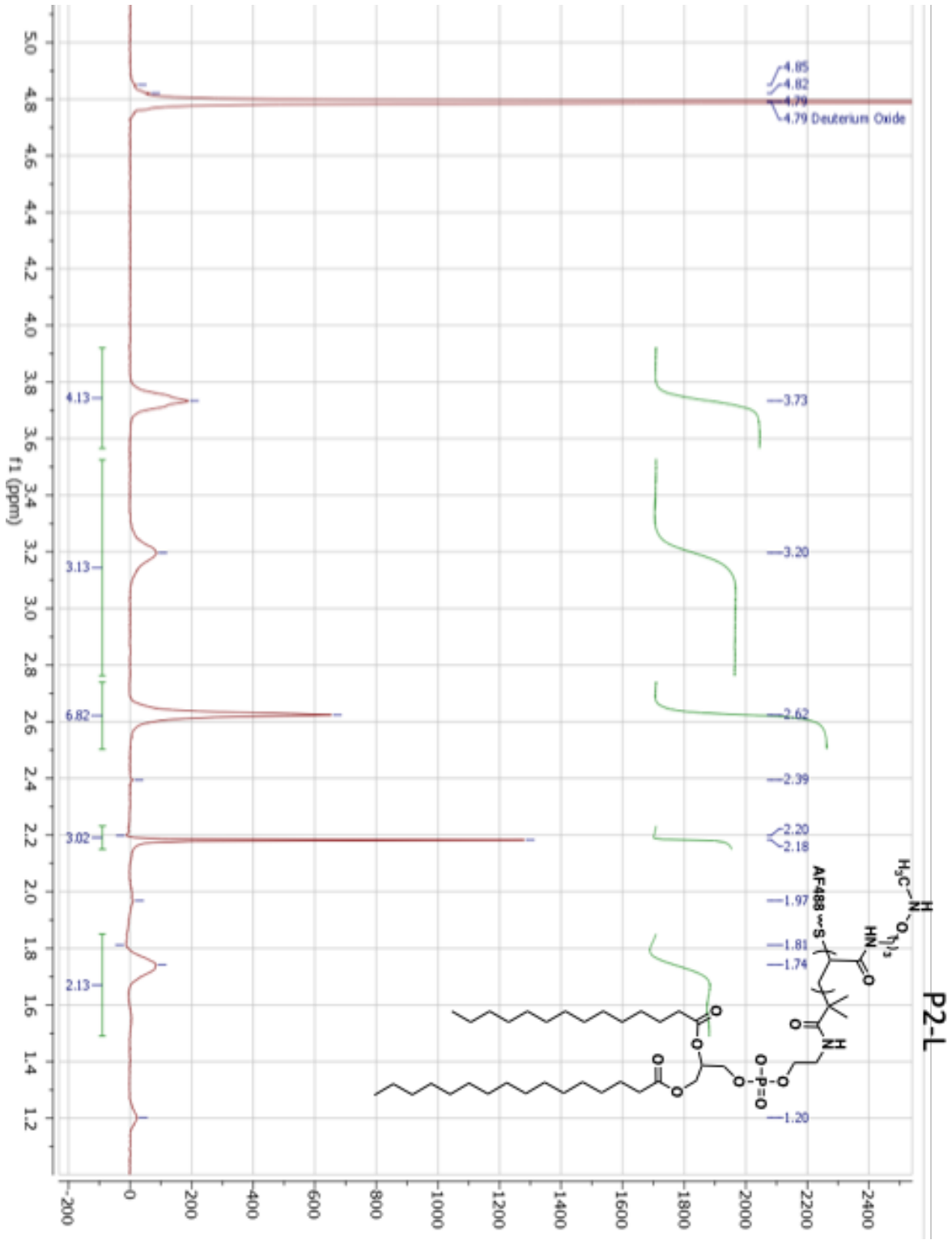

Figure 2.31. H NMR spectrum of **P2-L** (300MHz, D_2O)

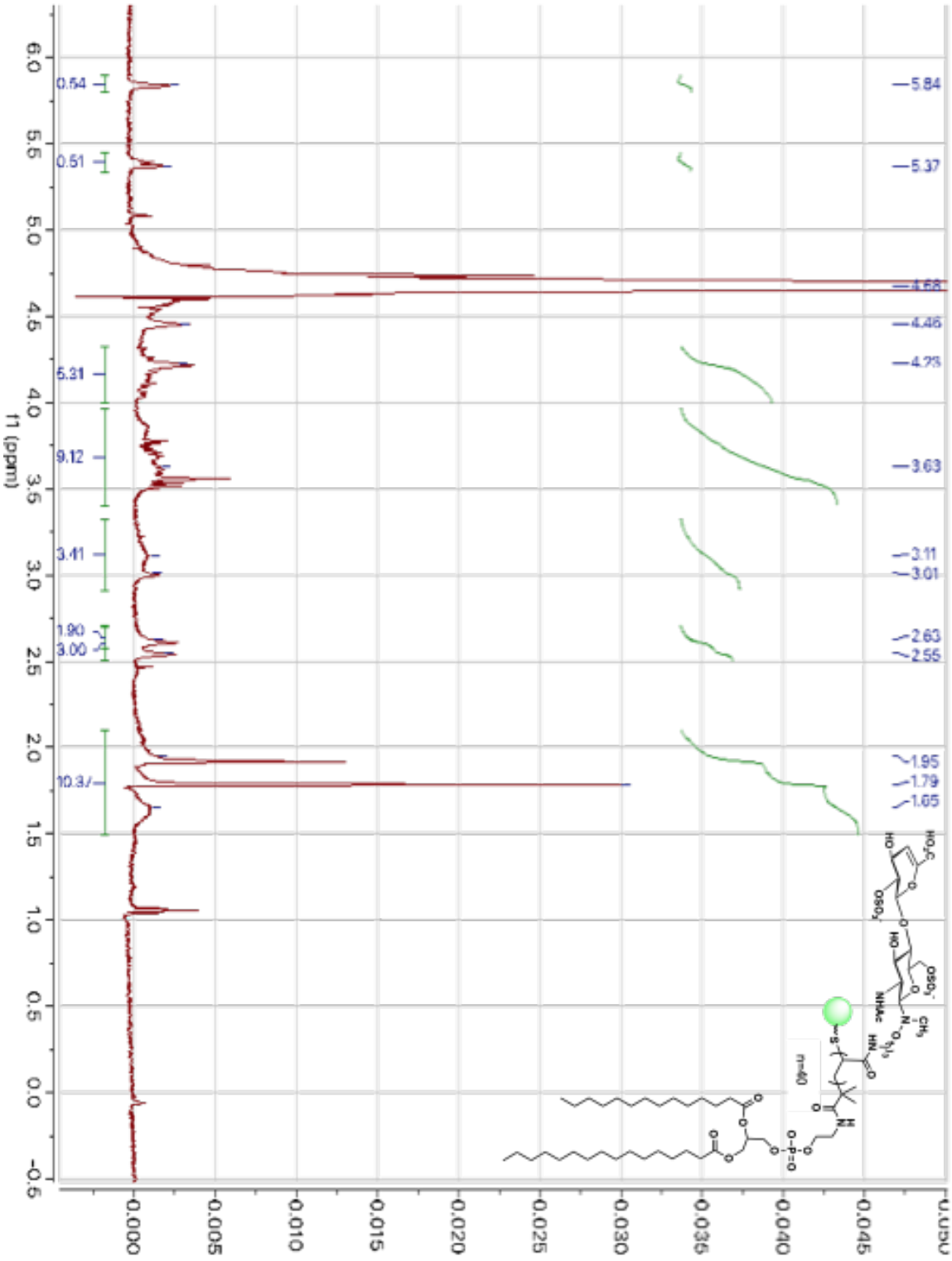

Figure 2.32. H NMR spectrum of **GP-S/D2A6** (300MHz, D_2O)

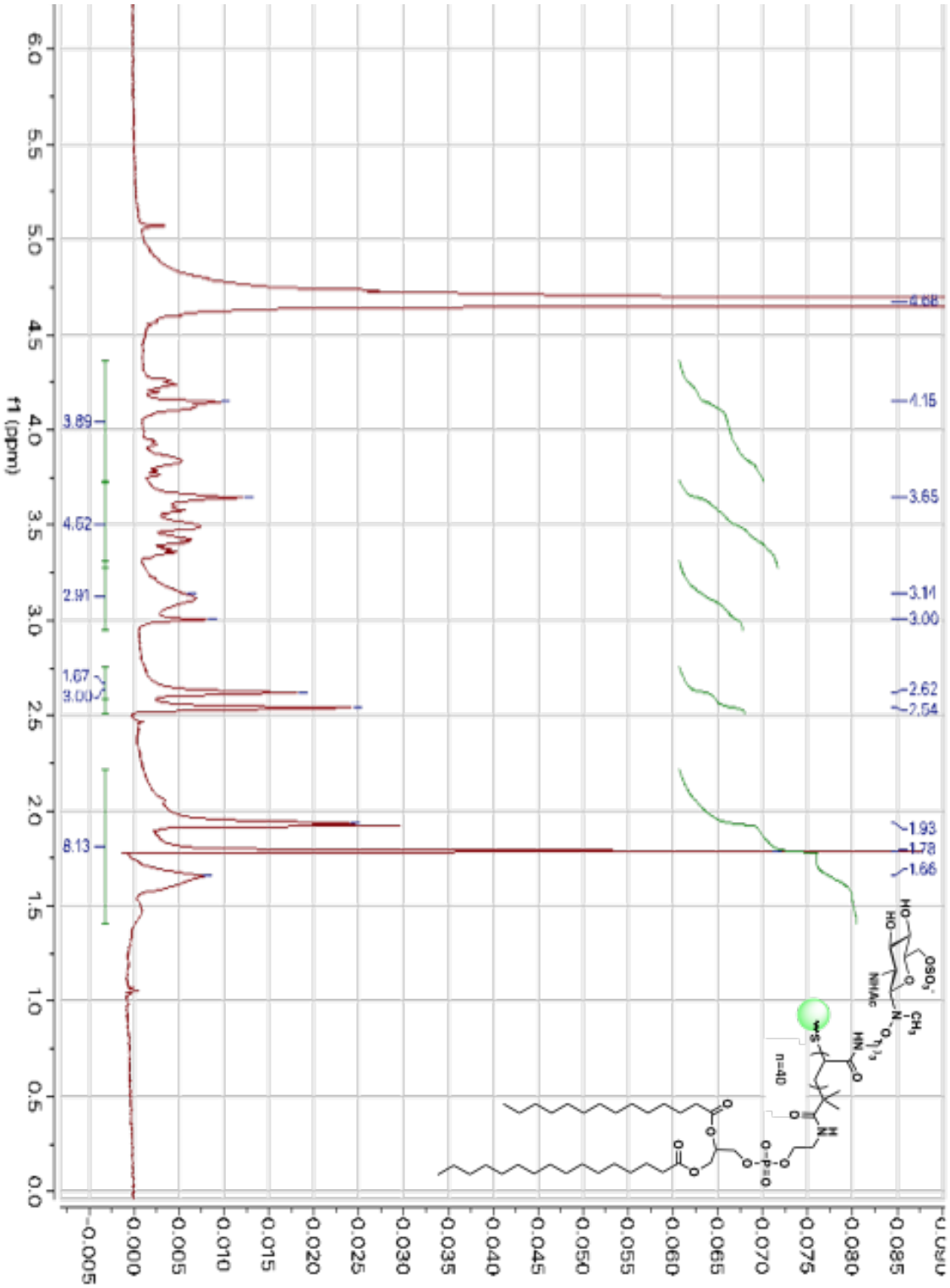

Figure 2.33. H NMR spectrum of **GP-S/GlcNAc6S** (300MHz, D_2O)

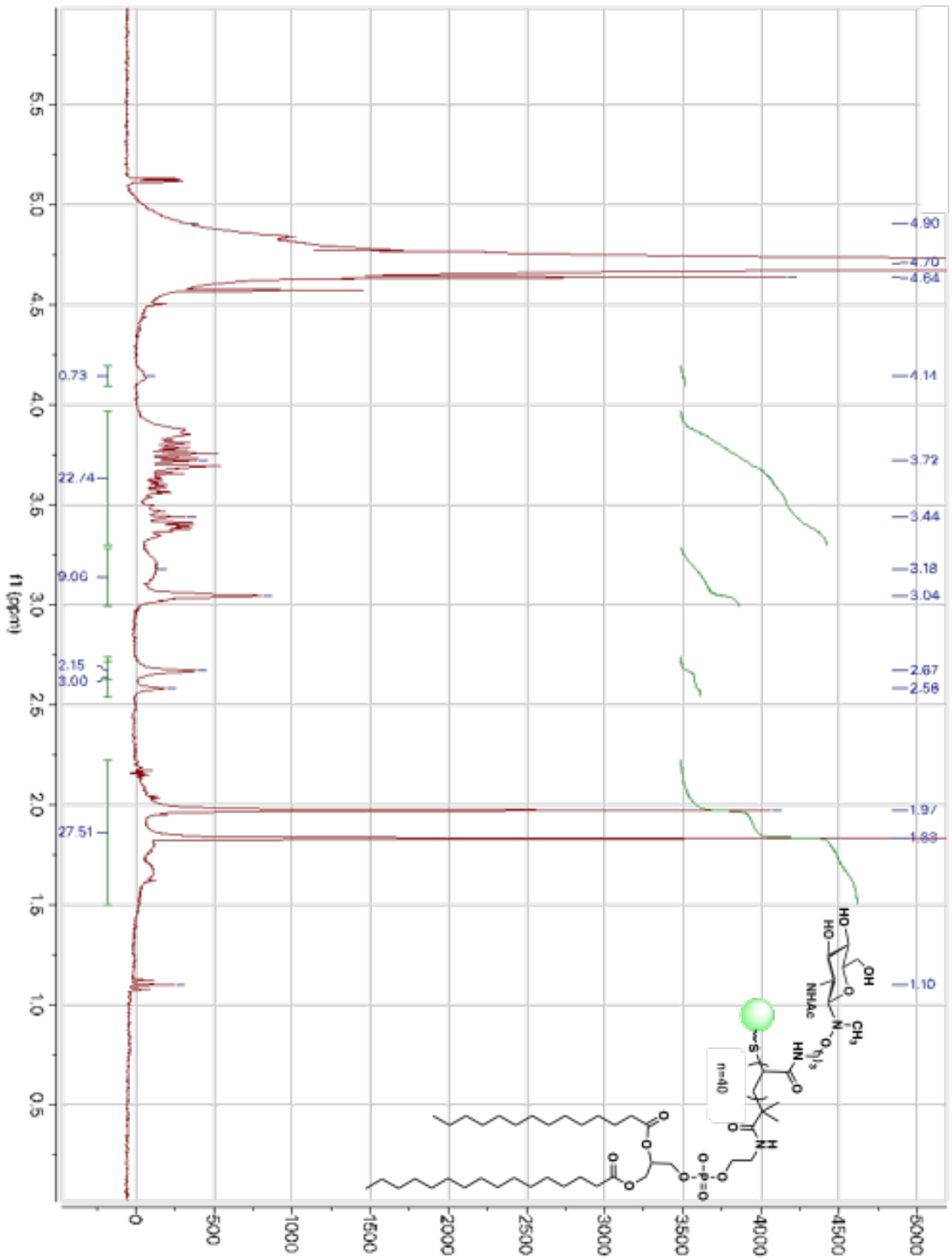

Figure 2.34. H NMR spectrum of **GP-S/GlcNAc** (300MHz, D_2O)

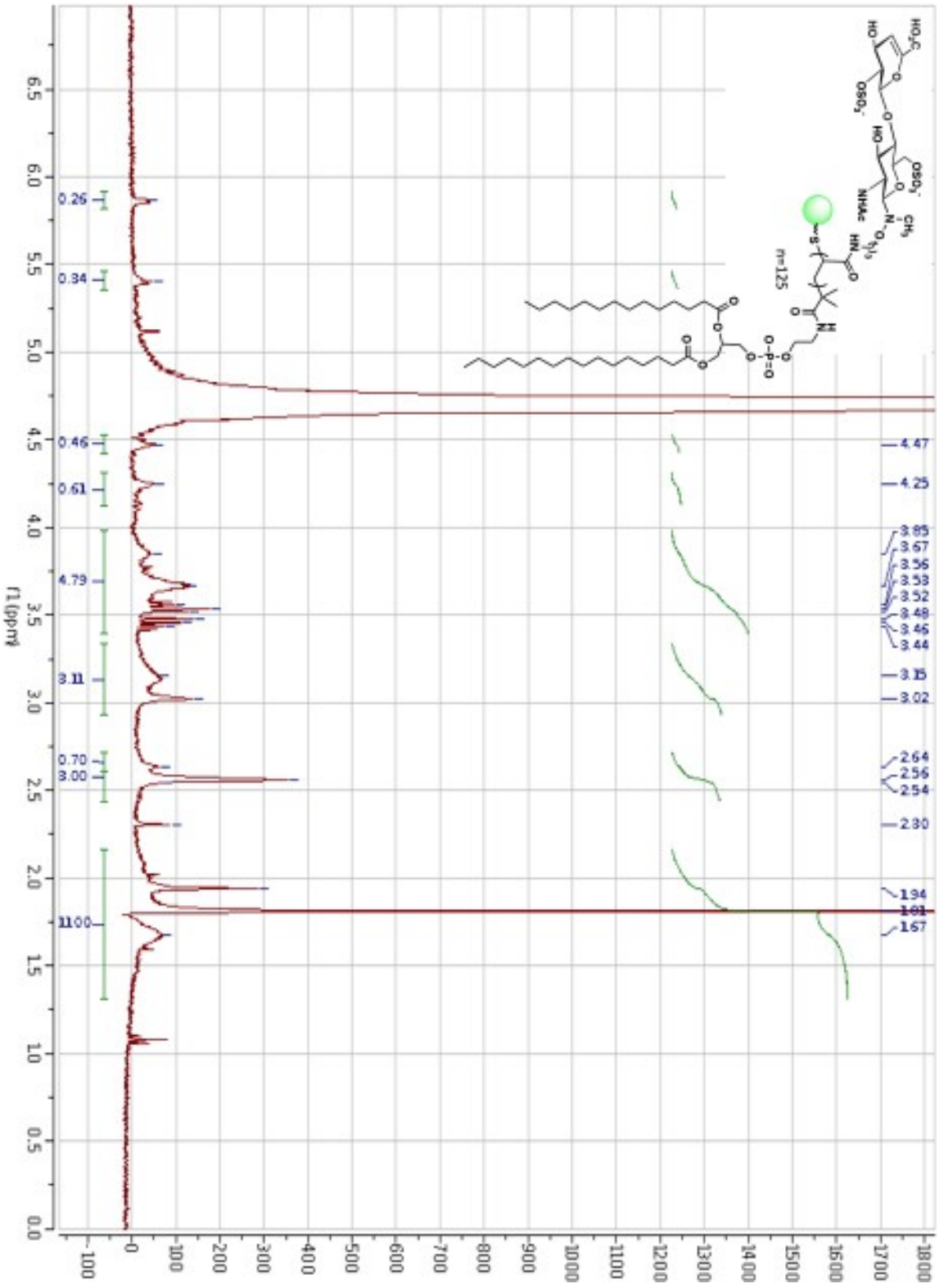

Figure 2.35. H NMR spectrum of **GP-M/D2A6** (300MHz, D_2O)

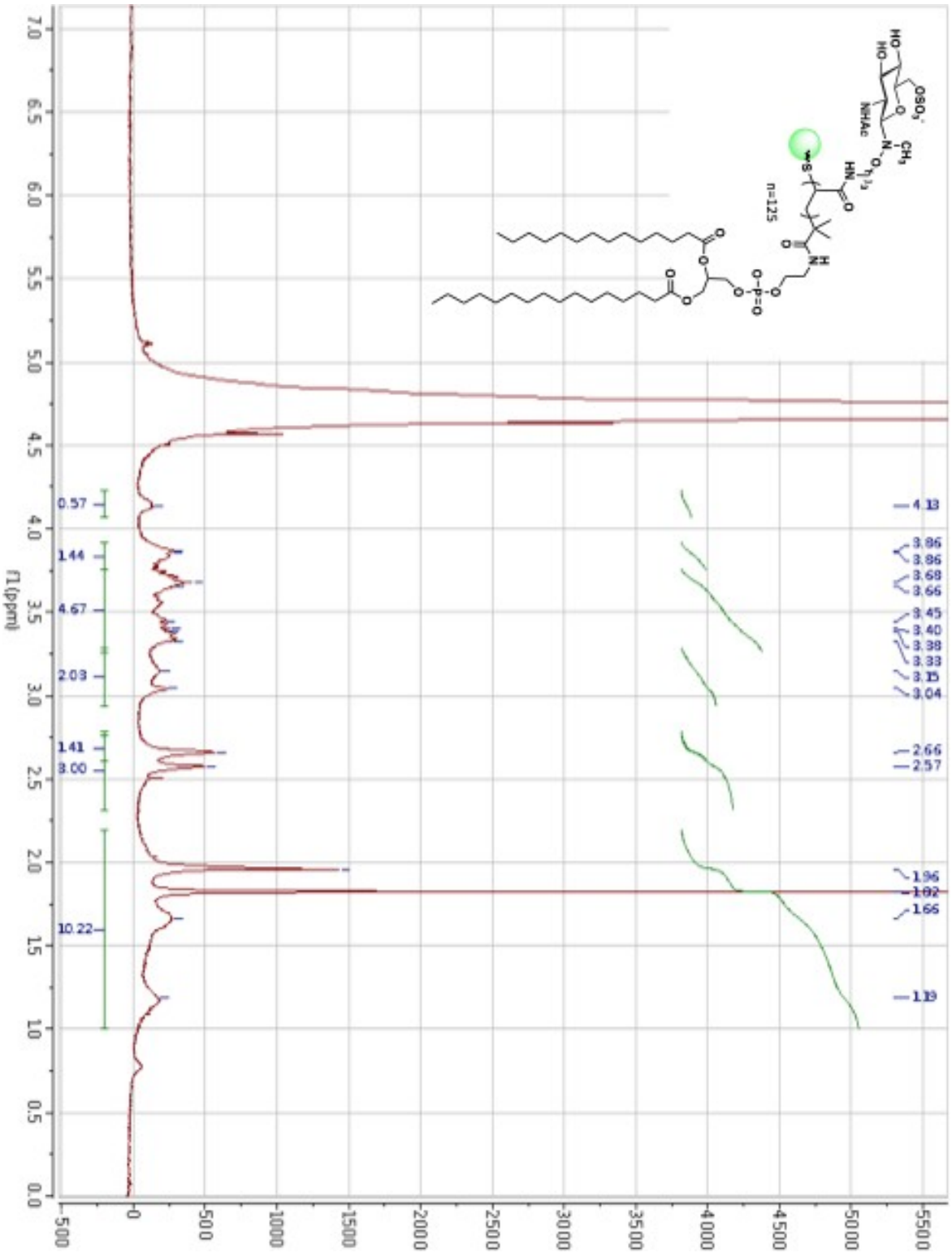

Figure 2.36. H NMR spectrum of **GP-M/GlcNAc6S** (300MHz, D_2O)

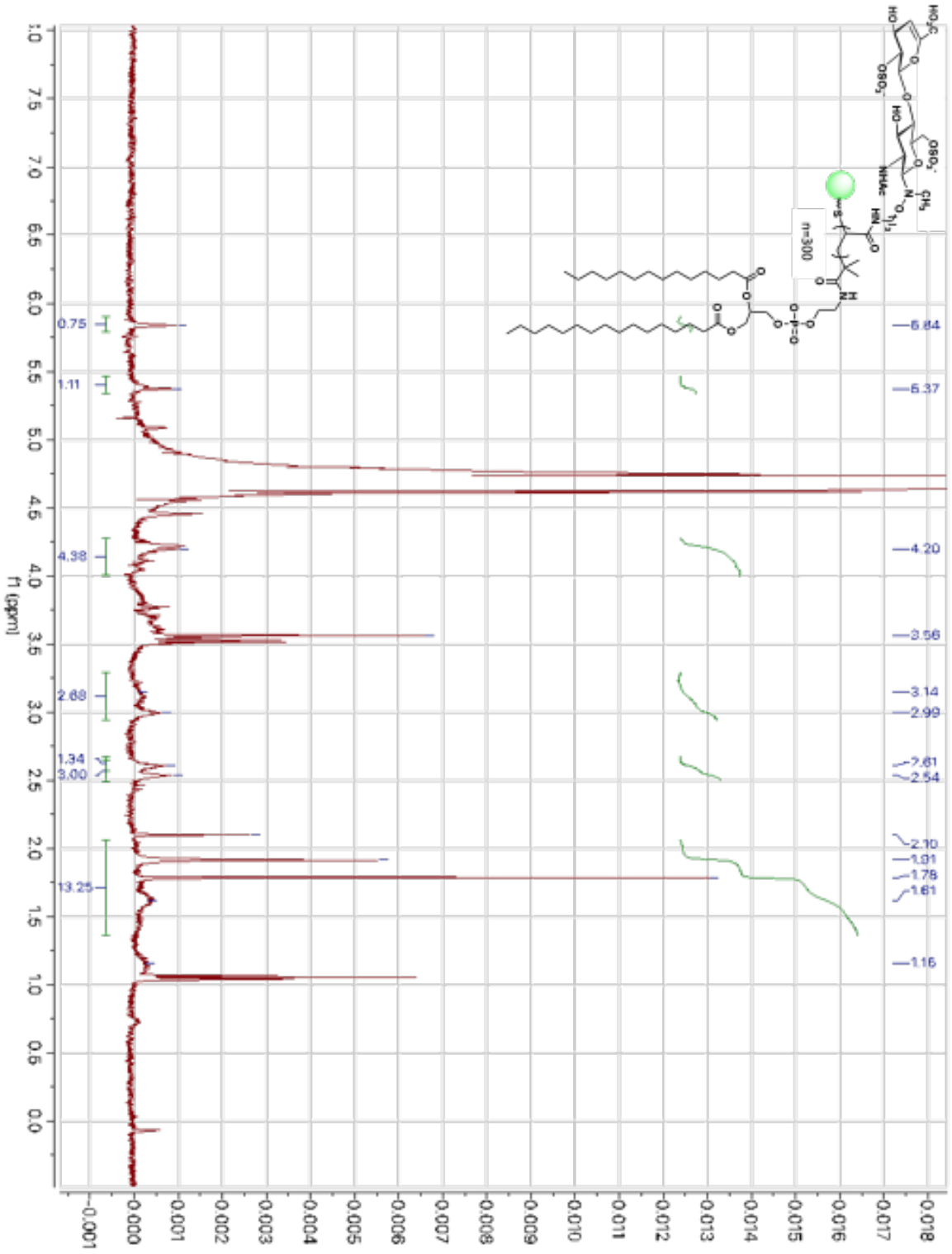

Figure 2.37. H NMR spectrum of **GP-L/D2A6** (300MHz, D_2O)

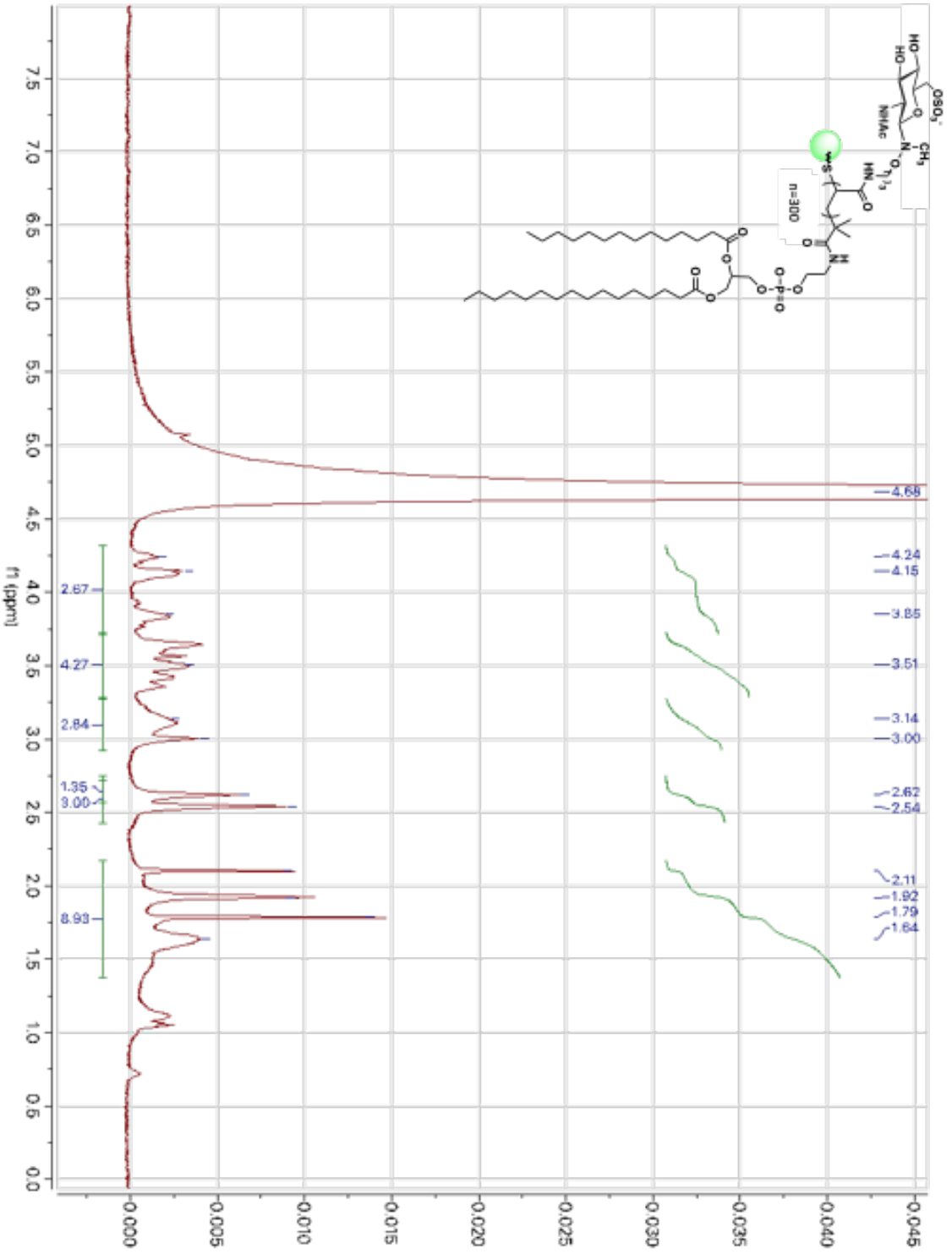

Figure 2.38. H NMR spectrum of **GP-L/GlcNAc6S** (300MHz, D_2O)

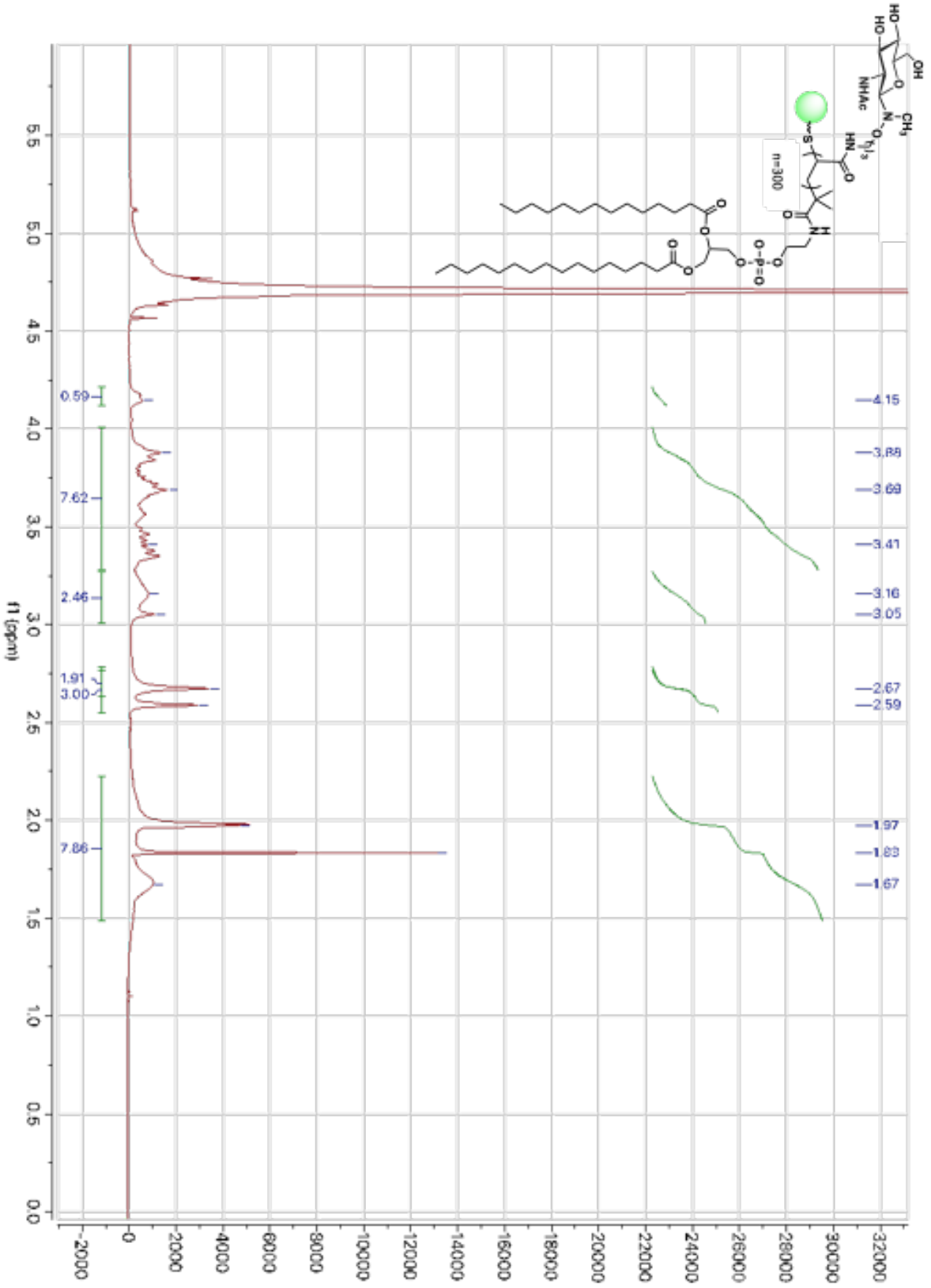

Figure 2.39. H NMR spectrum of **GP-L/GlcNAc** (300MHz, D_2O)

2.7 References

40. S. Moradi, H. Mahdizadeh, T. Šarić, J. Kim, J. Harati, H. Shahsavarani, B. Greber, J. B. Moore, Research and therapy with induced pluripotent stem cells (iPSCs): social, legal, and ethical considerations. *Stem Cell Research & Therapy*. **2019**, 10, 341.

41. T. Dvash, D. Ben-Yosef, R. Eiges, Human Embryonic Stem Cells as a Powerful Tool for Studying Human Embryogenesis. *Pediatr Res*. **2006**, 60, 111–117.

42. J. Bragança, J. A. Lopes, L. Mendes-Silva, J. M. Almeida Santos, Induced pluripotent stem cells, a giant leap for mankind therapeutic applications. *World J Stem Cells*. **2019**, 11, 421–430.

43. D. Antoni, H. Burckel, E. Josset, G. Noel, Three-dimensional cell culture: a breakthrough in vivo. *Int J Mol Sci*. **2015**, 16, 5517–5527.

44. J. Lee, M. J. Cuddihy, N. A. Kotov, Three-dimensional cell culture matrices: state of the art. *Tissue Eng Part B Rev*. **2008**, 14, 61–86.

45. A. M. Bratt-Leal, R. L. Carpenedo, T. C. McDevitt, Engineering the Embryoid Body Microenvironment to Direct Embryonic Stem Cell Differentiation. *Biotechnol Prog*. **2009**, 25, 43–51.

46. S. A. Ruiz and C. S. Chen, Emergence of patterned stem cell differentiation within multicellular structures, *Stem Cells*, **2008**, 26, 2921–2927.

47. Y. Sasai, Next-generation regenerative medicine: organogenesis from stem cells in 3D culture, *Cell Stem Cell*, **2013**, 12, 520–530.

48. J. A. Brassard and M. P. Lutolf, Engineering Stem Cell Selforganization to Build Better Organoids, *Cell Stem Cell*, **2019**, 24, 860–876.

49. P. Samal, C. van Blitterswijk, R. Truckenmüller and S. Giselbrecht, Grow with the Flow: When Morphogenesis Meets Microfluidics, *Adv. Mater.*, **2019**, 31, e1805764.

50. Y. S. Torisawa, B. H. Chueh, D. Huh, et al.,Efficient formation of uniform-sized embryoid bodies using a compartmentalized microchannel device, *Lab Chip*, **2007**, 7, 770776.

51. W. T. Fung, A. Beyzavi, P. Abgrall, N. T. Nguyen and H. Y. Li, Microfluidic platform for controlling the differentiation of embryoid bodies, *Lab Chip*, **2009**, 9, 2591–2595.

52. S. Gerecht, J. A. Burdick, L. S. Ferreira, S. A. Townsend, R. Langer and G. Vunjak-Novakovic, Hyaluronic acid hydrogel for controlled self-renewal and differentiation of human embryonic stem cells, *Proc. Natl. Acad. Sci*. U. S. A., **2007**, 104, 11298–1130

53. 14 K. A. Mosiewicz, L. Kolb, A. J. van der Vlies, et al., In situ cell manipulation through enzymatic hydrogel photopatterning, *Nat. Mater.*, **2013**, 12, 1072–1078.

54. A. P. Van Winkle, I. D. Gates and M. S. Kallos, Mass transfer limitations in embryoid bodies during human embryonic stem cell differentiation, *Cells Tissues Organs,* **2012**, 196, 34–47.

55. R. L. Carpenedo, A. M. Bratt-Leal, R. A. Marklein, et al., Homogeneous and organized differentiation within embry oid bodies induced by microsphere-mediated delivery of small molecules, *Biomaterials*, **2009**, 30, 2507–2515.

56. L. Ferreira, T. Squier, H. Park, H. Choe, D. S. Kohane and R. Langer, Human embryoid bodies containing nano– and microparticulate delivery vehicles, *Adv. Mater.,* **2008**, 20, 2285–2291.

57. A. M. Bratt-Leal, A. H. Nguyen, K. A. Hammersmith, A. Singh and T. C. McDevitt, A microparticle approach to morphogen delivery within pluripotent stem cell aggregates, *Biomaterials*, **2013**, 34, 7227–7235.

58. D. Xu and J. D. Esko, Demystifying heparan sulfate-protein Interactions, *Annu. Rev. Biochem*., **2014**, 83, 129–157.

59. D. C. Kraushaar, S. Dalton and L. Wang, Heparan sulfate: a key regulator of embryonic stem cell fate, *Biol. Chem*., **2013**, 394, 741–751.

60. G. J. Sheng, Y. I. Oh, S. K. Chang and L. C. Hsieh-Wilson, Tunable heparan sulfate mimetics for modulating chemokine activity, *J. Am. Chem. Soc*., **2013**, 135, 10898–10901.

61. R. S. Loka, E. T. Sletten, U. Barash, I. Vlodavsky and H. M. Nguyen, Specific Inhibition of Heparanase by a Glycopolymer with Well-Defined Sulfation Pattern Prevents Breast Cancer Metastasis in Mice, *ACS Appl Mater Interfaces*, **2019**, 11, 244–254.

62. M. L. Huang, R. A. Smith, G. W. Trieger and K. Godula, Glycocalyx remodeling with proteoglycan mimetics promotes neural specification in embryonic stem cells, *J. Am. Chem. Soc*., **2014**, 136, 10565–10568.

63. R. Lawrence, H. Lu, R. D. Rosenberg, J. D. Esko and L. Zhang, Disaccharide structure code for the easy representation of constituent oligosaccharides from glycosaminoglycans, *Nat. Methods*, **2008**, 5, 291–292.

64. G. Moad, E. Rizzardo and S. H. Thang, Living Radical Polymerization by the RAFT Process - A Second Update, *Aust. J. Chem.,* **2009**, 62, 1402–1472.

65. F. Peri, P. Dumy and M. Mutter, Chemo- and stereoselective glycosylation of hydroxylamino derivatives: A versatile approach to glycoconjugates, *Tetrahedron*, **1998**, 54, 12269–12278.

66. D. Lombardo, M. A. Kiselev, S. Magazù and P. Calandra, Amphiphiles Self-Assembly: Basic Concepts and Future Perspectives of Supramolecular Approaches, *Adv. Condens. Matter Phys*., **2015**, e151683.

67. D. C. Kraushaar, Y. Yamaguchi and L. Wang, Heparan sulfate is required for embryonic stem cells to exit from self-renewal, *J. Biol. Chem*., **2010**, 285, 5907–5916.

68. I. Raitman, M. L. Huang, S. A. Williams, B. Friedman, K. Godula and J. E. Schwarzbauer, Heparin-fibronectin interactions in the development of extracellular matrix insolubility, *Matrix Biol.,* **2018**, 67, 107–122.

69. M. Koike, S. Sakaki, Y. Amano and H. Kurosawa, Characterization of embryoid bodies of mouse embryonic stem cells formed under various culture conditions and estimation of differentiation status of such bodies, *J. Biosci. Bioeng*., **2007**, 104, 294–299.

70. Y. H. Chen, Y. Narimatsu, T. M. Clausen, et al., The GAGOme: a cell-based library of displayed glycosaminoglycans, *Nat. Methods*, **2018**, 15, 881–888;

71. H. Qiu, S. Shi, J. Yue, et al., A mutant-cell library for systematic analysis of heparan sulfate structure-function relationships, *Nat. Methods*, **2018**, 15, 889–899.

72. J. S. Chua and B. Kuberan, Synthetic Xylosides: Probing the Glycosaminoglycan Biosynthetic Machinery for Biomedical Applications, *Acc. Chem. Res*., **2017**, 50, 2693–2705.

73. Carrasco, M. R.; Alvarado, C. I.; Dashner, S. T.; Wong, A. J.; Wong, M. A. Synthesis of aminooxy and N-alkylaminooxy amines for use in bioconjugation. *J. Org. Chem*. **2010**, *75*, 5757-5759.

74. Godula, K.; Umbel, M. L.; Rabuka, D.; Botyanszki, Z.; Bertozzi, C. R.; Parthasarathy, R. Control of the molecular orientation of membrane-anchored biomimetic glycopolymers. *J. Am. Chemn. Soc.* **2009**, *131*, 10263–10268.

75. Peterson, A. M.; Tan, Z.; Kimbrough, E. M.; Heemstra, J. M. 3,3′-Dioctadecyloxacarbocyanine per- chlorate (DiO) as a fluorogenic probe for measurement of critical micelle concentration. *Anal. Methods*. **2015**, 7, 6877–6882.

76. Koike, M.; Sakaki, S.; Amano, Y.; Kurosawa, H. Characterization of Embryoid Bodies of Mouse Em- bryonic Stem Cells Formed under Various Culture Conditions and Estimation of Differentiation Status of Such Bodies. *J. Biosci. Bioeng*. **2007**, *104*, 294–299.

3 Embryonic Stem Cell Engineering with a Glycomimetic FGF2/BMP4 Co-Receptor Drives Mesodermal Differentiation in a Three-Dimensional Culture

3.1 Introduction

Embryonic stem cells (ESCs) isolated from developing embryos at the blastocyst stage are characterized by their pluripotency, an ability to undergo differentiation into all three primary germ layers: ectoderm, mesoderm, and definitive endoderm. Subsequently, these precursor cells can go on to produce the complete repertoire of cell types of the adult body.[1] As such, ESCs have been the focus of intense research to delineate the molecular mechanisms that govern their differentiation and to exploit these processes for therapeutic gain.[2] Murine ESCs (mESCs), which can be readily interrogated using genetic methods, have served as an important model for mapping the signaling pathways underlying early mammalian development and have provided useful tools for testing new approaches to harness the regenerative potential of stem cells.

The current model for germ layer specification in mESCs identifies members of the fibroblast growth factor (FGF), bone morphogenetic protein (BMP), and Wingless (Wnt) protein families as key regulators of this process (Figure 3.1).[1,4,5] Activation of the MAPK pathway by FGF2 is required for differentiation toward nestin^{+ive} neural precursor cells (NPCs) and β-III-tubulin^{+ive} neurons.6 The FGF signaling pathway, in conjunction with the Wnt and BMP pathways, is also required to induce mesodermal differentiation.[1,7,8] The emergence of nascent mesoderm is associated with the expression of the Tbox transcription factor, Brachyury, which is subsequently downregulated as the cells migrate and differentiate further (Figure 3.1A). The reemergence of Brachyury expression[7] together with fetal liver kinase (Flk1) at a later time point marks the formation of the

hemangioblast, which subsequently produces endothelial and hematopoetic cells.9 In culture, BMP4, via the Smad protein signaling pathway, downregulates FGF and Wnt signaling, suppresses neuroectoderm formation, and drives mESCs toward mesoderm, pointing to the importance of spatial and temporal regulation of BMP4 activity during development.[10,11]

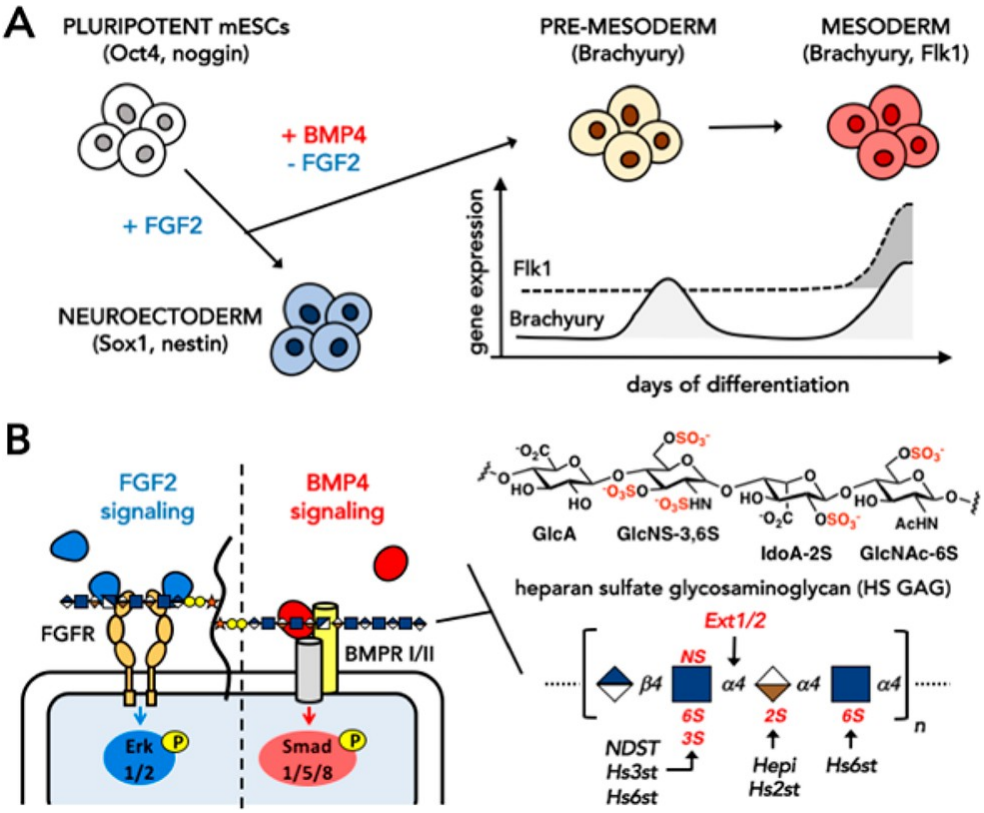

Figure 3.1. Growth factor signaling mediates mesodermal differentiation in mESCs. (A) BMP4 attenuates FGF2 signaling after initial exit of mESCs from the pluripotent state and drives differentiation toward early Brachyury+ive mesodermal precursors. Further mesodermal differentiation produces hemangioblast co-expressing both Brachyury and Flk1 markers. (B) Cell surface HS polysaccharides are required as co-receptors for both FGF2 and BMP4 to activate signal transduction. The enzymatic assembly of sulfated regions within HS.

While the coordinated expression of the FGF, Wnt, and BMP proteins provides one such control mechanism, the extracellular matrix and the cellular glycocalyx serve as coregulators in this process. In particular, heparan sulfate glycosaminoglycans (HS

GAGs) have been identified as a class of glycans involved in spatial patterning of growth factors and facilitating signal transduction at the cell surface.[12−14]

HS GAGs are polysaccharides attached to core polypeptides of proteoglycans containing sulfated regions that harbor binding sites for various growth factors and their receptors (Figure 1B).[15] The biosynthesis of HS is accomplished by the action of a heterodimeric complex of exostosin 1 and 2 (Ext1/ 2) glycotranferases, which promotes the addition of alternating N-acetylglucosamine (GlcNAc) and glucuronic acid (GlcA) residues to the growing polysaccharide chain. The GAG polymer is acted upon by a complex of N-deacetylase and N-sulfotransferase (NDST) enzymes that initiate the formation of the sulfated protein binding regions. Further elaboration by epimerases (Hepi) converting GlcA residues into iduronic acids (IdoA) and 2-, 3-, and 6-O-sulfotransferases (Hs2st, Hs3st, and Hs6st, respectively) then fine-tunes the composition of the sulfated domains, thus providing a structural basis for selectivity in protein recognition.[12,16]

Genetic manipulation of HS biosynthesis has illuminated the essential contributions of these biomolecules in embryonic development. Embryos produced from mice lacking the Ext1/2 glycotransferases fail to undergo gastrulation.17,18 This observation is mirrored in vitro, where Ext1−/− mESCs are restricted in their ability to exit the pluripotent state and differentiate into nestin^{+ive} NPCs, indicating the requirement for HS structures for proper FGF signaling.[19−21] BMP signaling and mesoderm differentiation are likewise impaired in these cells, showing delayed or absent expression of differentiation markers.22−24 In an embryoid body (EB) culture, under conditions that recapitulate the mesoderm differentiation process,[25] Ext1$^{-/-}$ mESCs showed elevated

Brachyury expression levels but did not express Flk1 and failed to form the hemangioblast.[23] Bypassing the requirement for HS in FGF signaling and lineage commitment using high concentrations of FGF2 partially restored differentiation of Ext1$^{-/-}$ mESCs into endoderm and nestin^{+ive} NPCs; however, this treatment failed to produce mesodermal cell types.[22] The mesodermal differentiation defect in Ext1$^{-/-}$ mESCs was attributed to the disruption in FGF and BMP, but not Wnt, signaling due to the absence of functional HS.

Soluble HS and heparin can restore differentiation in Ext1$^{-/-}$ mESCs. Experiments employing chemically and enzymatically altered heparinoids have provided insights into the structural requirements for HS in differentiation.[20,23,26,27] For instance, high levels of sulfation (NS, 2S, 6S) generally support the activity of both FGF2 and BMP4; however, the latter was shown to require extended heparin oligosaccharide sequences (DP of 12−20),[23] while relatively short HS chains (DP of ∼6) were sufficient to promote FGF2 signaling.[28] In addition, an increased stability of BMP4 was observed when soluble heparin was present during differentiation, suggesting a possible dual role for HS GAGs in co-reception of the signal at the cell surface and in protection against proteolytic degradation.[22]

Engineering of the stem cell glycocalyx with synthetic HS co-receptors has emerged as a strategy to control this process,[29−31] providing several advantages over the use of soluble heparin and heparinoid structures, which lack structurally well-defined growth factor binding sites and have to be introduced into a culture continuously throughout differentiation. In addition, exogenous heparinoids need to be applied over a

narrow concentration range, above which they can inhibit signaling activity via sequestration of growth factors away from the cell surface.[19,23,32]

In a recent example, chemically prefunctionalized heparinoids were covalently attached to proteins in the membranes of wild type mESCs via a genetically engineered halo tag.29 This approach, in conjunction with the removal of endogenous HS structures through heparinase treatment, provided a long-term remodeling of the glycocalyx and enhanced differentiation of mESCs toward NPCs and β-III-tubulin^{+ive} neurons. We have shown that HS glycomimetic co-receptors with affinity for FGF2, and carrying phospholipid anchoring units, could be introduced transiently ($t_{1/2}$ ∼9 h) into the glycocalyx of Ext1$^{-/-}$ mESCs, where they reconstituted signaling through MAPK activation via the FGF2/FGF receptor (FGFR) complex and restored differentiation toward neuroectoderm and nestin^{+ive} NPCs.[30]

In this study, we report that glycomimetic co-receptors with dual FGF2 and BMP4 activity allow for the exit of Ext1$^{-/-}$ mESCs from their pluripotent state toward Brachyury^{+ive}/ Flk1^{+ive} mesoderm in an EB culture, via the Smad protein signaling cascade. This study provides new evidence of the utility of glycocalyx engineering in manipulating the outcomes of the stem cell differentiation process.

3.2 Results

Considering the role of HS in promoting FGF and BMP signaling during mesodermal differentiation, we reasoned that a functional synthetic co-receptor for these proteins should include HS fragments capable of binding to both FGF2 and BMP4. The structural requirements for HS function in FGF2 binding and signaling have now been reasonably established,[33,34] with relatively short (DP of ∼6) fragments with high levels of N-sulfation and 2-O-sulfation having been identified as being necessary for FGF2 binding

with an additional 6-O-sulfate required for signaling. The structural requirements for HS in BMP4 signal transduction are still rather poorly defined.[35,36] While no HS binding site has been identified within the heterodimeric BMP receptor I and II (BMPR I/II) complex, the BMP4 protein is retained on a heparin affinity column indicating the presence of an HS recognition domain.[37−39] The HS binding domain is thought to reside in the disordered N-terminal region of BMP4,[40] complicating the crystallographic analysis of HS−BMP4 interactions. However, unlike the case for FGF2, evidence points to the requirement for longer (DP of >12) fragments of HS in BMP4 signaling.[23]

We set out to delineate the fine HS structure responsible for high-avidity binding of BMP4; therefore, we analyzed the interactions of this protein toward an array of chemoenzymatically derived HS oligosaccharides [HS 1−24 (Fig. 3.2)]. The array contained oligosaccharides ranging from tetrasaccharides to nonasaccharides with well-defined sulfation patterns. While we observed minimal binding of BMP4 to oligosaccharides devoid of sulfation (HS 1−6) or carrying only N-sulfated motifs (HS 7−12), the introduction of additional 2-O- and 6O-sulfation (HS 13−16 and HS 17−19, respectively) resulted in enhanced binding of BMP4 to the HS structures. Octasaccharides containing a combination of N-, 2-O-, and 6-O-sulfation motifs (HS 20−22) exhibited the strongest association with BMP4 according to their increasing level of sulfation. Interestingly, inclusion of a 3-O-sulfation modification (HS 24) led to weakened BMP4 binding despite the octasaccharide's higher negative charge density.

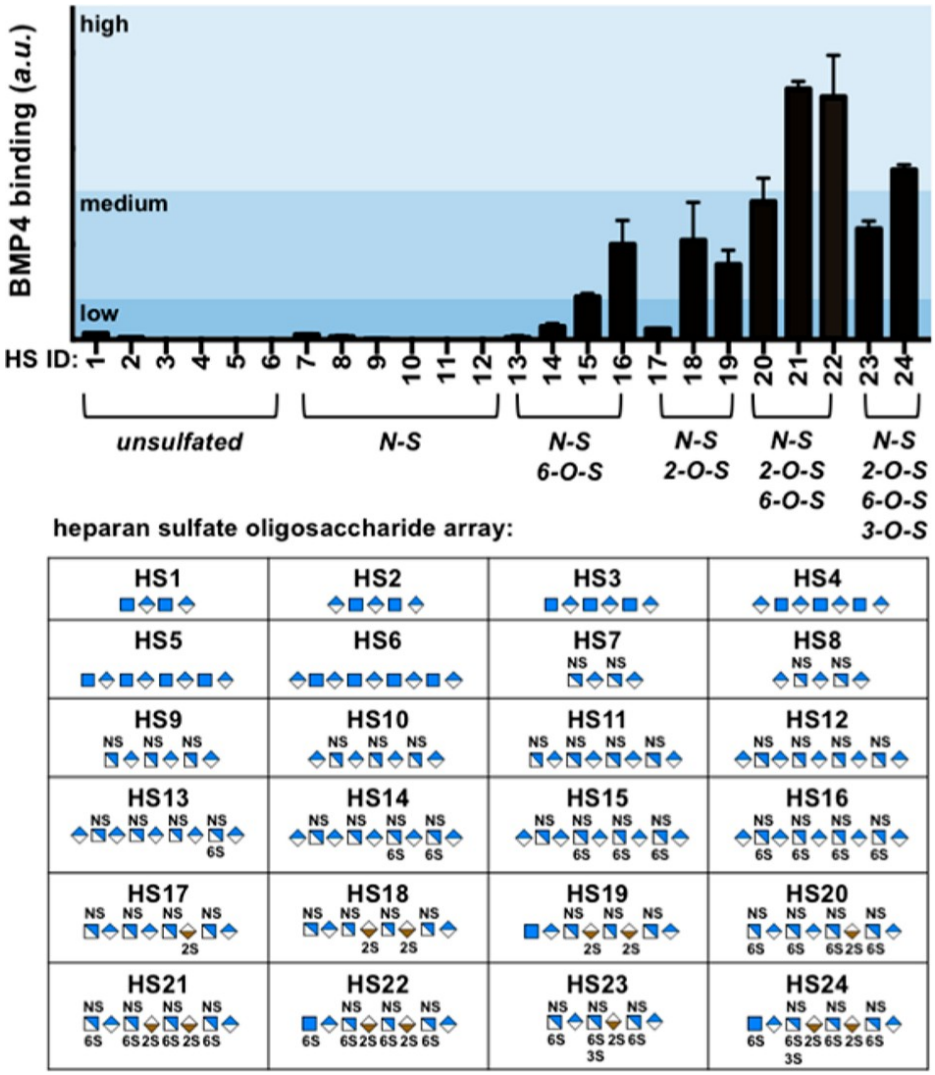

Figure 3.2. Analysis of interactions of BMP4 with chemically defined HS oligosaccharides. BMP4 exhibits a preference for binding to HS oligosaccharides with high-charge density regions containing combinations of N-, 2-O-, and 6-O-sulfation modifications. Addition of 3-Osulfate attenuates BMP4 binding.

With a clearer picture of the structural requirements for binding of HS to BMP4, we set out to generate a synthetic HSmimetic glycopolymer co-receptor with dual FGF2 and BMP4 activity capable of supporting mesodermal differentiation in Ext1$^{-/-}$ mESCs. Previously, we have produced a library of glycopolymers using an HS fragment-based strategy, where differentially sulfated HS disaccharides derived by heparinase depolymerization of HS polysaccharides were conjugated to polyacrylamide scaffolds.[30]

These HS fragments were conjugated to polymer side chains containing N-methylaminooxy functionality reactive toward the disaccharides' reducing end. While GAG disaccharides alone do not show a high affinity for growth factors, their multivalent presentation achieved by glycopolymers can reconstitute the activity of their parent GAGs.[41,42] From our initial library, two polymer structures containing disaccharides sulfated in both 2-O- and 6-Opositions with additional N-acetamido or N-sulfo modifications emerged (D2A6 and D2S6,[43] respectively) that exhibited high affinity for FGF2.[30] Both polymers also showed the ability to enhance MAPK signaling via the FGF2/FGFR complex and initiate neuroectodermal differentiation when introduced into the glycocalyx of Ext1$^{-/-}$ mESCs using passive membrane insertion via a phospholipid anchor. While both D2A6 and D2S6 disaccharides exhibited overlapping FGF2 binding profiles, the former afforded higher-valency conjugates with improved biological activities.

On the basis of our array binding data indicating the requirement of 2-O- and 6-O-sulfation for high-affinity binding to BMP4, we assessed the ability of the D2A6-modified polymer to engage this protein. Using RAFT polymerization, we have synthesized a biotinylated D2A6 glycopolymer, **P1-D2A6** (Fig. 3.3A; DP = 200; Đ = 1.19; valency = 155).

In addition, we prepared a control polymer containing the 6-Osulfated monosaccharide N-acetylglucosamine, **P1-GlcNAc6S** (Fig. 3.3A; DP = 200; Đ = 1.19; valency = 177), which was not expected to engage BMP4 despite its highly anionic character. We tested both polymers for their binding to BMP4 using a capture enzyme-linked immunosorbent assay (ELISA). I n this assay, BMP4 was immobilized via its antibody to

the plate surface and the binding of soluble biotinylated polymers P1 was detected using horseradish peroxidase (HPR) conjugated to streptavidin and the chromogenic reagent 3,3′,5,5′-tetramethylbenzidine (TMB). As anticipated, the **P1-D2A6**, but not **P1-GlcNAc6S**, polymer showed strong association with the immobilized BMP4 protein (EC_{50} =14 nM) , which was comparable to that of a biotinylated heparin control (EC_{50} = 13 nM) (Fig. 3.3B) . We used a similar assay to also confirm the binding of the polymers to FGF2 (Fig. 3.X), with both **P1-D2A6** and heparin showing similar binding affinities (EC_{50} values of 7 and 6 nM, respectively). These data demonstrate that the synthetic glycopolymer **P1-D2A6** successfully recapitulates the binding interactions between the natural HS polysaccharide and both BMP4 and FGF2 proteins in a glycan- and sulfation-dependent manner, while **P1-GlcNAc6S** does not engage either protein to an appreciable degree.

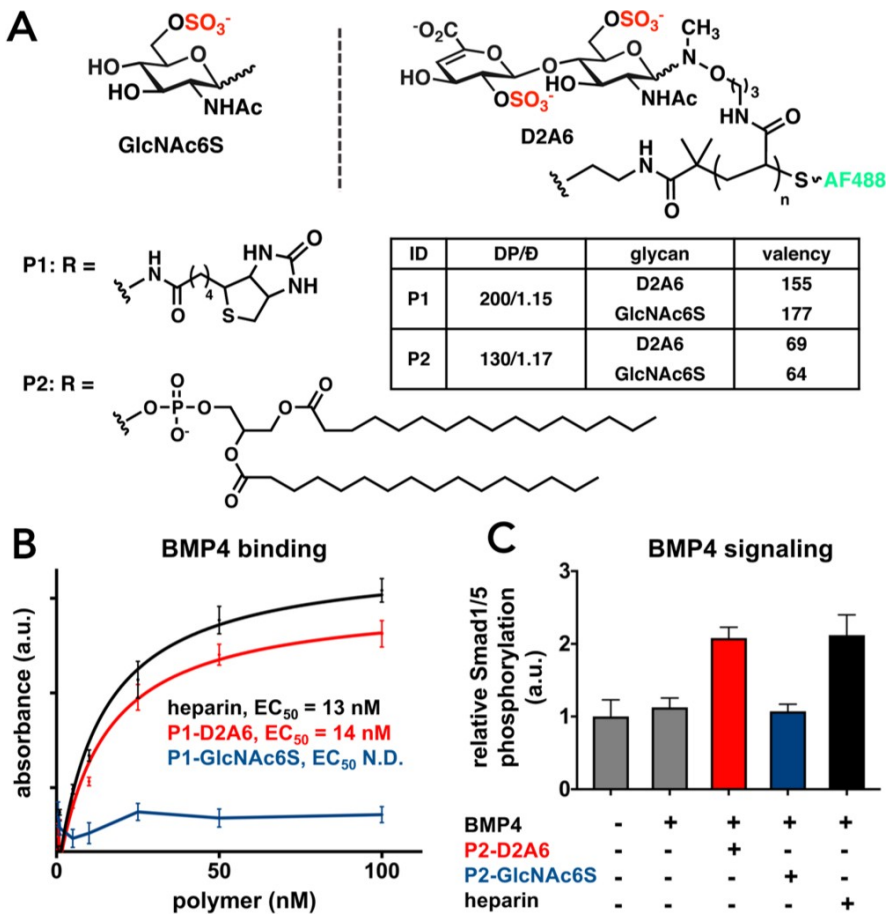

ID	DP/Đ	glycan	valency
P1	200/1.15	D2A6	155
		GlcNAc6S	177
P2	130/1.17	D2A6	69
		GlcNAc6S	64

Figure 3.3. Synthetic HS-mimetic glycopolymers act as functional coreceptors for BMP4. (A) Glycopolymers with low dispersity indices (Đ < 1.20) containing biotin (**P1**; DP = 200) or phospholipid (**P2**; DP = 130) modifications and bearing 2-O- and 6-O-sulfated HS disaccharides (D2A6) or N-acetylglucosamine 6-O-sulfate monosaccharides (GlcNAc6S) were generated via the RAFT technique. (B) In an enzyme-linked immunosorbent assay, HS-mimetic glycopolymer **P1-D2A6** exhibited binding to surface-immobilized BMP4 comparable to that of heparin (EC50 values of 14 and 13 nM, respectively). Glycopolymer **P1-GlNAc6S** showed a low affinity for BMP4. (C) Remodeling of Ext1$^{-/-}$ mESCs with lipid-conjugated glycopolymer **P2-D2A6**, but not **P2-GlcNAc6s**, enhances phosphorylation of Smad1/5 proteins in response to stimulation with BMP4. Reactivation of the Smad signaling pathway is also observed in the presence of soluble heparin (1 μg).

We have previously demonstrated the ability of the D2A6carrying glycopolymers to act as functional co-receptors for FGF2 in the activation of the MAPK pathway in Ext1−/− mESCs.30 To test whether the binding of BMP4 to P1-D2A6 may similarly translate to signaling activity in these cells, we synthesized membrane-targeting polymer analogues P2-D2A6 and P2-GlcNAc6S containing phospholipid anchors (Figure 3A; DP = 130; Đ = 1.17; valencies of 69 and 64, respectively) and monitored effects on Smad

protein phosphorylation downstream of BMP4 receptors I and II after glycocalyx remodeling. Ext1$^{-/-}$ mESCs in a monolayer culture were first remodeled with polymers **P2** by incubation (3 μM) for 1 h at 37°C. The cells were washed to removed unbound polymers and stimulated with BMP4 (2 ng) for 2 h. Conditions containing untreated cells and cells stimulated in the presence of heparin (1 μg) were included as negative and positive controls, respectively. After stimulation, cell lysates were collected and changes in levels of Smad1/5 phosphorylation (normalized to the Smad1 total protein concentration) were assessed using an ELISA (Figure 3B). The Ext1−/− mESCs remodeled with polymer P2-D2A6 or in the presence of soluble heparin (1 μg) showed a 2-fold enhancement of Smad1/5 phosphorylation compared to cells remodeled with **P2-GlcNAc6S** and in an untreated control (Fig. 3.3C), indicating that polymer **P2-D2A6** can act as a co-receptor for BMP4 at the surface of Ext1$^{-/-}$ mESCs and allow for signal transduction via the Smad signaling pathway. Thus, **P2-D2A6** should be able to support mesodermal formation in an Ext1$^{-/-}$ EB culture by, first, facilitating activation of FGF2 signaling and exit from the pluripotent state and by mediation of the BMP4 response to drive further mesodermal differentiation.

We set out to establish a protocol for glycocalyx remodeling with polymers **P2** in the three-dimensional EB structures[44] derived from Ext1$^{-/-}$ mESCs to test this hypothesis. During EB formation, the outer layer cells form close contacts and deposit extracellular matrix proteins creating a dense shell, which can pose a challenge for the delivery of materials into the inner core of the structures.[45,46] To ensure full incorporation of the glycopolymers throughout the EB structures, we optimized the remodeling conditions with respect to polymer concentration and incubation time and used confocal microscopy to

monitor the distribution of the fluorescently labeled (AF488) polymers (Fig. 3.4A). We observed a concentration-dependent polymer distribution across the EB structure (Fig. 3.X), with full penetration achieved for both polymers (3 μM) after 2 h at 37 °C. The outer EB regions showed increased brightness, likely due to both the higher number of compacted cells forming the EB shell and the increase in the level of ECM protein deposition leading to polymer retention and accumulation. To ensure that remodeling occurred through membrane insertion of the lipidated glycopolymers rather than their physical retention within the EB structure, EBs were dissociated with Accutase and the cells were analyzed via flow cytometry for the presence of the fluorescent polymer marker (AF488). A robust and equivalent increase in cell fluorescence was observed for both polymers P2 (Fig. 3.4C), indicating similar levels of incorporation of the polymers into the EBs regardless of their glycan structure.

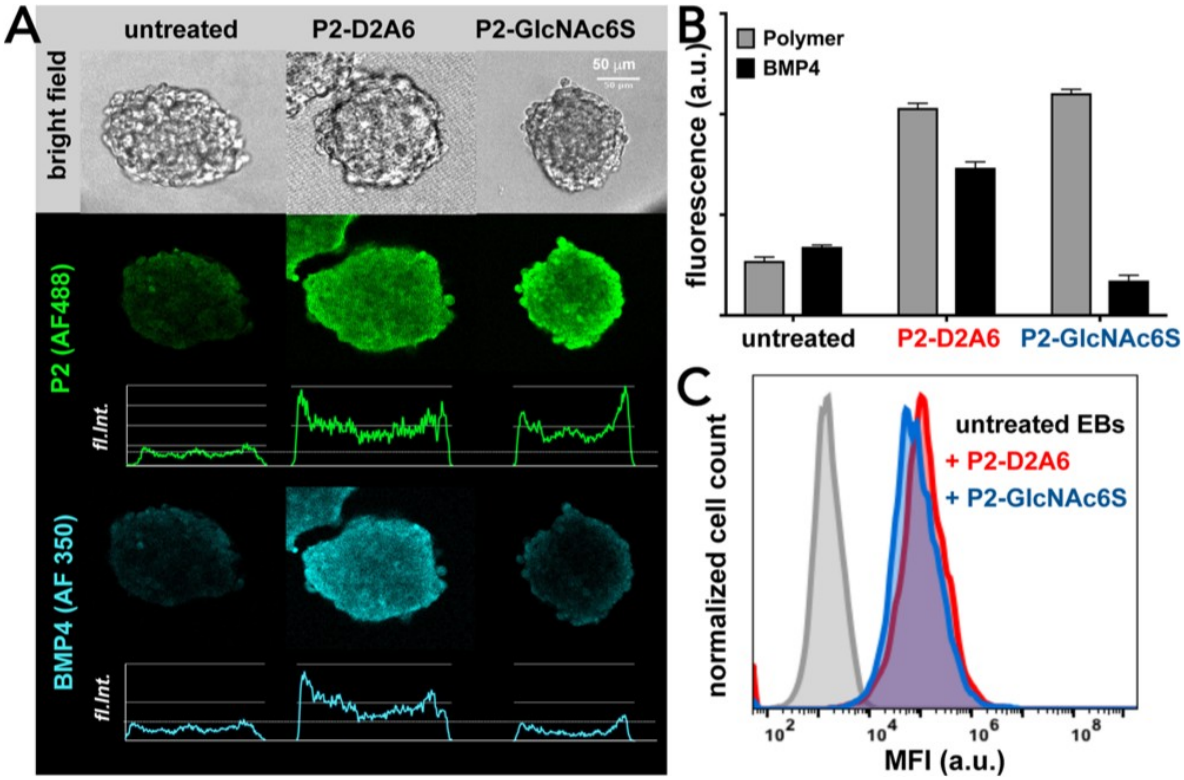

Figure 3.4. Glycocalyx engineering of Ext1$^{-/-}$ mESC embryoid bodies (EBs) with HS-mimetic glycopolymers P2. (A) Micrographs of day 0 EBs treated with AF488-labeled polymers **P2** show extensive remodeling with both polymers (3 μM, 2 h, 37 °C) independent of glycan structure (green). Only remodeling with polymer **P2-D2A6** provided an enhanced afffinity of BMP4 for the cell surface, as visualized by immunostaining with the AF350-labeled anti-BMP4 antibody (teal). (B) Total mean fluorescence intensity of polymers **P2** (AF488) and the anti-BMP4 antibody (AF350) measured at the midpoint of EB structures (n = 10) by confocal microscopy. (C) Total mean fluorescence intensity of cells remodeled with AF488-labeled polymers **P2** measured by flow cytometry after EB dissociation.

Next, we assessed the effects of incorporation of glycopolymers P2 within the EB structures on BMP4 association. The EBs were fixed and then incubated with BMP4 (100 nM, 18 h, 4°C), and the localization of the protein was visualized after immunofluorescence staining (Fig. 3.4A,B). Confocal microscopy indicated co-localization of the BMP4 and **P2-D2A6** signals. No enhancement in BMP4 binding was observed for EBs remodeled with polymer **P2-GlcNAc6S** compared to that of polymer-untreated EBs, which is in agreement with the BMP4 binding profiles of polymers **P1** determined by an ELISA (Fig. 3.3B). Thus, glycopolymer **P2-D2A6** can be effectively

diffused throughout the three-dimensional EB structure and provide binding sites for BPM4 within the Ext1$^{-/-}$ mESC glycocalyx. Having established that polymer **P2-D2A6** can act as a functional co-receptor for both FGF2 and BMP4 proteins and facilitate signal transduction through their associated MAPK and Smad signaling pathways, respectively, we next tested its ability to support mesodermal differentiation in Ext1$^{-/-}$ mESCs. Mesodermal differentiation in wild type mESCs in an EB culture is characterized by a rapid loss of pluripotency markers (i.e., SSEA-1, Oct4, or Noggin) and the emergence of mesodermal markers, such as Brachyury, at approximately day 2−3 of differentiation.[8] The Brachyury message is then transiently attenuated, until it reappears together with the expression of the kinase, Flk1, and they together mark the emergence of the hemangioblast.[7,23]

To test whether the remodeling of Ext1$^{-/-}$ EBs with synthetic FGF2/BMP4 co-receptor **P2-D2A6** may drive mesodermal commitment, we remodeled EBs with both polymers **P2** at day 0 of differentiation, after removing leukemia inhibitory factor from the medium and allowing EBs to form for 2 days (days −2 to 0). Conditions including polymer-untreated EBs and EBs differentiated in the presence of soluble heparin (1 μg), which has been demonstrated to restore HS-dependent signaling in Ext1$^{-/-}$ mESCs,[23] were included as negative and positive controls, respectively.

Differentiation was monitored in glycocalyx-remodeled EBs by collecting lysates over 10 days and assessing the mRNA expression patterns of embryonic, mesodermal, and neuroectodermal markers using reverse transcription quantitative polymerase chain reaction (RT-qPCR) analysis (Fig. 3.5). As expected, we observed rapid loss of the expression of embryonic markers *oct4*, *sox2*, and *noggin* under all conditions (Fig. 3.5

and Fig. 3.14) and the emergence of the *brachyury* marker by day 3 of differentiation, which was somewhat delayed in EBs treated with glycopolymer **P2-GlcNAc6S** (day 6, Fig. 3.5). *Brachyury* expression continued unabated (3−5-fold enhancement) in untreated EBs and EBs remodeled with **P2-GlcNAc6S**, which is characteristic for Ext1$^{-/-}$ mESCs lacking functional cell surface HS structures (Fig. 3.5 and Fig. 3.3.114). This message was downregulated by days 6 and 8 under conditions including soluble heparin (1 μg) and in EBs treated with polymer **P2-D2A6**, respectively, to reemerge again by day 10 of differentiation under both conditions concomitant with the expression of Flk1. Successful progress toward the formation of mesoderm under these conditions was corroborated by the progressive transcriptional upregulation of the *inhibitor of differentiation 1* (*id1*) factor, which is activated through BMP signaling and blocks neural differentiation.[11] In untreated EBs and EBs remodeled with **P2-GlcNAc6S**, expression of *flk1* and *id1* was absent throughout the course of differentiation, indicating their failure to successfully advance toward mesoderm. Closer examination of levels of transcripts for the neural markers *sox1*, *nestin*, and *fgf5* indicated some neural commitment[22,23,47] in EBs remodeled with polymers **P2-D2A6** and under conditions supplemented with heparin compared to EBs treated with **P2-GlcNAc6S** or in untreated control EBs. While the employed differentiation conditions are optimized to promote mesodermal differentiation in EBs, the formation of cell types associated with another germ layer is typically observed.[48]

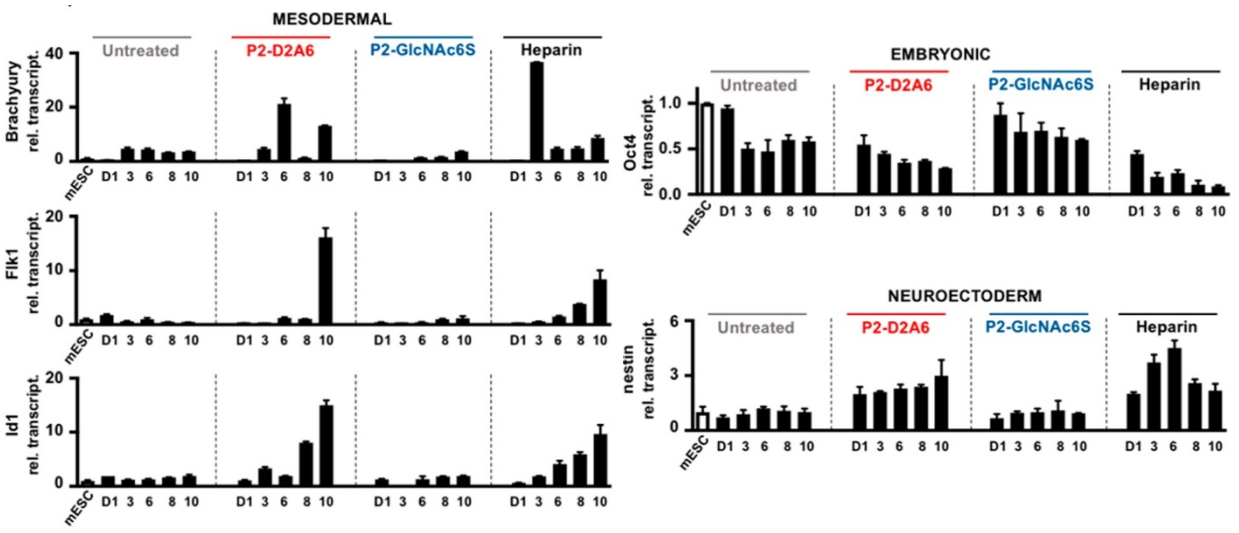

Figure 3.5. Mesodermal differentiation of Ext1$^{-/-}$ mESCs in an EB culture after glycocalyx remodeling with HS-mimetic glycopolymers P2. Relative transcriptional abundances of pluripotency (Oct4), mesodermal (Bachyury, Flk1, and Id1), and neuroectodermal (nestin) markers over 10 days of differentiation in an EB culture were determined by reverse transcription quantitative polymerase chain reaction (ΔΔCt; GAPDH and mESC). A rapid loss of pluripotency markers and the appearance of Brachyury expression were observed under all conditions. Only EBs remodeled with polymer P2-D2A6 (3 μM) or cultured in the presence of soluble heparin (1 μg) showed attenuation of Brachyury expression after day 6 or 3, respectively. Under these conditions, the Brachyury message reemerged together with the onset of medosdermal Flk1 marker expression by day 10 of differentiation.

The gene expression changes in EBs observed by RT-qPCR analysis were confirmed by the detection of cell surface markers of mesodermal formation (Flk1) and pluripotency (SSEA1) at day 10 of differentiation. EBs were dissociated with Accutase, and the cells were immunostained with AlexaFluor647 (AF647)-conjugated primary antibodies against either Flk1 or the embryonic marker, SSEA1, and analyzed using flow cytometry (Figure 6). In agreement with embryonic marker expression profiles detected by RT-qPCR analysis, we observed a significant decrease in the level of SSEA1 under all conditions compared to that of cells maintained in an embryonic culture (Figure 6, left), while only EBs differentiated in the presence of **P2-D2A6** or heparin produced Flk1^{+ive} cell populations [27 or 34%, respectively (Figure 6, right)].

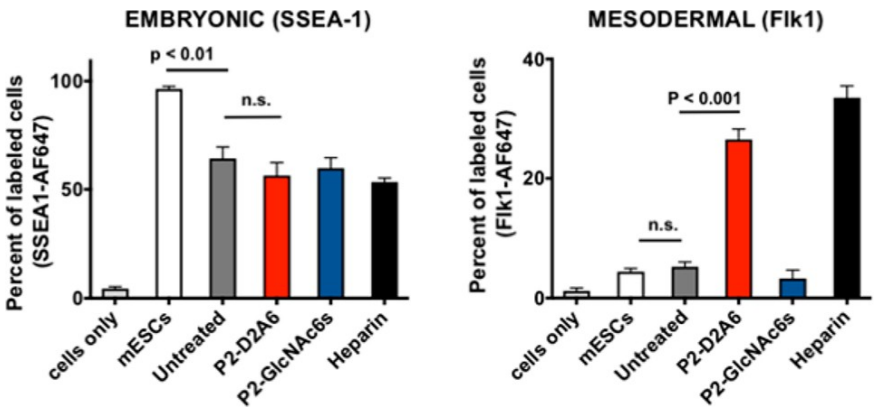

Figure 3.6. Expression of embryonic and mesodermal cell surface markers in glycocalyx-remodeled EBs on day 10 of differentiation. All conditions saw a significant decrease in the level of cell surface pluripotency marker SSEA1 as detected after immunostaining by flow cytometry in cells dissociated from day 10 EBs. Elevated levels of Flk1 protein expression were detected in cells from day 10 EBs only after remodeling with **P2-D2A6** (3 μM) or cultured in the presence of soluble heparin (1 μg).

3.3 Conclusions

Cell surface and extracellular matrix glycans, such as HS GAGs, have been increasingly identified as co-regulators of growth factor signaling during early development.[14,36,49] While current in vitro approaches for recapitulating the developmental process to derive specialized cells for therapeutic applications from isolated or induced pluripotent cells focus primarily on mapping the combinations of factors and their associated signaling pathways needed to guide the differentiation process, the contributions of glycans often remain unexplored and underutilized.[50,51]

The ubiquitous and tightly regulated expression of cell surface HS GAGs accompanies embryonic development and is characterized by alterations in the fine structures of their sulfated regions,[13,19] which serve as recognition elements for a large number of signaling proteins and their receptors. As such, these glycans offer a unique target for manipulating the cell differentiation process. While in limited instances the HS GAG structure−activity relationships have been delineated (e.g., in the organization of the

FGF2/FGFR signaling complex),[33] in many cases molecular level details of interactions of HS with proteins, including BMP4, are still lacking. Despite the yet incomplete understanding of selectivity in HS−protein interactions, chemical methods for manipulating the stem cell glycocalyx to harness HS functions and gain control over cellular differentiation have begun to emerge.[29−31] Early examples include the introduction of heparinoids or HS-mimetic glycopolymers onto the cell surface of enzymatically deglycosylated wild type mESCs or Ext1$^{-/-}$ mESC mutants with defects in HS biosynthesis, respectively, to promote FGF2 signaling and neural differentiation.

In the study presented here, we sought to expand this strategy to produce mesodermal cell lineages, which requires inputs from both FGF2 and BMP4 signaling pathways. First, we delineated the composition of sulfated regions in HS needed for BMP4 binding using an oligosaccharide microarray binding assay and then developed synthetic HS-mimetic coreceptors capable of promoting both BMP4 and FGF2 activity in the glycocalyx of Ext1$^{-/-}$ mESCs.

The microarray screen revealed a general positive correlation between the increasing overall negative charge of the HS fragments and the level of BMP4 association, with the strongest binding observed for octasaccharides containing a combination of N-, 2-O-, and 6-O-sulfation (Fig. 2). Notably, BMP4 binding was attenuated when the negative charge density was increased further by the introduction of 3O-sulfate groups. This observation suggests that while BMP4 is known to bind to heparin, which is a highly sulfated variant of HS, it may not interact with its most negatively charged regions containing the 3-O-sulfate modification, responsible for heparin's anticoagulant activity.

The enhanced association of BMP4 with HS oligosaccharides containing both 2-O- and 6-O-sulfation indicates overlapping binding preferences with FGF2, which requires both modifications for signaling.30 While differences in selectivity between FGF2 and BMP4 with respect to the sulfation patterns they recognize are not clear, prior studies identified a requirement for longer oligosaccharides (DP of >12) to allow for signaling through BMP4[23] compared to the relatively short (DP of ~6) fragments that are sufficient for FGF2 activity.[28]

On the basis of the similar binding preferences of FGF2 and BMP4, we identified a glycopolymer structure with the HS disaccharide motif, D2A6, containing both 2-O- and 6-Osulfation (Fig. 3.3A), which could act as a common coreceptor for both proteins. We have previously identified the ability of this polymer to bind to FGF2 and facilitate signal transduction via the FGF receptor.[30] We have now demonstrated that this polymer can also engage BMP4 with an avidity similar to that of heparin (Fig. 3.3B) and, when embedded within the cellular glycocalyx of $Ext1^{-/-}$ mESC via a lipid anchor, allowed for the activation of the Smad signaling pathway after BMP4 stimulation (Fig 3.3C). The D2A6 disaccharide motif was required for the biological activity of the glycopolymer, because an analogous polymer containing the 6-O-sulfated monosaccharide, GlcNAc6S, showed no significant binding to either FGF2 or BMP4 despite its highly polyanionic character.

The binding activity of the D2A6 glycopolymers toward FGF2 and BMP4 is notable and likely stems from the architecture of the synthetic mimetic materials, which is distinct from that of HS structures in several key respects. Mainly, N-deacetylation and N-sulfation of glucosamine residues are required for priming of nascent HS chains for further

elaboration of growth factor binding domains by HS epimerases and O-sulfotransferases,15 and numerous studies have pointed to the requirement of N-sulfation in HS for FGF2 binding and signaling.[33,34] Therefore, the D2A6 disaccharide is present only in minute quantities in heparinase digests of isolated HS polysaccharides and may not contribute to growth factor binding in native HS but provide sufficient affinity when presented in a multivalent fashion on polymer scaffolds.

Despite their macromolecular architecture (Mw ~ 50 kDa), the polymers diffused freely into EB structures formed from Ext1$^{-/-}$ mESCs and anchored via their lipid modifications to the outer leaflet of the cellular plasma membranes. Levels of polymer incorporation into the inner core of the EB structure were influenced by the concentration of the materials during remodeling. This behavior potentially affords the opportunity to pattern EBs and spatially control growth factor activity. Once embedded within the cellular glycocalyx, the polymers promoted association of BMP4 with the cell surface based on the structure of their glycan appendages and in agreement with their binding profiles established by an in vitro ELISA (Fig. 3.4). After induction of differentiation, BMP4 binding polymer P2-D2A6 was able to support the exit of Ext1−/− mESCs in an EB culture toward mesoderm and, eventually, the formation of Brachyury^{+ive}/Flk1^{+ive} mesodermal populations (Fig. 3.5 and 3.6). Untreated EBs and EBs treated with control polymer **P2-GlcNAc6S** were able to exit from their pluripotent state toward premesoderm (Brachyury^{+ive}) but failed to transiently attenuate Brachyury expression and successfully establish Flk1^{+ive} mesodermal cell types. The fact that the onset of Brachyury and Flk1 expression was somewhat delayed in Ext1$^{-/-}$ mESCs remodeled with **P2-D2A6** compared to those differentiated in the presence of heparin is worth noting. However, we observed

an overall high abundance of the Flk1 message and lower levels of expression of the neural markers, Sox1, nestin, and FGF5, at day 10 of differentiation under both conditions. The observed differences in timing and outcomes of differentiation between glycocalyx-engineered cells and cells cultured in the presence of soluble heparin may stem from the larger structural and functional heterogeneity of heparin compared to that of P2-D2A6 as well as the timing of their activities. While the presence of soluble heparin is required throughout the entire course of differentiation, **P2-D2A6** is introduced into the cellular glycocalyx only once at the induction of differentiation and has a cell surface residence half-life of ~9h.[30]

In conclusion, we have demonstrated that synthetic HS-mimetic co-receptors for FGF2 and BMP4 can act as functional surrogates for native HS GAG structures at the surfaces of mESCs and drive their mesodermal differentiation. The ease of chemical cell surface glycocalyx engineering with glycomaterials, together with the new information regarding HS specificity emerging from modern glycomics platforms, may enable, in the future, selective activation of signaling pathways in response to endogenous biochemical cues to direct stem cell differentiation.

3.4 Materials and methods

3.4.1 Reagents and Instrumentation

^{1}H NMR spectra were collected on using either a Bruker 300 MHz and Jeol 500 MHz NMR spectrometer. Analysis of the spectra were done using MestReNova software. GPC traces were collected on the Hitachi Chromaster. UV Vis spectra were collected using a quartz cuvette in a Thermo Scientific Nanodrop2000c spectrophotometer. Glycan ligations and cDNA reverse transcriptase reactions were done in a Biorad MyCycler

thermocycler (Hercules, CA). ELISA plates were read on the Spectra Max i3x plate reader (Molecular Devices). Confocal Microscopy images were taken using a Leica Sp5 microscope (Leica Biosystem Lab Solutions) and images were analyzed using ImageJ software. qPCR data was collected using a QuantStudio 7 Flex System (Thermo Scientific) and graphs were made in PRISM. Flow cytometry experiments were done on the Accuri C6 flow cytometer (BD Biosciences) and data was analyzed with Flowjo software.

All chemical reagents and solvents used for the synthesis of monomer **1**,[34] lipid chain transfer agent (**CTA**),[35] and polymeric precursors **P1** and **P2** were purchased from Aldrich Chemicals and used as received unless otherwise specified. RAFT polymerization was carried out under standard Schlenk technique conditions using inert atmosphere of N_2 by adopting previously published procedure.[23] Glycans and reactive fluorophores for the assembly of glycopolymers GP as well as all biological reagents and their sources (including catalog numbers) are listed in Table 3.1. Glycan conjugation reactions to assemble glycopolymers GP were maintained at 50°C using a Biorad MyCycler thermocycler (Hercules, CA).

Table 3.1. Biological Reagents

Material	Supplier	Catalog Number
FGF2	Cell Signaling Technologies	8910
BMP4	Peprotech	120-05
α-BMP4	Peprotech	500-M121
α-FGF2		
α-Flk1 Alexa Fluor 647 conjugate	Biolegend	121910
α-mouse Alexa Fluor 350 conjugate	Life Technologies	A11045
Streptavidin horse radish peroxidase conjugate	Cell Signaling Technologies	3999S
α-SSEA1 Alexa Fluor 647 conjugate	Santa Cruz Biotechnology	sc-21702
BCA Protein Assay	Thermos Sci Pierce Biotech	P123225
Heparin	Acros	AC411212500
Heparan Sulfate Glycan Array (8-sample)	Z Biotech	10604
DPBS (w/o Ca and Mg)	Mediatech Inc (Corning)	21-031-CM
Quick Spin Columns for radiolabeled DNA purification Sephadex G-50, fine	Roche Diagnostics	11273973001
1x TMB ELISA substrate	eBioscience	00-4201-56
BSA, Fraction V	Spectrum	A3611
Smad (Total/Phospho) InstantOne ELISA kit	Invitrogen	85-86183-11
Fetal Bovine Serum	Sigma Aldrich	12303C
PMSF	ThermoFisher Scientific	36978
Protease inhibitor cocktail	Thermo Sci Pierce Biotech	P178439
Cell lysate buffer	Cell Signaling Technologies	9803S
RNeasy mini kit	Qiagen	74104
cDNA kit	Applied Biosystems	4368814
GlcNAc6S sodium salt	Sigma	108321-79-5
ΔUA2S-GlcNAc6S Na_3	Dextra	H1005
Anti-mouse Alexa Fluor 647 conjugate	Cell Signaling Technologies	4410S
SyBr Green Mastermix	Life Technologies	4309155
Tween20	Amresco	M147
Accutase in DPBS	Sigma	A6964
SecureSeal 100 μM spacers (silicon)	Grace Biolabs	654008
Prolong gold anti-fade	Invitrogen	P36930
KO DMEM	Gibco- ThermoFisher Scientific	10829018
IMDM	GE Healthcare Life Sciences	SH3022802

3.4.2 Analysis of BMP4 binding in HS oligosaccharide microarray.

A PropPlate 8 multi-well chamber was added to a Heparan Sulfate Glycan Array (10604-S, Z biotech), and the subarrays were blocked in a 3% BSA solution in PBS for one hour at room temperature. All incubations were done with gentle rocking. The arrays were then washed twice with 200 µL of binding buffer (1% BSA, 0.05% Tween-20, and 0.1 mM Ca^{2+}, Mn^{2+}, and Mg^{2+} in PBS). BMP4 was diluted to 100 nM and incubated on the array for one hour at room temperature. All dilutions were made in the binding buffer. (NOTE: The subarrays that were to be used as an antibody control were left in binding buffer for this duration) The subarrays were washed three times with binding buffer and then incubated with a 1:500 dilution of anti-BMP4 primary antibody for one hour at room temperature, washed three times with binding buffer, followed by a one hour incubation with a 1:500 dilution of anti-mouse-AF647 secondary antibody. The arrays were then washed two times with binding buffer and 0.1% Tween-20 in PBS. The multi-well chamber was removed and the whole slide was submerged in the 0.1% Tween-20 solution and rocked for 15 minutes. After rinsing in MilliQ water and spin drying at 550 rpm for 5 minutes, the slide was imaged at a PMT of 420 for the 635 channel on the GenPix 4000B scanner.

3.4.3 Evaluation of growth factor binding to HS-mimetic glycopolymers P1 by ELISA.

10 µg of primary antibodies against BMP4 or FGF2 (Rabbit, 1-24, µM, Cell Signaling Technologies) were immobilized on 24 well plates overnight in Buffer A (DPBS + 1% BSA). Wells were washed DPBS, and 10 nM of BMP4 and FGF2 was added for 2 hr at room temperature. Following growth factor immobilization, wells were washed Buffer B (0.05% Tween20 in DPBS), blocked with Buffer A for 1 hr, and then treated with

biotinylated polymers **P1** or biotinylated heparin at increasing concentrations (0.1-200 nM) for 1 hr. Colorimetric analysis using streptavidin-HRP conjugate and TMB was used to determine EC_{50} values for polymer binding to the immobilized growth factors. Reaction was quenched with 2N sulfuric acid and absorbance was read at 450 nm with a plate reader. All conditions were done in triplicate.

3.4.4 Evaluation of Smad phosphorylation by ELISA.

Ext1$^{-/-}$ mESCs were seeded in 6 well plates coated with gelatin and grown to confluency. Cells were serum starved overnight (~18 h) before being incubated with HS-mimetic glycopolymers **P2** (3 μM) for 1 hr at 37 °C. After 1h, cells were washed and BMP4 was introduced and incubated with the cells for 2 h at 37 °C. Cell lysis buffer with PMSF and protease inhibitor cocktail (Cell Signaling Technologies) was used to lyse the cells. Protein concentrations were determined using a BCA assay. 50 μg of protein was mixed with phospho(Ser463/465)-Smad1 or Smad1(total) antibody cocktail (1:1 mix of capture antibodies and HRP conjugated detection antibodies) in a well of the InstaOne 96 well ELISA plate assay. Wells were washed after 1 hr with 1x wash buffer, and TMB detection substrate was added. The reaction was quench with 2N sulfuric acid, and then light absorbance (450 nm) was measured with the Spectra Max i3x plate reader (Molecular Devices) and levels of Smad1/5 phosphorylation and total Smad1 protein were normalized. Data was plotted and curve fits (non-linear regression) were determined using PRISM software.

3.4.5 Cell Culture

For embryonic culture, Ext1$^{-/-}$ mESCs (gift from Dr. Catherine Merry) were grown on gelatin-coated plates in knockout (KO)-DMEM + 10% FBS in the presence of LIF. To

form EBs, cells were trypsonized and spotted in 20 µl drops (1000 cells/ drop) on the lid of 150 mm petri dishes in IMDM + 15% FBS (2 mM glutamine, 300 µg/mL transferrin, monothioglycerol and 25 µg/mL ascorbic acid) and grown for 2 days in hanging drops. For differentiation, EBs were cultured using IMDM in petri dishes as a suspension culture for 10 days.

3.4.6 EB remodeling with HS-mimetic glycopolymers P2 and BMP4 binding.

Day 0 EBs were incubated with glycopolymers **P2** at increasing concentrations (0.3-3 µM) for 1 or 2 hrs in serum-free IMDM media. EBs were then washed with cold DPBS (-Ca^{2+}, -Mg^{2+}) and fixed paraformaldehyde. After fixing, the remodeled EBs were incubated with BMP4 (10 nm) overnight. Cells were washed with DPBS, blocked for one hour in 1% BSA in DPBS, and then probed overnight with anti-BMP4 antibody, followed by washing with blocking buffer and another overnight incubation with Alexafluor350 conjugated secondary antibody (A11045, Life Technologies). Immunostained EBs were mounted on glass slides in Prolong Gold anti-fade in wells made from three stacked 100 µm silicon spacers (Grace biolabs). Images (n=10) were taken using the Leica sp5 confocal microscope with the multiphoton laser at 20x magnification. Z-stacks of all EBs were taken, the images were analyzed in ImageJ, and the mean total fluorescence and line- average fluorescence in the z-plane at the midpoint of each EB were determined after background subtraction.

3.4.7 Gene expression analysis after differentiation.

At days 1, 3, 6, 8 and 10 of differentiation, mRNA was collected and analyzed by qRT-PCR. To extract mRNA from EBs, cells were lysed with cell lysis buffer (Qiagen) containing β-mercaptoethanol. RNA was isolated and purified using the RNeasy mini kit

(Qiagen). RNA concentrations and purity were determined using UV absorption (at l=260 and 280 nm) using a nanodrop. RNA (10 µg) was reverse transcribed into cDNA using the High Capacity Reverse Transcriptase kit (Applied Bioscience). 100 ng/mL of cDNA was used in 20 µL reactions with SyBr Green Mastermix (Life Technologies) in a 384 well plate using the QuantStudio™ 7 Flex System (Thermo Scientific). Data is representative of two biological experiments, and each PCR reaction was done in technical triplicate. Graphs were plotted using PRISM software.

3.4.8 Flow cytometry.

To monitor EB remodeling with glycopolymers **P2**, Day 0 EBs were incubated with the glycopolymers at increasing concentrations (0.3-3 µM) for 2 h at 37 °C. EBs were washed with DPBS and then dissociated for 15 min using Accutase in DPBS (Innovative Cell Technologies). Cells were analyzed for the presence of AlexaFluor 488 glycopolymer labels using the Accuri C6 flow cytometer (BD bioscience).

To monitor differentiation, EBs were differentiated in IMDM media for 10 days, before cells were dissociated using Accutase (15 min). Cells were fixed with 4% PFA and then blocked with 2% BSA/DPBS for 1 hr. The cells were probed with AlexaFluor647-conjugated Flk1 antibody or AlexaFluor647-conjugated SSEA1antibody (in 0.2% BSA/PBS). Fluorescence was measured using the Accuri C6 flow cytometer and analyzed using Flowjo software. Means and standard deviations were calculated from three independent biological experiments, and p-values were calculated using t tests with PRISM software.

*3.4.9 Synthesis of HS-mimetic glycopolymers **GP***

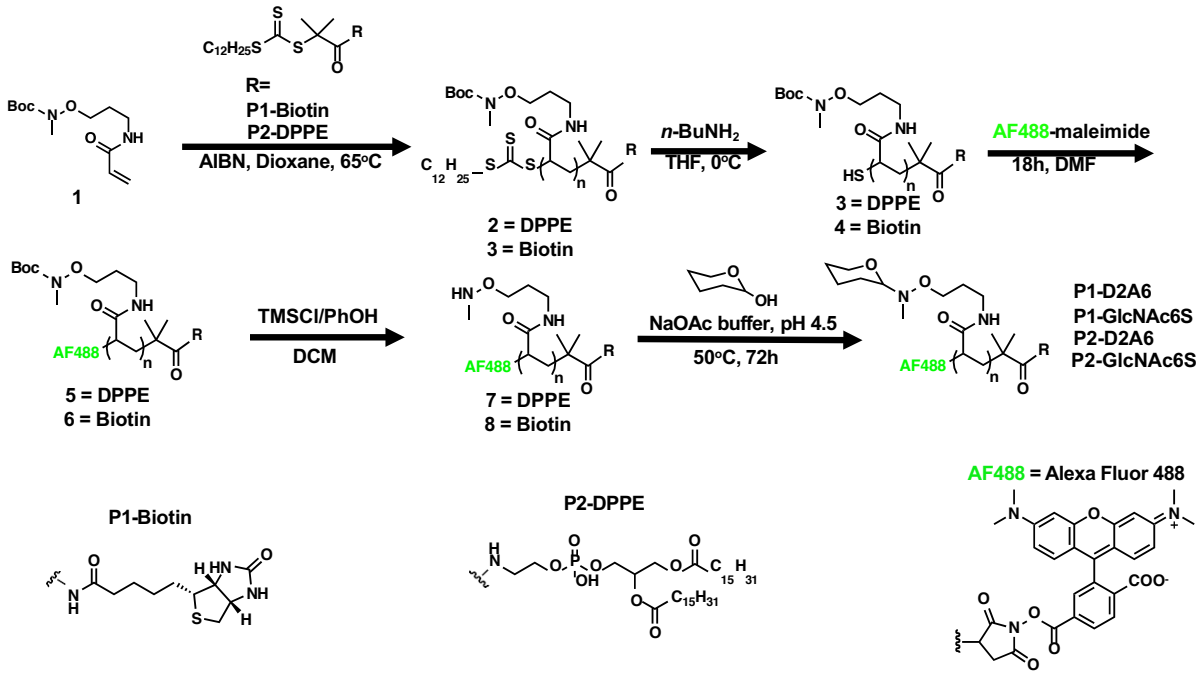

Scheme 3.1. Synthesis of HS-mimetic glycopolymers **GP**

3.4.9.1 Procedure for RAFT polymerization.

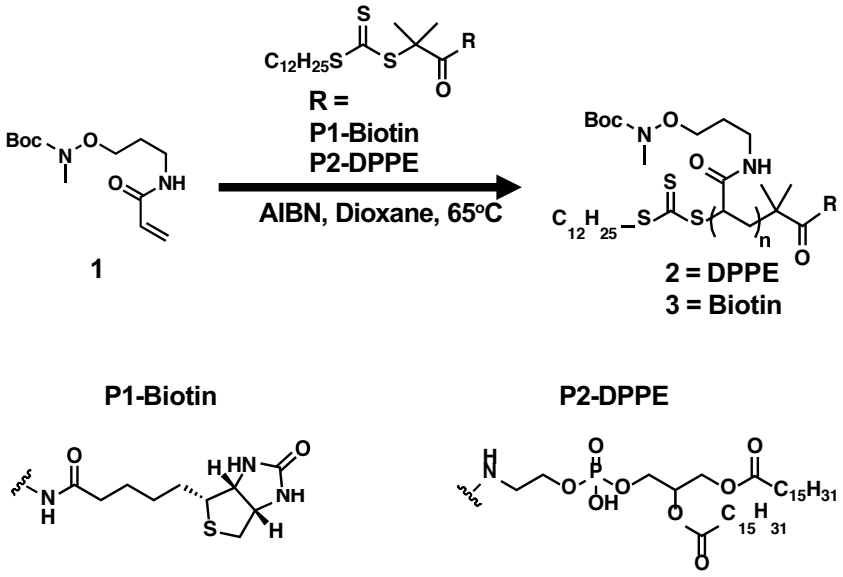

Scheme 3.2. RAFT polymerization

The procedure has been modified from methods previously described.[1] AIBN in anhydrous dioxane filtered through basic alumina (0.4 mg), monomer **1** (462 mg), DPPE-CTA R_1 (12.1 mg), and anhydrous dioxane were added to a 10-mL flame dried Schlenk flask with a magnetic stirring bar. The yellow solution was thoroughly degassed by three freeze-pump-thaw cycles and filled with N_2. The flask was heated at 65°C for 7 hr. The product was precipitated in hexanes three times. Following precipitation, the yellow-white polymer was concentrated in $CHCl_3$ and dried overnight to give the pale-yellow polymer **2** (88% yield). The polymer was characterized by H NMR (500 MHz, $CDCl_3$) and GPC (DMF, 0.2% LiBr, 70 °C). Procedure and characterization for polymer **3** was previously published with a Mw = 52.2 kDa, DP ≈ 200, Đ = 1.16.[3]

3.4.9.2 Procedure for end deprotection.

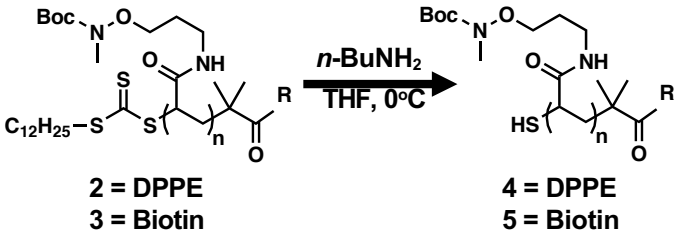

Scheme 3.3. Polymer end deprotection.

Polymer **2** (20.1 mg) was dissolved and 201 µL of degassed 20 mM n-butylamine in THF in a 10 mL flame dried schlenk flask. The reaction was run on ice for 2 h. The product was precipitated in excess hexanes 3 times before being concentrated in $CHCl_3$ three times and dried overnight. The resulting polymer 4 was a white solid (92% yield). Polymer **5** was prepared from Polymer **3** as described above to yield a white solid (85% yield). Polymer **4** and **5** were characterized using ^{1}H NMR ($CDCl_3$, 300 MHz, Fig. 3.X), UV Vis (310 nM) and GPC (DMF, 0.2% LiBr, 70 °C).

Table 3.2. Uv-Vis for determination of end deprotection efficiency.

Polymer (in DCM)	Absorbance (%$_{max}$: 310 nm)
2 (0.1 mg/mL)	0.636
3 (0.1 mg/mL)	0.039
4 (0.1 mg/mL)	0.572
5 (0.1 mg/mL)	0.068

3.4.9.3 Procedure for fluorophore ligation.

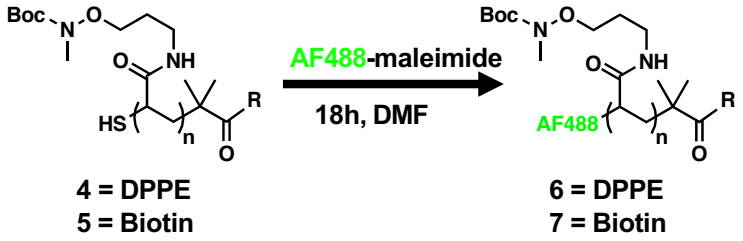

4 = DPPE
5 = Biotin

6 = DPPE
7 = Biotin

Scheme 3.4. Fluorophore ligation to polymers.

Polymer **4** (18.2 mg) was dissolved in 415 µL of a 2 mM AF488 C_5-maleimide (1.5 eq) solution in DMF in a 4 mL vial. The reaction was stirred in the dark, overnight after 3 freeze-pump-thaw cycles. The resulting polymer **6** was precipitated in hexanes three times (centrifugation for 3 min at 1000xg between precipitations) before concentrating with $CHCl_3$ and drying under vacuum. The product was taken to the next step without characterization. Polymer **7** was made as described above from polymer **5**.

Table 3.3. UV-vis for determination of fluorophore ligation efficiency to polymers.

Polymer (in H_2O)	Absorbance (%$_{max}$: 495 nm)
8 (0.2 mg/mL)	0.638
9 (.3 mg/mL)	0.507

3.4.9.4 Procedure of side chain deprotection.

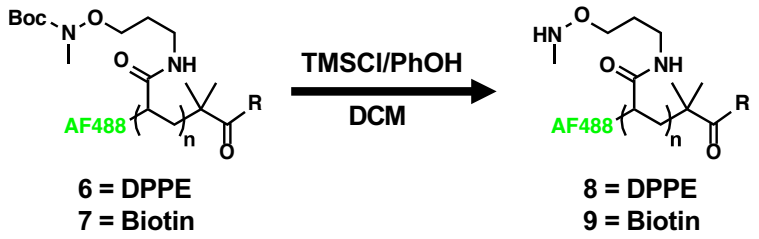

Scheme 3.5. Side chain deprotection.

Polymer **6** (8.5 mg) was dissolved in 500 µL of a freshly made solution of 1M TMS-Cl and 3M phenol in anhydrous DCM in a 4 mL vial. The solution was stirred at room temperature for 2 hrs in the dark. The product was precipitated in ether three times (centrifugation between washes) before being resuspended in water and isolated using a PD10 column. The product was lyophilized to form product **8** (labeling efficiency = 82%). The lyophilized product was characterized by ^{1}H NMR (300 MHz, D_2O) and UV Vis (λ_{max}: 495). Polymer **9** was prepared as described above with (labeling efficiency = 63%).

3.4.9.5 Procedure for glycan ligation.

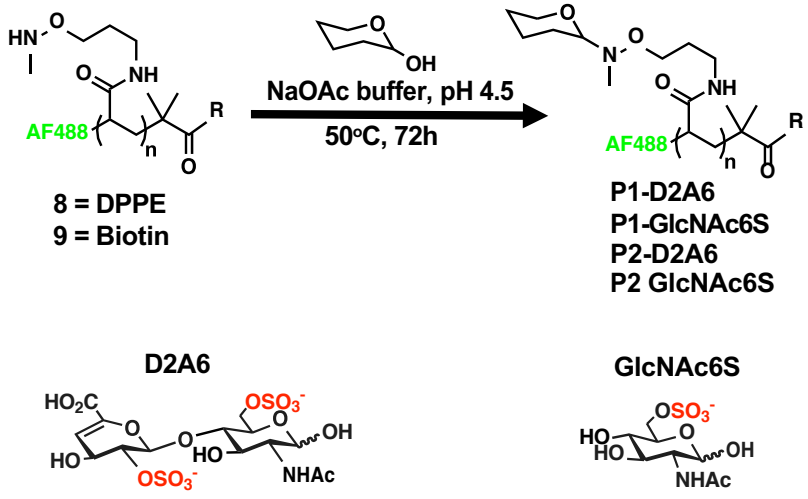

Scheme 3.6. Glycopolymer **P1** and **P2** assembly.

Polymer **8** was dissolved in sodium acetate buffer (1M NaOAc, 1M urea, pH 4.5) to form a 200 mM by side chain solution of the polymer. This solution was then added to a PCR tube containing 1.02 mg of D2A6 (1.1 eq) and the reaction was heated for 72 h at 50°C in a thermocycler. The resulting polymer **P2-D2A6** was purified using a DNA spin column and eluted with deuterated phosphate buffer (100 mM phosphate, 150 mM NaCl, pD 7.4). The polymer was analyzed by H NMR (500 MHz, deuterated phosphate buffer) and UV Vis (488 nm). Polymer **P2-GlcNAc6S** was made using GlcNAc6S and polymer **8**, while polymer **P1-D2A6** and **P1-GlcNAc6S** were made from polymer **9** using D2A6 and GlcNAc6S, respectively, as described above.

Table 3.4. GP ligation efficiency (LE) and valency.

Polymer ID	glycan	LE, %	valency
P1	**D2A6**	**77**	**155**
P1	**GlcNAc6S**	**83**	**177**
P2	**D2A6**	**54**	**69**
P2	**GlcNAc6s**	**49**	**64**

3.5 Acknowledgments

The authors thank C. Merry (University of Nottingham, Nottingham, U.K.) for providing us with Ext1$^{-/-}$ ESCs, C. Fisher (University of California, San Diego) for assistance with polymer characterization, the UCSD Microscopy Core facility (via p30 Grant NS047101 from the National Institute of Neurological Disorders and Stroke) for assistance with fluorescence confocal imaging, and the UCSD CFAR Genomics Core [via p30 Grant AI036214 from the National Institutes of Health (NIH)] for assistance with RT-qPCR analysis. This work was supported by the NIH Director's New Innovator Award [Eunice Kennedy Shriver National Institute of Child Health and Human Development (NICHD) Grant 1DP2HD087954-01]. M.R.N. was supported by the GAANN fellowship

from the U.S. Department of Education. E.M.T. is supported by the National Science Foundation GRPF Program. T.M.L. is supported by the Chemical Biology Interface Program (National Institute of General Medical Sciences Grant 5T32GM112584-03). M.L.H. is supported by the NIH Pathway to Independence Award (NICHD Grant 1K99HD090292-01). K.G. is supported by the Alfred P. Sloan Foundation (Grant FG-2017-9094).

Chapter 3, in full, is a reprint of the material as it appears: M. R. Naticchia, L.K. Laubach, E.M. Tota, T. M. Lucas, M.L. Huang, K. Godula. *ACS Chemical Biology* – Embryonic stem cell engineering with a glycomimetic FGF2/BMP4 co-receptor drives mesodermal differentiation in a three-dimensional culture. The dissertation author is the primary author of this manuscript.

3.6 Supporting Information

Embryonic stem cell engineering with glycomimetic FGF2 and BMP4 co-receptor drives mesodermal differentiation in 3D culture

Matthew R. Naticchia, Logan K. Laubach, Ember M. Tota, Taryn M. Lucas, Mia L. Huang, and Kamil Godula*

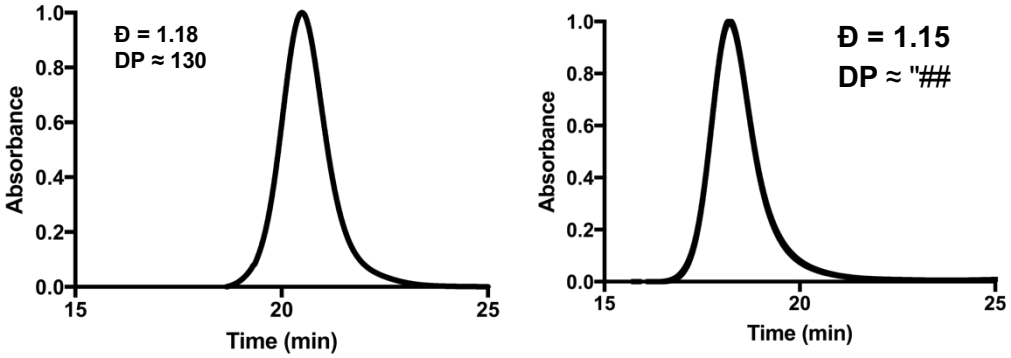

Figure 3.7. GPC trace of polymer **2** and **3** (left and right respectively)

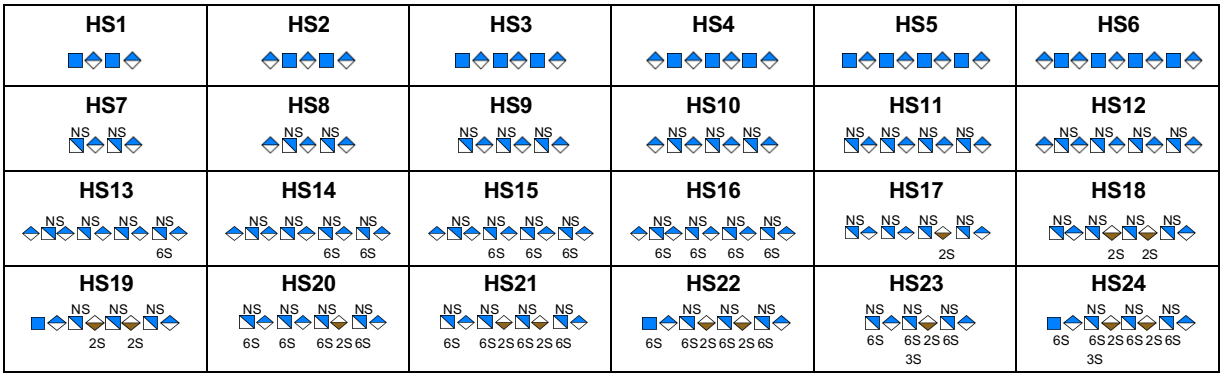

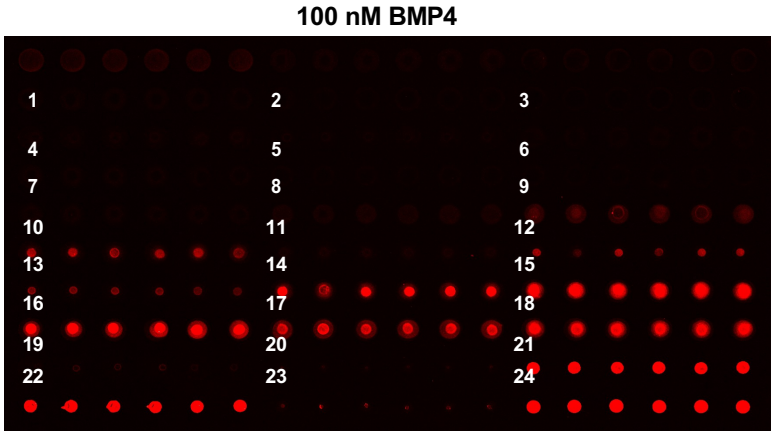

Figure 3.8. Fluorescence images of BMP4 binding to oligosaccharide array. To assess binding of BMP4 to the Z Biotech glycan array, arrays were first blocked with 3% BSA/PBS for one hour. Arrays were then incubated with 100 nM BMP4 for one hour at room temperature, before washing and immunostaining. Images were taken with the GenPix 4000B scanner to assess BMP4 binding to various HS oligosaccharides (6 spots per glycan).

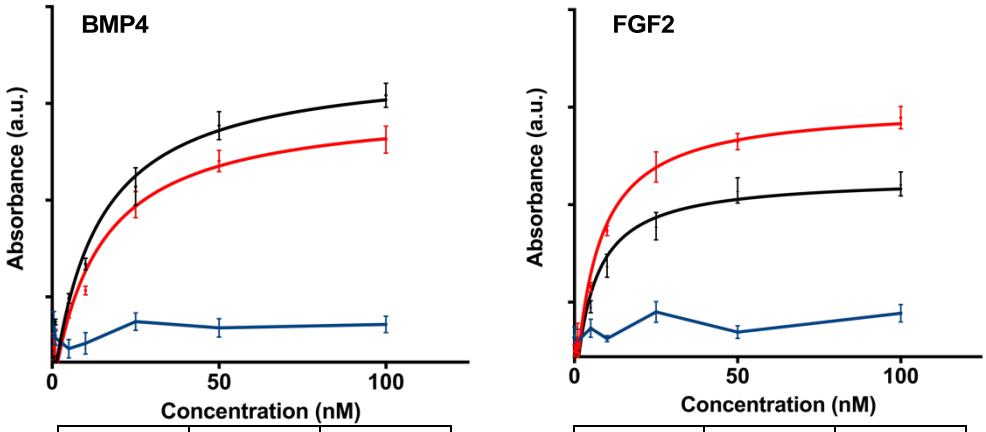

	BMP4	
	EC_{50} (nM)	R^2 value
P2-D2A6	14	0.9298
P2-GlcNAc6s	Not determined	No fit
Biotin-Heparin	13	0.943

	FGF2	
	EC_{50} (nM)	R^2 value
P2-D2A6	6.7	0.9287
P2-GlcNAc6s	Not detemined	No fit
Biotin-Heparin	5.5	0.8595

Figure 3.9. Polymers and biotinylated heparin bind immobilized growth factors. ELISA binding curves for BMP4 (left) and FGF2 (right) were evaluated and EC_{50} values were determined from the curves using PRISM software. Polymer **P1-GlcNAc6S** did not bind to either growth factor, but biotinylated heparin and P1-D2A6 bound both FGF2 and BMP4.

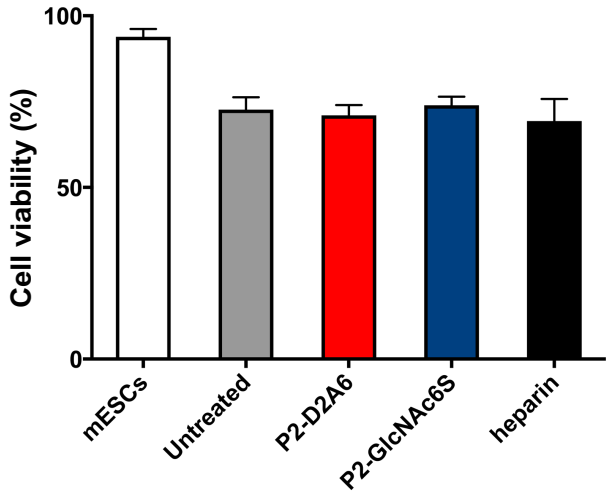

Figure 3.10. Cytotoxicity in EB culture. To assess whether the polymers (3 μM) were cytotoxic to cells under differentiation conditions, viability was tested using ethidium bromide homodimer (EtBr) and calcein AM as a live/dead stain. EBs were incubated with polymer for 2 hr in IMDM media and EBs were grown in IMDM differentiation media for 8 hr. After 8 hr, EBs were dissociated in Accutase for 15 min and stained with a solution of EtBr (50 μM) and calcien AM (50 μM) and analyzed with flow cytometry. Percentage of viable cells were determined by gating for fluorescence. EB formation and dissociation resulted in some loss in cell viability in all conditions with no significant decrease in cell viability resulting from polymer treatment.

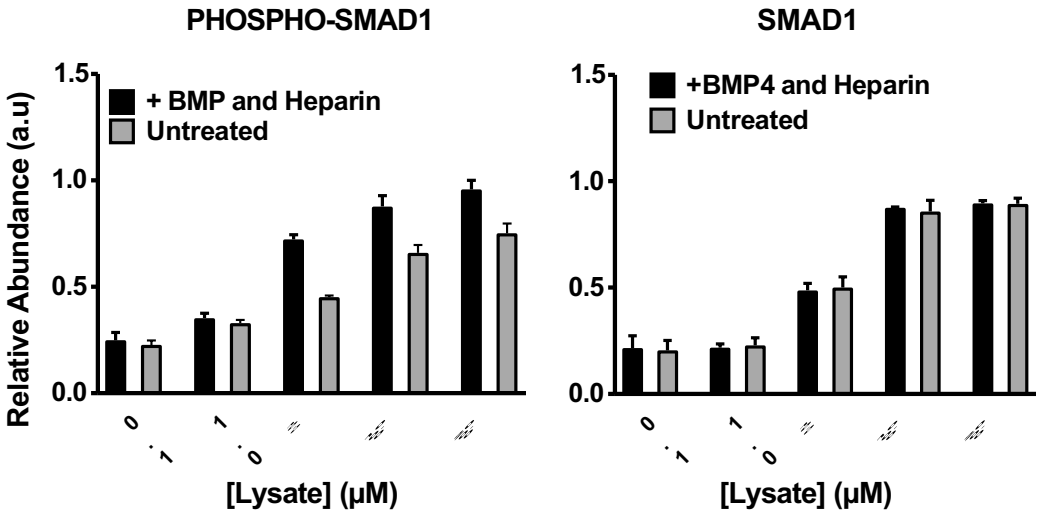

Figure 3.11. Determination of optimal lysate concentrations for Smad activity ELISA. Ext1$^{-/-}$ mESCs were seeded in 6 well plates and serum starved overnight. They were then incubated with heparin (1 μg) for 15 min at 37°C. The wells were washed and subsequently incubated with BMP4 (10 ng) with heparin for 2 hr. Cells were lysed with cell lysis buffer with PMSF and protease inhibitor cocktail. Protein concentrations were determined by BCA assay, and then increasing concentrations of protein (0-200 μg/mL) were added to InstantOne Smad ELISA plates with a 1:1 mixture of capture and detection antibodies. TMB was added for 15 min, then quenched with 2N sulfuric acid.

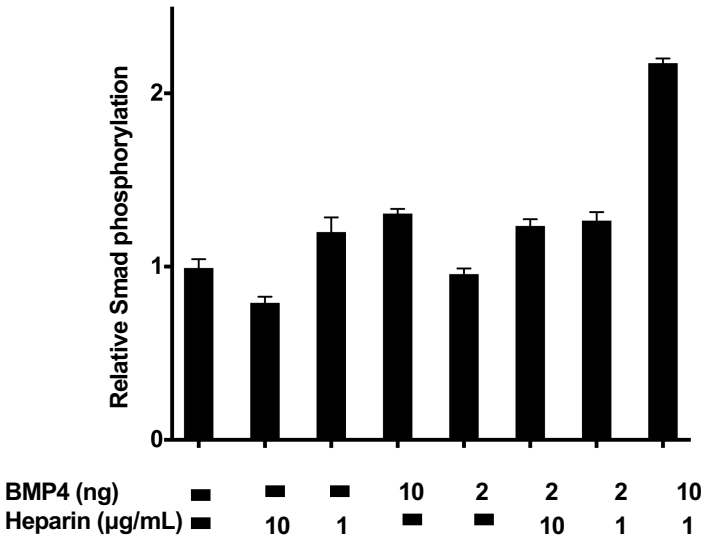

Figure 3.12. Smad1 phosphorylation is dependent on heparin and BMP4 concentrations. Ext1$^{-/-}$ mESCs were seeded in 6 well plates and serum starved overnight. They were then incubated with heparin (1 or 10 μg) for 15 min at 37°C. The wells were washed and subsequently incubated with BMP4 (2 or 10 ng) with heparin for 2 hr. Cells were lysed and protein concentrations were determined by BCA assay. Then increasing concentrations of protein (10 μg/mL) were added to InstantOne Smad ELISA plates.

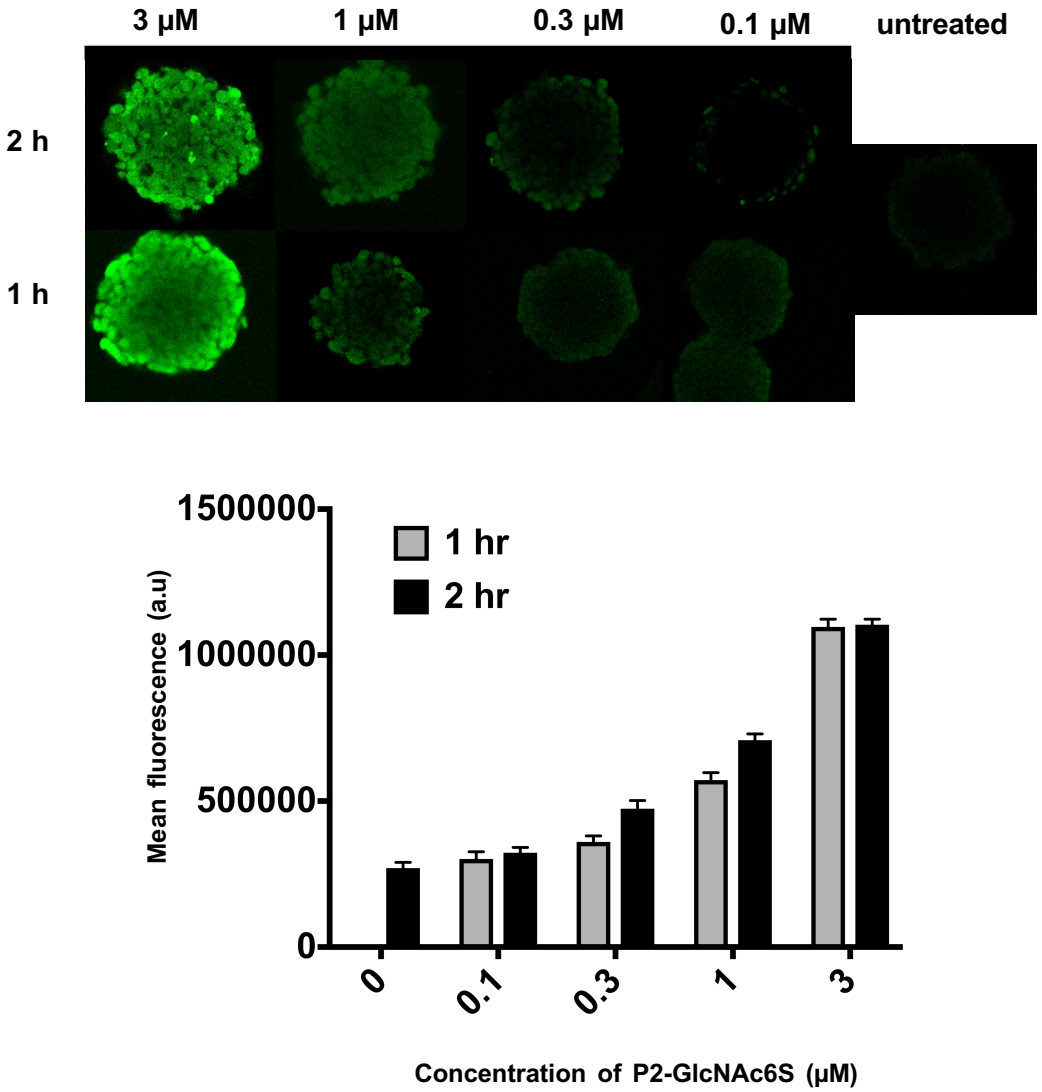

Figure 3.13. Concentration dependence of **P2-GlcNAc6S** incorporation into EBs. (Top) Ext1$^{-/-}$ mESCs were trypsinized and placed in 20 µL drops on the lid of a petri dish (Day -2) to form EBs. After two days, the EBs were washed with DPBS, and polymer **P2- GlcNAc6S** was introduced in serum free IMDM media. After 1 or 2 hrs, EBs were fixed, and mounted to glass slides. AF488 on polymers incorporated into Ext1$^{-/-}$ mESC EBs were imaged using confocal microscopy. Incorporation was found to be time and concentration dependent. (Bottom) The mean total fluorescence of the EBs (n= 10) at midpoint was determined and shows effects of concentration and time on levels of polymer incorporation.

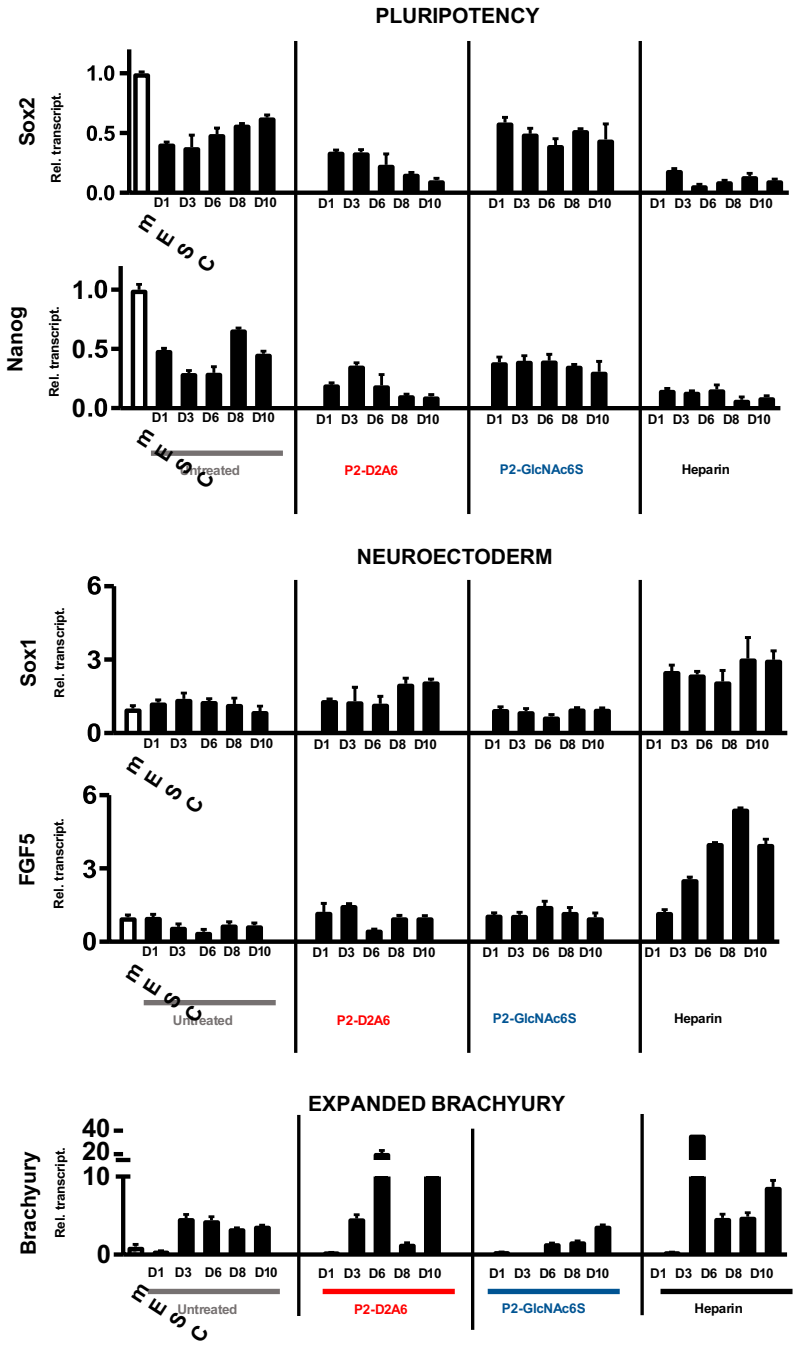

Figure 3.14. Expression of pluripotent and neuroectodermal markers after 10 days of EB differentiation. Ext1-/- mESCs were formed into EBs using the hanging drop method. Polymer **P2-D2A6** or **P2-GlcNAc6S** (3 μM) were incubated with EBs for 2 hr. EBs were then differentiated in IMDM media for 10 days, and lysates were collected throughout the differentiation. mRNA was purified using the RNeazy kit (QIAGEN) and then reverse transcribed to cDNA. Relative levels of expression were assed using qPCR with SyBr green and all values were normalized to GAPDH and mESCs (ΔΔCt).

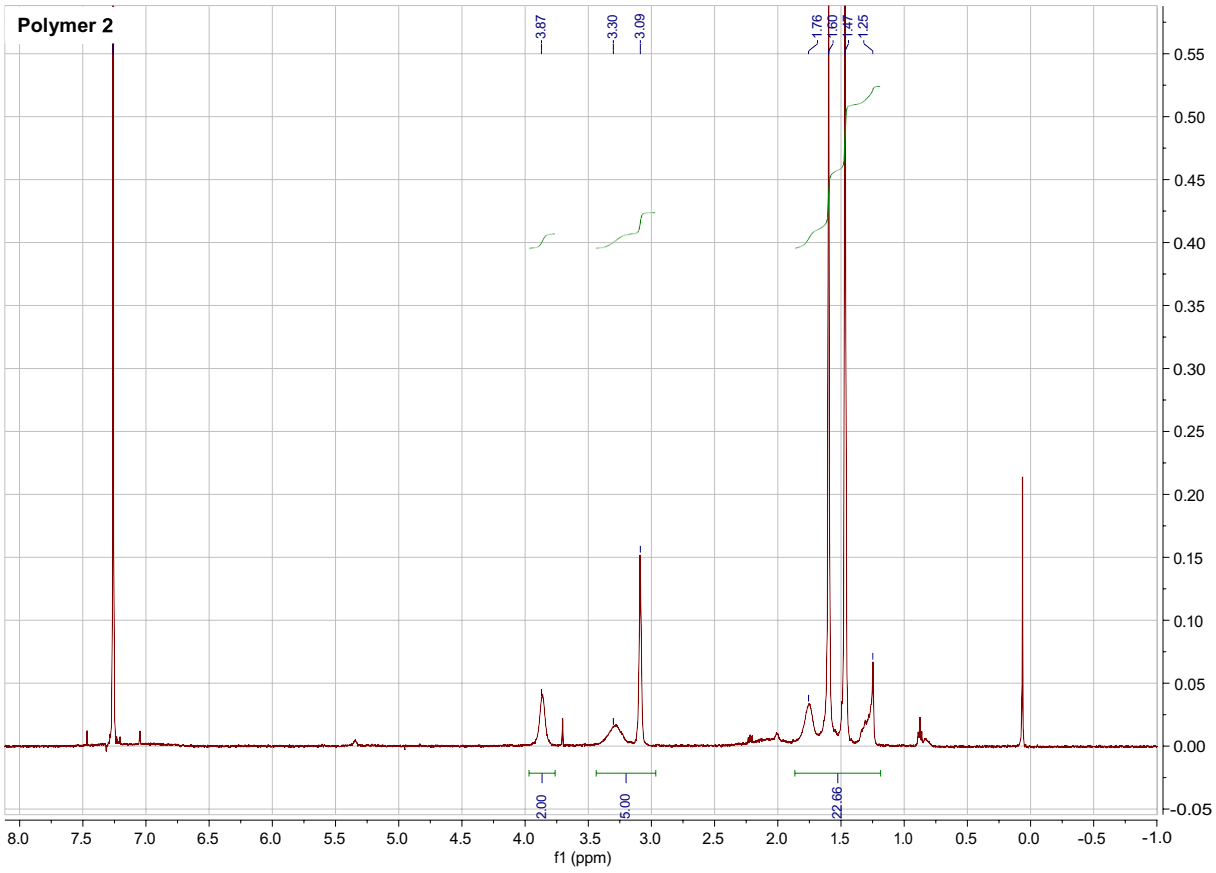

Figure 3.15. ^{1}H NMR of **2**. (500 MHz, $CDCl_3$)

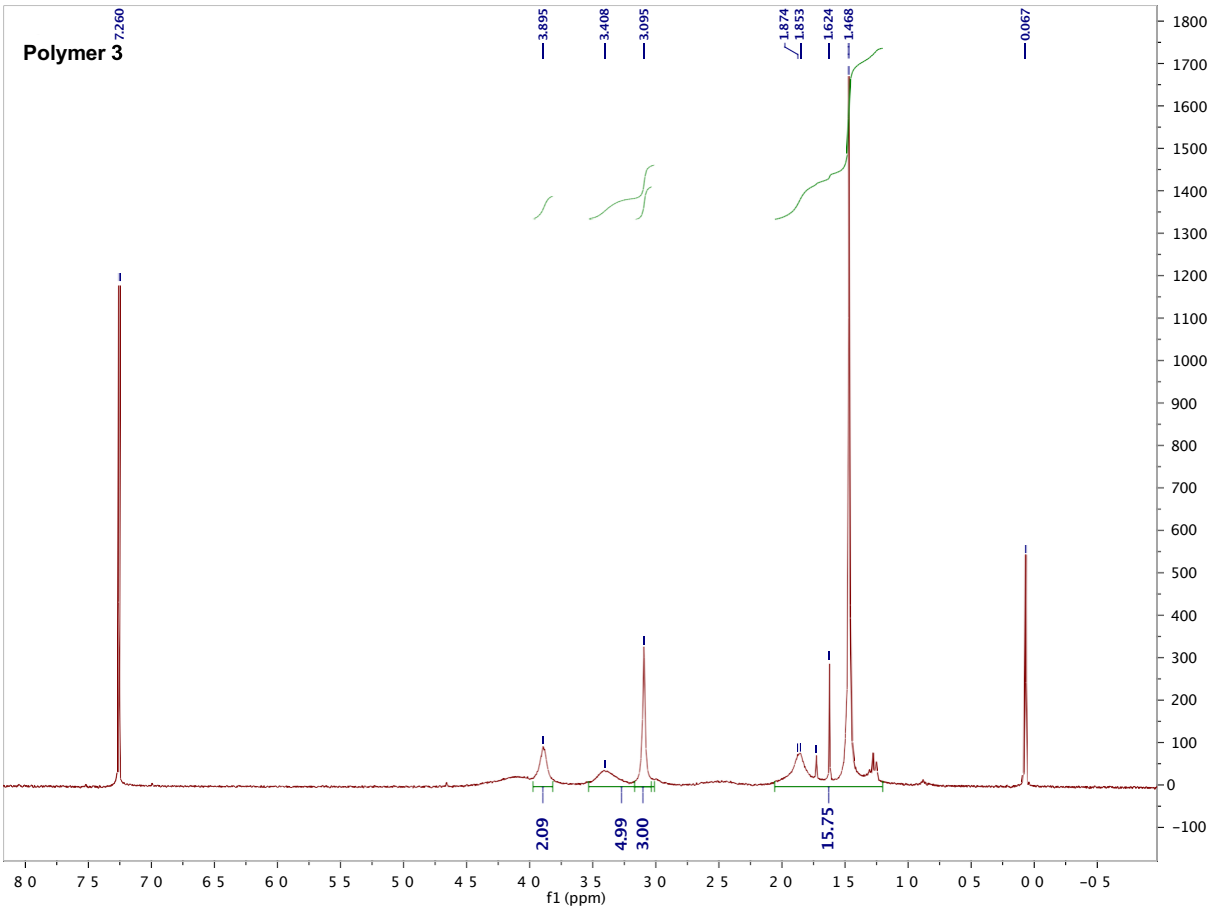

Figure 3.16. ^{1}H NMR of **3**. (300 MHz, $CDCl_3$)

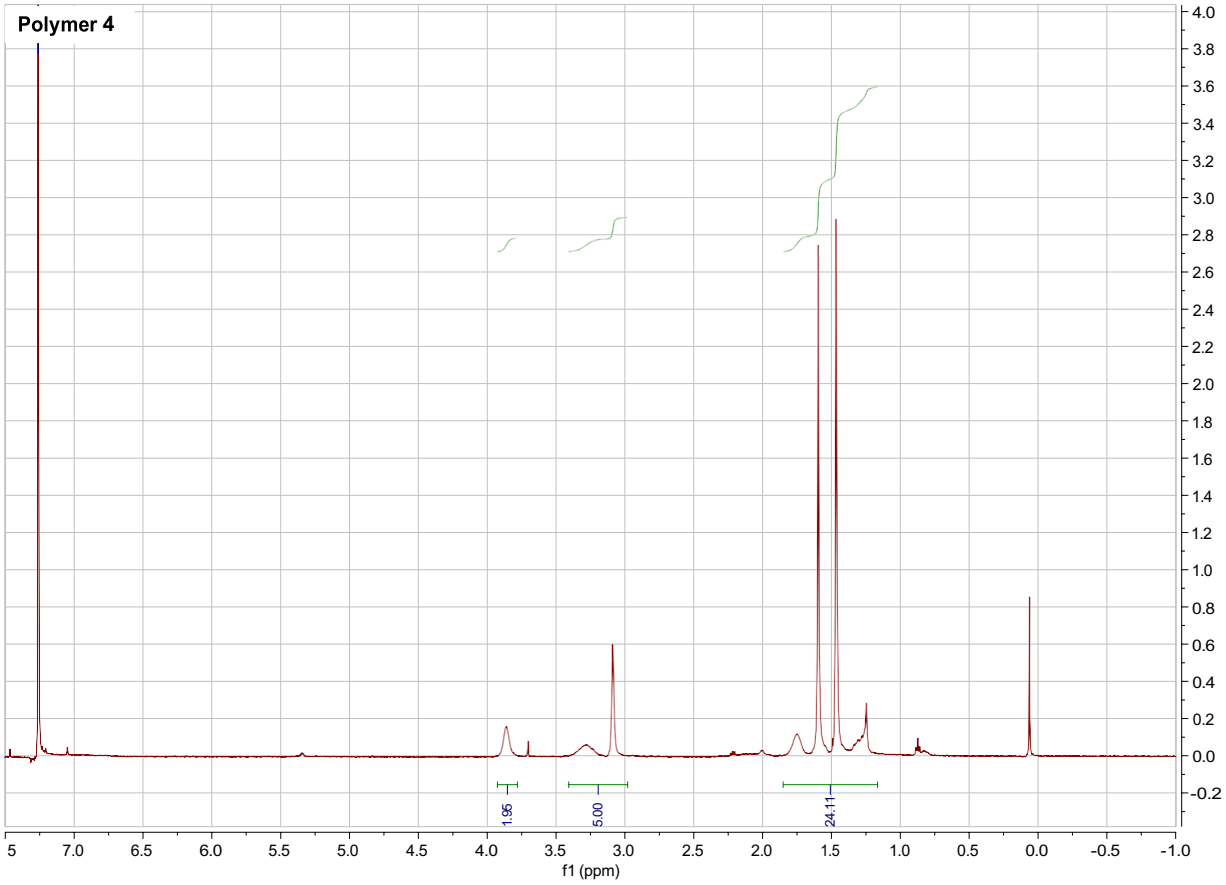

Figure 3.17. ^{1}H NMR of **4**. (500 MHz, $CDCl_3$)

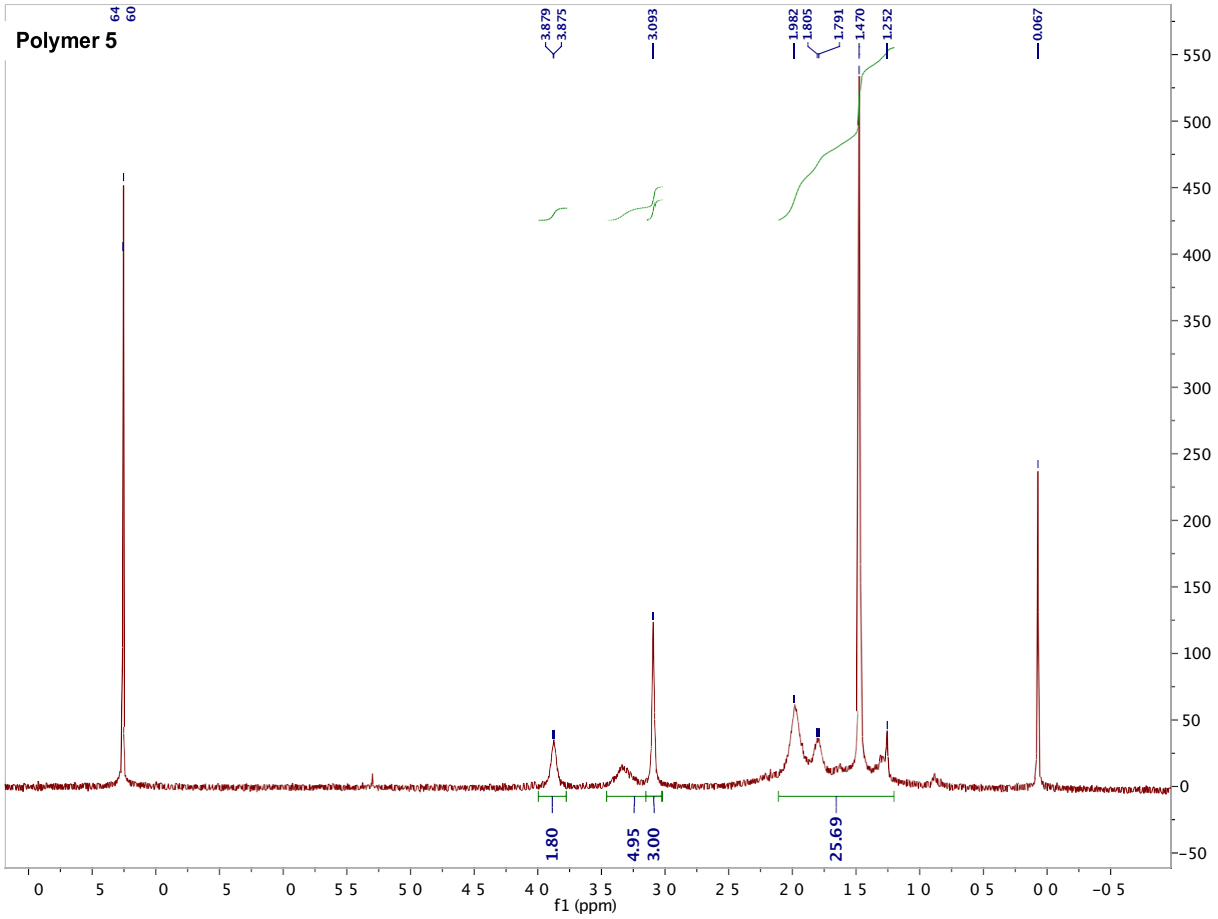

Figure 3.18. ^{1}H NMR of **5**. (300 MHz, $CDCl_3$)

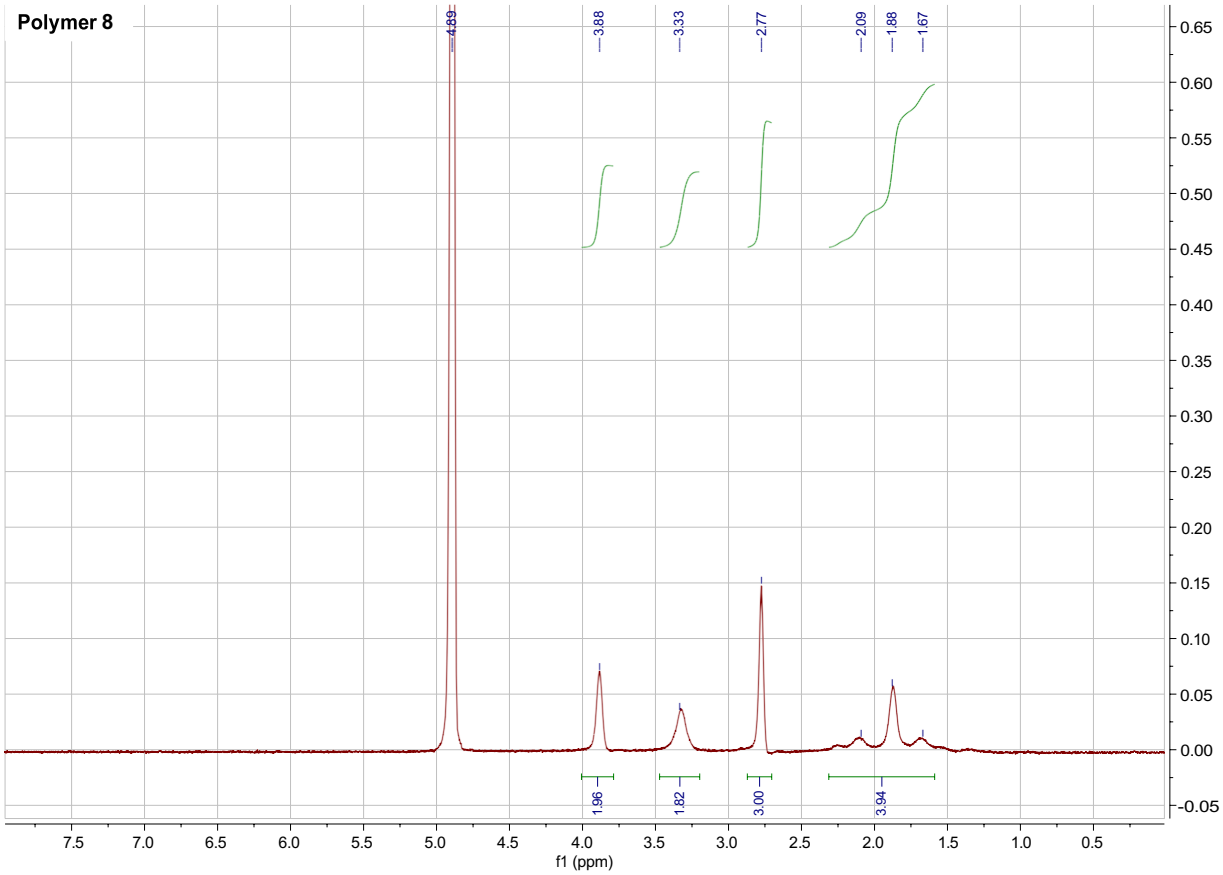

Figure 3.19. ^{1}H NMR of **9**. (500 MHz, D_2O)

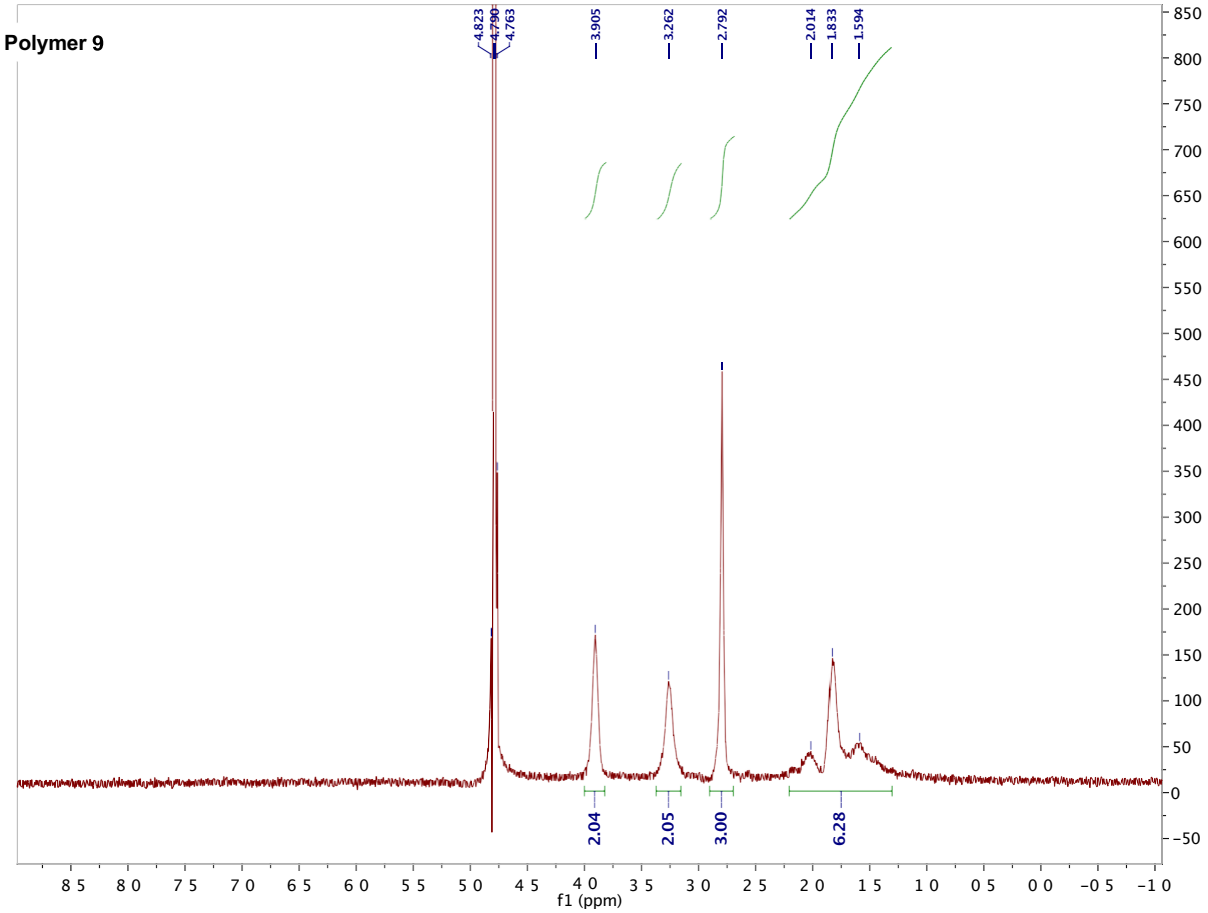

Figure 3.20. ^{1}H NMR of **9**. (300 MHz, D_2O)

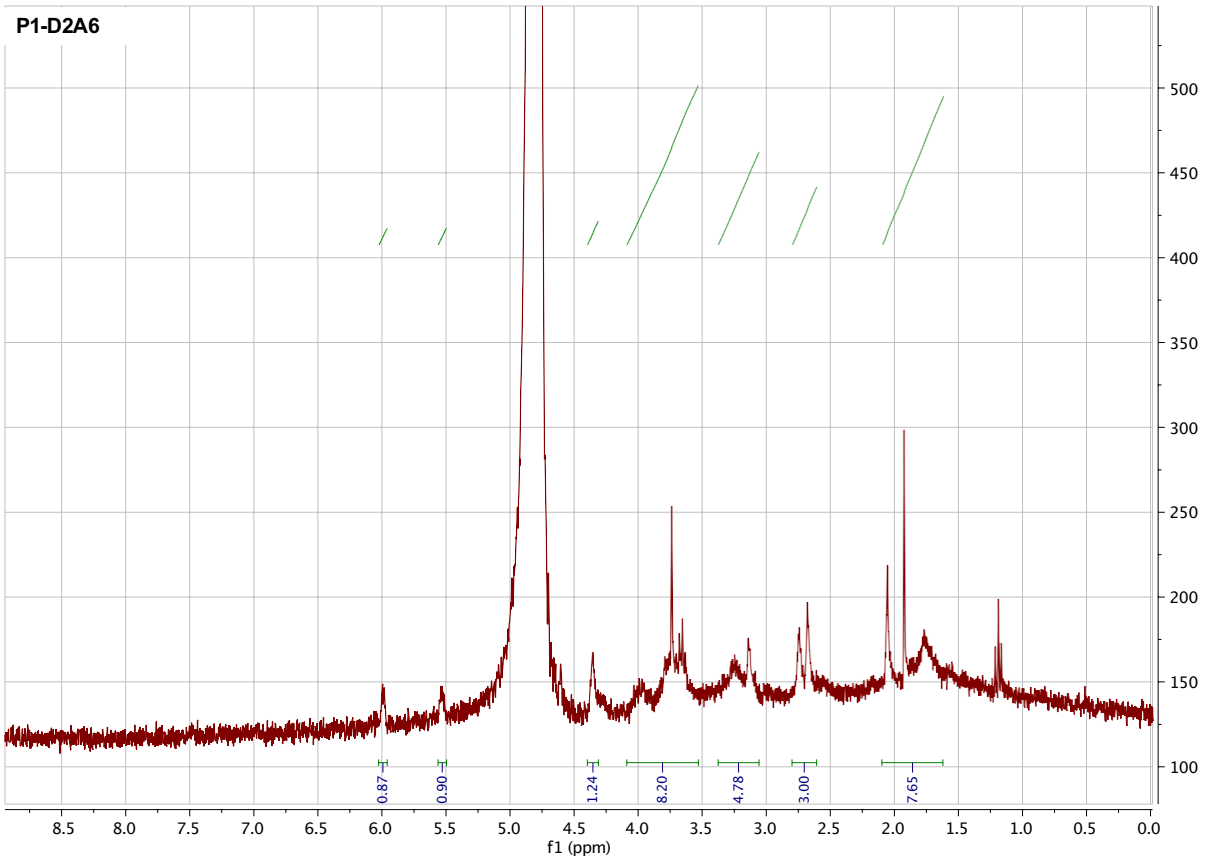

Figure 3.21. ^{1}H NMR of **P2-D2A6**. (500 MHz, D_2O)

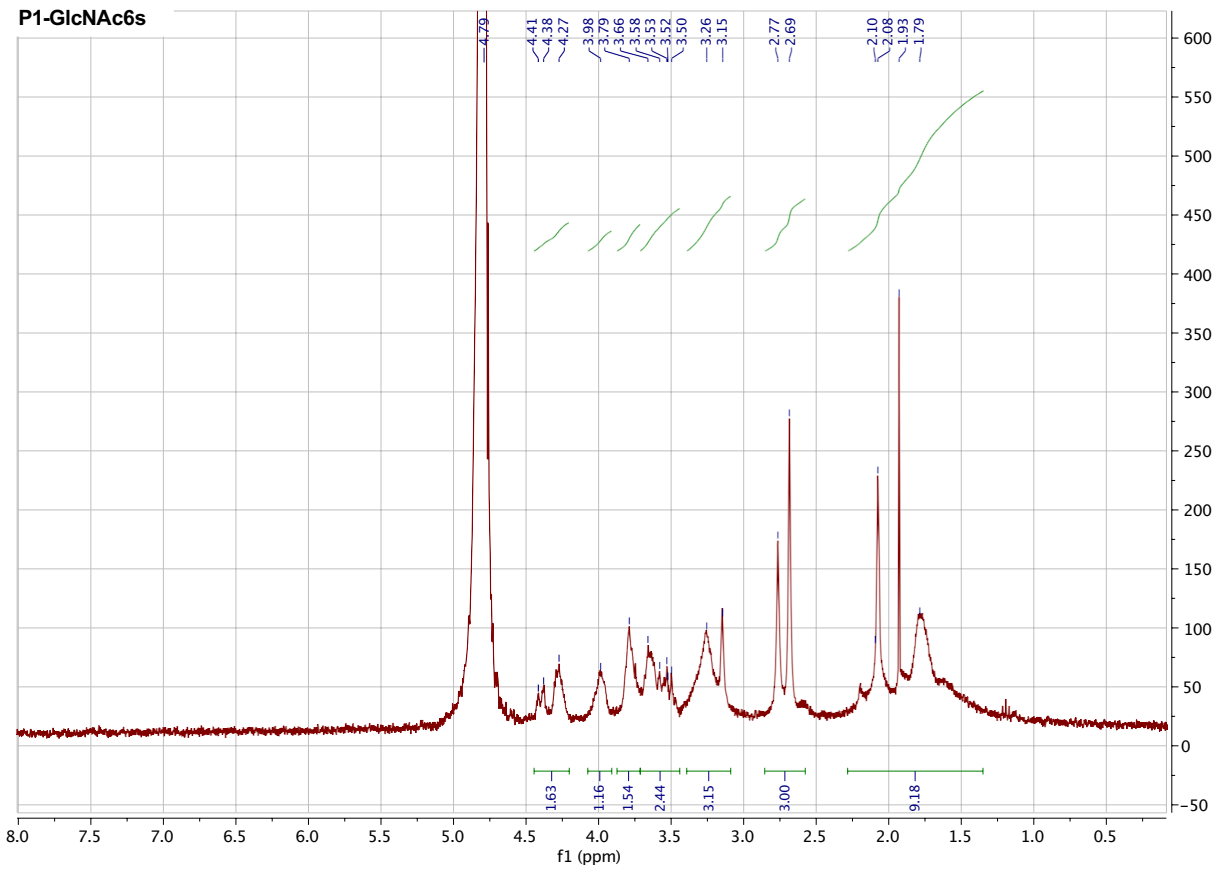

Figure 3.22. ^{1}H NMR of **P1-GlcNAc6S**. (500 MHz, D_2O)

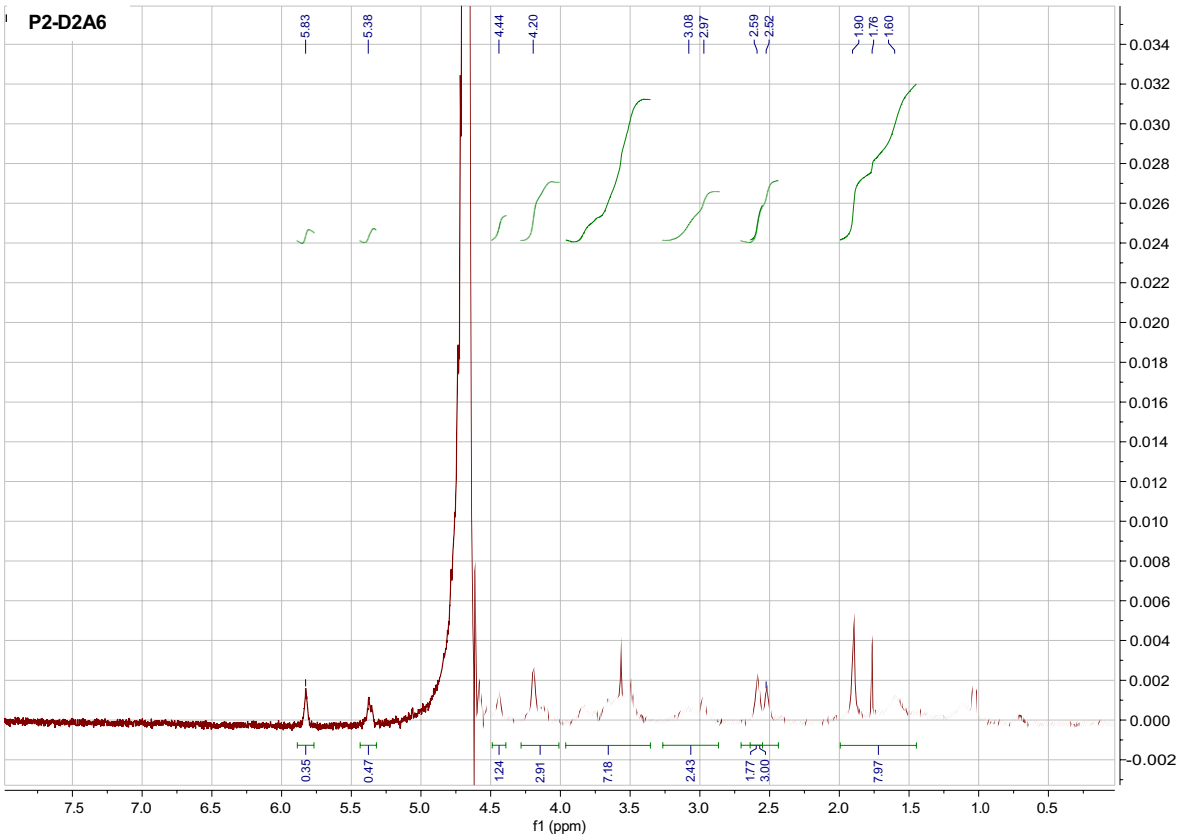

Figure 3.23. ^{1}H NMR of **P2-D2A6**. (500 MHz, D_2O)

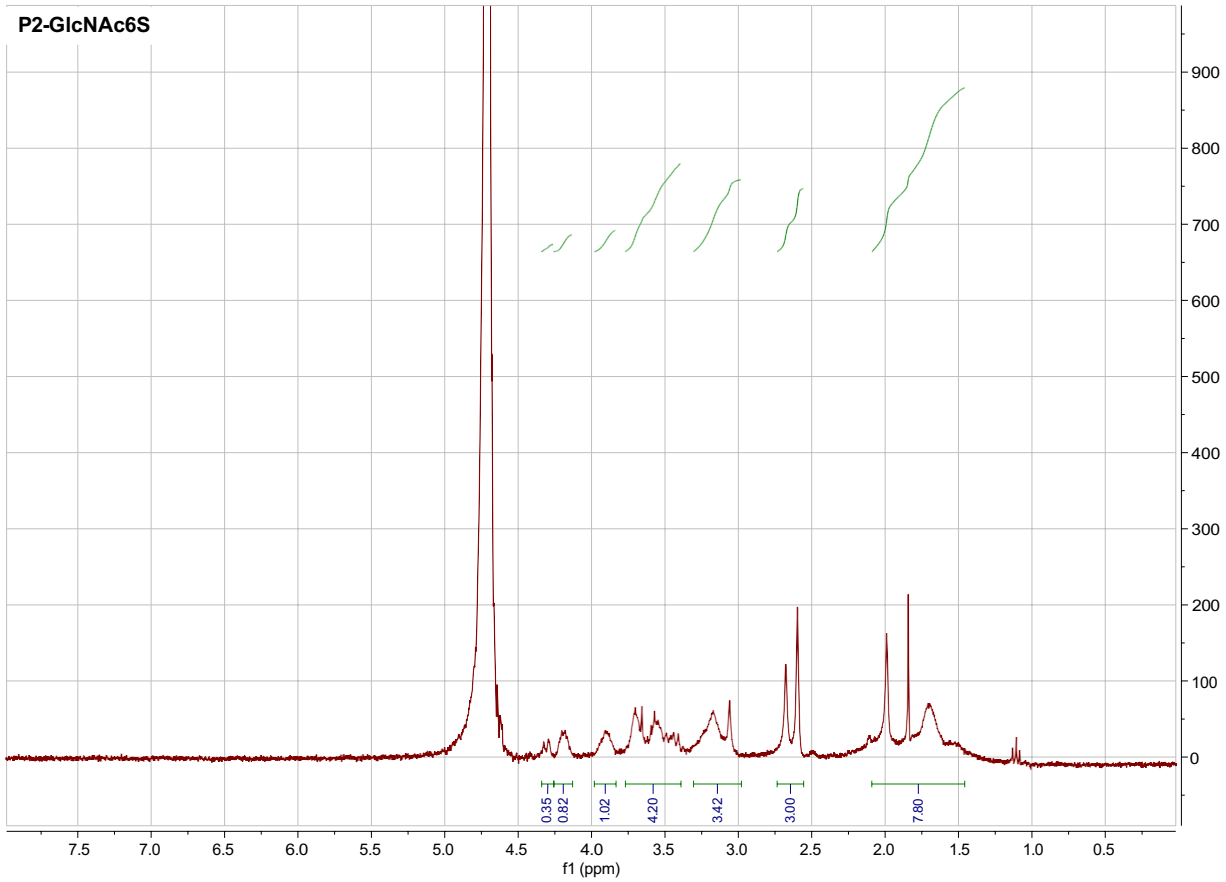

Figure 3.24. ^{1}H NMR of **P2-GlcNAc6S**. (500 MHz, D_2O)

3.7 References

1. D. A. F. Loebel, C. M. Watson, R. A. De Young, P. P. L. Tam, Lineage choice and differentiation in mouse embryos and embryonic stem cells. *Dev. Biol.* **2003**, 264,1−14.

2. C. E. Murry, and G. Keller. Differentiation of Embryonic Stem Cells to Clinically Relevant Populations: Lessons from Embryonic Development. *Cell*. **2008**, 132, 661−680.

3. P. P. L. Tam, and R. R. Behringer. Mouse gastrulation: the formation of a mammalian body plan. *Mech. Dev.* **1997**, 68,3−25.

4. G. M. Keller. In vitro differentiation of embryonic stem cells. *Curr. Opin. Cell Biol.* **1995**, 7, 862−869.

5. J. Heo, J. S. Lee, I. S. Chu, Y. Takahama, S. S. Thorgeirsson. Spontaneous differentiation of mouse embryonic stem cells in vitro: Characterization by global gene expression profiles. *Biochem. Biophys. Res. Commun.* **2005**, 332, 1061−1069.

6. B. Thisse, and C. Thisse. Functions and regulations of fibroblast growth factor signaling during embryonic development. *Dev. Biol.* **2005**, 287, 390−402.

7. Fehling, H. J., Lacaud, G., Kubo, A., Kennedy, M., Robertson, S., Keller, G., and Kouskoff, V. Tracking mesoderm induction and its specification to the hemangioblast during embryonic stem cell differentiation. *Development.* **2003**, 130, 4217−4227.

8. Tada, S., Era, T., Furusawa, C., Sakurai, H., Nishikawa, S., Kinoshita, M., Nakao, K., Chiba, T., and Nishikawa, S.-I. Characterization of mesendoderm: a diverging point of the definitive endoderm and mesoderm in embryonic stem cell differentiation culture. *Development.* **2005**, 132, 4363−4374.

9. Keller, G., Kennedy, M., Papayannopoulou, T., and Wiles, M. V. Hematopoietic commitment during embryonic stem cell differentiation in culture. *Mol. Cell. Biol.* **1993**, 13, 473−486.

10. Varga, A. C., and Wrana, J. L. The disparate role of BMP in stem cell biology. *Oncogene.* **2005**, 24, 5713−5721.

11. Malaguti, M., Nistor, P. A., Blin, G., Pegg, A., Zhou, X., and Lowell, S. Bone morphogenic protein signalling suppresses differentiation of pluripotent cells by maintaining expression of ECadherin. *eLife* **2013**, 2, No. e01197.

12. Bishop, J. R., Schuksz, M., and Esko, J. D. Heparan sulphate proteoglycans fine-tune mammalian physiology. *Nature.* **2007**, 446, 1030−1037.

13. Lin, X. Functions of heparan sulfate proteoglycans in cell signaling during development. *Development.* **2004**, 131, 6009−6021.

14. Kraushaar, D. C., Dalton, S., and Wang, L. Heparan sulfate: a key regulator of embryonic stem cell fate. *Biol. Chem.* **2013**, 394, 741−751.

15. Esko, J. D., and Selleck, S. B. Order Out of Chaos: Assembly of Ligand Binding Sites in Heparan Sulfate. *Annu. Rev. Biochem.* **2002**, 71, 435−471.

16. Xu, D., and Esko, J. D. () Demystifying Heparan Sulfate− Protein Interactions. *Annu. Rev. Biochem.* **2014**, 83, 129−157.

17. Lin, X., Wei, G., Shi, Z., Dryer, L., Esko, J. D., Wells, D. E., and Matzuk, M. M. Disruption of Gastrulation and Heparan Sulfate Biosynthesis in EXT1-Deficient Mice. *Dev. Biol.* **2000**, 224, 299− 311.

18. Stickens, D., Zak, B. M., Rougier, N., Esko, J. D., and Werb, Z. Mice deficient in Ext2 lack heparan sulfate and develop exostoses. *Development.* **2005**, 132, 5055−5068.

19. Johnson, C. E., Crawford, B. E., Stavridis, M., ten Dam, G., Wat, A. L., Rushton, G., Ward, C. M., Wilson, V., van Kuppevelt, T. H., Esko, J. D., Smith, A., Gallagher, J. T., and Merry, C. L. R. Essential Alterations of Heparan Sulfate During the Differentiation of Embryonic Stem Cells to Sox1-Enhanced Green Fluorescent Protein Expressing Neural Progenitor Cells. *Stem Cells*. **2007**, 25, 1913−1923.

20. Kraushaar, D. C., Yamaguchi, Y., and Wang, L. Heparan Sulfate Is Required for Embryonic Stem Cells to Exit from Selfrenewal. *J. Biol. Chem.* **2010**, 285, 5907−5916.

21. Spivak-Kroizman, T., Lemmon, M. A., Dikic, I., Ladbury, J. E., Pinchasi, D., Huang, J., Jaye, M., Crumley, G., Schlessinger, J., and Lax, I. Heparin-induced oligomerization of FGF molecules is responsible for FGF receptor dimerization, activation, and cell proliferation. *Cell* **1994**, 79, 1015−1024.

22. Kraushaar, D. C., Rai, S., Condac, E., Nairn, A., Zhang, S., Yamaguchi, Y., Moremen, K., Dalton, S., and Wang, L. Heparan Sulfate Facilitates FGF and BMP Signaling to Drive Mesoderm Differentiation of Mouse Embryonic Stem Cells. *J. Biol. Chem.* **2012**. 287, 22691−22700.

23. Holley, R. J., Pickford, C. E., Rushton, G., Lacaud, G., Gallagher, J. T., Kouskoff, V., and Merry, C. L. R. Influencing Hematopoietic Differentiation of Mouse Embryonic Stem Cells using Soluble Heparin and Heparan Sulfate Saccharides. *J. Biol. Chem.* **2011**, 286, 6241−6252.

24. Baldwin, R. J., ten Dam, G. B., van Kuppevelt, T. H., Lacaud, G., Gallagher, J. T., Kouskoff, V., and Merry, C. L. R. A Developmentally Regulated Heparan Sulfate Epitope Defines a Subpopulation with Increased Blood Potential During Mesodermal Differentiation. *Stem Cells* **2008**, 26, 3108−3118.

25. Desbaillets, I., Ziegler, U., Groscurth, P., and Gassmann, M. Embryoid bodies: an in vitro model of mouse embryogenesis. *Exp. Physiol.* **2000**, 85, 645−651.

26. Pickford, C. E., Holley, R. J., Rushton, G., Stavridis, M. P., Ward, C. M., and Merry, C. L. R. Specific Glycosaminoglycans Modulate Neural Specification of Mouse Embryonic Stem Cells. *Stem Cells*. **2011**, 29, 629−640.

27. Holley, R. J., Meade, K. A., and Merry, C. L. R. Using embryonic stem cells to understand how glycosaminoglycans regulate differentiation. *Biochem. Soc. Trans.* **2014**, 42, 689−695.

28. Pye, D. A., Vives, R. R., Turnbull, J. E., Hyde, P., and Gallagher, J. T. Heparan Sulfate Oligosaccharides Require 6-O-Sulfation for Promotion of Basic Fibroblast Growth Factor Mitogenic Activity. *J. Biol. Chem.* **1998**, 273, 22936−22942.

29. Pulsipher, A., Griffin, M. E., Stone, S. E., and Hsieh-Wilson, L. C. Long-Lived Engineering of Glycans to Direct Stem Cell Fate. *Angew. Chem., Int. Ed.* **2015**, 54, 1466−1470.

30. Huang, M. L., Smith, R. A. A., Trieger, G. W., and Godula, K. Glycocalyx Remodeling with Proteoglycan Mimetics Promotes Neural Specification in Embryonic Stem Cells. *J. Am. Chem. Soc.* **2014**, 136, 10565−10568.

31. Griffin, M. E., and Hsieh-Wilson, L. C. Glycan Engineering for Cell and Developmental Biology. *Cell Chem. Biol.* **2016**, 23, 108−121.

32. Khan, S. A., Nelson, M. S., Pan, C., Gaffney, P. M., and Gupta, P. Endogenous heparan sulfate and heparin modulate bone morphogenetic protein-4 signaling and activity. *Am. J. Physiol. - Cell Physiol.* **2008**, 294, C1387−C1397.

33. Pellegrini, L. Role of heparan sulfate in fibroblast growth factor signalling: a structural view. *Curr. Opin. Struct. Biol.* **2001**, 11, 629−634.

34. Powell, A. K., Yates, E. A., Fernig, D. G., and Turnbull, J. E. Interactions of heparin/heparan sulfate with proteins: Appraisal of structural factors and experimental approaches. *Glycobiology.* **2004**, 14, 17R−30R.

35. Khan, S. A., Nelson, M. S., Pan, C., Gaffney, P. M., and Gupta, P. Endogenous heparan sulfate and heparin modulate bone morphogenetic protein-4 signaling and activity. *Am. J. Physiol. Cell Physiol.* **2008**, 294, C1387−1397.

36. Kuo, W.-J., Digman, M. A., and Lander, A. D. Heparan Sulfate Acts as a Bone Morphogenetic Protein Coreceptor by Facilitating Ligand-induced Receptor Hetero-oligomerization. *Mol. Biol. Cell.* **2010**,21, 4028−4041.

37. Gandhi, N. S., and Mancera, R. L. Prediction of heparin binding sites in bone morphogenetic proteins (BMPs). *Biochim. Biophys. Acta, Proteins Proteomics* **2012,** 1824, 1374−1381.

38. Ruppert, R., Hoffmann, E., and Sebald, W. Human bone morphogenetic protein 2 contains a heparin-binding site which modifies its biological activity. *Eur. J. Biochem.* **1996**, 237, 295−302.

39. Jasuja, R., Allen, B. L., Pappano, W. N., Rapraeger, A. C., and Greenspan, D. S. Cell-surface heparan sulfate proteoglycans potentiate chordin antagonism of bone morphogenetic protein signaling and are necessary for cellular uptake of chordin. *J. Biol. Chem.* **2004**, 279, 51289−51297.

40. Hintze, V., Samsonov, S. A., Anselmi, M., Moeller, S., Becher, J., Schnabelrauch, M., Scharnweber, D., and Pisabarro, M. T. Sulfated Glycosaminoglycans Exploit the Conformational Plasticity of Bone Morphogenetic Protein-2 (BMP-2) and Alter the Interaction Profile with Its Receptor. *Biomacromolecules* **2014,** 15, 3083−3092.

41. Rawat, M., Gama, C. I., Matson, J. B., and Hsieh-Wilson, L. C. Neuroactive Chondroitin Sulfate Glycomimetics. *J. Am. Chem. Soc.* **2008,** 130, 2959−2961.

42. Sheng, G. J., Oh, Y. I., Chang, S.-K., and Hsieh-Wilson, L. C. Tunable Heparan Sulfate Mimetics for Modulating Chemokine Activity. *J. Am. Chem. Soc.* **2013**, 135, 10898−10901.

43. R. Lawrence, H. Lu, R. D. Rosenberg, J. D. Esko, L. Zhang. Disaccharide structure code for the easy representation of constituent oligosaccharides from glycosaminoglycans. *Nat. Methods.* **2008**, 5, 291−292.

44. C. Cerdan, S. H. Hong, M. Bhatia. Formation and Hematopoietic Differentiation of Human Embryoid Bodies by Suspension and Hanging Drop Cultures. *Current Protocols in Stem Cell Biology*. **2007**.

45. E. Sachlos and D. T. Auguste. Embryoid body morphology influences diffusive transport of inductive biochemicals: A strategy for stem cell differentiation. *Biomaterials* **2008,** 29, 4471−4480.

46. A. M. Bratt-Leal, R. L. Carpenedo, T. C. McDevitt. Engineering the embryoid body microenvironment to direct embryonic stem cell differentiation. *Biotechnol. Prog*. **2009**, 25,43−51.

47. T. Kunath, M. K. Saba-El-Leil, M. Almousailleakh, J. Wray, S. Meloche, A. Smith. FGF stimulation of the Erk1/2 signalling cascade triggers transition of pluripotent embryonic stem cells from self-renewal to lineage commitment. *Development.* **2007**, 134, 2895−2902.

48. M. Koike, S. Sakaki, Y. Amano, H. Kurosawa. Characterization of embryoid bodies of mouse embryonic stem cells formed under various culture conditions and estimation of differentiation status of such bodies. *J. Biosci. Bioeng.* **2007**, 104, 294−299.

49. N. Jastrebova, M. Vanwildemeersch, A. C. Rapraeger, G. Giménez-Gallego, U. Lindahl, J. Spillmann. Heparan Sulfate-related Oligosaccharides in Ternary Complex

Formation with Fibroblast Growth Factors 1 and 2 and Their Receptors. *J. Biol. Chem.* **2006**, 281, 26884−26892.

50. J. R. Klim, L. Li, P. J. Wrighton, M. S. Piekarczyk, L. L. Kiessling. A defined glycosaminoglycan-binding substratum for human pluripotent stem cells. *Nat. Methods*. **2010**, 7, 989− 994.

51. P. J. Wrighton, J. R. Klim, B. A. Hernandez, C. H. Koonce, T. J. Kamp, L. L. Kiessling. Signals from the surface modulate differentiation of human pluripotent stem cells through glycosaminoglycans and integrins. *Proc. Natl. Acad. Sci. U. S. A.* **2014**, 111, 18126−18131.

4 Small molecule inhibitor of heparan sulfate biosynthesis enables transient reprograming of stem cell glycocalyx to control differentiation

4.1 Introduction

With the ability to propagate and then differentiate into all three germ layers, embryonic stem cells (ESCs) are a versatile precursor for cell-based therapies.[1] These precursor cells can go on to produce a spectrum of terminally differentiated cells, which could be used in cancer immunotherapies[2], diabetes treatments[3], or regenerative medicine[4]. Despite the potential of stem cell therapy, currently the only FDA approved stem cell therapy is hematopoietic stem cell transplantation.[5] To further expand the use of stem cells as a therapeutic, we must first develop methods to control these differentiation pathways in a way that produces a high yield of the target cell lineage and a method that is easily reproducible. Many of the current methods require delivery of a high concentration of growth factor (GF) and suffer from poor reproducibility or off-target differentiation.[6]

In mouse embryonic stem cells (mESCs), germ layer specification is largely controlled by three families of growth factors: fibroblast growth factor (FGF), bone morphogenetic protein (BMP), and Wingless (Wnt) protein.[7,8] For neural speficiation, FGF2 is required for exit of the pluripotent state and further FGF2 signaling leads to differentiation toward nestin^{+ive} neural precursor cells (NPCs) and β-III-tubulin^{+ive} neurons. This process is initiated via the MAPK signaling cascade. [9] This signaling pathway also requires another co-receptor, heparan sulfate (HS), which spans both FGF2 and the tyrosine kinase receptors (FGFRs).[10] HS binds both FGF2 and FGFR through

electrostatic interactions in highly sulfated pockets along the long, linear glycan chain. These interactions are necessary for proper signaling, and subsequent differentiation.[11]

Synthetic tools have been developed to mimic HS and activate this signaling pathway in the absence of native HS. Soluble heparin was the first exogenous HS used to rescue signaling and differentiation in mESCs deficient in one of the HS biosynthetic proteins, Ext1. Knocking out the *ext1* gene arrests the cells in a pluripotent state and prevents differentiation. Soluble heparin can then serve the role of native HS and activate FGF2 or BMP4 signaling, resulting in neuroectoderm[13] or mesoderm[14] differentiation, respectively. Since then, more chemically defined HS mimetics have been designed in conjunction with genetic knockout cell lines, however none have been shown to override native HS activity in wild type cells. [15,16,17]

In order to use HS mimetics as a method for controlling stem cell specification in the context of therapeutics, genetic knockouts are not a viable option and a method for removing native HS for transient glycocalyx remodeling is required. Methods for enzymatic removal of HS with bacterial heparinases have been developed, but they often lead to incomplete digestions of HS chains and digestion would be necessary throughout differentiation to prevent replacement of the HS structures.[18] Antagonists, such as surfen[19], have been shown to prevent signaling and differentiation, but due to the nature of their interaction with HS, are incompatible with HS mimetics. Instead, small molecule inhibition of HS biosynthesis offers a facile method of removing native HS off the surface for glycocalyx engineering.

Several classes of inhibitors of HS biosynthesis have been developed. Broad spectrum metabolic inhibitors, such as 4-deoxy-GlcNAc, reduce the pool of functional

monosaccharides for chain elongation and effectively reduces HS on the surface of cells.[20] However, this method is not specific to HS or GAG biosynthesis and therefore is not an appealing class of compounds in conjunction with glycocalyx remodeling. To reduce off target effects, developing a small molecule inhibitor specific for one of the HS biosynthetic enzymes confers greater potential.

Considering the complexity of the HS biosynthesis pathway, intercepting one of the early steps in the polysaccharide chain assembly is ideal. Namely, we focused on inhibition of the transfer of the uridine-diphosphate galactose (UDP-Gal) nucleotide sugar to xylose residues *O*-linked to the proteoglycan polypeptide backbone by the galactyosyltransferase, β1,4-galactosyltransferase 7 (β4GalT7). This step initiates the assembly of a tetrasaccharide primer required for further elongation by glycan chain polymerases to produce HS chains. The primer sequence also initiates the biosynthesis of chondroitin sulfate (CS) chains, which are also involved in the regulation of a range of GF-singling pathways, thus providing a potentially versatile platform to also engineer the CS component of the stem cell glycocalyx. By acting on xylose, which is a monosaccharide uniquely found in HS and CS in the mammalian glycome,[21] β4GalT7 is an ideal target for selective editing of these structures without interference with other glycans, which may be important of stem cell functions (i.e., *N*- and *O*-glycans or glycolipids). As such, significant efforts have focused on generating chemically modified xylosides to manipulate HS and CS assembly. Originally developed to produce soluble HS and CS in Chinese hamster ovary (CHO) cells, *O*-aryl and *O*-alkyl xylosides can serve as soluble competitor substrates for β4GalT7 that can be elaborated by cells in to full length biologically active glycan chains.[22,23] These xylosides primers were later converted

into competitive inhibitors of β4GalT7, by replacing the C4-hydroxyl group in the monosaccharide with groups which cannot be extended by the enzyme.[24] Extensive structure-activity studies have found that very little modifications to the sugar moiety can be tolerated while maintaining binding to the enzyme.[25] The aglycone was found to be amenable to chemical modifications, resulting in a large library of xylosides being developed to date. Several compounds have shown good inhibitory activity *in vitro* and in various cell assays, with 4-fluoro-(-*O*-methylumbelliferyl)xyloside (4FMUX) being among the most commonly used.[26,27,28] To develop a stem cell glycocalyx engineering approach, whereby the activity of endogenous HS is overridden via chemical inhibition of its assembly with concomitant introduction of synthetically defined functional HS-mimetics,[29,30] we assessed the ability of the most active xylosides inhibitors to ablate HS production in mouse ESCs. Unfortunately, none of the previously reported compounds that attenuated HS expressing and FGF2 binding were able to fully inhibit differentiation and restrict the ESCs in their pluripotent state.

Therefore, we set out to develop a novel inhibitor of β4GalT7 that is compatible with glycocalyx remodeling (Fig. 4.1). We used the information gleaned from numerous structure-activity studies done with xyloside inhibitors to further modify xyloside inhibitors and develop a new class of non-xylose inhibitors. Our strategy utilized in silico docking methods as a way of verifying the potential of our rationally designed compounds. Through this method, we have developed a novel class of inhibitors that utilizes the metal binding site, for near-complete inhibition of HS biosynthesis. This inhibition prevents differentiation and enables reprogramming with HS mimetics.

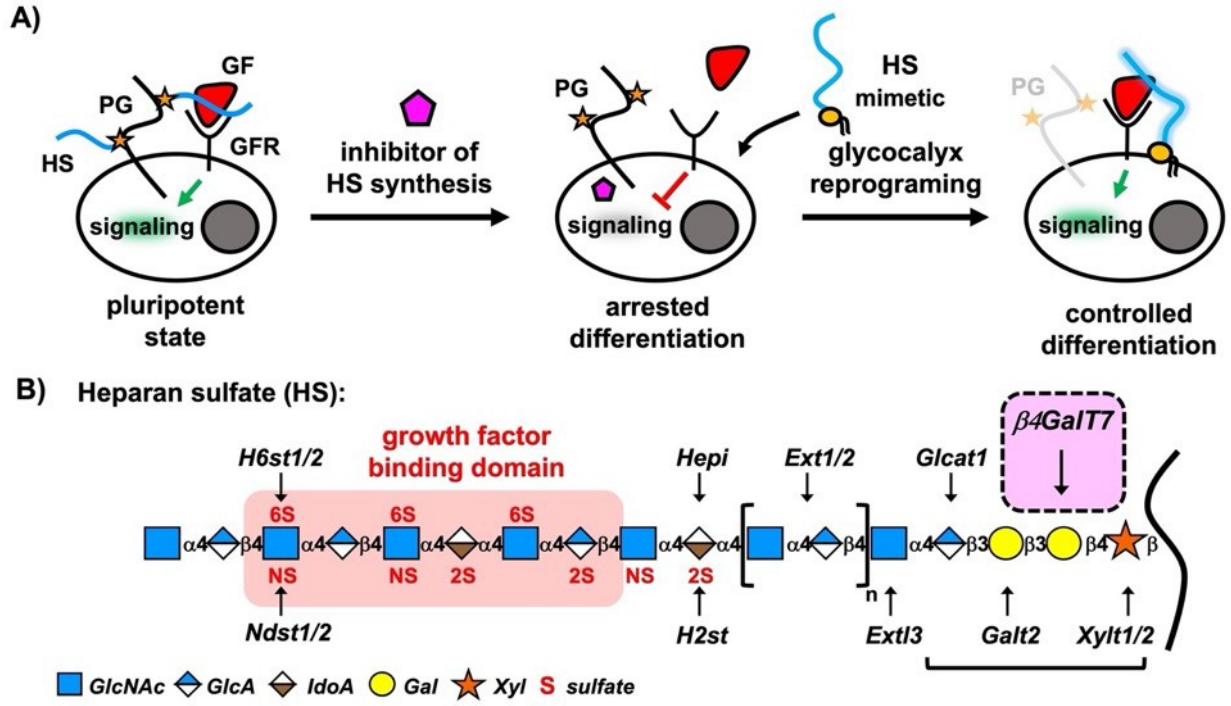

Figure 4.1. Glycocalyx remodeling strategy using inhibitor and HS-mimetics. A) Schematic of experimental design B) HS biosynthesis and target for inhibitors

4.2 Results

To develop compounds with improved activity in suppressing ESC differentiation via inhibition of HS, we used computational modeling to expand the set of potential inhibitors. Using 4FMUX as a starting point for rational design of additional inhibitors we used computational docking using crystal structures for β4GalT7. Based on the occupancy of its UDP-Gal binding site, the β4GalT7 enzyme accommodates two conformational states. The enzyme undergoes a conformational change from an "*open*" to a "*closed*" form upon UDP-Gal binding, which enhances binding of the *O*-xylosylated protein substrates to the active site of the enzyme and initiates catalysis.[31] Docking of 4FMUX into the UDP-Gal bound *closed* form of the enzyme (Fig 4.2A), confirmed previously identified key interactions for the inhibitor in the active site.[32,33] Namely, D228,

Y194, Y196, Y199, W224 as key amino acid side-chain residues involved in hydrogen bonding to the substrate, π-stacking and C-H/ π interactions.[25] We used these contacts and a space filling model to designing novel xyloside and primer structures with varying aglycones and linkers to the xyloside (compounds 1-10). Additionally, warhead targeting Tyrosine and Arginine were added to the end near the aglycone in an attempt to design a covalent inhibitor (compounds 11-16). Our final strategy was replacement of the xylose region with heterocyclic structures, which could have enhanced H-bonding with D228, Y194, Y196 and Y199, while also benefitting from improved membrane permeability, additional π-stacking interactions and hydrolytic stability over the glycosidic bond (compounds 16-19).

All proposed structures underwent docking to confirm the orientation of binding in the active site of the enzyme (see Table 4.1 and 4.2 for predicted interactions). Anticipating that the non-xyloside inhibitors may also engage the enzyme in its open form conformation, we performed docking analysis using a previously published structure of β4GalT7 crystallized in the absence of UDP-Gal.[34] Interestingly, close inspection of the docking data revealed that one of the non-xyloside compound **16**, benzotriazolyl dansyl sulfonamide (**BTADan)**, had several predicted docking orientations with the triazole ring oriented toward the Mn^{2+} in the active site of the enzyme (Fig. 4.2B). This led us to hypothesize a possible coordination of the molecule to the metal center. This contact was not observed for this molecule in the closed form of the enzyme or with any other structure with a triazole (Table 4.1).

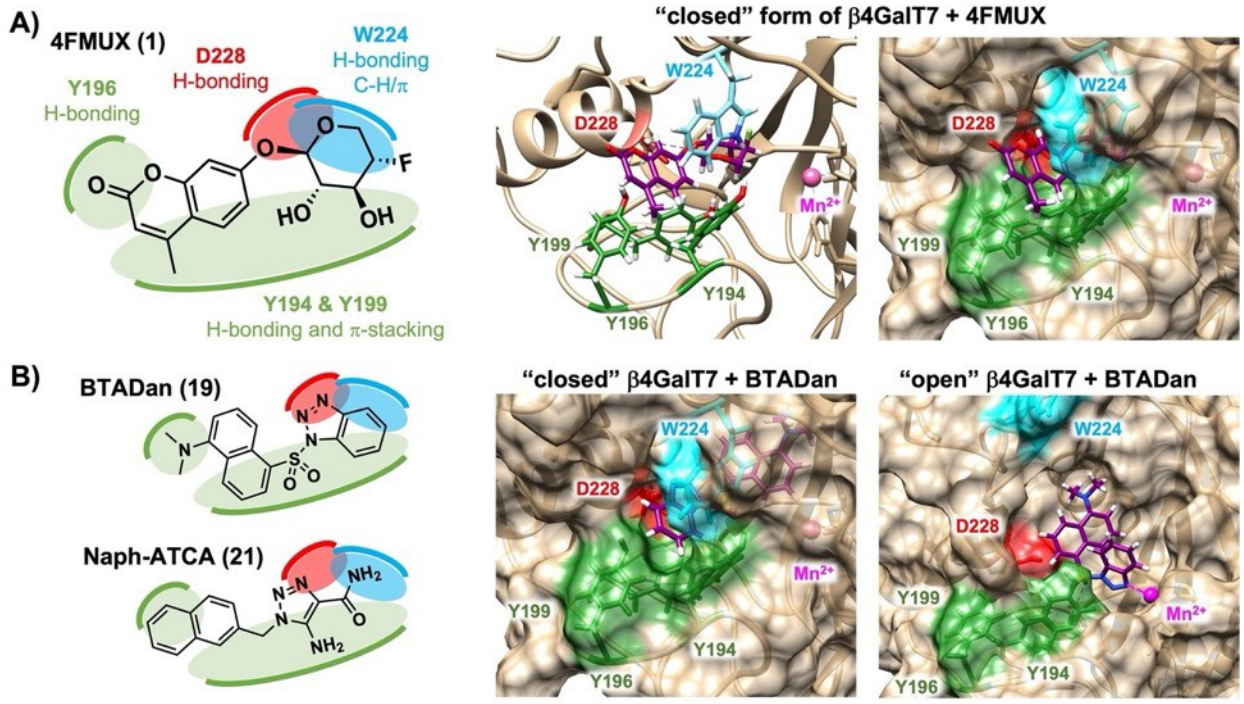

Figure 4.2. Design and docking of xylosides and non-xyloside inhibitors. A) In the closed form of the enzyme, 4FMUX is predicted to have π-stacking interactions with Y194 and Y199 along the aglycone, as well as H-bonding interactions between the hydroxyl groups at C2 and C3 of the xyloside and the hydroxyl groups of Y194 and Y199 (green). On the other face of the molecule, D228 and W224 form H-bonding interactions (red) and C-H/ π interactions (blue) with the xyloside. B) The design of the non-xylose inhibitors **BTADan** and **Naph-ATCA** with these interactions in mind (left). However, some predicted binding orientations of **BTADan** showed binding in the reverse direction in the closed form (middle). In the open form (right), another interesting feature arises, as the triazole is predicted to be within 3 Å of the metal center in the active site.

All new compounds were tested for β4GalT7 inhibition using an *in vitro* UDP-Glo enzymatic inhibition assay (Promega),[35] in which the transfer of UDP-Gal to 4MUX primer substrate is coupled to the generation of luminescence. All the compounds were tested at 0.5 mM concentration and achieved at least 20% activity (Fig. 4.8), so they were further tested for inactivation of HS in CHO cells via FGF2 binding **(**Fig. 4.3A). The cells were incubated with compounds at concentrations 500 μM for 24 hrs and their activity was assessed by staining with AF647-FGF2 by flow cytometry (Fig. 4.3A and Fig. 4.X). None of the new xyloside inhibitors showed enhanced activity over 4FMUX (Fig. 4.X); however, **BTADan** and **Naph-ATCA,** exhibited significant reduction of FGF2 binding, with **BTADan**

showing the strongest inhibition (Fig. 4.3A). Inhibition of HS by 4FMUX, **BTADan** and **Naph-ATCA** was further evaluated by increasing inhibitor concentration or extending the duration of the treatment. **BTADan** exhibited nearly complete inhibition of HS biosynthesis at higher concentrations and increased time (Fig 4.3A). To confirm the loss of FGF2 binding was due to loss of HS, we stained the inhibited cells with the anti-HS antibody 10E4 (Fig. 4.3). Loss of HS was consistent with the observed levels of FGF2 binding, with **BTADan** showing the strongest inhibition of HS in both dose and time dependent manner.

Although **BTADan** was predicted to have few H-bonding contacts in both the open and closed form in *our in-silico* docking, it was predicted to be near the Mn^{2+} in the active site of the open form of β4GalT7 (Fig. 4.2B). The metal center plays a critical role in the transition from the open to the closed conformation of the enzyme and is essential for catalysis. While we did not design the molecule with this interaction in mind, there have been reported inhibitors that utilize metal binding to prevent catalysis of glycosylation.[35,36] While some of these inhibitors displayed poor specificity or selectivity, a recent inhibitor has been designed using a fragment based approach that may behave similarly to our proposed inhibitor. This inhibitor was screened against human blood group glycotransferase B, and is thought to work by spanning the active site and bind to the metal center, preventing the necessary conformational change for catalysis to occur.[37] We were curious if **BTADan** owes its increased potency by binding in a similar manner so we hypothesized that coordination to the metal may prevent the conformational change of the enzyme, locking it in an open state and leading to the observed efficacy of the molecule despite fewer predicted interactions within the active site.

To validate this hypothesis, we performed fluorescence polarization studies with the apo form of the β4GalT7, **BTADan** and UDP-Gal. In the absence of Mn^{2+}, there was a significant reduction of **BTADan** binding, indicating a dependence on Mn^{2+} for binding (Fig. 4.3D). Furthermore, binding was independent of UDP-Gal (Fig. 4.3E), suggesting binding is only in the open form of the enzyme. The conformational change only occurs once UDP-Gal and the acceptor sugar have bound to the enzyme. Therefore, it is unlikely that **BTADan** binds the closed form of the enzyme.

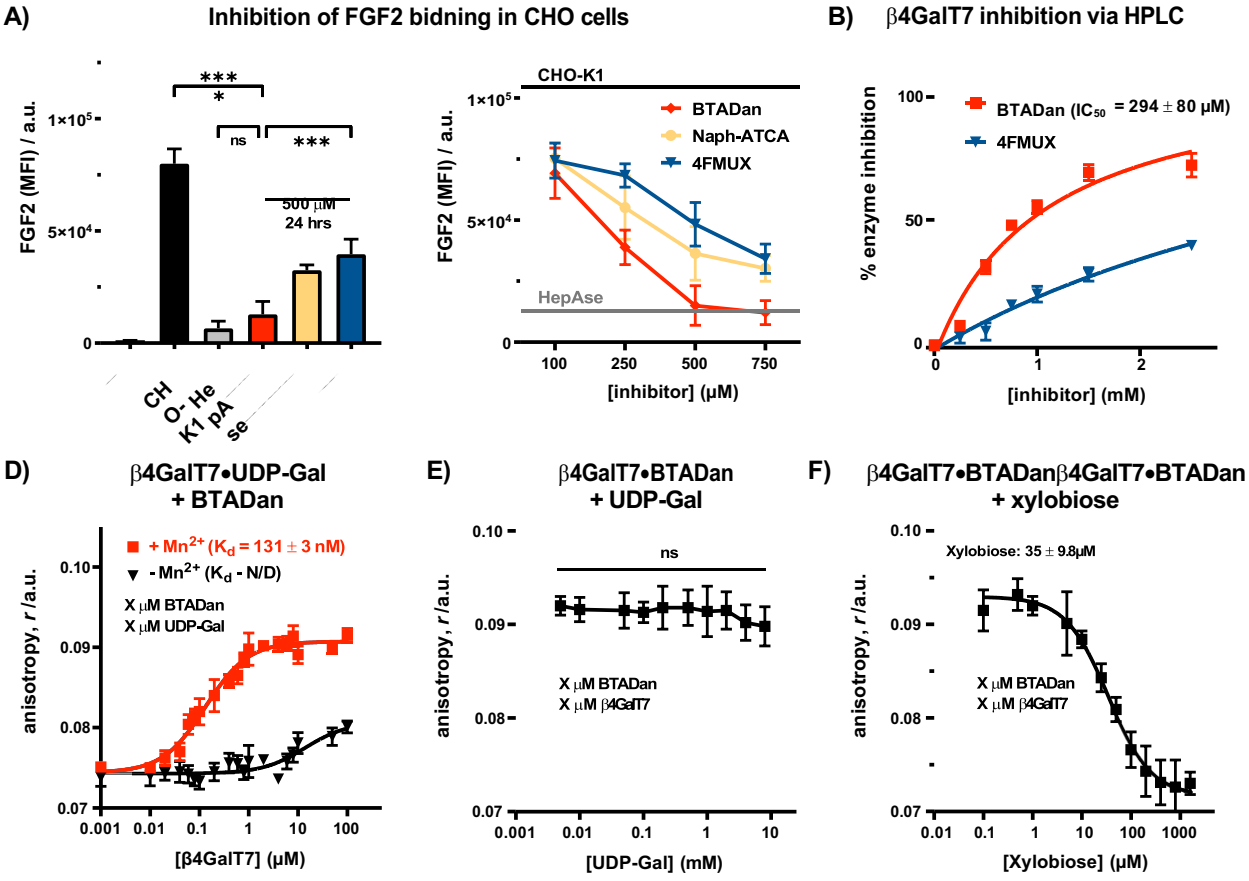

Figure 4.3. BTADan and Naph-ATCA CHO screen and in vitro characterization. A) CHO cells were incubated with 0.5 mM inhibitors for 24 h. After that time, they were washed and stained with AF647-FGF2 and visualized by flow cytometry. B) HPLC assay C) 50 µM **BTADan** was incubated with various concentrations of β4GalT7 (0.01 µM-100 µM) in the presence of 400 µM UDP-Gal with or without 2 mM Mn^{2+}. Fluorescence was observed and anisotropy calculated using a fluorimeter. D) 50 µM **BTADan**, 1 µM β4GalT7 and 2 mM Mn^{2+} were titrated with UDP-Gal and fluorescence anisotropy was recorded using a fluorimeter. E) 50 µM **BTADan**, 1 µM β4GalT7, 400 µM UDP-Gal and 2 mM Mn^{2+} were titrated with xylobiose.

With a prospective candidate in hand, we set to evaluate the potency and selectivity of the molecule in mESCs. We observed significantly more cytotoxicity in mESCs than CHO cells (Fig. 4.4B) but were able to see significant reduction of FGF2 binding at 100 μM concentrations when treated for 72 h (Fig. 4.4A,C,D). Decreased staining with the HS binding antibody 10E4 was also observed (Fig. 4.4E,F), indicating the loss of FGF2 binding was likely a result of inhibition of HS biosynthesis. To ensure that this molecule is selective for β4GalT7, and is not interacting with other glycosyltransferases, we isolated RNA from mESCs incubated with BTADan (100 μM, 72 h). We observed no change in mRNA expression of HS biosynthetic genes or pluripotency markers under these conditions compared to E14 mESCs (Fig 4.4G). To determine if BTADan was selective for HS biosynthesis, and not other glycosyltransferases, we used biotinylated lectins to stain for common cell surface glycosylation (1 h incubation, followed by 1 h incubation with streptavidin-AF647). After 72 h of 100 μM incubation with **BTADan**, there was no observable aberrant glycosylation on the surface of the mESCs as determined by flow cytometry (Fig 4.4I). Carbazole assays were used to further quantify the inhibition of HS biosynthesis. HS disaccharides derived from E14, *Ext1*$^{-/-}$ and **BTADan** treated E14 mESCs were collected using pronase (50^{o}C, 72 h). CS or HS was digested using bacterial chondroitinase or heparinase (respectively) and carbazole assay was used to measured total GAG content. Both *Ext1*$^{-/-}$ and **BTADan** treated E14 mESCs showed reduced isolated HS, with **BTADan** inhibited cells also having reduced chondroitin sulfate (Figure 4.4H).

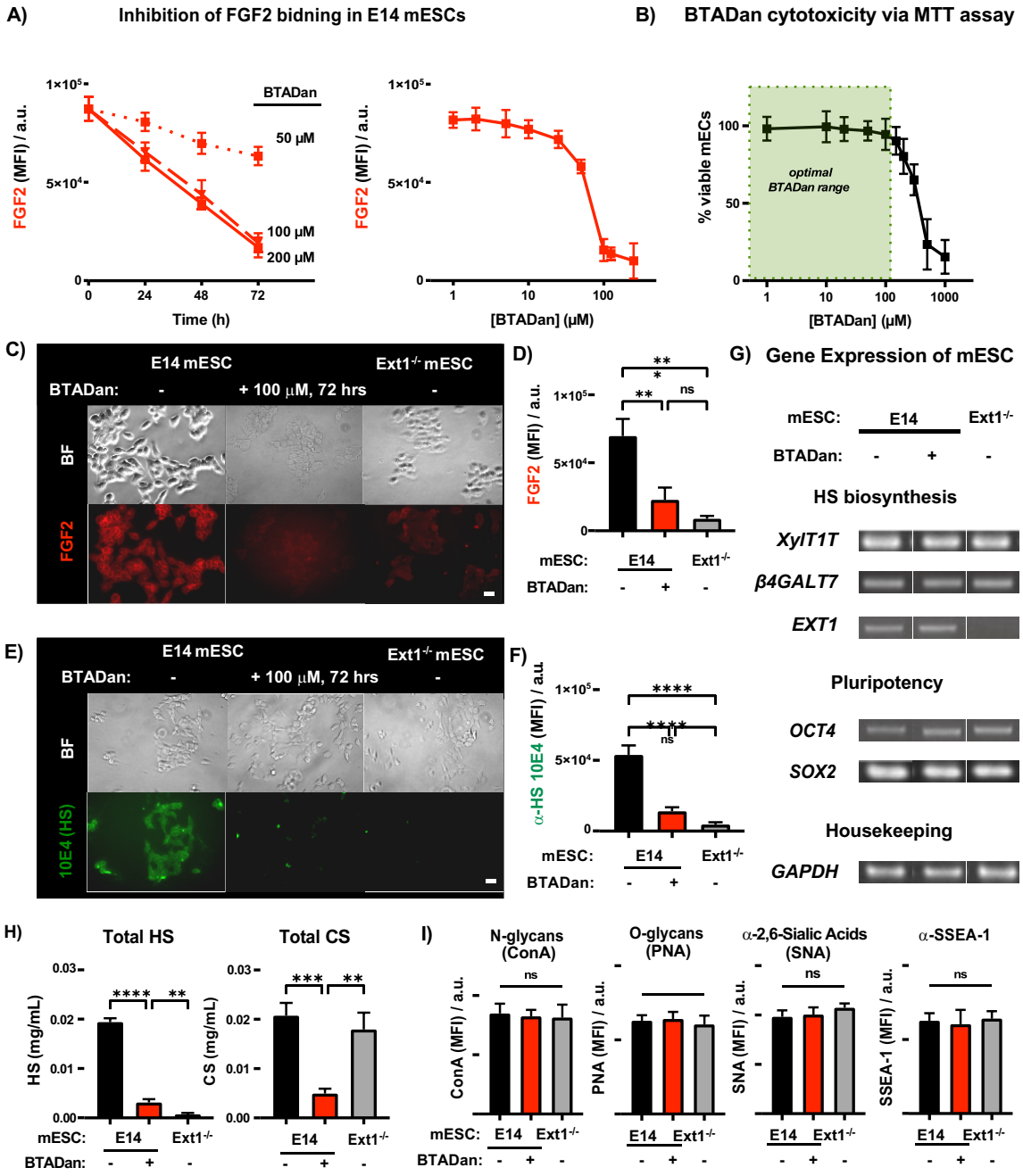

Figure 4.4. BTADan inhibition of HS biosynthesis in E14 mESCs. A) mESCs were incubated with BTADan (50, 100, 200 μM) for 24, 48 or 72 h. After that time, they were stained with 100 nM AF647-FGF2 and visualized by flow. B) Cells treated under the same conditions were used in an MTT assay[30] to test for cell viability. Cells incubated with BTADan (100 μM, 72 h) were fixed and stained with C) 100 nM AF647-FGF2 or E) α-HS (10E4, 1:200) and secondary (1:500). Images were taken on the Keyence Fluorescent Microscope. To confirm microscopy data, D) FGF2 stain F) and 10E4 stain were repeated and analyzed by flow cytometry. G) Gene expression H) Cells grown to confluency in T150 flasks and treated with standard **BTADan** inhibition were treated with pronase for 72 h at 50°C. GAGs were digested with chondroitinase or Hepase and GAG concentrations were determined using standard curves developed from carbazole assays I) Lectins (1:250) and streptavidin-AF647 (1:500) were incubated with fixed cells inhibited for 72 h with BTADan. Lectin stained cells were visualized by flow cytometry.

To determine if this reduction in HS was enough to prevent differentiation, we pre-treated Oct4-GFP (pluripotency marker) and Sox1-GFP (neuroectoderm marker) mESCs reporter cell lines with **BTADan** (72 h, 100 μM) and then switched to N2B27 neural differentiation media. After six days of differentiation, cells were evaluated by fluorescence microscopy (4.5A) and flow cytometry (4.5B). We observed significant reduction of Sox1 expression after 6 days compared to untreated mESCs and high levels of Oct4 were observed, indicating maintenance of pluripotency. This reduction of Sox1 (>60%) expression and maintenance of Oct4 expression was comparable to $Ext1^{-/-}$ mESCs (Fig 4.13). 4FMUX treatment was unable to arrest mESCs in a pluripotent state (Fig. 4.13). Similar treatment of *wt* mESCs, subsequent permeabilization (10% methanol) and staining for Sox1 and Oct4 showed similar trends (Fig 4.5B). This maintenance of pluripotency is likely due to a loss of FGF2 signaling through ERK phosphorylation. To test this, we pre-treated mESCs with BTADan (100 μM) for 72 h, and then serum starved them for an additional 12 h. Cells were then lysed and collected protein was analyzed by Western Blotting. Staining for phospho-ERK resulted in two-fold decrease in ERK phosphorylation over untreated mESCs (Fig 4.5C).

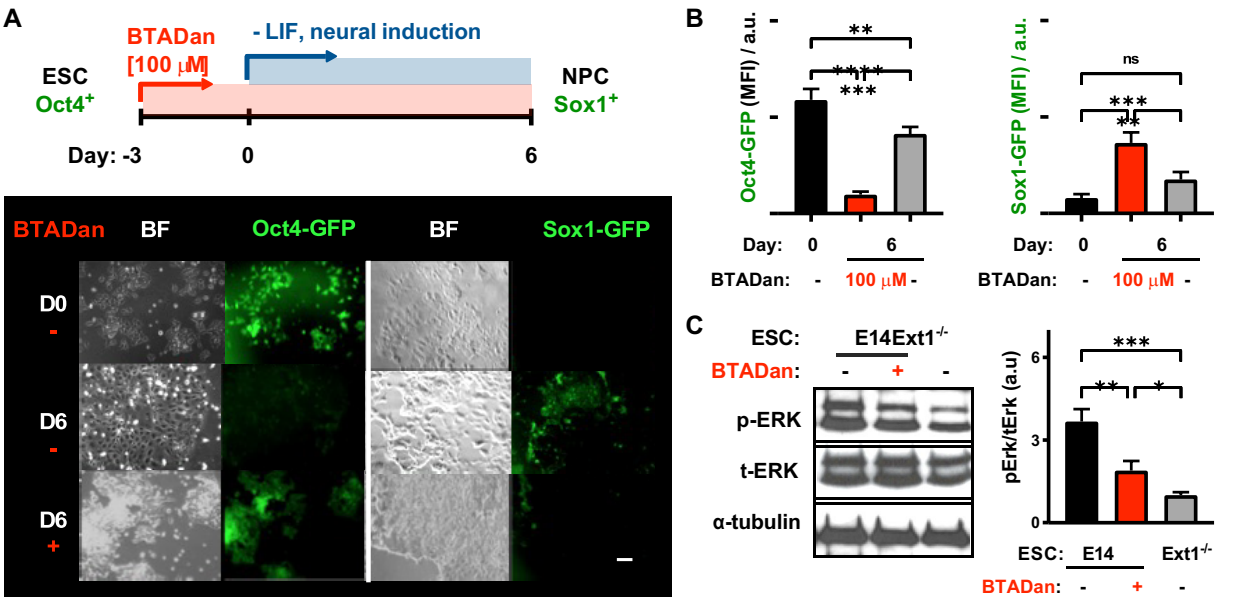

Figure 4.5. Inhibition of HS biosynthesis via **BTADan** prevents differentiation. A) Oct4-GFP and Sox1-GFP reporter cell lines were differentiated in the presence or absence of BTADan. Following 6 days of differentiation, cells were fixed and imaged. B) Differentiation conditions were repeated with Oct4-GFP and Sox1-GFP lines and analysis by flow cytometry C) E14 mESCs were plated in 6-well plates and incubated with BTADan (100 μM) for 72 h. Following inhibition, cells were stimulated with FGF2 (10 nM) for 45 min. Cells were lysed and phosphorylated ERK was visualized by Western Blot.

To be an effective inhibitor of HS for therapeutic purposes and one that can be used in conjunction with glycocalyx engineering methods, native HS structures should be seen upon removal of the inhibitor. The transient nature of small molecule inhibitors, and therefore reversibility, is a key aspect for our glycocalyx engineering approach. To test the reversibility of **BTADan**, mESCs were differentiated in neuroectodermal conditions for 10 days, and **BTADan** was removed after the third day. Cells were fixed at day 0, 3, 6 and 10, and stained for HS (10E4), Oct4 and Sox1. Unsurprisingly, mESCs left in **BTADan** for all ten days of differentiation showed no significant staining for 10E4 and Sox1, while maintaining high levels of Oct4 expression (Fig 4.6A). When **BTADan** was removed from the media, HS expression increased (Day 6, Fig 4.6A). By Day 10, Sox1 expression was observed in similar levels as untreated mESCs at Day 6, indicating recovery of HS and subsequent differentiation.

Additionally, glycocalyx engineering in conjunction with **BTADan** treatment should result in further differentiation. Previous studies by Dr. Cathy Merry and others have established that soluble heparin[28] or introduction of HS mimetics[29] can overcome HS deficiency in *Ext1*$^{-/-}$ mESCs and drive differentiation towards neuroectodermal lineages. Therefore, we introduced soluble heparin (5 μg/mL) at Day 0 of differentiation and continue treatment throughout the six days. By Day 10, we observed increased Nestin and βIII-tubbulin expression, further indicating the mechanism through which **BTADan** arrests mESCs in a pluripotent state is via reduction of HS biosynthesis (Fig 4.6C). This result was of particular interest for us, as we have previously used HS-mimetic glycopolymers (**GP**) to remodel the glycocalyx of *Ext1*$^{-/-}$ mESCs and drive differentiation. **GP-D2A6** has previously been shown to promote both neural and mesodermal differentiation in *Ext1*$^{-/-}$ mESCs. Incubation of **GP-D2A6** (1 h, 3 μM) with E14 mESCs pretreated with **BTADan** and subsequent differentiation does in fact result in increased Sox1 expression after six days of differentiation (Fig 4.6C). If BTADan is removed at Day 3 of the differentiation, the neural precursor cells will have normal HS expression on their surface (Fig 4.6 D). Therefore, BTADan is a promising inhibitor for use with glycocalyx engineering methods.

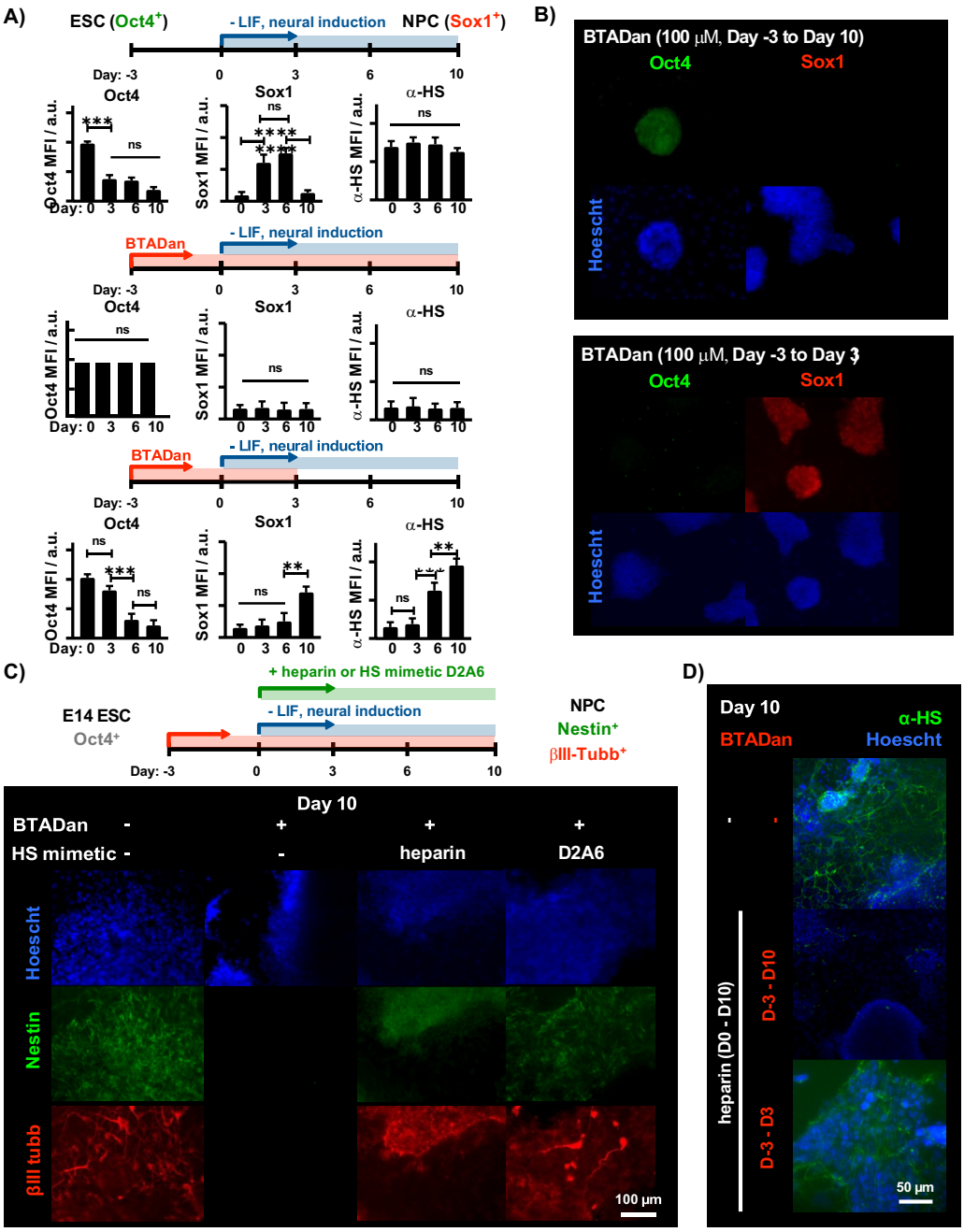

Figure 4.6. BTAdan inhibition is reversible and compatible with glycocalyx remodelling techniques. A) E14 mESCs (top) were differentiated for 10 days, with cells being fixed and permeabilized at Day 3, 6 and 10. To determine reversibility of inhibition, E14 mESCs were also differentiated in the presence of **BTADan** (100 μM, middle) throughout differentiation, or with **BTADan** from Day -3 to Day 3. Cells were stained for Oct4, Sox1 and HS (10E4) and visualized by flow cytometry. B) Under these conditions, fluorescence microscopy was also used to visualize the results. C) To determine if HS mimetics can be used in the presence of **BTADan** (100 μM), mESCs were grown for 10 days in neural differentiation conditions and then stained for Nestin (green) and βIII-tubulin (red). **BTADan** treated cells did not differentiate, but if HS mimetics were introduced either through soluble heparin or with glycocalyx remodeling with **GP-D2A6** (3 μM at Day 0), high levels of Nestin and βIII-tubulin are observed. D) Removal of **BTADan** at Day 3 during this differentiation allows for recovery of native HS (10E4, green) after differentiation.

4.3 Conclusions

Chemical tools for modulating stem cell differentiation offer a distinct advantage over genetic manipulations, as particularly for therapeutic purposes. Herein, we describe one such tool that allows for transient ablation of cell surface HS through inhibition of B4GalT7. This inhibitor is potent enough at sub-cytotoxic concentrations to prevent cell surface HS expression, resulting in suppression of downstream signaling associated with GF binding. This loss of binding and signaling results in arrest of the stem cells in a pluripotent state, similar to the phenotype of *Ext1*$^{-/-}$ mESCs. This method of inhibition is also compatible with glycocalyx remodeling, either with soluble heparin or cell surface engineering with glycopolymers, allowing for chemical control of differentiation. This provides a powerful tool for studying stem cell differentiation and increasing the therapeutic potential of glycocalyx engineering approaches.

In addition, this novel inhibitor gains much of its potency through coordination to a metal center within β4GalT7. While some compounds have been developed to target the metal centers of glycosyltransferases, the number of compounds is dwarfed by the number of xylosides that have been developed. With advances in metallo-based inhibitor designs, such as fragment-based designs[23,24] this could offer an exciting opportunity to revisit this strategy for potent and specific glycotransferase inhibition. These metal centers are ubiquitously found in the active site of glycosyltransferases and therefore could be targets for metal-binding small molecule inhibitors with greater potency and specificity for a wide range of glycan structures.

4.4 Materials and methods

4.4.1 Reagents and Instrumentation

Size exclusion chromatography (SEC) was performed on a Hitachi Chromaster system equipped with an RI detector and a 5 µm, mixed bed, 7.8 mm I.D. x 30 cm TSKgel column (Tosoh Bioscience). GlycoPolymer **P1** was analyzed in DMF (0.2% w/v LiBR, 70°C) using an isocratic method with a flow rate of 0.7 mL/min. Glycan conjugation reactions were performed in a Biorad MyCycler thermocycler (Hercules, CA). *Molecular modeling was done using pymol and previously published crystal structures of the open and closed form of the enzyme*. *ESC and CHO cultures* were performed using standard sterile cell culture techniques. CHO cells were grown in the presence of a cocktail of penicillin and streptomycin, while mESCs were grown without antibiotics. *Flow cytometry* analysis was performed on BD Accuri C6 flow cytometer and analyzed with FlowJo software. *Fluorescence microscopy* was done using a Keyence Widefield Microscope and images were analyzed using ImageJ software. *Statistical analysis* was performed using PRISM software. All biological experiments were performed in at least 3 experimental replicates and microscopy images were acquired and analyzed for at least 5 images per experimental condition. Included are representative images for each condition. All data were plotted as mean values ± standard deviation. Statistical analysis was performed using ANOVA.

4.4.2 Cell culture

CHO cells were grown without gelatin on tissue culture plates in 50:50 DMEM:F12 + 10% FBS. For embryonic culture, E14 and Ext1$^{-/-}$ mESCs (gift from Dr. Catherine

Merry) were grown on gelatin-coated plates in knockout (KO)-DMEM + 10% FBS in the presence of LIF.

4.4.3 Docking

Docking was done with a combination of Autodock Vina[37] and Schrodinger Glide[38] and images were made with UCSF Chimera software.

4.4.4 Synthesis of non-xyloside inhibitor

The synthesis of the non-saccharide inhibitors required one-to-two steps to synthesize (**BTADan**, **17**, **18, 19**). For **BTADan** and **17**, 1H-benzotriazole was dissolved in anhydrous pyridine, to which dansyl chloride (**BTADan**) or tosyl chloride (**17)** was added to the solution. After 5 hours, the solvent was removed *in vacuo* and the product was purified on SiO_2 (0-100% EA in hexanes) to afford title compounds **BTADan** or **17**. Compounds **18** and **19** were synthesized by dissolving benzyl bromide (**19**) or 2-(bromomethyl)-naphthalene (**18**) in acetone, to which NaN_3 dissolved in water was added to the stirred solution overnight. The solvent was removed, taken up in ethyl acetate, and washed with water and brine. The organic layer was dried over Na_2SO_4 and condensed *in vacuo*. The azido compound was then dissolved in anhydrous DMSO and used without further purification.

4.4.5 UDP-Glo

Full-length β-1,4-galactosyltransferase 7 (β4GalT7) with an *N*-terminus GST tag was purchased from Novus Biologics, LLC (Littleton, CO) for use in the assay. A UDP-GLO™ glycosyltransferase assay kit was purchased from Promega (Madison, WI) that was specific for galactosyltransferase and UDP-galactose detection. The literature procedure accompanied with the assay kit was modified to account for β4GalT7's unique

environmental conditions. For this assay, a buffer was used containing 50 mM Tris-HCl, 150 mM NaCl, 5 mM $MnCl_2$, and 0.02% Tween 20; with the pH adjusted to 6.5 with 1 M HCl and filtered through a 0.22 μm membrane. All reagents that accompany the kit, should be diluted with this buffer, unless otherwise noted. This includes dilutions with UDP-Gal, β4GalT7, acceptor substrate, and inhibitors (in 10% DMSO-buffer solution). White, half-volume, flat bottom 96-well plates are used for the assay.

Two standard curves are initially generated to determine (1) the amount of luminescence produced vs. the concentration of free UDP in solution and (2) the amount of β4GalT7 required to produce a 67-fold signal-to-noise ratio, per manufacturer guidelines. Once those values are produced and the reagents required for the assay are mixed, the procedure is followed as written. The nucleotide detection reagent that is provided with the assay kit is stated to quench glycosyltransferase, but this has not been determined empirically in-house.

Acceptor substrate (4MUX) and donor substrate (UDP-Gal) were diluted to 400 μM (1 mM stock solution). Inhibitors were added at 500 μM to the enzyme, and then acceptor and substrate was added. Reaction was run for 30 min, quenched and analyzed by plate reader.

4.4.6 HPLC

A solution of UDP-Gal (400 μM) and β4GalT7 (100 μM) was made in a 96 well plate. For this assay, a buffer was used containing 50 mM Tris-HCl, 150 mM NaCl, 2 mM $MnCl_2$, and 0.02% Tween 20; with the pH adjusted to 6.5 and filtered through a 0.22 μm membrane. 4MUX accepter substrate (400 μM) and increasing concentration of 4FMUX

or BTADan were added to the enzyme mix. After 30 m, the reaction was quenched, centrifuged and run through a C18 column by HPLC (Agilent, C18 column).

4.4.7 Flow Cytometry

To monitor EB remodeling with glycopolymers **P2**, Day 0 EBs were incubated with the glycopolymers at increasing concentrations (0.3-3 μM) for 2 h at 37 °C. EBs were washed with DPBS and then dissociated for 15 min using Accutase in DPBS (Innovative Cell Technologies). Cells were analyzed for the presence of AlexaFluor 488 glycopolymer labels using the Accuri C6 flow cytometer (BD bioscience).

To monitor differentiation, EBs were differentiated in N2B27 Neurobasal media for 10 days, before cells were dissociated fixed with 4% PFA and permeabilized in cold methanol. They were then blocked with 2% BSA/DPBS for 1 hr. The cells were probed with Oct4 antibody or Sox1 antibody (in 0.2% BSA/PBS) for 1 h, then washed with DPBS and stained with AF488 or AF647 labeled secondary antibody. Fluorescence was measured using the Accuri C6 flow cytometer and analyzed using Flowjo software. Means and standard deviations were calculated from three independent biological experiments, and p-values were calculated using ANOVA analysis with PRISM software.

4.4.8 GAG composition

Cells were grown to 80% confluency in sterile T150 flasks. After 72 h in media treated with **BTADan** (100 μM), cell surface glycans were collected using pronase treatment (72 h, 50°C). Glycans were collected using size exclusion columns. Solutions were incubated for 48 h with either heparinase or chondroitinase and digested disaccharides were removed through a size exclusion column. The remaining HS or CS

was used in a carbazole assay as previously described[REF] to determine concentration of GAG in solution.

4.4.9 Lectin Staining

E14 mESCs were plated and grown in the presence of LIF and inhibitor for three days (Day -3 to Day 0). At Day 0, cells were lifted using 0.05% trypsin-EDTA, stained with biotinylated-lectins (100 nM) for 30 min at 37°C, and then AF647-Streptavidin was added for an additional 30 min. Lectin staining was visualized using the BD Accuri C6 Flow Cytometer and analyzed using Flowjo software.

4.4.10 Neural Differentiation

Differentiation towards neural lineages was done in N2B27 media as previously reported.[29] Cells were plated and grown for three days in the presence of inhibitor (100 μM) and LIF. At Day 0, media was switched to N2B27 media and media was changed every day and additional inhibitor added. Cells were fixed at Day 6 to stain for Oct4 (1:1000) and Sox1 (1:500), or further differentiated to Day 10 to stain for Nestin (1:250) and βIII-tubulin (1:250) and subsequent fluorescently labeled secondary antibodies (1:500). For transient inhibition experiments, inhibitor was no longer added after Day 3, and cells continued to differentiate until Day 10.

4.5 Acknowledgements

Chapter four, in full, is currently being prepared for submission for publication. M. R. Naticchia, S. Verespy, D. Kozirovskiy, C. Seitz, Z. Gaieb, M. L. Huang, B. Timm, R. Amaro, K. Godula. Small molecule inhibitor of heparan sulfate biosynthesis enable transient reprogramming of stem cell glycocalyx to control differentiation. The dissertation author was the primary researcher and author of this material.

4.6 Supporting Information

Supporting Information

Small molecule inhibitor of heparan sulfate biosynthesis enables transient reprograming of stem cell glycocalyx to control differentiation

Matthew R. Naticchia, [‡,[a]] Stephen Verespy,[‡ ,†,[a]] David Kozirovskiy,[§,[a]] Christian Seitz,[[a]]

Zied Gaieb[[a]], Mia L. Huang, Bryce Timm, Rommie Amaro,[[a]] and Kamil Godula[*[a,b]]

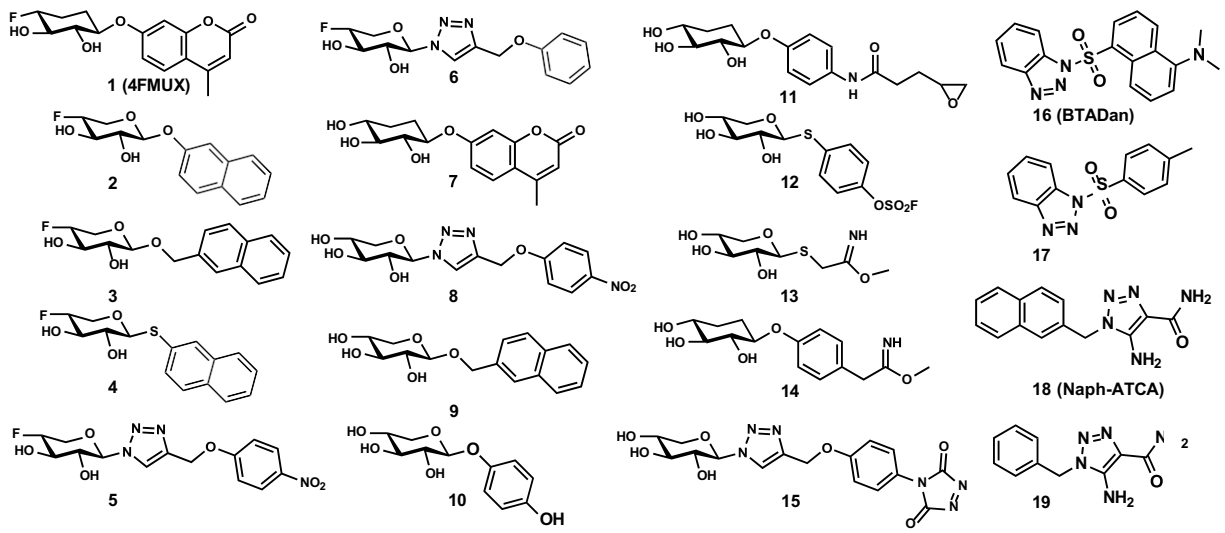

Figure 4.7. Library of inhibitors and primers.

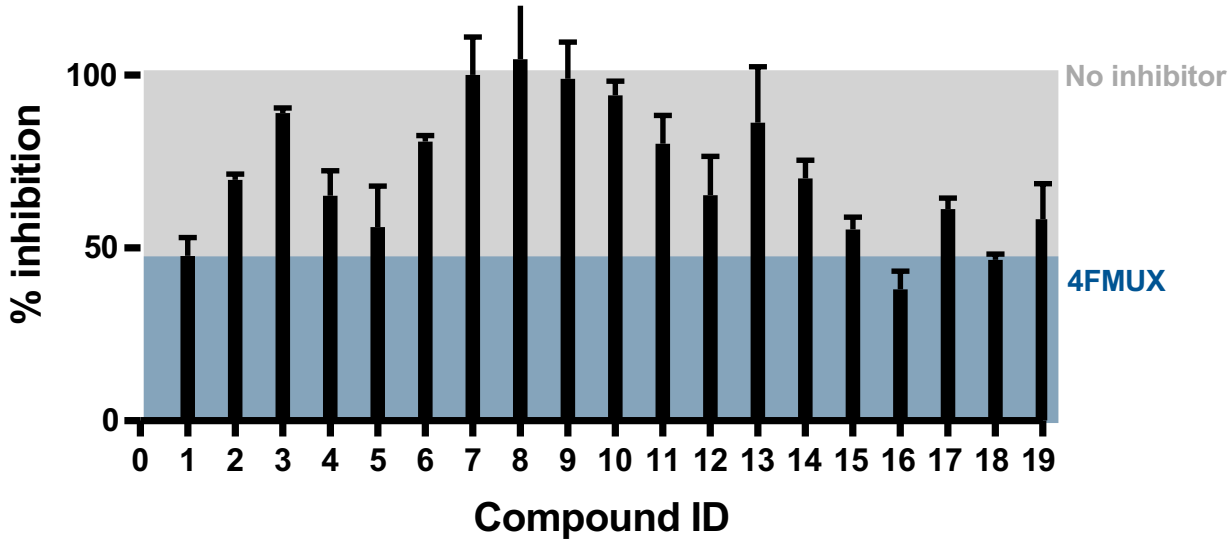

Figure 4.8. Enzymatic (UDP-Glo) screen of inhibitors. 4FMUX (1) inhibited enzymatic activity at 47% (blue line). Xyloside inhibitors (1-6) showed similar, primers (7-10) and covalent inhibitors (11-15) and two of the non-xyloside inhibitors (17 and 19) showed worse inhibition compared 4FMUX, but two non-xylose inhibitors showed the same or increased inhibition (16 and 18).

Table 4.1. Docking of inhibitors to open form (4IRP). Yellow indicates predicted π-stacking.

Compound ID	Y194	Y196	Y199	W224	D228	Mn^{2+}
Xylobiose	3.36 Å	N/a	2.28 Å	3.49 Å	2.2	N/a
1 (4FMUX)	4.30 Å	N/a	2.06 Å	3.37 Å	2.14 Å	N/a
2	3.97 Å	N/a	1.84 Å	N/a	3.87 Å	N/a
3	4.43 Å	N/a	1.89 Å	N/a	N/a	N/a
4	3.47 Å	N/a	2.14 Å	3.58 Å	2.29 Å	N/a
5	4.01 Å	N/a	2.19 Å	3.46 Å	2.16 Å	N/a
6	2.24 Å	N/a	2.43 Å	3.37 Å	2.10 Å	N/a
7	3.80 Å	N/a	3.01 Å	N/a	1.99 Å	N/a
8	4.23 Å	N/a	3.99 Å	N/a	2.40 Å	N/a
9	4.31 Å	N/a	1.99 Å	N/a	N/a	N/a
10	4.01 Å	N/a	2.19 Å	3.46 Å	2.16 Å	N/a
11	N/a	1.98 Å	2.17 Å	N/a	N/a	N/a
12	3.64 Å	N/a	2.65 Å	3.88 Å	2.61 Å	N/a
13	4.11 Å	N/a	3.11 Å	4.21 Å	2.15 Å	N/a
14	3.87 Å	N/a	3.69 Å	N/a	3.47 Å	N/a
15	3.90 Å	N/a	2.87 Å	N/a	3.19 Å	N/a
16 (BTADan)	3.18 Å	N/a	2.50 Å	N/a	N/a	2.31 Å
17	3.44 Å	N/a	3.80 Å	N/a	N/a	N/a
18 (Naph-ATCT)	3.46 Å	N/a	N/a	4.96 Å	3.37 Å	N/a
19	3.42 Å	N/a	2.07 Å	N/a	3.33 Å	N/a

Table 4.2. Docking of inhibitors to closed form (4IRQ). Yellow indicates predicted π-stacking.

Compound ID	Y194	Y196	Y199	W224	D228	Mn^{2+}
Xylobiose	3.36 Å	N/a	2.28 Å	3.49 Å	2.2	N/a
1 (4FMUX)	4.93 Å	3.95 Å	4.25 Å	2.55 Å 3.53 Å	3.01 Å	N/a
2	3.58 Å	4.12 Å	3.99 Å	2.39 Å 3.33 Å	3.26 Å	N/a
3	2.39 Å	3.88 Å	4.16 Å	4.16 Å	4.16 Å	N/a
4	2.12 Å	2.77 Å	4.74 Å	2.03 Å	1.87 Å	N/a
5	2.93 Å	3.96 Å	3.88 Å	3.16 Å	3.14 Å	N/a
6	2.74 Å	3.87 Å	3.59 Å	2.89 Å	2.99 Å	N/a
7	4.42. Å	3.59. Å	3.87. Å	2.94 Å	3.22 Å	N/a
8	2.92 Å	4.00 Å	3.34 Å	1.99 Å 3.84 Å	2.75 Å	N/a
9	3.16 Å	3.87 Å	3.59 Å	2.16 Å 4.01 Å	3.38 Å	N/a
10	3.59 Å	4.14 Å	3.59 Å	N/a	1.89 Å	N/a
11	3.70 Å	2.14 Å	2.13 Å	3.88 Å	2.53 Å	N/a
12	4.20 Å	N/a	2.56 Å	N/a	3.77 Å	N/a
13	3.91 Å	3.42 Å	2.12 Å	3.63 Å	3.10 Å	N/a
14	4.11 Å	N/a	3.19 Å	N/a	2.49 Å	N/a
15	3.78 Å	3.11 Å	3.66 Å	4.19 Å	2.78 Å	N/a
16 (BTADan)	4.16 Å	N/a	4.91 Å	3.74 Å	2.29 Å	N/a
17	4.33 Å	N/a	N/a	3.54 Å	2.78 Å	N/a
18 (Naph-ATCT)	4.47 Å	2.93 Å	4.66 Å	3.52 Å	2.45 Å	N/A
19	4.70 Å	2.84 Å	2.73 Å	3.59 Å	2.03 Å	N/a

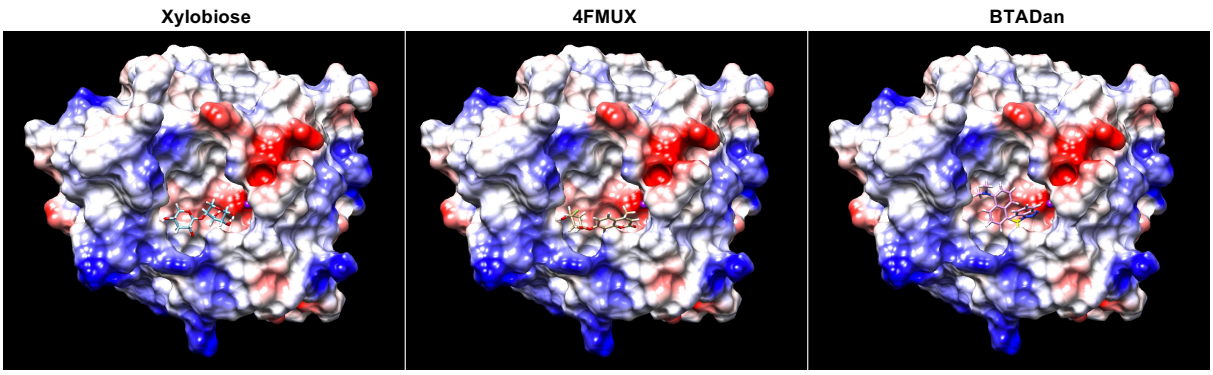

Figure 4.9. Surface potential of B4GalT7 in the open confirmation (4IRP) with xylobiose (middle), 4FMUX (middle), and BTADan (right) bound in the active site.

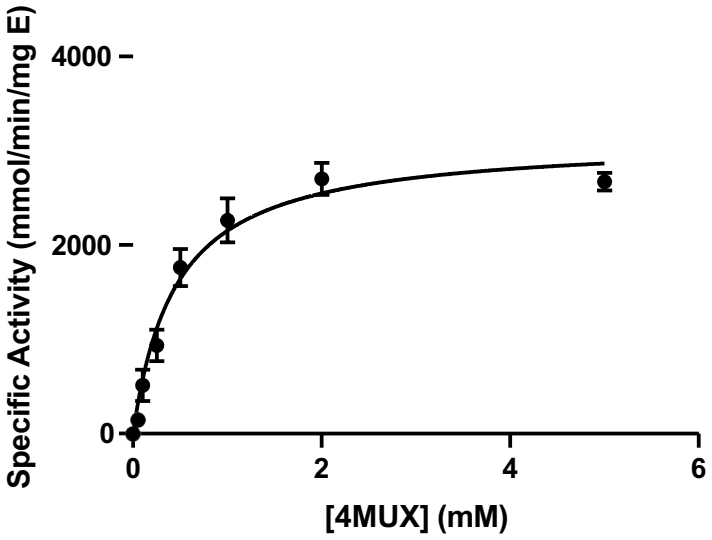

Figure 4.10. Efficiency of 4MUX as a substrate for b4GalT7 as analysed by HPLC. An increasing concentration of 4MUX was incubated with UDP-Gal (400 μM), β4GalT7 (100 μM). For this assay, a buffer was used containing 50 mM Tris-HCl, 150 mM NaCl, 2 mM $MnCl_2$, and 0.02% Tween 20; with the pH adjusted to 6.5 and filtered through a 0.22 μm membrane. After 30 m, the reaction was quenched, centrifuged and run through a C18 column HPLC (Agilent, C18 column). The K_m of 4MUX for the enzyme was determined to be 0.454 mM.

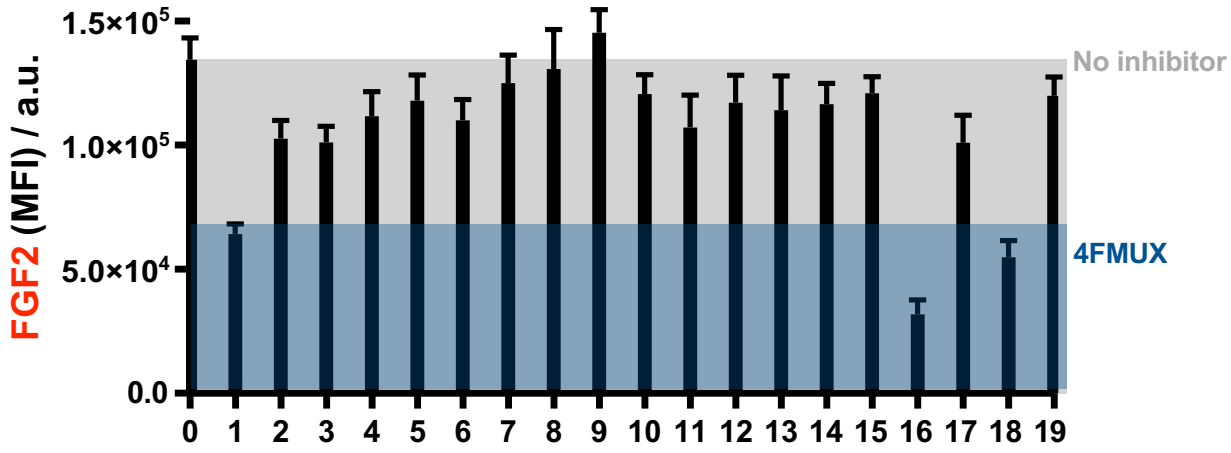

Figure 4.11. Full inhibitor CHO screen. Inhibitors (500 μM) were incubated with CHO cells for 24 h. Binding of AF647-FGF2 (100 nM, 1 h) to these CHO cells was visualized with flow cytometry.

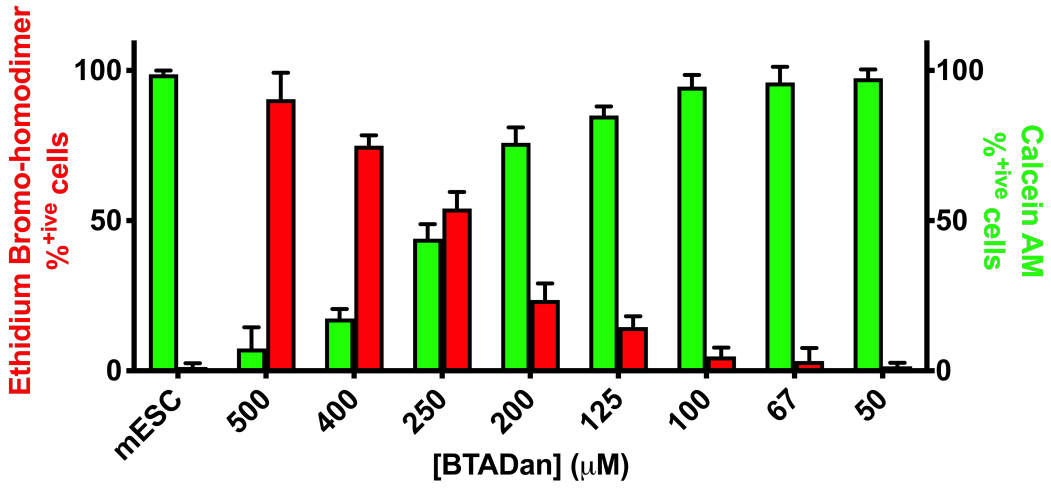

Figure 4.12. Cytotoxicity of **BTADan** in mESCs. E14 mESCs were treated with 100 μM **BTADan** for 24 h. After 24 h, cells were lifted with trypsin and stained with a Calcein AM/ Et Br homodimer cocktail. After 30 min incubation on ice, cellular fluorescence was visualized by flow cytometry.

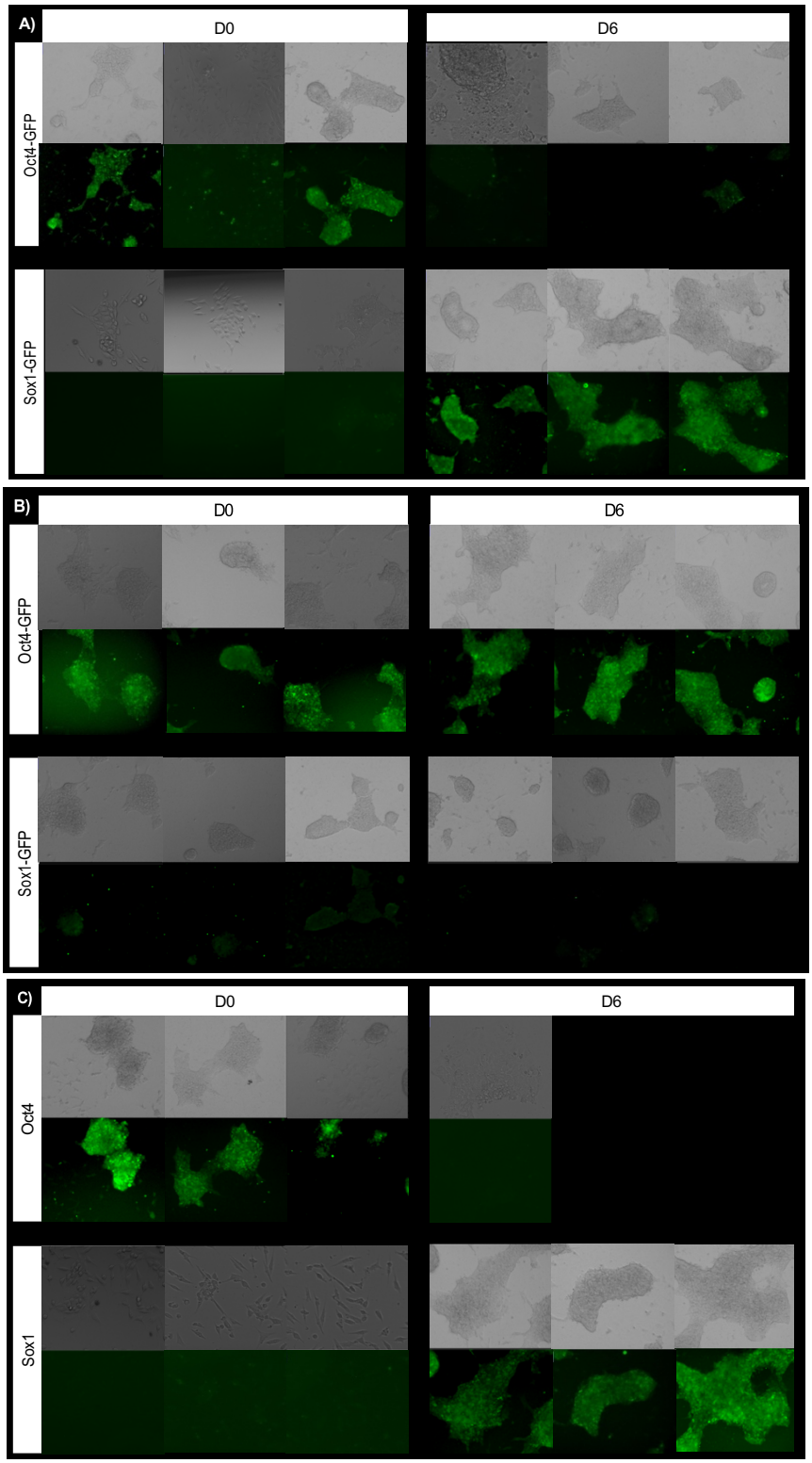

Figure 4.13. Extended Oct4 and Sox1 stained mESCs. A) Neural differentiation of mESC occurred for 6 days and cells were stained at Day 0 and Day 6. B) Neural differentiation after 72h pre-treatment with 100 μM **BTADan** and continued inhibition throughout differentiation. C) Neural differentiation after 72h pre-treatment with 100 μM 4FMUX and continued inhibition throughout differentiation.

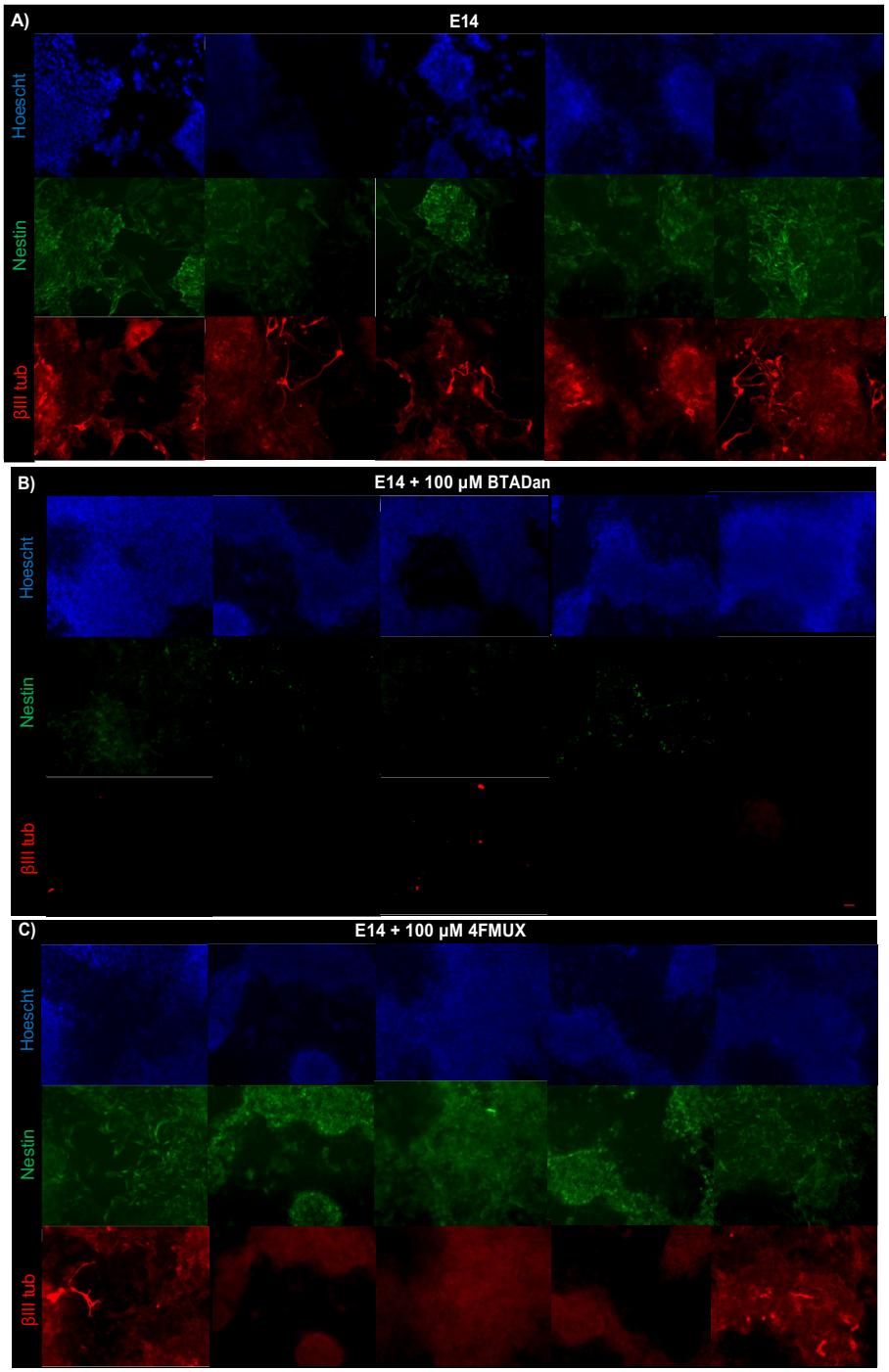

Figure 4.14. Extended Nestin and βIII-tubulin images. A) Neural differentiation of E14 mESCs for 10 days, and stained for Nestin (green) and βIII-tubulin (red). B) Neural differentiation in the presence of 100 μM BTADan. C) Neural differentiation in the presence of 100 μM 4FMUX. D) Neural differentiation in the presence of 100 μM BTADan and 5 μg/mL heparin. E) Neural differentiation in the presence of 100 μM BTADan and incorporated with 3 μM P1-D2A6 at D0 for 1 h.

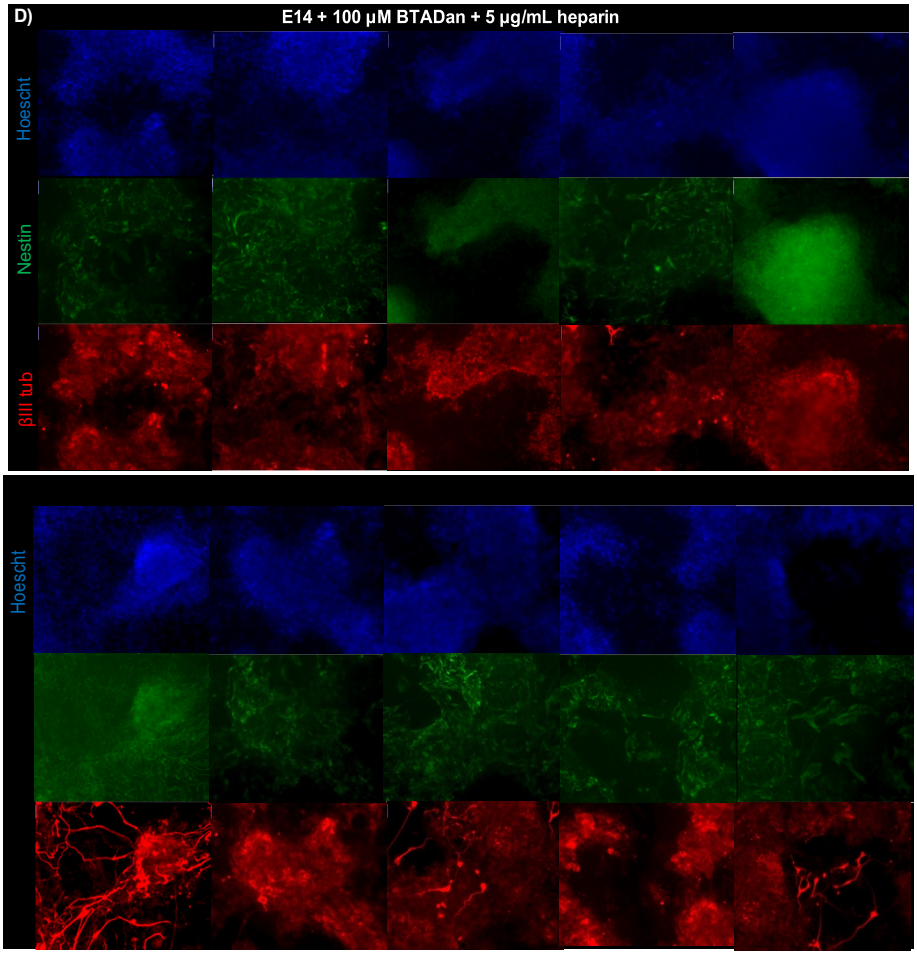

Continued. Extended Nestin and βIII-tubulin images. A) Neural differentiation of E14 mESCs for 10 days, and stained for Nestin (green) and βIII-tubulin (red). B) Neural differentiation in the presence of 100 µM **BTADan.** C) Neural differentiation in the presence of 100 µM 4FMUX**.** D) Neural differentiation in the presence of 100 µM **BTADan** and 5 µg/mL heparin**.** E) Neural differentiation in the presence of 100 µM **BTADan** and incorporated with 3 µM **P1-D2A6** at D0 for 1 h**.**

4.7 References

1. S. Moradi, H. Mahdizadeh, T. Šarić, J. Kim, J. Harati, H. Shahsavarani, B. Greber, J. B. Moore, Research and therapy with induced pluripotent stem cells (iPSCs): social, legal, and ethical considerations. *Stem Cell Research & Therapy.* **2019.** 10, 341.

2. D.-T. Chu, T. T. Nguyen, N. L. B. Tien, D.-K. Tran, J.-H. Jeong, P. G. Anh, V. V. Thanh, D. T. Truong, T. C. Dinh, Recent Progress of Stem Cell Therapy in Cancer Treatment: Molecular Mechanisms and Potential Applications. *Cells*. **2020**. 9, 563.

3. J. B. Sneddon, Q. Tang, P. Stock, J. A. Bluestone, S. Roy, T. Desai, M. Hebrok, Stem Cell Therapies for Treating Diabetes: Progress and Remaining Challenges. *Cell Stem Cell*. **2018**. 22, 810–823.

4. V. Tabar, L. Studer, Pluripotent stem cells in regenerative medicine: challenges and recent progress. *Nature Reviews Genetics*. **2014**. 15, nrg3563.

5. A. Golchin, T. Z. Farahany, Biological Products: Cellular Therapy and FDA Approved Products. *Stem Cell Rev and Rep*. **2019.** 15, 166–175.

6. W. Zakrzewski, M. Dobrzyński, M. Szymonowicz, Z. Rybak, Stem cells: past, present, and future. *Stem Cell Res Ther*. **2019**. 10, 68.

7. B. Thisse, C. Thisse, Functions and regulations of fibroblast growth factor signaling during embryonic development. *Dev. Biol.* **2005.** 287, 390–402 (2005).

8. M. Schuldiner, O. Yanuka, J. Itskovitz-Eldor, D. A. Melton, N. Benvenisty, Effects of eight growth factors on the differentiation of cells derived from human embryonic stem cells. *PNAS*. **2000.** 97, 11307–11312.

9. T. Kunath, M. K. Saba-El-Leil, M. Almousailleakh, J. Wray, S. Meloche, A. Smith, FGF stimulation of the Erk1/2 signalling cascade triggers transition of pluripotent embryonic stem cells from self-renewal to lineage commitment. *Development*. **2007.** 134, 2895–2902.

10. N. Jastrebova, M. Vanwildemeersch, A. C. Rapraeger, G. Giménez-Gallego, U. Lindahl, D. Spillmann, Heparan Sulfate-related Oligosaccharides in Ternary Complex Formation with Fibroblast Growth Factors 1 and 2 and Their Receptors. *J. Biol. Chem.* **2006.** 281, 26884–26892.

11. N. Jastrebova, M. Vanwildemeersch, U. Lindahl, D. Spillmann, Heparan Sulfate Domain Organization and Sulfation Modulate FGF-induced Cell Signaling. *J Biol Chem*. **2010.** 285, 26842–26851.

12. C. E. Pickford, R. J. Holley, G. Rushton, M. P. Stavridis, C. M. Ward, C. L. R. Merry, Specific Glycosaminoglycans Modulate Neural Specification of Mouse Embryonic Stem Cells. *STEM CELLS*. **2011.** 29, 629–640.

13. R. Kleene, M. Schachner, Glycans and neural cell interactions. *Nat. Rev. Neurosci.* **2004.** 5, 195–208.

14. H. J. Fehling, G. Lacaud, A. Kubo, M. Kennedy, S. Robertson, G. Keller, V. Kouskoff, Tracking mesoderm induction and its specification to the hemangioblast during embryonic stem cell differentiation. *Development*. **2003.** 130, 4217–4227.

15. M. L. Huang, R. A. A. Smith, G. W. Trieger, K. Godula, Glycocalyx Remodeling with Proteoglycan Mimetics Promotes Neural Specification in Embryonic Stem Cells. *Journal of the American Chemical Society*. **2014.** 136, 10565–10568.

16. K. A. Meade, K. J. White, C. E. Pickford, R. J. Holley, A. Marson, D. Tillotson, T. H. van Kuppevelt, J. D. Whittle, A. J. Day, C. L. R. Merry, Immobilization of Heparan Sulfate on Electrospun Meshes to Support Embryonic Stem Cell Culture and Differentiation. *J Biol Chem*. **2013.** 288, 5530–5538.

17. A. Pulsipher, M. E. Griffin, S. E. Stone, J. M. Brown, L. C. Hsieh-Wilson, Directing neuronal signaling through cell-surface glycan engineering. *J. Am. Chem. Soc.* **2014**. 136, 6794–6797.

18. C. K. M. Tripathi, J. Banga, V. Mishra, Microbial heparin/heparan sulphate lyases: potential and applications. *Appl Microbiol Biotechnol*. **2012.** 94, 307–321.

19. M. L. Huang, A. L. Michalak, C. J. Fisher, M. Christy, R. A. A. Smith, K. Godula, Small Molecule Antagonist of Cell Surface Glycosaminoglycans Restricts Mouse Embryonic Stem Cells in a Pluripotent State. *STEM CELLS*. **2018.** 36, 45–54

20. Y. Tsuzuki, T. K. N. Nguyen, D. R. Garud, B. Kuberan, M. Koketsu, 4-Deoxy-4-fluoro-xyloside derivatives as inhibitors of glycosaminoglycan biosynthesis. *Bioorganic & Medicinal Chemistry Letters*. **2010.** 20, 7269–7273.

21. A. Varki, R. D. Cummings, J. D. Esko, P. Stanley, G. W. Hart, M. Aebi, A. G. Darvill, T. Kinoshita, N. H. Packer, J. H. Prestegard, R. L. Schnaar, P. H. Seeberger, *Essentials of Glycobiology.* Cold Spring Harbor Laboratory Press, **2017**.

22. T. A. Fritz, F. N. Lugemwa, A. K. Sarkar, J. D. Esko, Biosynthesis of heparan sulfate on beta-D-xylosides depends on aglycone structure. *Journal of Biological Chemistry*. **1994.** 269, 300–307.

23. T. A. Fritz, J. D. Esko, Xyloside priming of glycosaminoglycan biosynthesis and inhibition of proteoglycan assembly. *Methods Mol. Biol.* **2001**. 171, 317–323.

24. D. R. Garud, V. M. Tran, X. V. Victor, M. Koketsu, B. Kuberan, Inhibition of Heparan Sulfate and Chondroitin Sulfate Proteoglycan Biosynthesis. *J Biol Chem*. **2008**. **283**, 28881–28887.

25. A. Siegbahn, S. Manner, A. Persson, E. Tykesson, K. Holmqvist, A. Ochocinska, J. Rönnols, A. Sundin, K. Mani, G. Westergren-Thorsson, G. Widmalm, U. Ellervik, Rules for priming and inhibition of glycosaminoglycan biosynthesis; probing the β4GalT7 active site. *Chemical Science*. **2014.** 5, 3501–3508.

26. S. Dahbi, J.-C. Jacquinet, I. Bertin-Jung, A. Robert, N. Ramalanjaona, S. Gulberti, S. Fournel-Gigleux, C. Lopin-Bon, Synthesis of a library of variously modified 4-methylumbelliferyl xylosides and a structure–activity study of human β4GalT7. *Organic & Biomolecular Chemistry*. **2017**. 15, 9653–9669.

27. J. S. Chua, B. Kuberan, Synthetic Xylosides: Probing the Glycosaminoglycan Biosynthetic Machinery for Biomedical Applications. *Acc. Chem. Res.* **2017.** 50, 2693–2705.

28. M. Saliba, N. Ramalanjaona, S. Gulberti, I. Bertin-Jung, A. Thomas, S. Dahbi, C. Lopin-Bon, J.-C. Jacquinet, C. Breton, M. Ouzzine, S. Fournel-Gigleux, Probing the Acceptor Active Site Organization of the Human Recombinant β1,4-Galactosyltransferase 7 and Design of Xyloside-based Inhibitors. *Journal of Biological Chemistry*. **2015.** 290, 7658–7670.

29. M. L. Huang, R. A. A. Smith, G. W. Trieger, K. Godula, Glycocalyx Remodeling with Proteoglycan Mimetics Promotes Neural Specification in Embryonic Stem Cells. *Journal of the American Chemical Society*. **2014**. 136, 10565–10568.

30. M. R. Naticchia, L. K. Laubach, E. M. Tota, T. M. Lucas, M. L. Huang, K. Godula, Embryonic Stem Cell Engineering with a Glycomimetic FGF2/BMP4 Co-Receptor Drives Mesodermal Differentiation in a Three-Dimensional Culture. *ACS Chem. Biol.* **2018.** 13, 2880–2887.

31. P. K. Qasba, B. Ramakrishnan, E. Boeggeman, Structure and Function of β-1,4-Galactosyltransferase. *Curr Drug Targets*. **2008**. 9, 292–309.

32. Y. Tsutsui, B. Ramakrishnan, P. K. Qasba, Crystal Structures of β-1,4-Galactosyltransferase 7 Enzyme Reveal Conformational Changes and Substrate Binding. *J Biol Chem*. **2013**. 288, 31963–31970.

33. L. Scietti, A. Chiapparino, F. De Giorgi, M. Fumagalli, L. Khoriauli, S. Nergadze, S. Basu, V. Olieric, L. Cucca, B. Banushi, A. Profumo, E. Giulotto, P. Gissen, F. Forneris, Molecular architecture of the multifunctional collagen lysyl hydroxylase and glycosyltransferase LH3. *Nat Commun*. **2018,** 9, 3163 ()

34. S. Wang, J. A. Cuesta-Seijo, D. Lafont, M. M. Palcic, S. Vidal, Design of Glycosyltransferase Inhibitors: Pyridine as a Pyrophosphate Surrogate. *Chemistry – A European Journal*. **2013**. 19, 15346–15357.

35. S. Niewiadomski, Z. Beebeejaun, H. Denton, T. K. Smith, R. J. Morris, G. K. Wagner, Rationally designed squaryldiamides - a novel class of sugar-nucleotide mimics? *Org Biomol Chem*. **2010.** 8, 3488–3499.

36. R. Jørgensen, L. L. Grimm, N. Sindhuwinata, T. Peters, M. M. Palcic, A Glycosyltransferase Inhibitor from a Molecular Fragment Library Simultaneously Interferes with Metal Ion and Substrate Binding. *Angewandte Chemie*. **2012**. 124, 4247–4251.

37. O. Trott, A. J. Olson, AutoDock Vina: improving the speed and accuracy of docking with a new scoring function, efficient optimization and multithreading. *J Comput Chem*. **2010**. 31, 455–461.

38. R. A. Friesner, R. B. Murphy, M. P. Repasky, L. L. Frye, J. R. Greenwood, T. A. Halgren, P. C. Sanschagrin, D. T. Mainz, Extra Precision Glide: Docking and Scoring Incorporating a Model of Hydrophobic Enclosure for Protein−Ligand Complexes. *J. Med. Chem.* **49**, 6177–6196 (2006).

.

Appendix for Chapter 3: Primer sequence

Table A.1. Primer sequences

Gene	Forward	Reverse
gapdh	TGCCTGCTTCACCACCTTCT	CCAATGTGTCCGTCGTGGAT
oct4	TTGCCTTGGCTCACAGCATC	TGTTCCCGTCACTGCTCTGG
sox2	TTCGAGGAAAGGGTTCTTGCTG	TCCTTCCTTGTTTGTAACGGTCCT
nanog	TTTGGAAGCCACTAGGGAAAG	CCAGATGTTGCGTAAGTCTCATA
sox1	GGCCGAGTGGAAGGTCATGT	TCCGGGTGTTCCTTCATGTG
fgf5	CCTTGCGACCCAGGAGCTTA	CCGTCTGTGGTTTCTGTTGAGG
brachyury	TTGAACTTTCCTCCATGTGCTGA	TCCCAAGAGCCTGCCACTTT
flk1	CACCTGGCACTCTCCACCTTC	GATTTCATCCCACTACCGAAAG